UNIVERSITÉ DE NANTES
ECOLE POLYTECHNIQUE DE L'UNIVERSITÉ DE NANTES

_____

ÉCOLE DOCTORALE
MOLÉCULES, MATIÈRES ET MATÉRIAUX EN PAYS DE LA LOIRE (3MPL)

Année 2012

N° attribué par la bibliothèque

Fabrication et propriétés mécaniques de ciments phosphocalciques poreux pour la substitution osseuse

THÈSE DE DOCTORAT

Discipline: Science des Matériaux

Spécialité: Science des Matériaux

Présentée
et soutenue publiquement par

Jingtao ZHANG

Le 2 juillet 2012, devant le jury ci-dessous

Président	Tanguy ROUXEL, Professeur	Université de Rennes 1
Rapporteurs	Maria Pau GINEBRA, Professeur	Universitat Politecnica De Catalunya
	Moussa GOMINA, Chargé de Recherche	CRISMAT, Caen
Examinateurs	Verena SCHNITZLER, Docteur	Société GRAFTYS
	Franck TANCRET, Professeur	Université de Nantes
	Jean-Michel BOULER, Professeur	Université de Nantes
Invité	Pierre WEISS, Professeur	Université de Nantes

Directeur de thèse : Franck TANCRET, Professeur *Université de Nantes*
Co- directeur de thèse : Jean-Michel BOULER, Professeur *Université de Nantes*

TABLE OF CONTENTS

Introduction

A few millions patients each year need bone grafts or bone graft substitutes to repair defects caused by trauma, aging and diseases. A large number of synthetic bone graft substitutes, which are based on ceramics, cements, polymers or metals, are used. Among them, Calcium Phosphate Cements (CPC), which were first reported in the 1980s (Brown et al., 1983; LeGeros et al., 1982), are interesting due to their injectability and in situ setting properties (Julien et al., 2007; Khairoun et al., 2002; Rupprecht et al., 2003), allowing minimally invasive surgery. Mechanical properties of CPC are critical for their successful application and have been widely investigated. However, most of them were measured in order to gain some “engineering information” on specific cements, in view of medical applications, but only rare studies considered the mechanical behavior of CPC as a scientific subject as itself. Nevertheless, an approach based on concepts of material mechanics would probably be valuable to better understand the overall mechanical behavior of this whole category of materials. The present work is therefore primarily focused on the understanding of the relations between microstructure (porosity, pore size and distribution, crystal shape/size) and mechanical properties (Young’s modulus, fracture toughness, flexural and compressive strength). The knowledge gained should allow, in the end, to improve mechanical properties by controlling the microstructure, and to find a better compromise between mechanical and biological behaviors. In this aim, this document is organised as follows. The first Chapter will mainly review the recent developments of CPC. But before detailing these aspects, the structure of human bone will be briefly described, and its fracture mechanisms explained. In addition, besides CPC, several typical bone graft substitutes will be presented. Then, CPC will be described from the viewpoints of chemistry, handling properties and mechanical properties. The latter being the main focus of this work, a special attention will be drawn to existing literature on the mechanical behavior of CPC, in order to identify what are the principal issues which would merit further investigation in order to better understand these aspects. In short, it will be shown that there is a lack of a comprehensive and comparative study of the relations between processing, microstructure and mechanical properties of CPC, performed as a systematic investigation of the influence of microstructural parameters on mechanical properties and their reliability, while working within a general frame where most other parameters are fixed. In addition, because

modelling can help to better understand and control the mechanical properties of materials, some analytical models describing the mechanical behavior of porous brittle materials will be reviewed. To achieve these aims, the procedures used to fabricate and characterise a set of CPC with systematically varying microstructures will be described in the second Chapter. The third Chapter will then investigate, in a systematic manner, the influence of microstructural parameters like porosity on elastic and fracture properties of dried CPC. The possibility to use analytical models to describe mechanical properties as a function of porosity will also be studied; they will be adapted when necessary. Then, the fourth Chapter will mainly focus on the comparison between the mechanical properties of wet and dried CPC, as well as on strength reliability which will be studied within a statistical approach of fracture.

Despite their advantages over bioceramics, CPC without any additives usually display poor injectability and cohesion and, even if optimisation is possible, their mechanical properties often remain rather low, which in all need to be further improved. To this end, the possibility to produce and develop composite CPC with enhanced handling and mechanical properties will be studied, which will be addressed in the fifth and last Chapter. To achieve this, several polymeric additives will be chosen following a critical review of their potential properties. The handling properties of the resulting composite CPC will be evaluated, and their mechanical properties measured and related to microstructure. Finally, because calcium phosphate bone substitutes containing pores of several tens or hundreds of micrometers are known to present a good potential of osteointegration, the possible fabrication of foamed composite cements will also be explored.

Chapter 1 Literature review and aims

1.1 Bone structure and fracture

Bone is a remarkable rigid organ within the vertebrates, performing several key functions such as providing structural support and protection to various organs of the body, producing blood cells and storing minerals for the metabolism (Hing 2004). Bones are full of cracks, which form and grow as a result of daily loading activities or diseases. However, bone has a property which, up to now, cannot be obtained in artificial materials, although constant progress is made in the field of "self-healing" materials (Cordier et al., 2008): it is "smart" enough to detect and repair the cracks before they become long enough to be dangerous. This self-repair ability of bone, called remodeling, is controlled by two kinds of specialized cells: osteoclasts, which resorb bone by releasing a powerful acid and enzyme, and osteoblasts, which make new bone. These cells together form a basic multicellular unit (BMU)- a cavity, about 200 μm in diameter, moving at a speed of 40 μm per day along the length of bone (Fig. 1-1) (Taylor et al., 2007).

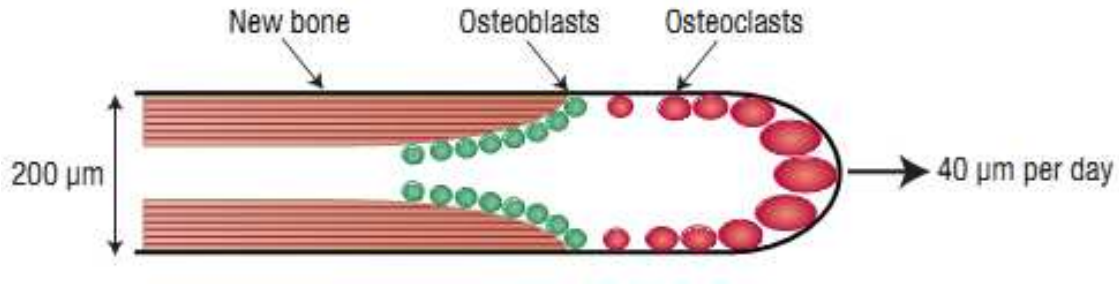

Fig. 1-1 Schematic diagram describing the remodeling of human bone. Reprinted from Taylor et al. (2007)

Although having this fascinating nature, bone still cannot prevent catastrophic breaking and defects caused by trauma, aging, diseases (i.e. osteoporosis or cancer) and congenital defects, which are greatly affecting millions of sufferers across the whole world. Just taking osteoporosis for instance, it causes more than 8.9 million fractures worldwide annually and over one third of all osteoporotic fractures occur in Europe (Ström et al., 2011). In France, about 120 000 cases of fracture caused by osteoporosis have been reported in 2001 (Maravic et al., 2005). The number of new bone fractures is

still increasing steadily, which on the one hand will affect the quality of life of millions of people and on the other hand cause a heavy burden to the whole society.

The structure and properties of bone have been widely investigated and well understood, and to fully understand the aims of the present work it is meaningful and necessary to introduce the structure and properties of our bones.

1.1.1 Structure of bone

Most biological materials with predominant mechanical properties have a hierarchical structure consisting of several different levels. Bone is not an exception. The structure of bone can be described in five hierarchical levels as shown in Fig. 1-2 (Rho et al., 1998). Specifically, the structures and levels are: (1) cortical and cancellous bone at macrostructural level; (2) haversian systems and osteons at sub-millimeter scale; (3) lamella at micron level; (4) fibrillar collagen and embedded mineral at submicron scale; (5) mineral crystals, collagen and organic proteins at nanometer level. These complicated hierarchical structures make bone heterogeneous and anisotropic.

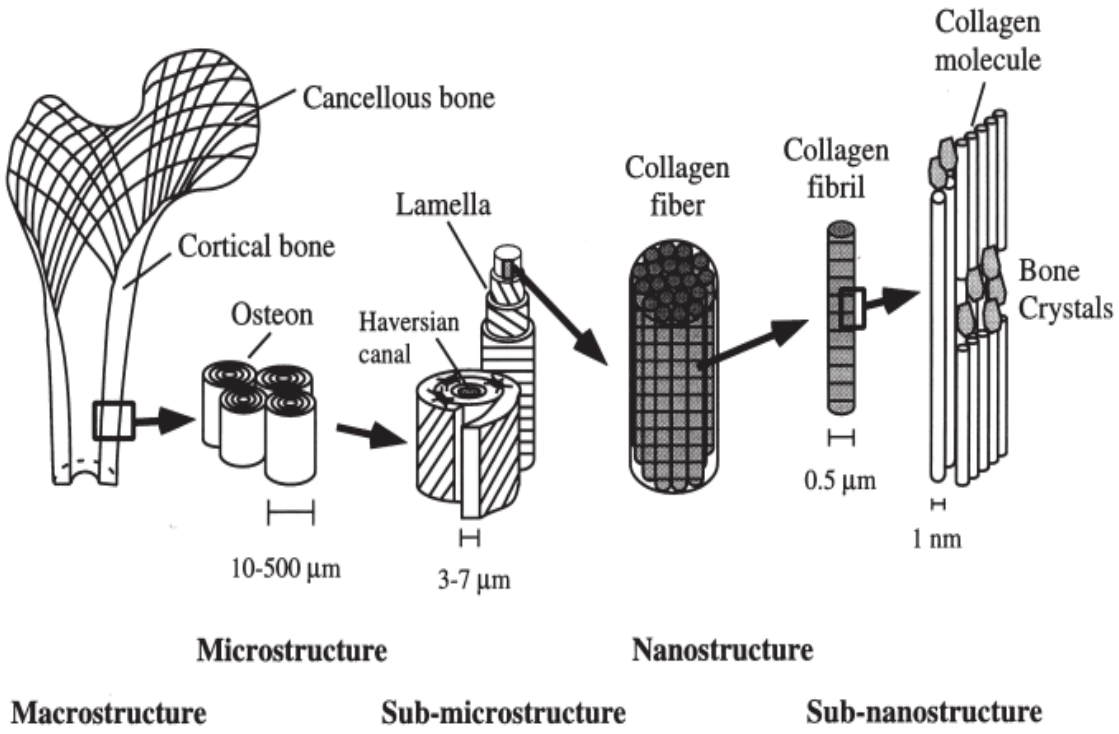

Fig. 1-2 Hierarchical structure of bone. Reprinted from Rho et al (1998)

From a chemical point of view, bone comprises an organic matrix (25%), a mineral

part (65%) and water (10%) (the percentages between parentheses represent typical constituents of bone in weight) (Olszta et al., 2007). The organic matrix mainly consists of 90% type I collagen whose molecule is composed of a triple helix of peptide chains. These molecules are covalently bonded by intra- and intermolecular crosslinks providing for the tensile strength (Eyre et al., 1984; Knott et al., 1998).

Bone mineral is an apatitic calcium phosphate containing 4%-6% carbonate by weight and small amounts of magnesium, sodium, potassium, citrate, fluoride and other trace components (Glimcher et al., 1981). This carbonated apatite, named dahllite, is also the mineral component of teeth and some invertebrate skeletons (Lowenstam et al., 1989). The plate-like bone crystals, with dimensions of 50 nm in length, 25 nm in width and 2.5-4 nm in thickness, are probably the smallest crystals formed physiologically (Fratzl et al., 1992). Recently, Xie and Nancollas (2010) found that the size and morphology of the apatite nanocrystals were strongly controlled by citrate molecules which cover approximately one sixth of the available apatite surface area in bone. Both collagen and minerals have a great influence on mechanical properties of bone: on the one hand the collagen can improve the fracture toughness[1], and on the other hand mineral can confer strength and stiffness[2].

Water exists throughout the tissue in several forms: freely mobile in vascular-lacunar-canalicular space, bound to the collagen network, and bound to the mineral phase. Due to their polarity, water molecules can attach to collagen (glycine, hydroxyproline, carboxyl and hydroxylysine) through hydrogen bonds and to different mineral ions such as Ca^{2+} and PO_4^{3-}. Because of the above interaction, water also influences the mechanical properties of bone. Nyman et al. (2006) surveyed the influence of water removal on the strength and toughness of cortical bone, speculating that the loss of water in the collagen phase decreased the toughness of bone, and that a loss of water related to the mineral phase decreased both bone strength and toughness.

1.1.2 Fracture of bone

As mentioned above, bone can repair itself through remodeling; however it cannot yet completely prevent propagation of cracks to a certain length that is long enough to cause catastrophic failure. Thus it seems to be essential to understand how cracks propagate in

[1] Fracture toughness is defined in 1.1.2

[2] Stiffness is the resistance of an elastic body to deformation, which can also be understood as “rigidity”.

bone, which is of crucial importance for clinical questions, such as the treatment of osteoporosis and other diseases associated with bone fragility. In addition, the following analysis will bring elements for the development of crack-resistant materials for bone replacement.

Fracture toughness, K_c, also called the critical stress intensity factor, is a property which is used to describe the ability of a material containing cracks or notches to resist crack propagation. The resistance of bone to cracking can also be characterized by fracture toughness. Like in other composite materials, the fracture toughness of bone is obviously larger than that of its constitutents (organic and mineral). Furthermore, Nalla et al. (2005) and Vashishth (2004) found that K_c is not constant during crack propagation, but increases with increasing crack extension; this phenomenon is called an R-curve behavior ("R" stands for "resistance", and an R-curve is the plot of resistance to cracking, i.e. toughness, as a function of crack extension, see Fig. 1-3), and is due to the existence of microscopic phenomena called toughening mechanisms.

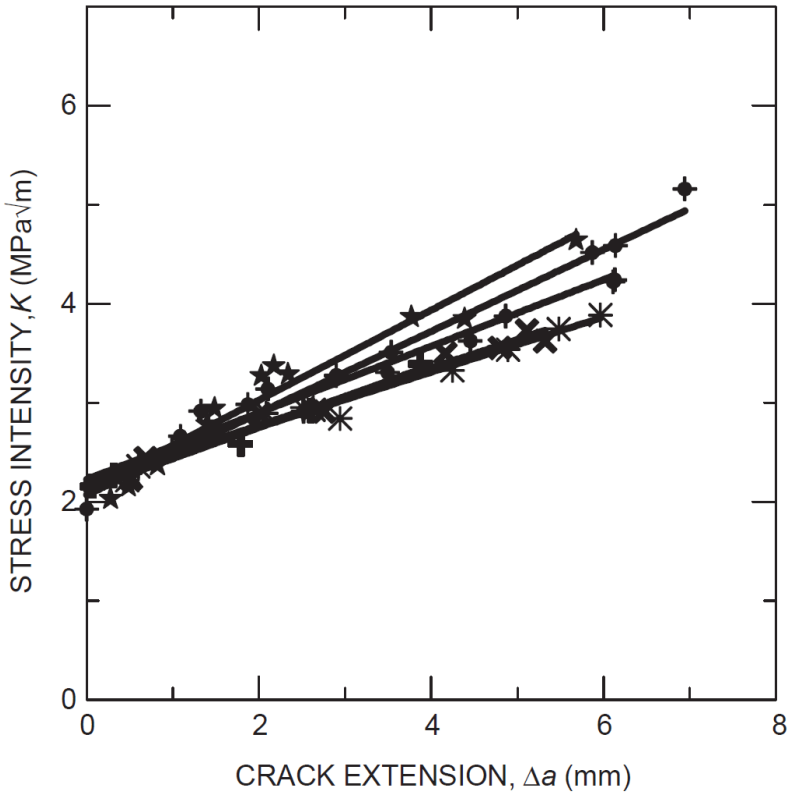

Fig. 1-3 $K_c(\Delta a)$ resistance curve for stable crack extension in bone, showing rising behaviors (R-curves). Reprinted from (Nalla et al 2005)

Launey and Ritchie (2009) postulated that there are several toughening mechanisms in

cortical bone, including crack bridging by unbroken ligaments (Nalla et al., 2005), crack deflection (Peterlik et al., 2006), microcracking (Vashishth, 2004) and viscoplasticity (Fantner 2005), which can be sorted into "intrinsic toughening" (crack initiation toughness) and "extrinsic toughening" (crack growth toughness), and which can also be used to explain rising R-curves. Fig.1-4 depicts the above toughening mechanisms in cortical bone.

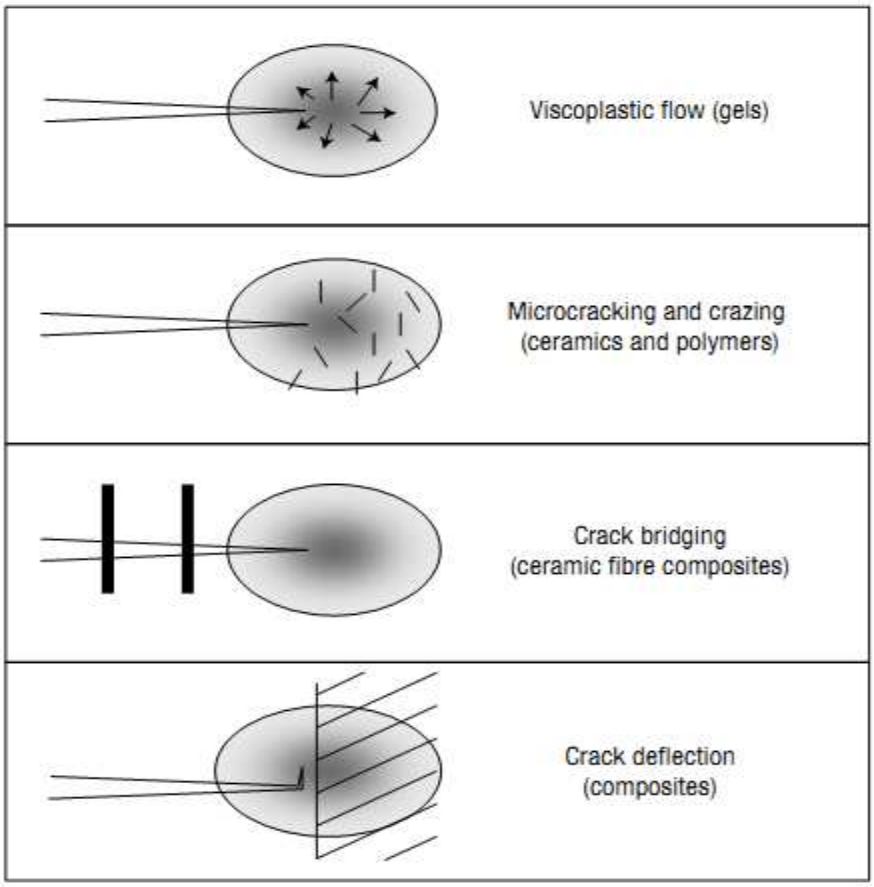

Fig.1-4 Toughening mechanisms in cortical bone, and their analogy with effective mechanisms acting in synthetic materials. Reprinted from (Peterlik et al., 2006)

Among these toughening mechanisms, Nalla et al. (2004A) found that crack bridging is the major contributor to the increasing R-curve as compared to microcracking basing on their different effects on compliance (compliance is the inverse of stiffness), specifically crack bridging decreases compliance, but in contrast, microcracking increases compliance. Nalla et al. (2004B) also surveyed the influence of aging on the toughness of human cortical bone through an evaluation of the R-curve, finding that crack-growth resistance deteriorates with increasing age and associating this to weaker bridges caused by lower collagen quality and to a possible change in the collagen network

integrity.

Koester et al. (2008) measured the toughness of human cortical bone with realistically short cracks in both transverse and longitudinal orientations. The authors found that after only 500 μm of cracking, the fracture toughness is more than five times higher in transverse (breaking) direction than in the longitudinal (splitting) direction, owning to different toughening mechanisms, specifically crack deflection on breaking and crack bridging on splitting (Fig.1-5). Furthermore, they identified the major role of microcracks: inducing primary forms of toughening in human cortical bone, that of crack deflection and crack bridging.

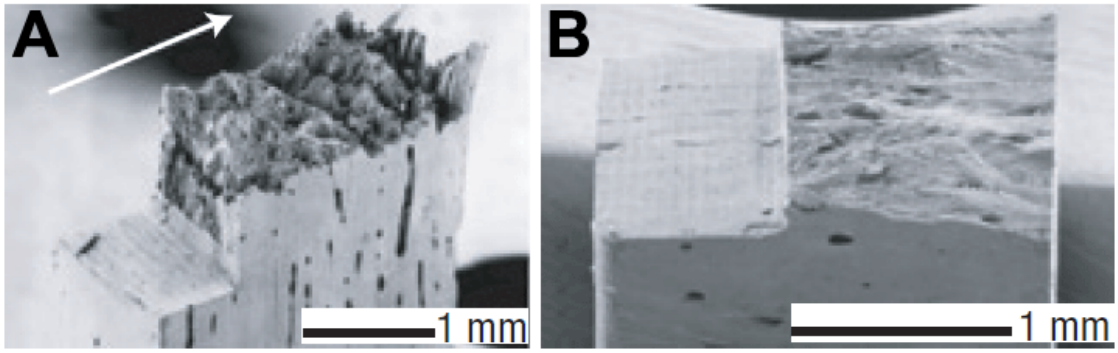

Fig.1-5 ESEM (Environmental Scanning Electron Microscope) fractographic images of broken surfaces of compact-tension samples of human cortical bone. (a) Fracture in transverse orientation, showing a rough fracture surface due to crack deflection. (b) Fracture in longitudinal orientation, showing a relatively flat fracture surface. Reprinted from Koester et al. (2008)

In conclusion, fracture of bone is a very complicated process which is related to not only its composition but also simultaneous operation of several toughening mechanisms owning to its hierarchical structure. Crack bridging and crack deflection are the two primary toughening mechanisms.

1.2 Bone graft substitutes

Owing to diseases and traumatic events, nearly three million patients worldwide need to undertake bone grafting operations each year (Greenwald et al., 2001). Bone grafting, firstly established two centuries ago, is the procedure to replace missing or damaged bones with materials from either patient themselves (autograft) or donors (allograft) (Hing 2005A; Meeder et al., 1994).

Currently, autografting is still considered to be ideal since the bone harvested from the

patients themselves contains living cells and growth factors. However, autografting has some limitations such as an additional operation on a second surgical site with associated donor site pain and morbidity, as well as the obvious short supply of bone sources. Alternatively, modern allografting using donor bone from a regular bone bank might partly overcome the limitation of bone supply; however after sterilization treatments, the bone will lose the biological factors and have impaired strength (Hing et al., 2005B). Furthermore, there are still concerns regarding immunological reaction between patient and donor bone, as well as disease transmisison (Barriga et al., 2004); thus healing can be in some cases unpredictable (Togawa et al., 2004).

Because of the above drawbacks, there is an increasing demand for synthetic bone substitutes which are free from the limitation of bone supply, consistency and disease. Moreover, there is the potential to use many of these scaffolds in conjunction with the own cells of the patient or recombinant growth factors to speed up or to improve the quality of bone regeneration, which is known as “tissue engineering” (Reddi 2000). There is a wide range of synthetic materials that have been proposed and developed as bone substitutes: metals such as tantalum, titanium, iron, or magnesium; polymers such as polylactides, polyglycolides, polyurethanes, or polycaprolactones; ceramics such as alumina, zirconia or calcium phosphates (CaP) and calcium phosphate cements obtained from tricalcium phosphate (TCP), dicalcium phosphate (DCP), tetra calcium phosphate (TTCP) and hydroxyapatite (HA) (Bohner 2010A). These synthetic bone substitutes will be reviewed briefly in the following subsections in conjunction with special attention to calcium phosphate cements.

1.2.1 PMMA

Polymethylmethacrylate (PMMA), sometimes called acrylic cement, is a synthetic polymer. Due to its excellent processability, PMMA has been extensively used in prosthesis fixation since 1960 (Charnley 1960). In 1985, Galibert et al. (1987) started to inject PMMA into vertebral lesion with a radiologically guided therapeutic technique named percutaneous vertebroplasty (PV). In these applications, PMMA acts as an intermediary phase and is used to fix the implant to bone or structurally reinforce the vertebrae, transmitting the applied force and body weight uniformly to surrounding tissues.

Despite its successful application, PMMA still has some well-known shortcomings.

The autopolymerization reaction of PMMA is exothermic, leading to an increase in temperature and thus causing necrosis of tissues (Lewis 1997). Furthermore, there is a weak interface between PMMA and bone due to the formation of a thin layer of fibrous tissue, allowing for micromovements and finally causing implant loosening (Driessens et al., 1994). Other shortcomings such as aging, lack of pores of sufficient size (macropores) to allow cell ingrowth, release of unreacted monomer and low mechanical properties have been also reported (Lewis 1997).

Many efforts have been made to overcome the above shortcomings. Meyer et al. (1973) reported that preparing PMMA at low temperature can significantly decrease the peak temperature of autopolymerization while compared to PMMA prepared at higher temperature. Dunne and Orr (2002) demonstrated that the level of heat release for PMMA during autopolymerization is significantly lower under vacuum than under atmospheric conditions. Ormsby et al. (2010) incorporated multiwalled carbon nanotubes (MWCNTs) into PMMA. The authors found that the addition of MWCNTs can not only significantly reduce the heat produced during autopolymerization but also improve mechanical properties. Contributions have been also made to improve mechanical properties or bioactivation by addition of carbon or aramid fibers (Saha et al., 1984), hydroxyapatite (Vallo et al., 1999) and bioglass (Heikkila et al., 1996). However, it is sometimes hard to improve both mechanical properties and bioactivity of PMMA owing to the deterioration of mechanical properties with a large amount of added bioactive particles, or to the lack of bioactivity when the amount of added bioactive particles is small, indicating that a balance between mechanical properties and bioactivity should be considered when bioactive particles are added.

Furthermore, macropores larger than 100 μm are essential for new bone growth. Puska (2003) prepared macroporous PMMA by using a resorbable bio-oligomer which is based on an amino acid of trans-4-hydroxy-L-proline and can be dissolved in moist environments. As expected, the resulting porosity inside the PMMA structure decreases its mechanical properties. Nevertheless, in some cases, PMMA with suitable but not high mechanical properties can produce a better treatment effect. Grados et al. (2000) reported that there is a small but actual increased risk of vertebral fracture in adjacent region of a cemented vertebra after a long-term observation on 25 patients who received PV treatments on vertebral osteoporotic fractures, indicating the side effect of an overly rigid reinforcement. According to this observation, Boger et al. (2007) prepared a porous scaffold with suitable mechanical properties compared to those of cancellous bone by

mixing PMMA with a sodium hyaluronate polymer solution which is used to create pores inside the PMMA structure.

In summary, despite improvements in mechanical properties and other related properties, PMMA is a bio-inert polymer which cannot be absorbed and replaced by human bone; therefore it is now imperative to find bone substitutes with better biocompatibility and bioactivity.

1.2.2 Ceramics

Since the term “bioceramics” first appeared in an abstract published in 1971 (Blakeslee et al., 1971), bioceramics have been used as bone substitutes for 40 years. Bioceramics can be classified in two families: bioinert (actually no material should be considered as completely inert, but such a material exhibits extremely slow kinetics of reaction into a level that they can be considered as “almost inert”) and bioactive. Bioinert ceramics have nearly no interaction with surrounding living tissue. Alumina and zirconia are often considered two prototypes of bioinert ceramics. However, these bioinert ceramics are rarely used as bone fillers. Since a soft tissue interlayer always shields the bone from the inert implant, this shielding promotes micro-motion and subsequently causes implant loosening (Chevalier et al., 2009).

Great effort has been made to improve the mechanical properties of these bioceramics. In the 1990s, yttria-stabilised zirconia (YSZ) became an attractive alternative as a structural bioceramic due to its superior fracture toughness and strength as compared to alumina. This improvement in facture toughness and strength can be attributed to a toughening mechanism by phase transformation, which involves the transformation of a metastable tetragonal phase to a monoclinic phase. This transformation thus causes volume expansion and introduces additional stresses in front of the crack tip hindering crack propagation (volume expansion and introduced additional stresses can offset part of the applied force and therefore ease the stress applied to a crack tip) (Chevalier et al., 2009; Claussen et al., 1980). Table 1-1 summarizes mechanical properties of different ceramics.

Table 1-1 Mechanical properties of different bioceramics. (PSZ = partially stabilized zirconia; TZP = tetragonal zirconia polycrystals). Reprinted from Chevalier et al. (2009)

Material	Toughness (K_{IC}, MPa $m^{1/2}$)	Strength (MPa)	Vickers hardness
Alumina	4.2	400-600	1800-2000
Zirconia	5.4	1000	1200-1300
Hydroxyapatite	0.9	50-60	500
Tricalcium phosphate	1.3	50-60	900
Mg-PSZ	8	600	1000
12Ce-TZP	7.8	700	1000-1100
Micro-nano-alumina-zirconia	6	600	1800
Nano-nano-Ce-TZP-alumina	8.4	900	1300
Silicon nitride	10	1000	2500

Most of these bioactive ceramics are based on calcium orthophosphates such as TCP, HA and biphasic calcium phosphate (BCP). Calcium orthophosphate based bioactive ceramics have been widely used in all areas of the human skeleton (Dorozhkin 2010). Most of the studies on these materials can be sorted into two main categories: optimization of microstructure and the achievement of a proper chemical activity (Hing et al., 2005B). With regard to the microstructure, it is worth mentioning in this study that microporosity refers to pores smaller than 10 μm, whereas macroporosity corresponds to pores of at least tens of micrometers, which are their common meaning in the community of biomaterials. Both microporosity and macroporosity play a great role in bone substitutes. On the one hand, microporosity allows for impregnation of biological fluids, and on the other hand, the presence of macropores is considered essential for cell migration (Hing et al., 1999). “Cell-size” macropores of minimum 100 μm are proposed to favor bone colonization of the implant. However, pore sizes larger than 300 μm are recommended due to enhanced new bone formation and to the formation of capillaries (Karageorgiou et al., 2005). Gauthier et al. (1998) evaluated bone ingrowth in BCP with two different macropore diameters, 300 μm and 564 μm, and two different macroporosity percentages, 40% and 50%. Their results suggest that macropore size has a great influence on bone ingrowth. However, von Doernberg et al. (2006) showed that macroporosity plays an important role but that macropore size has very limited effect on *in vivo* response. It can probably be argued that this is true as long as macropore size remains within an appropriate range. Moreover, recent research has shown that macroporous HA bioceramics containing micropores can further promote bone ingrowth (Woodard et al., 2007). Besides macropores and micropores, other microstructural features such as pore geometry, pore distribution and pore interconnectivity can all

modify the interaction between bone and implant. Chemistry also plays a crucial role on the bioactivity of bioceramics. Chemical modification through ion substitution, such as silicon into HA or TCP, can produce materials with superior biological performance as compared to those without ion substitution (Pietak 2007). In conclusion, both microstructural features and the chemical composition have a great influence on the biological behavior of bioceramics. This relationship can be attributed to physiochemical properties of the implant surface and to their impact on competitive protein growth factors (Hing et al., 2005B).

Despite great progress in the last forty years, and a promising future, there are still many challenges in terms of bioactivity, gene activation and mechanical properties (fracture toughness, reliability), the latter needing to be improved to be used as load bearing substitutes.

1.2.3 Calcium phosphate cements (CPC)

Calcium phosphate cements are highly biocompatible materials which are gradually replaced by new bone *in vivo*. Since the first patent on CPC proposed by Brown and Chow in 1983 (Brown et al., 1983), many CPC with varying compositions have been investigated and are commercially available (Bohner et al., 2005B).

A CPC is produced by a chemical reaction between two phases, a solid and a liquid which, when mixed, form a paste which progressively sets and hardens into a solid mass; this is similar to the cements used in civil engineering. The solid phase comprises one or several calcium phosphate (CaP) compounds. Water, or a calcium- or phosphate-containing solution is used as liquid which may contain chitosan, alginate or citric acid to allow the dissolution of the initial CaP compounds until the over-saturation of the solution, thus inducing the reprecipitation of crystals. The chemistry and kinetics of CPC setting will be described in more detail later. The hardening of the cement takes place through the entanglement of needle-like or plate-like crystals (Fig. 1-6). Currently, there are only two possible final products for the CPC reaction: brushite (Dicalcium Phosphate Dihydrate: DCPD) or apatite such as hydroxyapatite or calcium-deficient hydroxyapatite (CDHA) (Bohner 2007).

As mentioned previously, a porous microstructure is a critical factor to guaranty healing success. In the case of CPC, fortunately, most of them contain an intrinsic interconnected microporosity which is useful for impregnation of biological fluids.

Espanol et al. (2009) used mercury intrusion porosimetry curves to describe the porous structure developed in CPC, observing that the cements show a clear bimodal pore size distribution with two peaks which are attributed to inter-crystallite voids (smaller than 0.1μm) and to voids between aggregates (larger than 0.1μm). However, similar to other bone substitutes, it would be also desirable to create macropores[3] of at least tens of micrometers in CPC to favor bone colonization of the implant. Like bioceramics, both pore size and pore quantity have great effect on bone ingrowth into CPC although their respective influence remains controversial (Gauthier et al., 1998; von Doernberg et al., 2006), but their influence on strength is not questionable since, obviously, the strength decreases with increasing porosity and pore size (Karageorgiou et al., 2005). For this reason, the poor mechanical properties of CPC, especially weak fracture toughness and low reliability, prohibit them from being used in load-bearing places and need further enhancement (Bohner 2010B). This point will be further detailed in section 1.5.

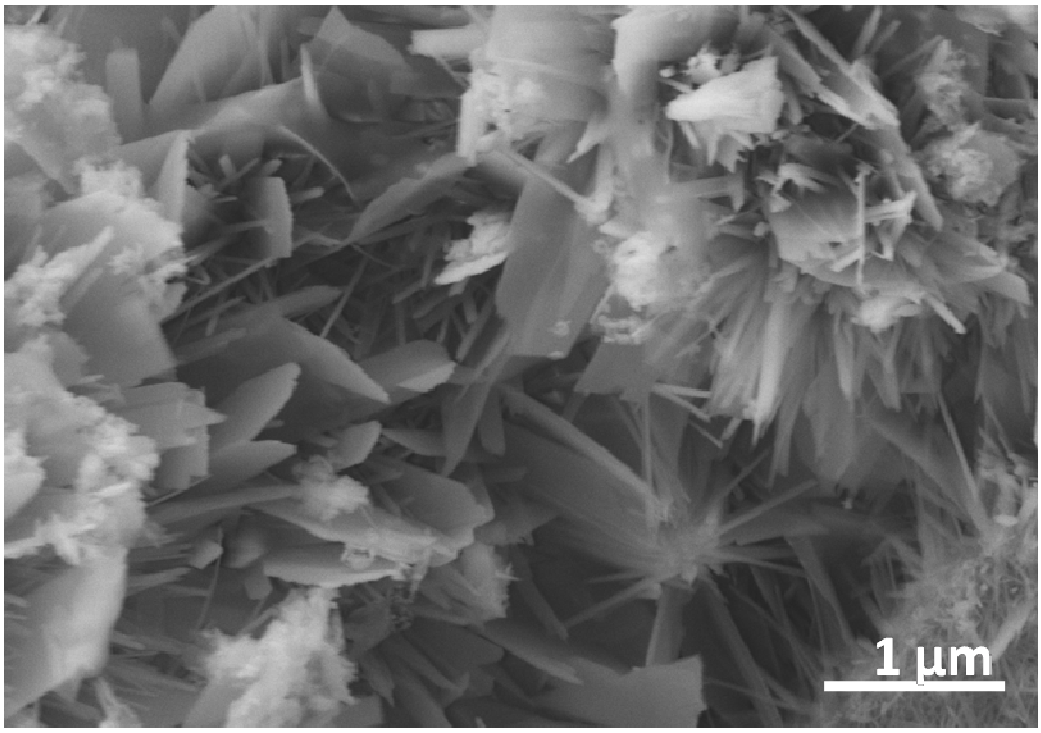

Fig.1-6 SEM micrograph of a CPC fracture surface showing needle-like and plate-like crystals

Besides advantages such as high biocompatibility, bioactivity and osteoconductivity, CPC have a unique advantage over bioceramics: they can be easily manipulated and shaped and, in some cases, be injected into a defect area, not only avoiding invasive

[3] Various methods have been used to create macropores in CPC, and they will be detailed in section 1.5.2.2.

surgical procedures but also providing intimate adaptation to the surrounding bone even for irregularly shaped cavities. Moreover, the final composition of hardened CPC is more similar to the calcium phosphates found in the mineralized tissues than bioceramics, with high specific surface area, exhibiting greatly improved (re)activity and allowing possible applications in tissue engineering or drug delivery (Bohner 2001).

The advantages and disadvantages of the above mentioned bone graft substitutes are summarized in table 1-2.

Table 1-2 Comparison of properties of several bone substitutes. The signs of "—", "+", "++" represent the levels of various properties in an ascending desired order.

Category	Final composition	Biocompatibility	Heat release	Degradability	Strength
Autograft bone	HA	++	++	++	+
Allograft bone	HA	+	++	++	+
Metal	Metal	—	++	—	++
Ceramic	HA	++	++	—	+
CPC	HA	++	++	+	+(—)

1.3 Chemistry and kinetics of CPC setting

1.3.1 Chemistry of CPC setting

Despite numerous combinations of calcium and phosphate-containing compounds in CPC, the chemistry of the setting reaction in these cement systems is similar and can be explained and understood by analyzing the solubility behavior of the compounds involved (Chow 2001). The chemical process during the setting reaction mainly involves two mechanisms: dissolution and precipitation. The driving forces controlling dissolution and precipitation can be explained by the competition between the ion activity product of a compound and its solubility product. Specifically, a precipitate tends to dissolve if its solubility product is larger than the ion activity product, and vice versa. Solubility product constants for some CPC at different temperatures are shown in Table 1-3.

Moreover, the solubility of a compound can be characterized in a schematic manner using a solubility phase diagram (Fig.1-7) (Chow 2009), which describes the evolution of solubility of a compound —in the form of logarithm of the total calcium concentration— as a function of the pH.

Table 1-3 Solubility product, K_{sp}, of some CPCs at 25°C and 37°C. Reprinted from Fernandez et al. (1999)

Ca/P ratio	Compound	Formula	-log (K_{sp}) at 25°C	-log (K_{sp}) at 37°C
0.5	Monocalcium phosphate monohydrate (MCPM)	$Ca(H_2PO_4)_2 \cdot H_2O$	1.14	-
0.5	Monocalcium phosphate anhydrous (MCPA)	$Ca(H_2PO_4)_2$	1.14	-
1	Dicalcium phosphate dehydrate (DCPD)	$CaHPO_4 \cdot 2H_2O$	6.59	6.63
1	Dicalcium phosphate (DCP)	$CaHPO_4$	6.90	7.02
1.33	Octacalcium phosphate (OCP)	$Ca_8H_2(PO_4)_6 \cdot 5H_2O$	96.6	95.9
1.5	α-Tricalcium phosphate (α-TCP)	$\alpha\text{-}Ca_3(PO_4)_2$	25.5	25.5
1.5	β-Tricalcium phosphate (β-TCP)	$\beta\text{-}Ca_3(PO_4)_2$	28.9	29.5
1.67	Hydroxyapatite (HA)	$Ca_5(PO_4)_3(OH)$	58.4	58.6
2.0	Tetracalcium phosphate (TTCP)	$Ca_4(PO_4)_2O$	38-44	42.4

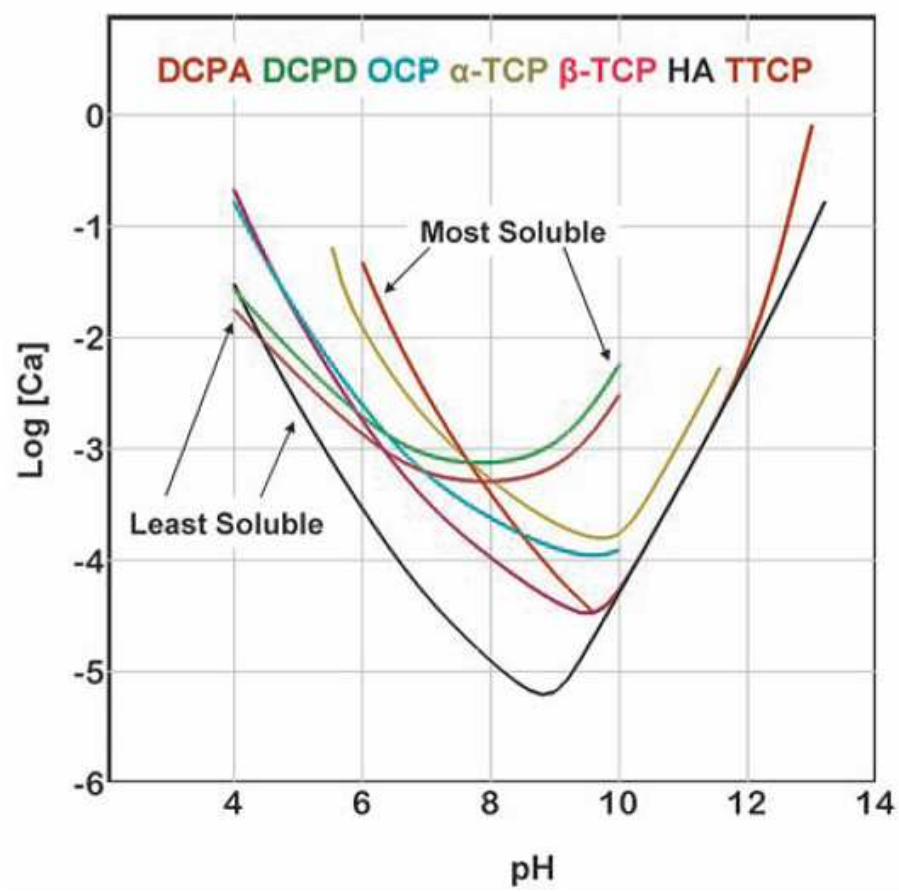

Fig.1-7 Solubility phase diagrams of different CPCs in a two dimensional graph. Reprinted from Chow et al. (2009)

Fig.1-7 shows the solubility phase diagram of some CPC which are in a ternary system $Ca(OH)_2$-H_3PO_4-H_2O at 37 ^oC. This solubility phase diagram is very important to understand the setting reaction of CPC since it can give information about the relative stability (and solubility) of various CaP in different pH values, which actually is the major parameter influencing the setting reaction. More specifically, each curve in this diagram, known as a solubility isotherm, indicates the solubility of a CaP. At a given pH, a CaP

with isotherm lying below that of another CaP is more stable (less soluble) than the other. The point where two isotherms intersect is regarded as “a single point” at which the solution is saturated concerning both CaP that are equally stable.

As can be seen from Fig.1-7, HA is the least soluble CaP above pH of approximately 4.4, below which DCPA becomes the least soluble. However, these curves would indicate a slightly different result from the two possible final products for the CPC reaction: on the one hand brushite (DCPD) and on the other hand apatite such as hydroxyapatite (HA) or calcium-deficient hydroxyapatite (CDHA) (Bohner 2007) (the solubility phase diagram of CDHA is similar to that of HA, so it is not shown in Fig.1-7). The fact that below a pH of 4.4 the final phase is brushite instead of monetite (Dicalcium Phosphate anhydrous: DCPA) is probably due to a complicated kinetic driven process (Konigsberger et al., 2006). In contrast, TTCP is the most soluble CaP for a pH below 7.6, above which DCPD is the most soluble.

Since HA is the most stable phase in a rather wide range of pH, with a pH higher than 4.4 most CaP would convert to HA as the final product. TTCP+DCPA and TTCP+DCPD are two such combinations which can react to HA with just water as the liquid phase. In principle, a slurry prepared from TTCP and another CaP should also form HA finally. However, the single points of TTCP and other CaP are not as far above the HA isotherm as are the TTCP+DCPA (DCPD) single points, indicating that the driving force for the HA forming reaction is much weaker for the combination of TTCP and another CaP than that of TTCP+DCPA (DCPD). This can be solved by adding setting accelerators in solution such as sodium phosphate (Bohner, 2007). Except for TTCP, α-TCP is the second most soluble CaP in neutral and acid pHs. Therefore, a slurry (pH>4.4) of α-TCP and another CaP, such as DCPA, DCPD or MCPM, or calcium-containing compounds like calcium carbonate or calcium hydroxide, will also convert to HA using a phosphate solution.

In spite of the above features about the solubility of CaP, some other factors such as Ca/P ratio, temperature (Fig.1-8) and CO_3^{2-} concentration are all considered to have an effect on the solubility phase diagram (Fernandez et al., 1999A).

As can be seen in Fig.1-8, temperature has a significant influence on the solubility isotherms of HA and DCPA but not of $CaCO_3$. The solubility of HA and DCPA decreases with increasing temperature. The lower the isotherms, the higher the driving force for the formation of HA. Thus increasing the temperature of the setting reaction can accelerate the process of HA formation.

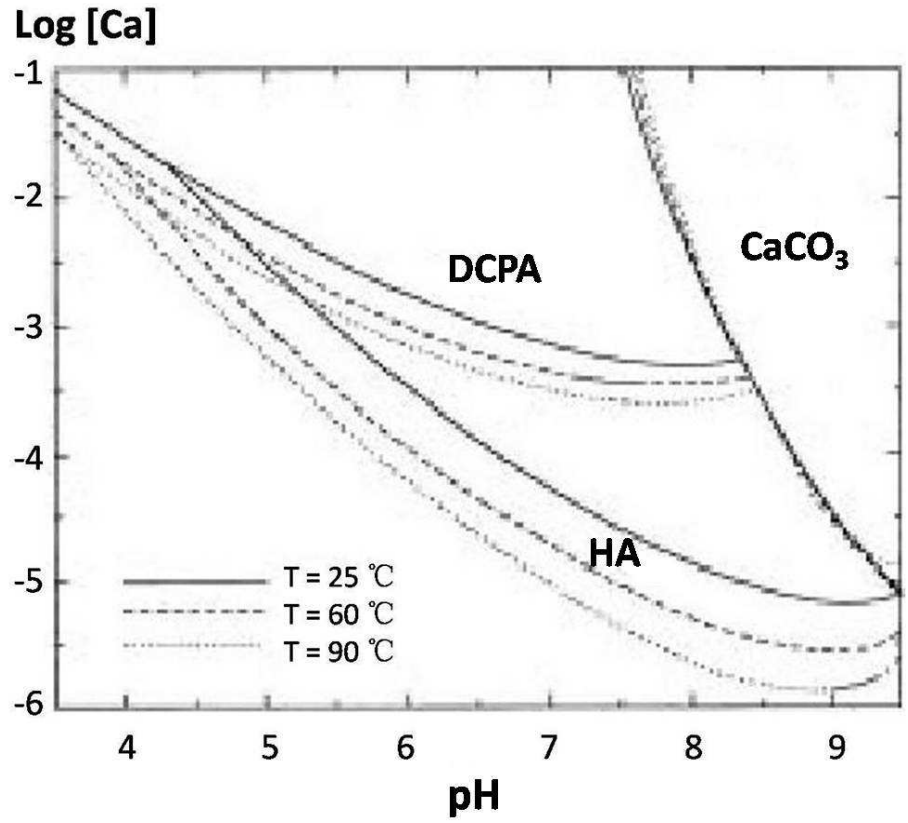

Fig.1-8 Effect of different temperatures on the isotherms of $CaCO_3$, DCPA and HA. Reprinted and adapted from Fernandez et al. (1999A)

1.3.2 Kinetics of CPC formation

Although solubility phase diagrams can be used to predict the thermodynamic behavior of CPC, they cannot always explain the observed setting and hardening behavior, and kinetics must also be considered.

Understanding the mechanisms controlling the setting process of CPC will help to have a comprehensive knowledge about their kinetics and then to better control their microstructure which determines their applications for different purposes. Currently, many CPC substitutes are based on the hydrolysis of α-TCP powder which is also the material used throughout this study, so this subsection will mainly focus on the setting kinetics of CPC based on α-TCP. Many studies have focused on the effects of particle size (Durucan et al., 2002A; Ginebra et al., 2004; Brunner et al., 2007A), crystallinity (Gbureck et al., 2004A; Camire et al., 2005; Brunner et al., 2007B), temperature (Ginebra et al., 1995; Tenhuisen et al., 1998; Durucan et al., 2000) and various constituents (Tenhuisen et al., 1994, 1999; Durucan et al., 2002B). Many methods such as X-ray diffraction (XRD) (Fernandez et al., 1996; Ginebra et al., 1997), isothermal calorimetry

(Tenhuisen et al., 1998; Bohner et al., 2006A) and measurement of compressive strength (Fernandez et al., 1996; Ginebra et al., 1997) have been used to study the evolution of setting reaction with time.

Fernandez et al. (1996) estimated the extent of conversion of α-TCP to CDHA by using the height of several selected peaks obtained by XRD, assuming a quasi-constant ratio between peak height and peak area. The authors found that the extent of conversion can be fitted with an exponential equation as a function of hardening time. Ginebra et al. (1997) calculated the relative amounts of different phases existing in the specimen by using an external standard method, and then used the calculated results to estimate the extent of conversion of α-TCP to CDHA. They got a similar conclusion as Fernandez et al. (1996) that the extent of conversion of α-TCP to CDHA could be exponentially fitted as a function of hardening time.

Moreover, both groups of authors also surveyed the evolution of compressive strength of CPC with hardening time and described it with exponential equations. Furthermore, they found a linear correlation between the compressive strength and the extent of conversion. Ginebra et al. (1999) further established a relationship between depth of reaction evolution and reaction time, and proposed an α-TCP hydrolysis kinetics with two rate-limiting mechanisms. The first mechanism, surface area of reactants, controls the reaction for the initial stage; in contrast, after 16 h the other mechanism, “diffusion through the hydrated layer”, leads the rest of the reaction.

Ginebra et al. (2004) investigated the effect of different particle sizes of α-TCP on the kinetics of setting reaction by combining data from XRD and compressive strength measurements. The results showed that fine particles have a much faster rate of hydrolysis than coarse particles. This could be easily explained by considering the fact that a higher specific area accelerates the process of dissolution.

Despite its simplicity to use, XRD has a limited ability for quantitative phase analysis especially for badly crystallized or amorphous phases, so that a more accurate method would be required to interpret the rate of hydrolysis and reaction mechanisms. Isothermal calorimetry is a commonly used technique for the study of reaction kinetics. Durucan et al. (2002A) surveyed the setting kinetics of CPC based on α-TCP with three particle sizes by means of isothermal calorimetry. Their result is consistent with the conclusion deduced from XRD that the setting reaction shows a strong dependence on particle size. Moreover, by comparison to the model suggested by Ginebra et al. (1999), the authors proposed a slightly different kinetic model that α-TCP hydrolysis reaction was considered to be

initially controlled by a surface mechanism, and subsequently by a nucleation and growth mechanism. Brunner et al. (2007A) analyzed the reactivity of three amorphous α-TCP nanoparticles synthesized through spray flame, as well as that of microsized α-TCP. The authors observed a pronounced increase in reactivity for these nanoparticles while the total energy release during hardening was constant.

Gbureck et al. (2004A) reported that prolonged high-energy milling of α-TCP provokes a pronounced increase in thermodynamic and kinetic solubility which could be attributed to the formation of amorphous α-TCP. Camire et al. (2005) related milling time and reactivity by means of isothermal calorimetry. It is noted that the total energy release during the hardening reaction is two- to threefold higher for α-TCP milled with prolonged time than that without any milling. The authors verified that the improved reactivity is not only due to a decrease in particle size and a concomitant increase in specific surface area, but mainly to amorphous α-TCP resulting from a longer milling time.

Recently, Bohner et al. (2009) calcined microsized α-TCP at different temperatures for various durations and assessed its reactivity as measured by isothermal calorimetry. No pronounced changes in composition, particle size and crystal size are observed, nevertheless the calorimetric data show that the induction time (time to start the reaction) increases from several minutes for α-TCP without calcination to 2-3 hours for α-TCP with calcination, which is speculated to be due to the disappearance of surface defects during the calcination process.

It is well known that temperature has a significant effect on the kinetics of chemical reactions. In general, a high temperature accelerates the reaction rate while a low temperature plays an opposite role, which is the same for the hydrolysis of α-TCP. Ginebra et al. (1995) found that with temperature increasing from 22 °C to 37 °C, the time to reach a certain extent of conversion is sharply reduced and compressive strength is pronouncedly improved. Tenhuisen et al. (1998) used isothermal calorimetry to study the effect of different temperatures on hydrolysis of α-TCP. The result shows that temperature has a significant effect on the reactivity, as demonstrated by the increasing heat release rate, and on the growth rate as indicated by a decrease in surface area of the CDHA with increasing temperature from 30 °C-75 °C.

Kinetics of CPC setting also depends on the composition of both the solid and liquid phases. Durucan et al. (2002B) assessed the reactivity of α-TCP associated with several calcium salt additives including DCPA, DCPD, $CaCO_3$, and $CaSO_4 \cdot ½H_2O$ by means of isothermal calorimetry. The authors reported that all the additives delay the formation of

HA in an ascending order: DCPA < DCPD < $CaSO_4 \cdot ½H_2O$ < $CaCO_3$; the latter nearly inhibits the formation of HA. Different liquid phases also influence the reaction rate of CPC. Tenhuisen et al. (1994) surveyed the effects of acetic and citric acids on the formation of HA. It was noted that the kinetics of hardening strongly depends on both the concentration and type of acid. Acetic acid accelerates reaction due to increased solubilities of the reactant phases at lower pH. Conversely, retardation by citric acid is related to the complexing and adsorbing ability of citrate ions which are adsorbed onto α-TCP crystals and apatite nuclei, thus retarding both the formation of crystal nuclei and their further growth and entanglement.

To sum up, there are many factors, such as particle size, crystallinity, temperature, composition and even physical modification of the reactant (Bohner et al., 2009), influencing the setting reaction of α-TCP. Furthermore, besides the methods mentioned above, new methods might be desirable to characterize the kinetics of CPC.

1.4 Handling properties of CPC

Despite numerous advantages as bone substitutes, CPC have some critical drawbacks which limit their potential clinical application. Among these drawbacks, a relatively long setting time (the time when the cement can resist a certain applied force) is one of the issues needing to be addressed. Another drawback is their poor injectability[4], which is often the consequence of phase separation between the liquid and the solid inside the injection device. Furthermore, in most cases, the injected paste tends to disintegrate upon early contact with blood or other physiological solutions due to its weak cohesion[5] in early age. All of the above drawbacks are considered to be challenges that must be overcome for wide applications of CPC. To this end, the above handling properties will be detailed and the methods used to improve them will be introduced in the following subsections.

1.4.1 Setting time

As mentioned previously, compared to bioceramics, one of the most attractive advantages for CPC is that it can set in situ in an aqueous environment at body

[4] Injectability is defined in section 1.4.3

[5] Cohesion is defined in section 1.4.2

temperature. However, it takes a certain time (minutes, or even hours) for the cement to be strong enough to resist an applied force, which is often defined as the setting time. Then a difference is made between the initial setting time (the time when the cement can withstand a small fixed pressure exerted by a large Gillmore needle[6]) and the final setting time (the time when the cement can withstand a high fixed pressure exerted by a sharp Gillmore needle) (Driessens et al., 1994). Generally speaking, a cement paste with a long setting time could cause problems due to its inability to support stresses within this time period. For instance, a severe inflammatory response occurred when the CPC was unable to set and disintegrated (Ueyama et al., 2001). For this reason, a great attention has been paid to the factors influencing the setting time of CPC. Actually, it is worth mentioning that the setting time, generally of the order of minutes or hours, is just the starting period of the whole hardening process of CPC which may last for several days or longer. Thus, as discussed in section 1.3.2, all the factors which promote fast kinetics could reduce the setting time of CPC: (i) smaller particle size (high specific surface), (ii) low crystallinity, (iii) accelerators in liquid and solid compositions, (iv) high setting temperature, as well as (V) low liquid-to-powder ratio (L/P ratio) (Dorozhkin 2008). Nevertheless, it does not mean that the shorter the setting time, the better. A too short setting time may cause the cement to be unworkable before the surgeon finishes performing implantation. Thus it is critical to prepare a cement with a suitable setting time (a few minutes) so that it can set slowly enough to provide sufficient time for the surgeon to perform implantation but fast enough to prevent delaying the operation or causing the above-mentioned problems (Dorozhkin, 2008).

1.4.2 Cohesion and anti-washout ability

Weak cohesion and anti-washout are other two major drawbacks which limit broad application of CPC. Cohesion is defined as the ability of a CPC to harden in a static aqueous environment without disintegrating into small particles (Khairoun et al., 1999). The definition of the “anti-washout ability” (thereafter just called “anti-washout”) is similar to that of cohesion except that the former is evaluated in a dynamic aqueous environment. Because of their similarity, cohesion time and anti-washout time are usually examined as a whole although the latter is longer. A CPC with weak cohesion could cause

[6] Gillmore needle is a standard device used to measure the setting time of a hydraulic-cement paste according to ASTM-C266-08

serious problems because of its inability to maintain integrity in an aqueous environment. For example, a study (Bernards et al., 2005) showed that when in contact with blood, CPC used for vertebroplasty caused blood clotting, which was provoked by interfacial reactions between blood and solid particles released from the CPC. Therefore, great efforts have been paid to enhance the cohesion of CPC. Since a high cohesion results from strong attractive forces between particles, factors which can enhance van der Walls forces (attractive) and which can decrease electrostatic forces (repulsive) can be used to improve cohesion. Thus, similar to the methods used to decrease the setting time, the same strategies such as using a smaller particle size and decreasing the L/P ratio can be applied to enhance cohesion. Moreover, another effective approach to improve cohesion is to increase the viscosity of the mixing liquid. To this end, numerous biopolymers, such as sodium alginate (Ishikawa et al., 1995A), hydroxypropyl methyl cellulose (HPMC) (Cherng et al., 1997), hyaluronic acid (Alkhraisat et al., 2009), chitosan (Liu et al., 2006) and modified starch (Wang et al., 2007), have been admixed either to the powder or to the liquid of CPC. Small amounts of these biopolymers can already significantly improve the cohesion and anti-washout of CPC. Based on these studies, Bohner et al. (2006B) performed a theoretical and experimental study to test the effect of various parameters potentially affecting the cohesion of cement pastes. Their results suggested that the two best methods to increase the cohesion of a cement paste are to decrease the particle size of the paste or to use a viscous solution. However, despite the prominent effect of these viscous solutions on the improvement of the cohesion of CPC, they may in some cases compromise setting time and mechanical properties (Khairoun et al., 1999).

1.4.3 Injectability

One of the most important advantages of CPC as compared to bioceramics is that they do not need pre-fabrication and can be injected with a syringe. Many methods have been set up to measure injectability of CPC. Khairoun et al. (1998) measured the injectability of a cement paste by measuring the percentage of a paste that could be extruded from a syringe fitted with a needle. They considered a bad injectability if phase separation happened between the solid and the liquid, which resulted in plugging, and hence partial extrusion. According to this method, the more the cement could be extruded, the more injectable the cement was. Bohner et al. (2005A) pointed out that Khairoun et al. did not measure the injectability of a paste, but rather its ease of injection. Thus they re-defined

the injectability of paste as the ability to stay homogeneous during injection, independent of the injection force.

Generally speaking, in most cases, CPC alone (i.e. when only constituted of a mixture of an inorganic powder and a saline solution) has a rather bad injectability. In order to overcome this weakness, numerous works have been conducted to investigate the factors improving the injectability of CPC. Khairoun et al. (1998) surveyed the factors which control the injectability of CPC, and found that it was significantly enhanced by increasing the L/P ratio and injecting soon after cement mixing. Ishikawa (2003) observed that a cement paste made of round particles was more injectable than one made of irregular particles. Furthermore, various polymers have been added to CPC, either in the powder or in solution, to try to improve injectability. Andrianjatovo et al. (1995) observed an obvious improvement of injectability by adding polysaccharides. Burguera et al. (2006) added an HPMC solution to CPC and obtained a strongly improved injectability. According to various observations, Bohner et al. (2005A) conducted a theoretical and experimental study on the injectability of CPC. They found that, among all the parameters (including decreasing particle size, increasing L/P ratio, using round particles, using deagglomerated particles, using particles with a broad size distribution, adding ions or polymers decreasing particle interactions and increasing the viscosity of the mixing liquid) which could be used to improve the injectability of CPC, the most adequate and applicable strategy is to increase the viscosity of the liquid. Indeed, except for the decrease in particle size, the last method is the only one which, on the one hand, improves the injectability of CPC, and on the other hand, does not compromise cohesion.

In summary, according to the above review, we can conclude that the best way to improve cohesion and injectability of CPC is to use a viscous solution as the liquid phase. However, these viscous solutions may compromise the setting time or the strength.

1.5 Mechanical properties of CPC and mechanical models

For most biomedical applications, the two most important properties of materials are mechanical properties (“strength”) and chemical properties (reactivity). Any biomaterial with high reactivity but with low strength will be useless. Thus, both mechanical properties and reactivity should be taken into account when developing a new biomaterial. For instance, one of the main parameter influencing both biological activity and mechanical properties is porosity. The following section will focus on the mechanical

properties of CPC and on mechanical models describing their dependence on porosity.

1.5.1 Definition of basic mechanical properties (Young's modulus, fracture toughness, strength)

1.5.1.1 Young's modulus

The Young's modulus (E), which is one of the so-called elastic moduli, is a measure of the stiffness of an elastic material. It is an intrinsic property of a material and is defined as the ratio of stress (σ) over strain (ε) in the domain where Hooke's (elastic) law holds. It depends on the magnitude of the interatomic stiffness of a material within the elastic range when suffering tensile or compressive forces, and is also dependent on the density of bonds in the material. It also indicates the amount of reversible deformation that will happen in a material when a load is applied. From the definition of stress and strain, Young's modulus can be calculated as follows (Hooke's law):

$$E = \frac{\sigma}{\varepsilon} \tag{1-1}$$

1.5.1.2 Fracture toughness

Fracture toughness, K_{IC}, is a property which is used to describe the ability of a material containing plane defects to resist crack propagation. The subscript "I" refers to the mode I of crack propagation, i.e. crack opening under a normal tensile stress perpendicular to the crack plane. The subscript "C" indicates that K_{IC} is the critical value of the stress intensity factor, K_I, i.e. the value provoking crack extension. Similar to Young's modulus, fracture toughness is an intrinsic property of a material and can be calculated with the following equation:

$$K_{IC} = Y\sigma_r c^{1/2} \tag{1-2}$$

σ_r is the material strength (fracture stress), Y is a geometrical factor depending mainly on the shape of the plane defect on which the fracture initiates, and c is a characteristic length of this defect. From this relation, given the fact that K_{IC} is an intrinsic property, it can be deduced that the fracture stress, σ_r, is not an intrinsic property.

1.5.1.3 Flexural strength and compressive strength

Strength (or fracture stress) is defined as the maximum stress that a material can withstand before fracture occurs. It can be measured in compression (compressive strength) or in bending (flexural or bending strength); in the latter case fracture occurs due to tensile stresses on one side of the specimen. As stated above, both strengths are not intrinsic properties of the material, but depend on fracture toughness and defect size in the material, although fracture in compression can proceed through quite complex phenomena (Bazant et al., 1997).

1.5.2 Mechanical properties of CPC

It is well known that, from a material science point of view, the mechanical properties of a material are determined by its microstructure. Different fabrication routes and parameters result in a variety of microstructural features. Thus, microstructure is the crucial connecting link between fabrication and mechanical properties. Any attempt to directly relate mechanical properties to fabrication without relating both to microstructure will be completely impractical and meaningless for theoretical understanding and effective design for targeted properties. Therefore, microstructure-mechanical properties relations will be taken into account throughout the following subsections.

As mentioned previously, bioceramics have been widely used as bone substitutes and numerous results about their mechanical properties and simulations have been reported. Therefore, it is of great interest and beneficial to review the mechanical properties of bioceramics before reviewing mechanical properties of CPC although the fabrication route is different. However, low strength and high brittleness prohibit their use in many stress-bearing locations, which would require an improvement in mechanical properties. Thus, various strategies are implemented to reinforce them, and these methods will be also reviewed. Finally, since one of the main limitations for CPC is its mechanical reliability, which has rarely been reported, the reliability of other materials will be briefly discussed so as to provide some useful references for CPC.

1.5.2.1 Mechanical properties of bioceramics

Mechanical properties of bioceramics are strongly dependent on microstructural features such as pores, grain size and second phases, but the influence of these features are generally different, the magnitude of the impact of porosity on properties being

generally larger than that of the other two parameters.

The relationships between microstructure and mechanical properties can be well understood by considering sintering, which is the major ceramic process and produces an extensive range of microstructures. The two most important changes during sintering are porosity and grain size that are to some extent correlated with each other. Maximal mechanical properties usually result from opposite property trends with porosity and grain size and their corresponding decrease and increase with processing temperature and time. Therefore, with ongoing sintering, mechanical properties usually increase with decreasing porosity, but decrease with increasing grain size, despite some exceptions (Rice et al., 1981A, 1981B), leading to a variable maximum depending on microstructure (Fig. 1-9).

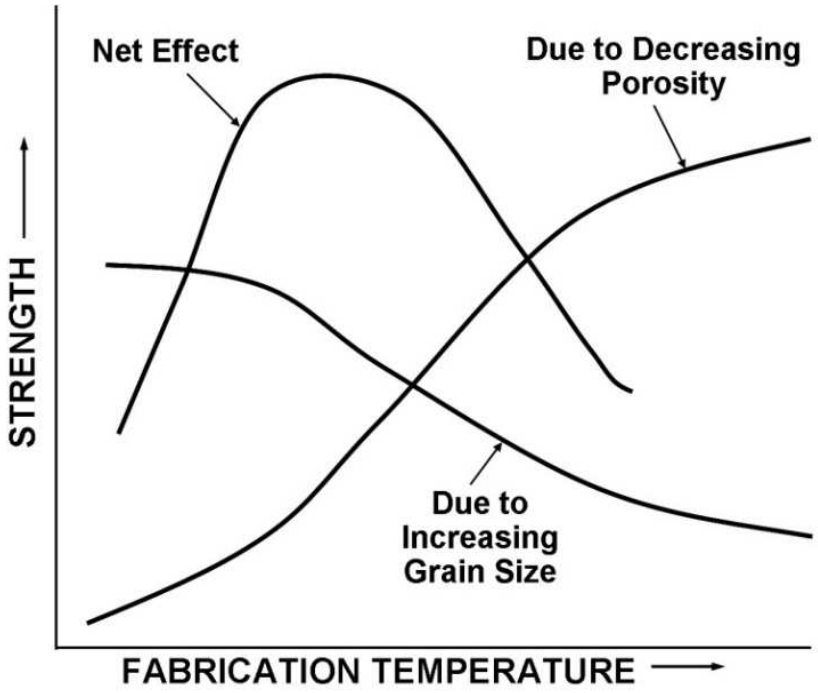

Fig.1-9 Schematic of mechanical properties depending on both decreasing porosity and increasing grain size with increasing sintering temperature or time. Reprinted from Rice (1998)

In general, pore size, fraction and shape (anisotropy) have a significant influence on mechanical properties of ceramics. Ceramics are essentially brittle in nature, thus they are sensitive to the most critical defects which can be pores.

Bouler et al. (1996) investigated the influence and interactions of five synthesis factors including chemical composition, percentage of macropores, mean size of macropores, isostatic compaction pressure and sintering temperature on compressive strength of macroporous biphasic calcium phosphate (BCP) using a factorial design method (FDM).

The results derived from FDM showed that compressive strength can be described by a first-order polynomial equation, with percentage of macroporosity and sintering temperature being the two major influences.

Liu (1997) fabricated porous HA ceramics with different macropore size and fraction by adding polyvinyl butyral (PVB) as a porogen and investigated their compressive strength. He demonstrated that specimens with smaller macropores exhibit a higher strength than those with larger macropores. Nevertheless, the strength is likely to be insensitive to macropore size at high levels of porosity (Fig. 1-10).

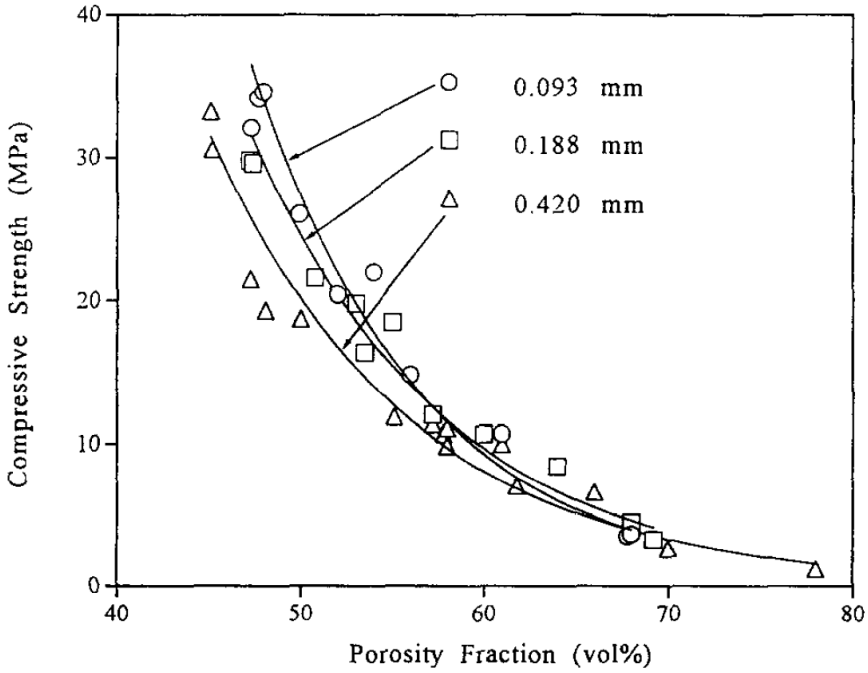

Fig.1-10 Evolution of compressive strength as a function of porosity created with different sizes of starting PVB particles (Liu 1997)

Furthermore, porosity-strength relations for these HA ceramics could be described by an exponential function, as proposed by Rice (1993, 1996), with different exponents which are related to the pore characteristics. Generally speaking, a higher exponent is related to a larger pore size, indicating a stronger dependence of strength on porosity for larger pores (Bignon 2003, Kingery 1976). However, Liu (1997) got a contrary result, with small pores being associated to a larger exponent; a similar conclusion on flexural strength was reported in his later work (Liu 1998). He speculated that the contradiction between experimental results and theoretical expectations is related to differences in the geometry of macropores left after burning off PVB agglomerates, which are particularly significant at higher contents of PVB phase (their shape is substantially deviated from the

original near-spherical geometry of a single PVB particle). Moreover, it is also showed from Fig.1-10 that at a given porosity, the compressive strength decreases with increasing size of macropores, which further proves the detrimental influence of macropore size and is consistent with the work of Griffith (1920), which relates strength (at a given porosity) to critical flaw size. The effect of macropores produced with other porogens (Lu 2003) and fabrication techniques (Miranda et al., 2007; Rodriguez-Lorenzo et al., 2002; Deville et al., 2006) on mechanical properties of bioceramics are reported elsewhere showing similar conclusions to those of Liu (1997, 1998).

Moreover, micropores are also detrimental to the mechanical properties of bioceramics (Le Huec et al., 1995), and this effect is usually controlled by sintering at different temperatures and for various times (Bignon et al., 2003; Milosevski et al., 1999; Thangamani et al., 2002).

As mentioned previously, the influence of porosity on mechanical properties of bioceramics has been widely studied, however, most studies focused on the effect of total porosity or macroporosity and microporosity alone; only a few authors made the distinction between the two types of porosity (Le Huec et al., 1995; Pecqueux et al., 2010; Tancret et al., 2006). Le Huec et al. (1995) evaluated the effects of macroporosity (> 100μm, 6.5%-30% in volume) and microporosity (< 100μm, 20%-40% of the total volume) on the compressive strength of HA (Fig.1-11).

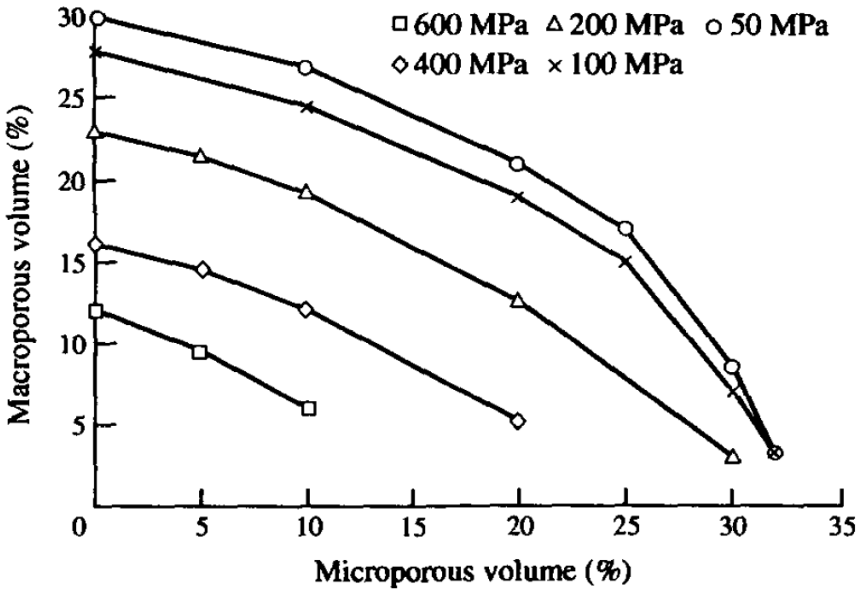

Fig.1-11 Isoresistance curves as a function of micropore volume and macropore volume. Various marks represent the fracture resistance of the samples. Reprinted from Le Huec et al. (1995).

This graph shows that, over the range of porosity studied, an infinite number of macroporosity-microporosity couples can produce any given value of compressive strength.

Pecqueux et al. (2010) prepared macroporous BCP bioceramics with varying macroporosity and microporosity and systematically investigated their mechanical properties (Young's modulus, fracture toughness and compressive strength) (Fig.1-12).

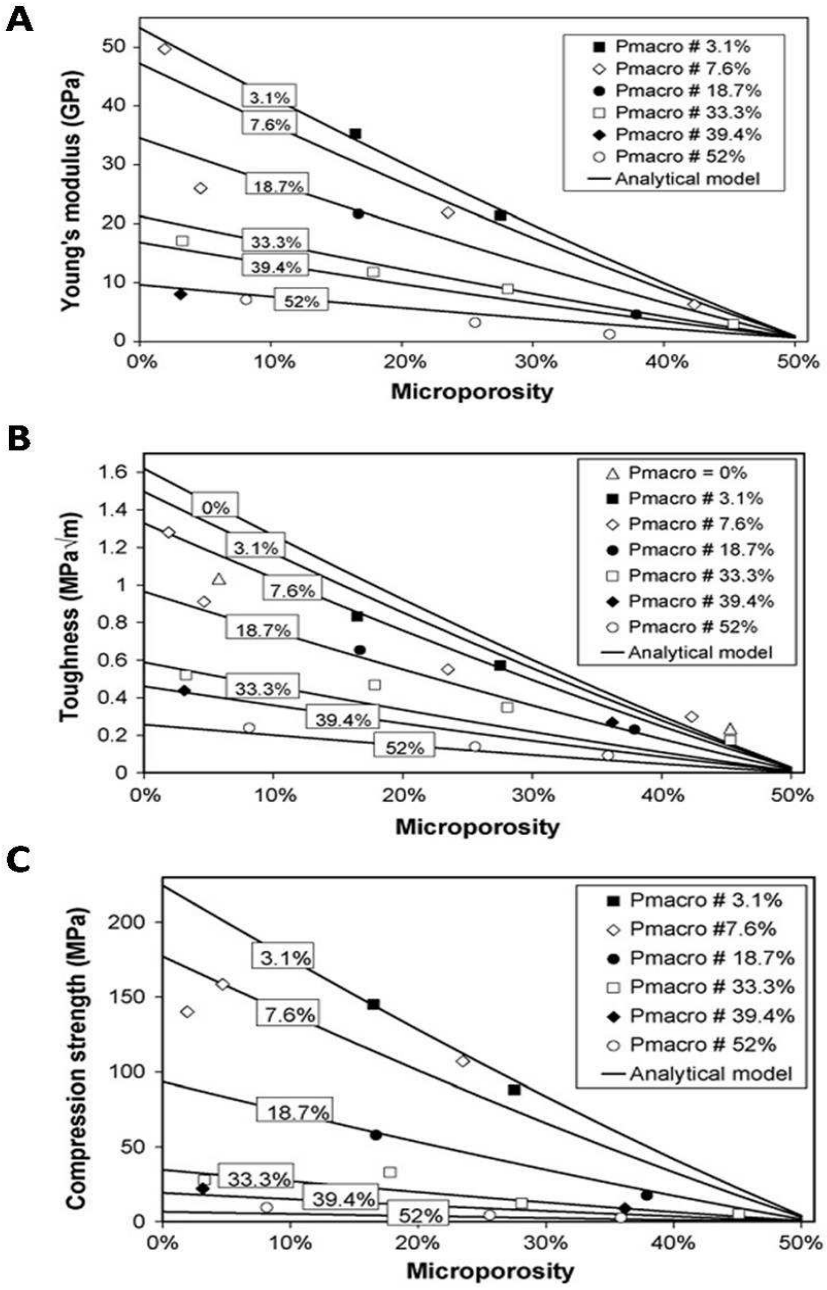

Fig.1-12 Experimental and modeled mechanical properties: (A) Young's modulus, (B) toughness, (C) compressive strength as function of microporosity, for different macroporosities. Solid lines are calculated variations for given macroporosities. Reprinted from Pecqueux et al. (2010)

Besides pore size and fraction, pore shape (isotropy or anisotropy) influences mechanical properties. Hing et al. (1999) found that anisotropy has a significant effect on the compressive modulus of porous HA but has no influence on its compressive strength.

A varying composition or the presence of a second phase is another factor influencing mechanical properties of bioceramics. Raynaud et al. (2002) fabricated BCP with variable Ca/P atomic ratio under hot pressing at 1100 °C and 1200 °C for 30 min and measured compressive strength and toughness of these ceramics. The authors found that after hot pressing at 1100 °C a relative deviation of 1% of the Ca/P ratio of initial powder leads to very different mechanical characteristics. After hot pressing at 1200 °C, both compressive strength and toughness were lower than after hot pressing at 1100 °C. The authors attributed this decrease to two reasons: increase of grain size with increasing temperature and residual stresses induced during phase transformation from β-TCP to α-TCP. Similarly, in a recent review Wagoner Johnson et al. (2011) pointed out that β-TCP is detrimental to strength, and that mechanical properties of BCP decrease with increasing amount of β-TCP although the details of pore size and pore fraction of the BCP studied are often missing. Finally, apart from the presence of a second phase, an influence of ion substitution such as fluoride for hydroxyl groups on mechanical properties of sintered hydroxyfluorapatites with the same density has also been reported (Gross et al, 2004).

In conclusion, there are many factors such as pore (size, fraction and morphology), grain size and second phase influencing the mechanical properties of bioceramics. Therefore, all these parameters should be balanced and controlled so as to optimize the overall performance for extensive applications.

1.5.2.2 Mechanical properties of CPC

Unlike bioceramics which need sintering at high temperature, CPC are formed through a dissolution-reprecipitation process at room or body temperature. During this process, an entangled network of apatite crystals is formed, which is responsible for the mechanical properties of CPC. With time, apatite crystals continue growing and the entangled network becomes denser (Fig.1-13) until CPC achieves its maximal strength.

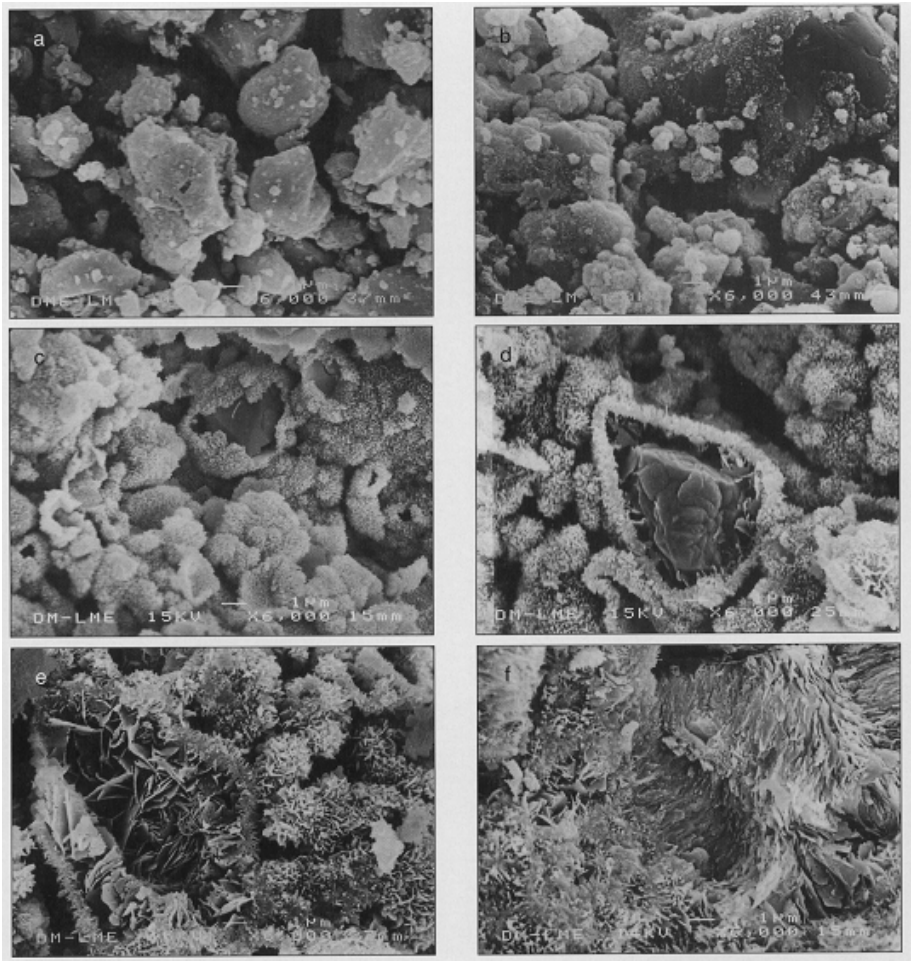

Fig.1-13 SEM micrographs of α-TCP based cement after different times of reaction: (a) 15 min; (b) 1h; (c) 4 h; (d) 8 h; (e) 64 h; (f) 360 h. Reprinted from Ginebra (1997)

The mechanical properties of CPC have been extensively studied. Most of them were assessed using compressive or diametrical tensile strength (DTS) tests (Barralet et al., 2004; Bermudez et al., 1993; Chow et al., 2000; Fukase et al., 1990; Ginebra et al., 1997; Gbureck et al., 2003; Hofmann et al., 2009; Ishikawa et al., 1995A; Martin et al., 1995; Pina et al., 2010). In contrast, few studies about toughness and reliability are reported (Barralet et al., 2002A; Barralet et al., 2002B; Morgan et al., 1997; Zhang et al., 2006). As for bioceramics, mechanical properties of CPC are strongly dependent on their microstructure such as porosity, crystal size and crystallinity. Furthermore, these microstructural features are related to all the technological factors involved in the fabrication of the cement. Therefore it is imaginable that all the factors such as chemical composition of the cement, relative proportion of the reactants in the mixture, powder or liquid additives acting as accelerators or retarders, particle size, L/P ratios, pressure applied during sample preparation and ageing conditions will affect its mechanical

properties.

One special feature of CPC is that they are intrinsically porous. The pores resulting from the setting process are normally of the order of micrometers. They are left by extra aqueous solution after hydrolysis of CPC. During this hydrolysis process the aqueous solution usually plays two roles. Firstly, it works as ion carrier to dissolve the solid phase. Secondly, it participates, as a reactant, to the formation of HA. The porosity of CPC, usually varying between 30% and 50%, is significantly dependent on the L/P ratio: the higher the L/P ratio, the higher the microporosity (Dorozhkin, 2008). Like bioceramics, CPC are naturally brittle and therefore they are very sensitive to large defects which can be, for instance, pores. The mechanical properties of CPC are inversely correlated to porosity. The higher the porosity, the lower the mechanical performance (Fig.1-14).

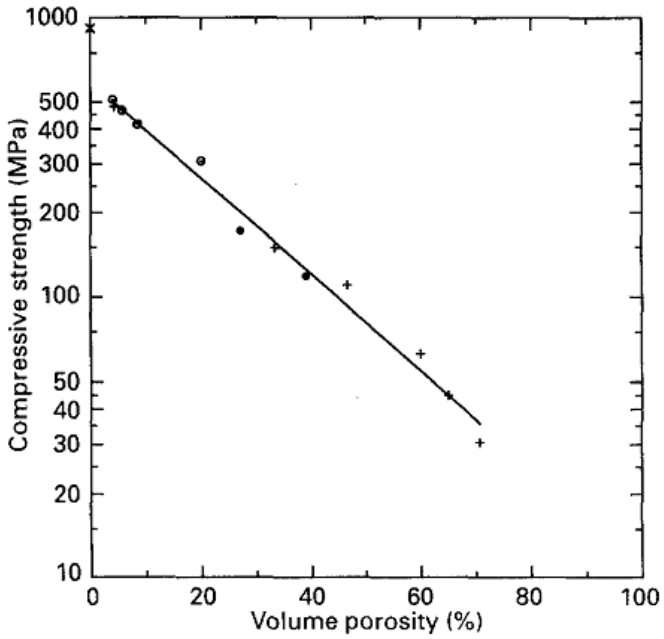

Fig.1-14 Evolution of compressive strength with increasing microporosity. Reprinted from Martin et al. (1995) [7]

Besides intrinsic microporosity allowing for impregnation of biological fluids, macroporosity (larger than 100 μm) is also desirable to enable bone ingrowth into CPC concomitantly improving its bioresorption and accelerating its replacement by new bone.

[7] The data points in the graph are a combination of data from several studies which are shown with different marks. Among these marks, only solid circles are the measurements of compressive strength of CPC, the rest marks are measurements of ceramics. This graph is chosen here because it is, to the best of our knowledge, the only one relating compressive strength with microporosity which results from different L/P ratios and modeling them. The modeling work will be detailed in 1.5.3

So far, the most common techniques used to create macropores in CPC are porogen leaching producing macropores after setting (Cama et al., 2009; Fernandez et al, 2005; Barralet et al., 2002B; Li et al., 2009; Qi et al., 2009; Takagi et al., 2001; Xu et al., 2001) and gas foaming creating macropores before setting (Almirall et al., 2004; Del Real et al., 2002). Nevertheless, neither method is exempt from its own drawbacks. On the one hand, for porogen leaching, it is necessary to add a large amount of a porogenic agent to guarantee interconnectivity. On the other hand, for gas foaming, the liberation of gas after the implantation of the cement paste could have harmful effects for the organism.

In order to avoid these problems, Ginebra (2007) proposed a new method to fabricate macroporous CPC by mixing the cement paste with a pre-prepared foam. Although the resulting macropres enhance bone ingrowth and osseointegration, it is extensively accepted that since CPC is brittle and sensitive to its largest defects, its strength could be reduced drastically by macropores, being several times or even orders of magnitude lower than that without macropores. Xu (2001) prepared macroporous CPC with almost 71% total porosity by adding mannitol in a mass fraction of 40%. In that study, all the measured mechanical properties including Young's modulus, work of fracture and flexural strength decreased sharply from 8.5 GPa, 0.032 kJ/m^2, 15 MPa without macroporosity to 0.8 GPa, 0.005 kJ/m^2, 1.5 MPa with 46% macroporosity respectively. Fig.1-15 shows the compressive strength of CPC as a function of macroporosity.

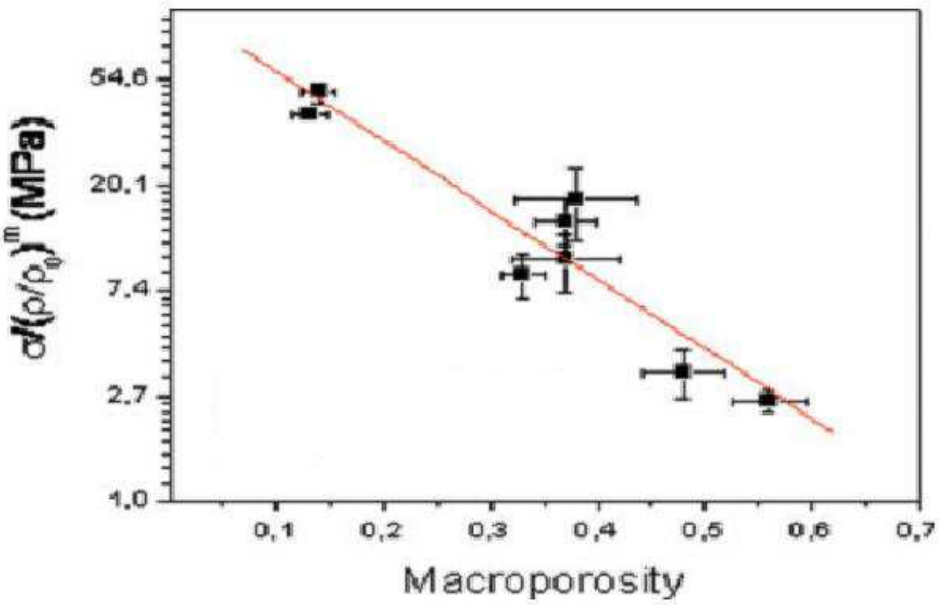

Fig.1-15 Evolution of compressive strength of CPC with increasing macroporosity. In the ordinate, $(\rho/\rho_0)^m$ is a constant in the present case . Reprinted from Ginebra et al. (2007)

Besides the effect of macropore fraction, similar to bioceramics, macropore size also significantly affects mechanical properties of CPC. Bai et al. (2010) fabricated macroporous CPC with equivalent total porosity but with different macropore sizes, finding that the compressive strength of CPC is inversely proportional to macropore size. Moreover, this difference on compressive strength becomes more evident after immersion in a dynamically flowing phosphate buffered saline (PBS) solution for up to 24 weeks (Fig.1-16).

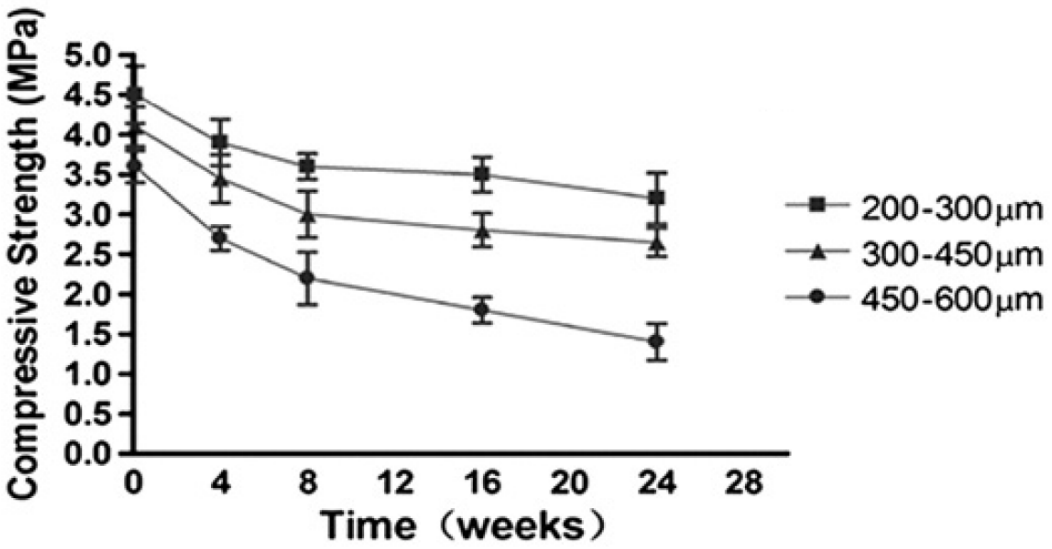

Fig.1-16 Compressive strength of CPC with different macropore sizes as a function of immersion time in a dynamically flowing PBS solution. Reprinted from Bai et al. (2010)

The amount of different additives functioning as accelerators and retarders and mixed in with the powder or liquid phase of the cement also have important effects on the mechanical properties of CPC by controlling the degree of cement setting and finally its microstructure. CDHA powders are solid phase additives frequently employed as seeds to promote the formation of apatite in CPC (Bermudez et al., 1993, 1994; Brown et al., 1991; Durucan et al., 2002B; Liu et al., 1997; Yang et al., 2002). Brown et al. (1991) indicated that CDHA seeds accelerated the initial setting reactions but did not appear to have major long-term effects on the extent of reaction or on microstructural development. Both Bermudez et al. (1994) and Yang et al. (2002) observed that by adding certain amounts of CDHA seeds the setting time of CPC decreased and concomitantly compressive strength increased; however, conversely, excess CDHA prolonged the setting time and decreased compressive strength. Furthermore, in contrast to these studies, Liu et al. (1997) argued that both setting time and compressive strength decreased with increasing amount of

CDHA seeds. Besides the addition of accelerator to the solid phase, adding accelerators to the liquid phase has also been reported. Ishikawa et al. (1995C) used a cement liquid containing PO_4^{3-} anions in a TTCP+DCPA system, finding that both DTS and formation of HA during the first three hours were significantly increased by the phosphate. However, the phosphate produced no significant effects on the properties of the cement after 24 h. Unlike cement accelerators, cement retardants delay setting, which is nevertheless positively correlated with a higher strength (Bohner et al., 2000; Durucan et al., 2002B; Fernandez et al., 1998). Fernandez et al. (1998) found that incorporation of 10 wt% $CaCO_3$ improved compressive strength of CPC by 40% compared to samples free of $CaCO_3$. Similarly, Bohner et al. (2000) demonstrated that the addition of SO_4^{2-} pronouncedly improved diametral tensile strength of a β-TCP based cement. The improvements of strength are mainly attributed to a refinement of the cement structure (for instance, the incorporation of carbonate in the apatite causes a decrease in crystallite size, thus resulting in an increase of final mechanical properties). Other major cement retardants that have been tested as increasing the cement mechanical properties are pyrophosphates or carboxylic acids (citric acid or glycolic acid) which allow easier mixing of the cement and processing with a decreased L/P ratio, thus resulting in improved mechanical properties (Barralet et al., 2004; Marino et al., 2007). However, each of these additives has an optimal concentration. Moreover, the addition of free ions (Sr^{2+}, Mg^{2+}, Si^{4+}) to the cement system usually has a retardant effect on setting. Nevertheless, they do not always have a beneficial effect on cement strength. Lilley et al. (2005) found that the compressive strength of Mg substituted HA decreased with an increasing amount of added Mg. The authors attributed this to increased porosity which was related to the addition of Mg. Similarly, Saint-Jean et al. (2005) revealed that the substitution of HA by Sr was detrimental to its compressive strength. The authors suggested that this inferior strength was related to the presence of larger voids between the crystals.

As mentioned previously, particle size significantly affects the kinetics of CPC setting, thus controlling the amount and size of entangled crystals which are responsible for strength. The smaller the particle size, the faster the conversion of starting materials into hydration product, which would lead to more entangled crystals and thus to an increase in strength (Liu et al., 2003). Otsuka et al. (1995) reported an increase of the compressive strength of a CPC when the specific surface of the precipitated phase increased. However, Ginebra et al. (2004) argued that there was no improvement of final strength of CPC

prepared from a fine powder. The authors explained that a fine initial powder could lead to a more compact microstructure but with a smaller fraction of empty space between crystals and some cavities where initial particles were located, which had a weakening effect; in contrast, a coarse initial powder could result in a less densely packed but more homogenous microstructure.

The aging condition is another factor influencing the mechanical properties of CPC, although in most cases it is made in a Ringer's solution at 37°C. At higher temperatures the rate of transformation of starting particles into CDHA is faster and the microstructure of CPC is more homogeneous and dense, leading to a higher strength, which is much apparent in the early stage of hardening (Ginebra et al., 1995). However, with the increase of hardening temperature, the growth rate of precipitated CDHA crystals is also faster, resulting in larger crystal size (TenHuisen et al., 1998), which might have a detrimental effect on final strength.

In summary, mechanical properties of CPC strongly depend on microstructure which is related to all the technological factors involved in the fabrication such as chemical composition, powder or liquid additives acting as accelerators or retarders, particle size, L/P ratio and ageing conditions. Moreover, a general conclusion is obtained: crystalline structures that are more compact with smaller crystals seem to give better mechanical properties than less compact ones with larger crystals.

1.5.2.3 Reinforcement of mechanical properties of CPC

Despite numerous advantages compared to bioceramics, it is widely accepted that CPC need further improvements on mechanical properties, especially on fracture toughness, to broaden their potential clinical applications such as, among others, the repair of multiple fractures of long bones, fixing of cemented articulation prostheses or substitution of vertebral bodies.

Various methods have been used to improve mechanical properties of CPC. Since porosity is the most detrimental factor to mechanical properties, one simple and predominant strategy to improve them is to reduce the size and volume fraction of pores in CPC to get a denser matrix. Since macropores are more essential than micropores for bone ingrowth, many efforts have been made to reduce the size and fraction of micropores so as to get a denser CPC matrix without compromising their biological performance (or in a limited range). Uniaxially, biaxially or isostatically compacting the cement paste prior to hydration have proved to be an effective method. Chow et al. (2000)

demonstrated that compaction pressure rather than compaction time could pronouncedly increase tensile and compressive strengths as compared to CPC obtained by simple mixing, even though the pressure is very low (2.8 MPa). Barralet et al. (2002A) showed that with increasing compaction pressure between 18 and 106 MPa, the porosity decreased from 50 to 31% (Fig.1-17), which resulted in an increase in the wet compressive strength from 4 MPa to 37 MPa. Ishikawa et al. (1995B) applied compaction pressures up to 173 MPa, reducing the porosity of CPC down to approximately 26%-28%. However, the authors found that, when compaction pressures above 100 MPa were applied, only a little decrease in porosity was reached and the DTS was not pronouncedly improved.

Although the above approaches to increase the strength of CPC by improving particle packing of the powder reactants with a pressurizing technique work effectively, they have the same function as decreasing L/P ratios (see Fig.1-17), which would influence the workability and injectability of the cement and might prohibit its application in minimally invasive surgery. Additionally, since these processes provoke a decrease in porosity, they might also affect the biological performance. In this sense, further improvement should be considered to balance handling properties and mechanical properties of CPC or to improve them at the same time.

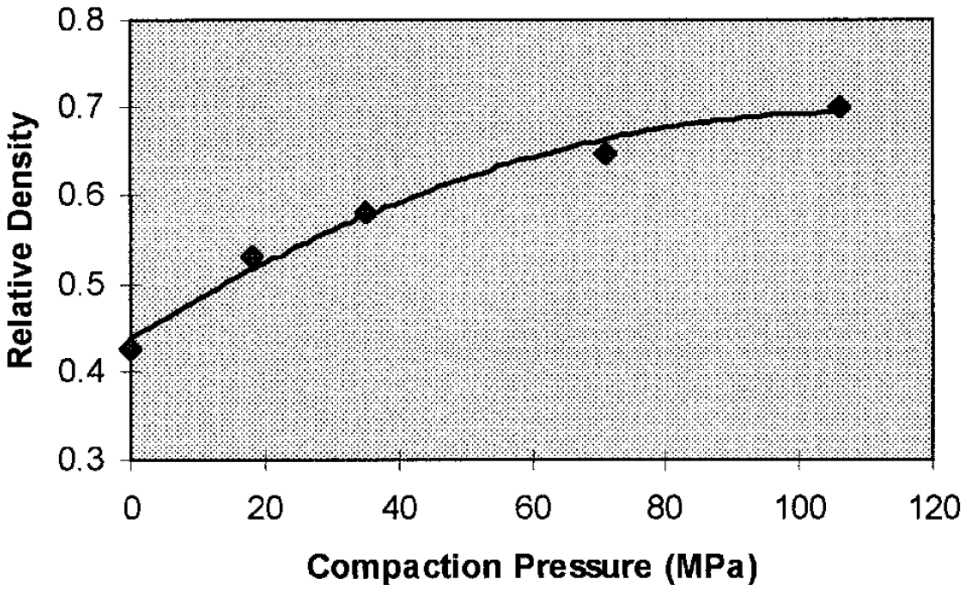

Fig.1-17 Effect of compaction pressure on the relative density of CPC. Reprinted from Barralet (2002A)

Sarda et al. (2002) added certain amounts of citric acid to the cement liquid to study

their effect on the injectability and setting properties of an α-TCP based cement. It was found that citric acid retards the formation of HA but improves injectability and strength. One of the reasons for this improvement of strength is in fact just a reduced porosity, due to the possibility to decrease the L/P ratio resulting from an improved mixing behavior. However, another strengthening mechanism is also proposed. It is well known that the more homogeneous and denser the microstructure, the higher the strength. As mentioned previously, the mechanical properties of CPC come from an entangled network of apatite crystals. Citrate ions adsorb onto the surface of reactants and of newly formed apatite nuclei, providing Coulomb repulsion, which counterbalances the Van der Waals attraction between them. In this way, the particles, instead of agglomerating in the liquid, slide along each other easily and disperse homogeneously (Fig.1-18). Then growth and entanglement of apatite crystals are based on these initially more homogeneous microstructures of small apatite nuclei, and thus produces a stronger matrix.

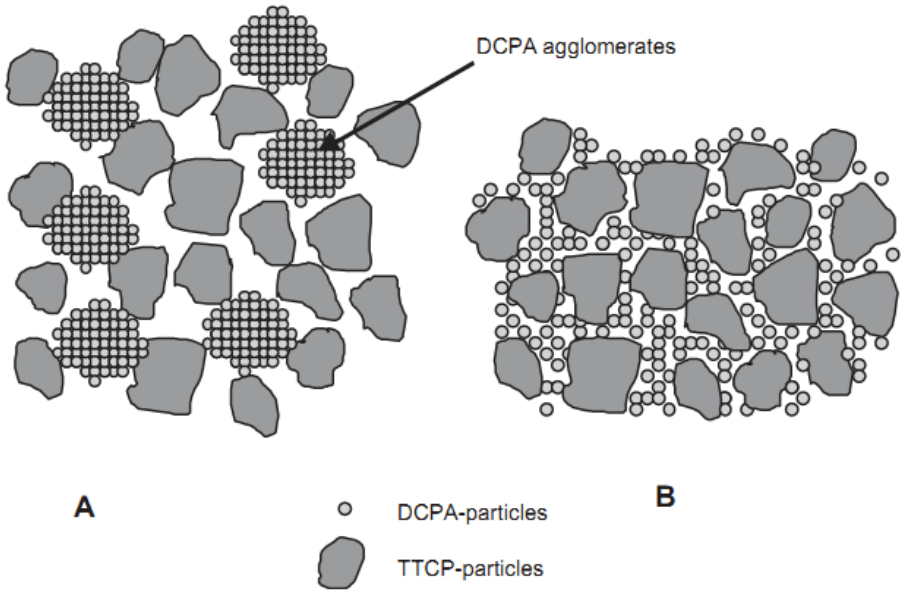

Fig.1-18 Schematic illustration of the microstructure of cement pastes formed with water (A) and sodium citrate (B). Reprinted from Gbureck (2004B)

According to this prominent effect of citric acid on improvement of strength, Barralet et al. (2003) and Gbureck et al. (2004B) added sodium citrate to the cement liquid in conjunction with compacting of the resulting cement paste, achieving a compressive strength as high as 180 MPa and 154 MPa respectively, which are in the strength range of cortical bone, demonstrating a potential application of this CPC system in load-bearing places. The effect of citric acid combined with other additives such as chitosan, glucose

or sodium hyaluronate on mechanical properties have been reported elsewhere (Yokoyama et al., 2002; Liu et al., 2006; Kai et al., 2009). The authors also noted increased strength of CPC by adding different amounts of citric acid or sodium hyaluronate. Moreover, besides the previous strengthening mechanism proposed by Sarda and Barralet, they suggested that there is a chelate reaction between citric acid and calcium, which could account for the increase of strength.

Another main strategy to improve mechanical properties of CPC is to add fibers to their matrix. Actually reinforcement with fibers has been extensively developed in the field of hydraulic cements and concretes for civil engineering and building applications. The incorporation of fibers into a brittle cement matrix has been proved to be an effective method to improve fracture toughness as well as tensile and flexural strength (Beaudoin et al., 1990).

As for civil engineering, choosing the proper fiber is the premise of successful reinforcement of CPC composites. Generally speaking, a fiber with high tensile strength is essential. However, not only fiber type is important. Other factors, such as fiber length, volume fraction, orientation and fiber/matrix adhesion are also critical for the final properties of the composite. Cement paste or precursor powder can be mixed with fibrous materials having different structures (Fig.1- 19).

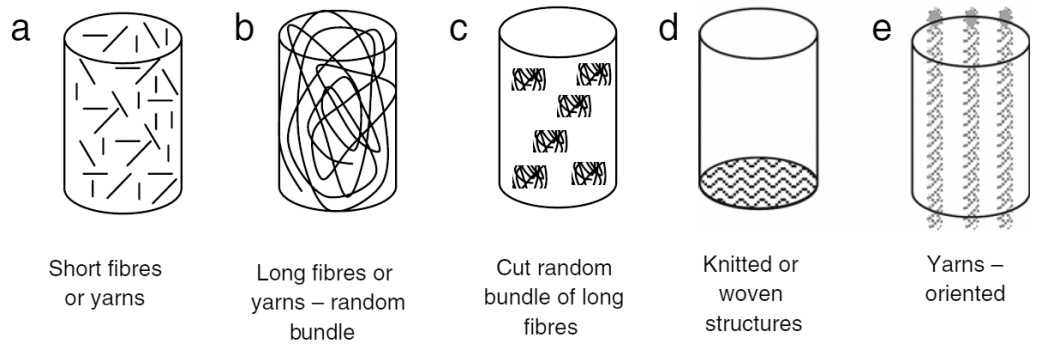

Fig.1-19 CPC composite reinforced with fibers of different forms. Reprinted from Canal (2011)

Moreover, to be used in CPC, specific requirements must be taken into account in the selection of the fibers. First of all they must be biocompatible. Furthermore, in some cases, they can be used not only as a reinforcement for the cement matrix at early stage of hardening but also as porogen to create pores after complete hardening. Then in addition to being biocompatible, they must also be biodegradable. Various fibers have been employed in the reinforcement of CPC until now. They can be classified into two

categories: (I) non-resorbable fibers including polyamides (Dos Santos et al., 2000; Xu et al., 2000), carbon fibers (Wang et al., 2007; Xu et al., 2000) and glass fibers (Xu et al., 2000), and (II) resorbable fibers which are natural or synthetic polyesters such as polylactide (PLA) (Zuo et al., 2010), polyglycolide/polylactide copolymers (PLGA) (Burguera et al., 2005; Gorst et al., 2006; Xu et al., 2002, 2004A) and poly-ε-caprolactone (PCL) (Zuo et al., 2010).

Xu et al (2000) investigated the CPC reinforcement by adding polyamides with different lengths and volume fractions. The authors found that both fiber volume fraction (with fixed fiber length) and fiber length (at constant fiber volume fraction) have significant effects on mechanical properties (flexural strength, Young's modulus and work of fracture). The mechanical properties gradually increased with increasing fiber volume fraction. However, high fiber volume might compromise their workability, making them difficult to be mixed and wetted by the CPC paste. Similarly, increasing fiber length progressively improves the mechanical properties of the composite CPC except for the longest fibers. The authors ascribed this to heterogeneous distribution of the longest fibers. This negative effect of heterogeneous fiber distribution was also observed in Dos Santos's study (Dos Santos et al., 2000), where compressive strength of composite CPC showed a great variability. Being considered as the shortest "fibers", carbon nanotubes (CNT) have also been used as reinforcing agents in CPC (Wang et al., 2007). The authors mineralized CNT with an HA nanoparticle layer to improve their wettability towards CPC. Compared to pristine CNT which only slightly improved the compressive strength of the CPC, the mineralized CNT significantly improved mechanical properties of CPC due to the enhanced interfacial bonding between them. However, the addition of non-resorbable fibers to CPC could be a meaningful strategy only for non-resorbable CPC. The incorporation of these non-resorbable fibers to resorbable CPC could cause fiber release in the surrounding tissues, with the subsequent biocompatibility risks (Canal et al., 2011)

Unlike non-resorbable fibers, the reinforcement of CPC with resorbable or biodegradable fibers relies on a different strategy. On the one hand, the addition of resorbable fibers can provide early temporary reinforcement at the implant site. On the other hand, after fiber degradation, the resulting macropores can facilitate bone ingrowth. Xu et al. (2002) investigated the evolution of mechanical properties (flexural strength, Young's modulus and work of fracture) of CPC reinforced with 8 mm long PLGA fibers at 25% fiber volume. Their results showed a threefold increase in flexural strength and a

hundred times increase in work of fracture but, in contrast, no prominent differences were observed in the Young's modulus. With increasing immersion time, the mechanical properties of the composite CPC progressively decreased at different rates with fiber degradation. Laminar-like mesh consisting of knitted fibers was also used to improve mechanical properties of CPC (Xu et al., 2004A). Similar to their previous study (Xu et al., 2002), by adding mesh, the authors observed a threefold increase in flexural strength and 150 times increase in work of fracture. After 84 days of immersion and mesh dissolution, interconnected macropores suitable for bone ingrowth were created in the CPC. Recently, Zuo et al. (2010) tried to improve mechanical properties of CPC by using ultrafine PLA fibers with controllable diameter made with an electrospinning technique. However, due to their hydrophobic properties, most fibers displayed an obvious separation from the CPC matrix. The flexural strength and Young's modulus decreased gradually with the addition of fibers. Conversely, the work of fracture progressively increased with increasing fiber content, which was attributed to an increased flexibility of the CPC.

Moreover, in conjunction with fibers, various additives such as chitosan lactate or HPMC have been incorporated to CPC to attempt to improve different properties. Zhang et al. (2005) incorporated chitosan lactate to CPC-fiber composite as an additional reinforcing agent. Their results show significantly improved mechanical properties with respect to the separate contributions of fibers or polymer alone. Xu et al. (2006) added HPMC at a mass fraction of 1% to a macro CPC-fiber composite, as a gelling agent. The incorporation of HPMC maintains the injection force of CPC-fiber composite of different fiber volume fractions within a low range (6 – 10 N), which greatly facilitates injection.

Among the above studies, three mechanisms of fiber reinforcement (fiber bridging, crack deflection and frictional sliding) appear to be operative. Firstly, when the matrix started to crack, the fibers bridged the crack to resist its further opening and propagation. Secondly, crack deflection by the fibers caused multiple cracking in the matrix, consuming more energy in more newly formed surfaces. Finally, the frictional sliding of fibers against the matrix during pullout further consumed the applied energy and further increased the fracture resistance of the composite (Xu et al., 2001).

In summary, basing on the above review, two main strategies can be proposed for enhancing the mechanical properties of CPC. First, under the premise of remaining critical factors for bone ingrowth or other biological performance, a more dense and homogeneous matrix consisting of smaller crystals would be desirable to improve the

intrinsic mechanical properties of CPC. Second, incorporation of fibers into the CPC could supply extra enhancement to intrinsic mechanical properties of CPC. However, deliberate selection of fibers with proper type, length and volume fraction should be taken into account.

1.5.2.4 Reliability of mechanical properties of CPC

As discussed previously, mechanical properties of CPC are critical for their successful application in surgery and have been extensively studied. However, most of them were evaluated using strength tests. On the contrary, few studies mentioned fracture toughness and reliability which are real limitations for CPC, rather than strength per se. For this reason, some examples on the reliability of ceramics (Bhamra et al., 2002; Cordell et al., 2009; Salehi et al., 2008; Villora et al., 2004) and dental cements (Fleming et al., 1999) with different microstructures resulting from various fabrication processes will be briefly discussed in the following subsection so as to provide some useful references for CPC.

The reliability of a brittle material can be characterized using Weibull statistics. The basic Weibull probability function (Weibull, 1939, 1951) using the strength data ranked in an ascending order is usually written as

$$P_f = 1 - \exp\left[-\left(\frac{\sigma_r - \sigma_u}{\sigma_0} \right)^m \right] \tag{1-3}$$

where P_f is the probability of failure, σ_r is the fracture strength, σ_u is the threshold stress below which no failure occurs in the material, σ_0 is a normalizing parameter determined from the stress at which 1/e of the population survive and m is called the Weibull modulus; the meaning of the latter will be discussed later. Davies (1973) showed that $\sigma_u = 0$ can be taken as a safe stress level for brittle materials; then equation (1-3) can be reduced to the form

$$P_f = 1 - \exp\left[-\left(\frac{\sigma_r}{\sigma_0} \right)^m \right] \tag{1-4}$$

The Weibull modulus, m, is a dimensionless number used to characterize the variability in measured strength of components made from brittle materials, which arises from the presence of flaws having a distribution in size and orientation (Karageorgiou et al., 2005).

A high value of m indicates a sharp distribution of strength data while a low value represents a large scatter. It should be noted, however, that the Weibull model is based on an empirical description of the probability of failure of individual volume elements of the material (i.e. not relying on fracture mechanics), and as such cannot be considered a physically sound model. Nevertheless, because of its practical applicability, it has become the most widely used model to describe fracture statistics in brittle materials.

Cordell et al. (2009) used Weibull modulus to determine the strength reliability (compressive strength and flexural strength) of porous HA ceramics with the same total porosity but with different pore sizes. The authors found that Weibull modulus for bending test increased (more reliable) with decreasing pore size while the Weibull modulus for compression test decreased (less reliable) with decreasing pore size. They attributed the opposite trend of Weibull modulus to the different distribution of pore sizes in bending and different number of pores per unit volume in compression.

Fleming et al. (1999) investigated the influence of different preparation methods (mechanical mixing of encapsulated cement and manual mixing) on the reliability of zinc phosphate dental cements. They observed that the dental cement prepared with the former method had smaller average strength and Weibull modulus (lower reliability) than with the latter method. Moreover, both average strength and reliability of the cement prepared with mechanical mixing could be enhanced by an improved capsule design. The authors attributed the discrepancy on strength and reliability of dental cements prepared with different methods to the effect of entrapped air bubbles. The cement prepared using mechanical mixing contains more bubbles which are detrimental to strength and reliability. On the contrary, the problem could be eased or avoided in the hand-mixed cement.

Villora et al. (2004) analyzed the strength and reliability of three series of ceramic Raschig rings prepared from industrial and urban waste, using three different green processes: uniaxial pressing, extrusion and slip casting. The authors found that the Raschig rings made from extrusion had the lowest strength, but at the same time had the highest Weibull modulus compared to that made from other methods. They ascribed the results to the effect of defects produced during the fabrication process of the rings. Large and uniform defects are observed in extruded rings. In contrast, small defects but with variable sizes are found in the rings prepared with other methods.

Salehi et al. (2008) studied the effect of moisture content on strength and reliability of ceramic Raschig rings made from kaolinitic-illitic clay through an extrusion process. The

authors found that the Weibull modulus of the rings decreased with increasing moisture content. They related the decreasing reliability to inhomogeneously distributed pores brought by an excess moisture content.

Bhamra et al. (2002) assessed the effect of surface roughness on the flexural strength and reliability of an alumina reinforced all-ceramic dental crown material. The authors identified a pronounced increase in flexural strength and Weibull modulus for the material with a smooth surface compared to that with a rough surface.

In summary, Weibull modulus (strength reliability) is strongly dependent on the microstructure of the material. The more homogeneous the microstructure, the higher the material reliability. Weibull modulus has been widely used to characterize the strength reliability of various materials. However, surprisingly, this method has been rarely applied to CPC. For this reason, it will be desirable to use Weibull statistics to evaluate the mechanical reliability of CPC in addition to mean values of properties.

1.5.3 Modeling of mechanical properties

As mentioned previously, the mechanical properties of CPC are strongly dependent on their porosity (intrinsic micropores and incorporated macropores). To optimize the overall mechanical behavior of CPC, it is thus necessary to understand how their microstructural parameters (micro- or macroporosity) influence mechanical properties. To this end, it would be useful to model the mechanical properties of CPC as a function of the amount and morphology of porosity. However, unfortunately, there are very few studies attempting to model mechanical properties of CPC with their porosity, may it be either microporosity, macroporosity or total porosity (Ginebra et al., 2007; Martin et al., 1995; Zhang et al., 2006). Martin and Brown (1995) measured the compressive strength of CPC with different microporosities and plotted it in conjunction with results from other studies as a function of microporosity using an exponential law. Similarly, Ginebra et al. (2007) measured the compressive strength of foamed-CPC and plotted it with macroporosity by means of an exponential law. In contrast, Zhang et al. (2006) prepared CPC with various amounts of macropores created by mannitol particles as porogen. The authors measured Young's modulus, flexural strength and work of fracture of the macroporous CPC and plotted them as a function of total porosity using power laws. Until now, many models have been proposed to describe the mechanical behavior of porous materials. Nevertheless, showing all these models here would be at the same

time extremely long and not appropriate, so the following section will briefly review several well-known or relevant models; the knowledge gained could help to extend the application of modeling principles to mechanical properties of CPC.

Rice (1996, 1998) reviewed several existing models, suggesting that the variation of Young's modulus of all porous materials, regardless of their structure, depends only on their minimum solid area (MSA) which corresponds to the minimum relative area occupied by the matrix over a section of the specimen normal to the applied stress. A representation of the MSA is shown schematically in Figure.1-20 for different porous structures.

Moreover, basing on the concept of MSA, the author demonstrated that most of the existing models reviewed could be mathematically approximated in a common manner using an exponential law of the form:

$$E = E_0.e^{-bp} \tag{1-5}$$

In this equation, E is the Young's modulus of the porous material, E_0 is the Young's modulus of the fully dense material, p is the porosity of the material and b is a constant related to pore characteristics.

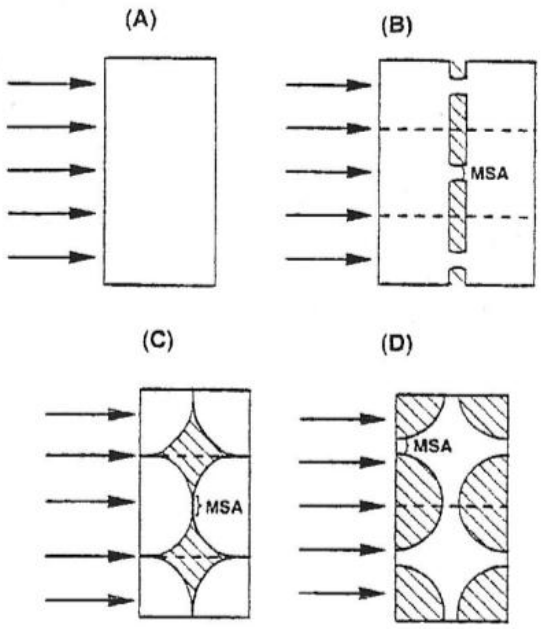

Fig.1-20 Schematic illustration of the MSA for materials with different structures. (A) dense material, (B) material containing pores lying in one plane, (C) material consisting of contacting spheres, and (D) material comprising isolated pores. Reprinted from Rice (1996)

Gibson and Ashby (1982, 1999) have extensively studied the influence of various forms of porosity on the mechanical properties of materials. In particular, they used a power law to describe the mechanical properties of cellular materials whose structure is represented in Figure.1-21 by stacks of open cells.

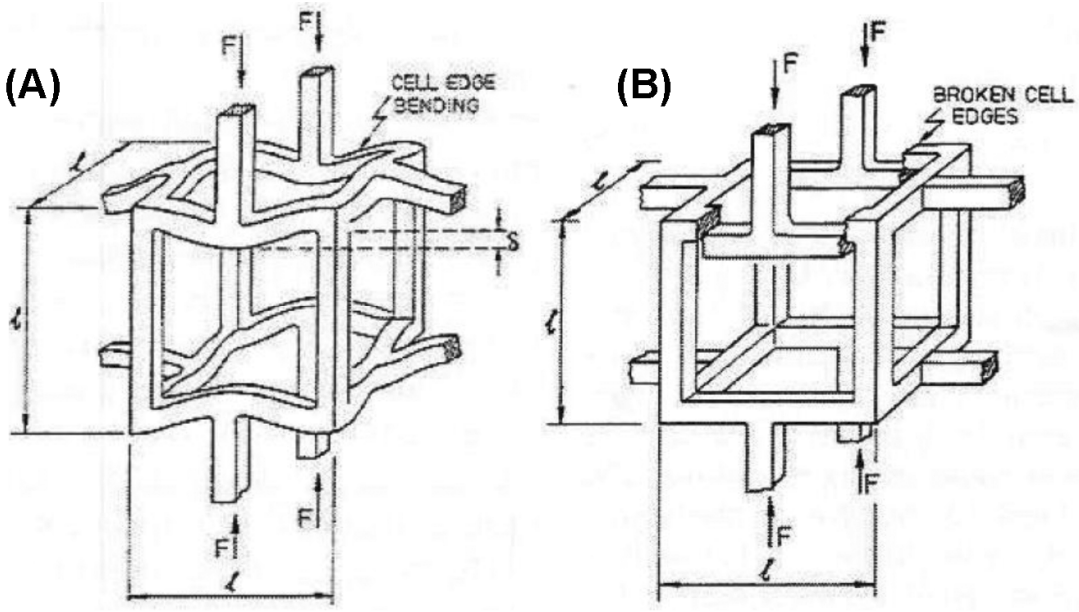

Fig.1-21 Deformation (left) and break (right) of a brittle cellular material subjected to a compressive stress. Reprinted from Gibson et al. (1982)

The mechanical property of an open cell material is then described by the following power law:

$$\frac{E}{E_0} = C.(1-p)^2 \tag{1-6}$$

where C is a constant comprised between 0.8 and 1.

In order to better understand the effect of porosity on Young's modulus, Wagh et al. (1991) developed a new procedure to gradually and randomly introduce pores into a dense material and then investigate the influence of the resulting porosity on the Young's modulus. To achieve this, they began from an initially dense body consisting of a stacking of identical bricks. Then, a random size reduction algorithm is applied to the bricks so as to produce a gradually increasing porosity (Fig.1-22).

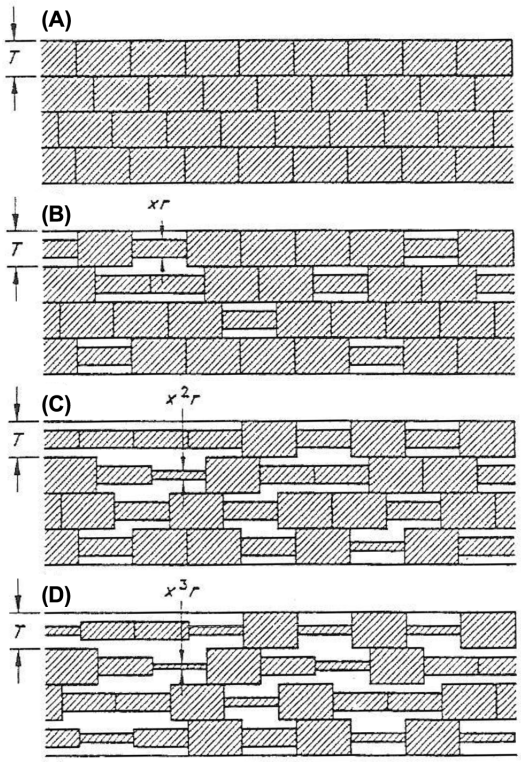

Fig.1-22 Schematic illustration of gradual and random introduction of pores into a dense material. One dimensional simulation of material channels. (A) Uncontracted structures, (B) radii of the cylinders are reduced by a factor of x, (C) the reduction is repeated choosing cylinders again at random. Note that same cylinder may be chosen and in that case the radius is reduced by a factor x^2, and (D) third simulation presents a more realistic picture of ceramic structures. Reprinted from Wagh et al. (1991)

The material maintains its cohesion until nearly 100% porosity. Then the authors deduced by calculation the relation between Young's modulus and porosity using a power law:

$$E = E_0.(1-p)^n \tag{1-7}$$

where n is a parameter depending on the "tortuosity", or "disorder", of the porosity, which was later confirmed using numerical simulation (Pecqueux, 2009). Moreover, Wagh et al. (1993) proposed an approach, based on energetic considerations during fracture, to set an equivalence between Young's modulus and toughness models for brittle materials. This procedure was later corrected by Arato (1996) and Tancret et al. (1997) to show that, if one can write the evolution of Young's modulus as a function of porosity as

$$E = E_0 . f(p) \tag{1-8}$$

with f(p) a dimensionless function of porosity, then the relationship between fracture toughness and porosity is given by

$$K_{IC} = K_{IC0} . f(p) \tag{1-9}$$

where K_{IC} and K_{IC0} are the fracture toughnesses of the porous and of the fully dense materials, respectively. Moreover, by assuming that the critical flaw size of the material is almost constant in certain cases, Tancret et al. (2006) extended the above approach to fracture stress, which can be written as:

$$\sigma_r = \sigma_{r0} . f(p) \tag{1-10}$$

where σ_r is the strength of the porous material and σ_{r0} is the strength of the fully dense material.

Tancret et al. (2006) prepared macroporous BCP bioceramics with almost constant macroporosity and varying microporosity and developed a new model on Young's modulus combining the effect of both macropores and micropores and extended this model to other mechanical properties such as fracture toughness and compressive strength. The development of the new model is detailed in the following section. For this new model, at the macropore scale, a closed porosity model is firstly used, like the one in equation (1-7). However, the value of porosity in the new model must be macroporosity, p_{macro}, i.e. the fraction of the total volume occupied by macropores. Therefore, the model is written as:

$$E = E_{0m} . (1 - p_{macro})^n \tag{1-11}$$

E_{0m} is the Young's modulus of the "continuous matrix", which is actually, at the "micro scale", itself microporous. Thus it is imperative to define E_{0m} as a function of microporosity, p_{micro}, the latter being the fraction of the "matrix" volume occupied by micropores. Because this matrix is the result of the incomplete sintering of a pressed powder, a model proposed by Jernot et al. (1982) and having been successfully proved in various sintered materials is used and can be written as follows:

$$E_{0m} = E_0.[N_C(1-p_{micro}) - (N_C - 1)(1-p_{micro})^{2/3}] \quad (1\text{-}12)$$

where N_C is the average number of neighbours of each grain in the microstructure. By combining equation (1-11) and (1-12), the new model containing the two types of porosities is finally written as:

$$E = E_0.[N_C(1-p_{micro}) - (N_C - 1)(1-p_{micro})^{2/3}].(1-p_{macro})^n \quad (1\text{-}13)$$

Furthermore, based on the aforementioned development from equation (1-8) to (1-10), equation (1-13) can also be used to describe to the evolution of fracture toughness and compressive strength and therefore a general equation is obtained:

$$X = X_0.[N_C(1-p_{micro}) - (N_C - 1)(1-p_{micro})^{2/3}].(1-p_{macro})^n \quad (1\text{-}14)$$

where X and X_0 are the mechanical properties (Young's modulus, toughness or strength) of the porous and fully dense materials, respectively. Experiments were conducted to prove the proposed models (see equation (1-14)). However, they were not completely validated because of a lack of available experimental data (only one level of macroporosity and a narrow range of microporosity). Thus, Pecqueux et al. (2010) from the same group performed more experimental measurements of several properties (Young's modulus, fracture toughness and compressive strength) on extended ranges of both macroporosity and microporosity and further validated these models with a satisfying result in the case of Young's modulus and toughness. Compressive strength, however, could not be described using the same exponent n as the other two properties. This was interpreted in terms of a subcritical crack growth inside "clusters" of macropores during compressive loading, before catastrophic failure occurs. These groups of macropores, hence constituting the actual critical flaws at final fracture, are more likely to be present in highly macroporous ceramics, which could explain a higher exponent n for strength than for elastic modulus and toughness, through an increase of the critical flaw size with macroporosity.

In summary, this section reviewed several main existing models used to describe the evolution of mechanical properties with porosity. Two major models based on exponential and power laws have been extensively used. The role of modeling is interesting and useful since, even if it cannot be used as a proper predictive tool, it is a

way to explain and understand experimental observation. Thus it is desirable to try and model the mechanical properties of CPC so as to optimize their mechanical behavior.

1.6 Aims of the study

According to the above literature review, we can draw some conclusions which show the current status on the study of mechanical properties of CPC and then further lead to the goals of this PhD thesis.

Numerous calcium phosphate based materials are commercially available nowadays. Among them, α-TCP has attracted great interest due to its capacity to hydrolyze into CDHA which, compared to stoichiometric HA, is more similar to biological apatite in terms of structure and chemical composition. Mechanical properties of CPC are critical for their successful application in surgery and have been extensively studied. However, most of them were evaluated using strength tests such as compressive strength and diametrical tensile strength. On the contrary, few studies mentioned fracture toughness which is one of the real limitations for CPC, rather than strength per se. Moreover, besides the lack of a systematic study on the mechanical properties of CPC, there is also almost nothing on the evolution of mechanical properties with microporosity (L/P ratio) and macroporosity considered separately, as well as on its modeling which is considered to be a useful tool not only for a better understanding of the mechanical behavior but also to help in the design of materials with desirable mechanical properties. Furthermore, the role of particle size on mechanical properties of CPC has not been studied either with a similar approach although its effect on kinetics is well understood. From these observations, it appears that one of the main weaknesses of the existing literature is the lack of a comprehensive and systematic comparative study of the relations between processing, microstructure and mechanical properties of CPC, produced by a unique team although, of course, each individual publication is scientifically sound and valuable. To address this issue, we will first synthesize large batches of pure α-TCP and define standard fabrication and testing procedures of CPC, for comparative purposes and systematic parametric studies; this will be addressed in Chapter 2.

It will then become possible to measure systematically elastic and fracture properties of CPC, and in particular toughness since this property has rarely been investigated, as a function of initial particle size, microporosity (obtained by varying the L/P ratio) and macroporosity (obtained by using recrystallized mannitol as a porogen). This will be

dealt with in Chapter 3 along with an attempt to describe mechanical properties with analytical models as already proposed for calcium phosphate bioceramics. For experimental simplicity, mechanical properties will first be measured in dry conditions. Chapter 4 will extend partly such investigations.

However, it also appears from the literature that a high variability of measured strength values exists from one team to the other, which could be due to variability introduced during processing and testing (setting and hardening kinetics, effect of testing in dry or wet conditions). Once more, it would be interesting to bring some light on these issues for materials prepared in comparable conditions; among others, this will be explored in Chapter 4. Nevertheless, even with fixed conditions, variability in strength still exists, implying reproducibility (reliability) issues, which is another real limitation for CPC. This has never attracted much attention in spite of its huge practical importance. It will thus be addressed using Weibull statistics in Chapter 4, to try and establish links between processing, microstructure and mechanical reliability.

From another point of view, in a recent study (Pecqueux et al., 2010), the authors proposed that the critical flaw size of BCP bioceramics increased with increasing macroporosity, due to subcritical crack growth during compressive loading inside "clusters" of macropores. From a scientific point of view, there is also a need to confirm this evolution of the critical flaw size with macroporosity in CPC. An interesting point to identify the role of macropores as critical flaws (and the possible subcritical crack growth during loading) would be the comparison between bending and compressive strengths, which will be also studied in Chapter 4.

Finally, as stated in the literature, CPC remain very brittle from their nature, with quite low mechanical properties, thus it would be necessary to develop new materials with optimized properties (handling/biological/mechanical), which could in particular be less brittle and exhibit a sort of tolerance to damage. However, it appears that the "fibers" option has been largely investigated and seems to compromise the handling properties of CPC. In contrast, composite cements with HPMC seem to be interesting from the cohesion viewpoint, although, once more, no systematic study is available on the effect of the addition of HPMC on both handling and mechanical properties (for instance on fracture toughness). This will be investigated in Chapter 5. Finally, silanized HPMC (Si-HPMC) is a rather "new" biomaterial in the stage of research and development, with interesting biological and rheological properties. Its combination with calcium phosphates for bone and joint repair has been reported but only on the polymer-rich side

(Si-HPMC being the “matrix” in which CaP particles are embedded) (Weiss et al., 2008). Given what has been seen in the literature on the role of viscosity on cohesion and injectability, it would therefore be of great interest to try and incorporate it to CPC. This will also be tried in Chapter 5, in an attempt to develop biomaterials with an improved overall performance for bone substitution.

Chapter 2 Materials and methods

2.1 Preparation and characterization of materials

This section mainly introduces the process of synthesizing α-TCP and mannitol and preparing CPC by using the above synthesized materials. α-TCP is used as the main composition of the solid phase of CPC throughout this study. Mannitol is selected here as a porogen to create macropores because it has the appropriate solubility, is nontoxic and is physiologically biocompatible (Xu et al., 2001).

2.1.1 Synthesis of α-TCP powder

TCP has three crystalline polymorphs: β-TCP, the low temperature form; and the high temperature forms, α-TCP and α′-TCP. In practice α′-TCP is less interesting since it only exists at temperatures higher than 1430 °C and spontaneously transforms to α-TCP on cooling below the transition temperature. On the contrary, β-TCP is stable at room temperature and converts to α-TCP above 1125 °C, but it can be maintained as a metastable phase during rapid cooling to room temperature (Carrodeguas et al., 2011; Yashima et al., 2003).

However, despite having the same chemical composition, α-TCP and β-TCP are considerably different in their structure and solubility, which in turn determines their biological properties and possible clinical applications. β-TCP is applied mainly for preparing biodegradable bioceramics which are shaped as dense or porous granules and blocks, whereas α-TCP is used mainly in the form of powder for the preparation of CPC, although some commercial bioceramic granules and blocks made of α-TCP can be found on the market. Table 2-1 shows the structural parameters of these TCP polymorphs.

At present, there are two major routes for synthesizing α-TCP: (1) thermal transformation of a single precursor with a molar ratio Ca/P ≈ 1.5 (either CDHA; amorphous calcium phosphate, ACP; or β-TCP); (2) solid-state reaction of a mixture of solid precursors at high temperatures.

In this study, α-TCP powder was synthesized by a high-temperature solid-state reaction between DCPA and calcium carbonate, as follows:

$$2\ CaHPO_4 + CaCO_3 \rightarrow \alpha\text{-}Ca_3(PO_4)_2 + CO_2 + H_2O \quad (2\text{-}1)$$

Table 2-1 Structural data of polymorphs of TCP. Reprinted from Carrodeguas et al. (2011)

Property	$Ca_3(PO_4)_2$ polymorph		
	β-$Ca_3(PO_4)_2$	α-$Ca_3(PO_4)_2$	α′-$Ca_3(PO_4)_2$
Symmetry	Rhombohedral	Monoclinic	Hexagonal
Space group	R3C	$P2_1/a$	$P6_3/mmc$
a (nm)	1.04352(2)	1.2859(2)	0.53507(8)
b (nm)	1.04352(2)	2.7354(2)	0.53507(8)
c (nm)	3.74029(5)	1.5222(3)	0.7684(1)
α (°)	90	90	90
β (°)	90	126.35(1)	90
γ (°)	120	90	120
Z	21	24	1
V (nm^3)	3.5272(2)	4.31(6)	0.19052(8)
V_0 (nm^3)	0.1680(2)	0.180(6)	0.19052(8)
D_{th} (g cm^{-3})	3.066	2.866	2.702

The commercial DCPA powder ($CaHPO_4$, Alfa Aesar, Germany) and calcium carbonate powder ($CaCO_3$, VWR, BDH, Prolabo) with a molar ratio 2:1 were mixed together in a blender for about 1 h. After blending, about 45 g of the mixture were transferred to a tubular plastic probe cover (Protex, Japan), vacuumed and shaped into a cylindrical bar within a mould. The cylindrical bars were then cold isostatically pressed (NOVA, Swiss) under a pressure of 120 MPa for three minutes. Then, the pressed bars were calcined in a furnace (VECSTAR, UK) at 1360 °C for 15 h and subsequently quenched to room temperature in a flow of compressed air. The calcining temperature of 1360 °C is chosen according to a pretest which indicates formation of pure α-TCP at this temperature (Fig. 2-1)[8]. Heating at higher temperatures and/or for longer times would lead to microstructural coarsening (Durucan et al., 2002B; Kingery 1976), i.e. to the production of large crystals and hence to a lower specific area associated to a low rate of hydrolysis. Cooling with compressed air is helpful to accelerate the quenching speed of the calcined bars during cooling to avoid reverting of α-TCP to β-TCP although it was reported in a recent review that this process might not be necessary (Carrodeguas et al., 2011).

After calcination, the bars were broken and ground to a coarse powder, using a Retsch

[8] It is worth reminding that the CPC studied in this thesis has α-TCP as the only active reactant, so proper sintering schedules and quenching method is critical to get as pure α-TCP as possible. The temperature of 1360 °C is chosen since it is the lowest temperature to reproducibly get large batch of "pure" α-TCP in our present lab condition. Moreover, this temperature cannot be compared among different labs and needs to be adjusted since it is strongly influenced by many factors such as: purity of precursors, amount of green body and type of furnace.

ZM100 Centrifugal Grinding Mill. The coarse powder was subsequently milled for 1 h in a Retsch RM100 Mortar Grinder to get a finer powder. No other phases than α-TCP were detected by XRD (Fig. 2-1).

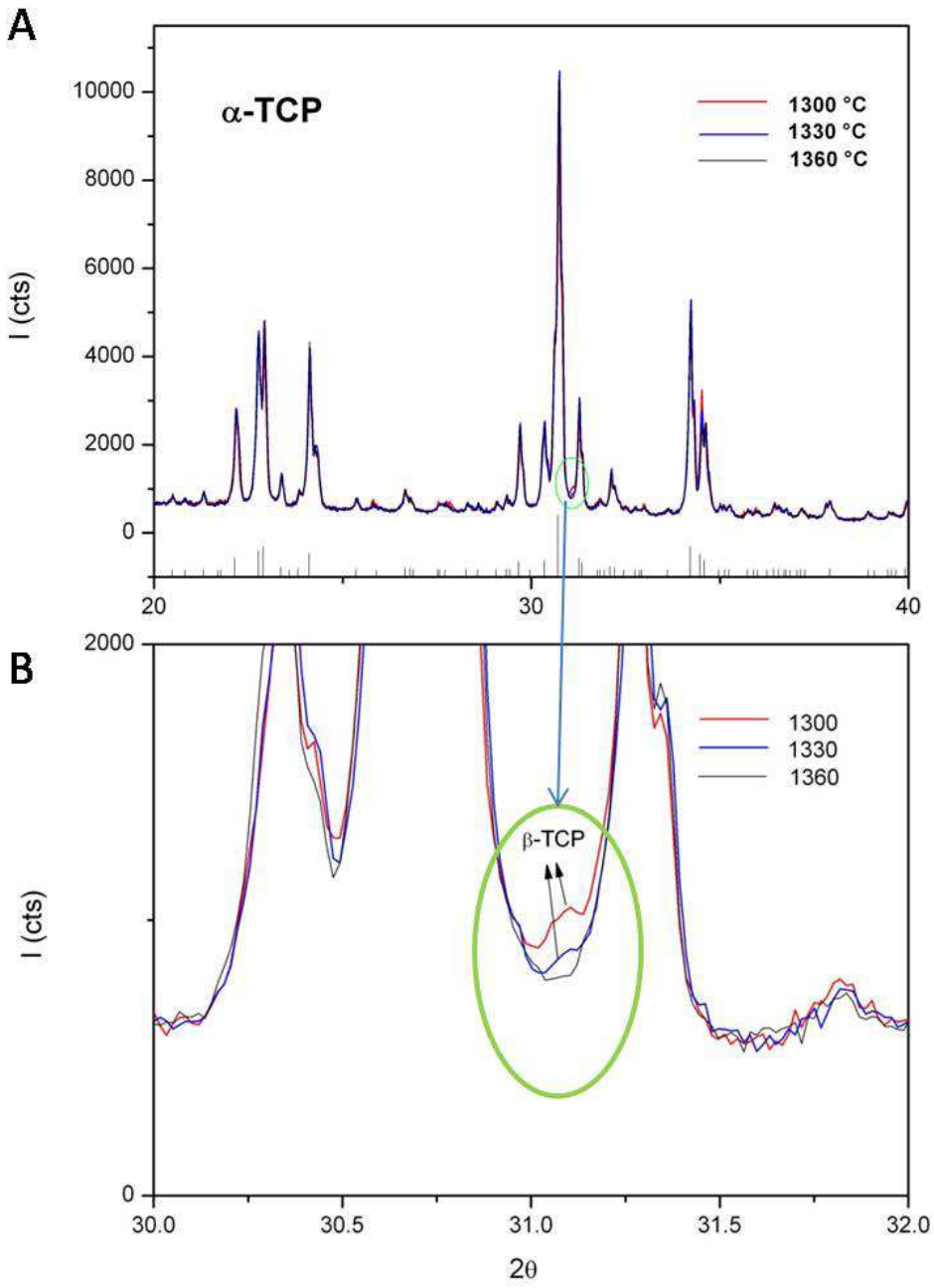

Fig. 2-1 (A) XRD pattern of α-TCP powder synthesized at different temperatures; (B) a small amount of β-TCP is observed in the α-TCP calcined at 1300 °C and 1330 °C respectively. No β-TCP is seen in α-TCP prepared at 1360 °C.

In addition, it is worth noting that it was indeed at the beginning of the study expected to get three batches of α-TCP with distinct particle sizes (specific surface area): “small” ($d < 1$ μm), “middle” ($5 < d < 10$ μm) and “large” (10 μm $< d$). As mentioned previously,

since α-TCP is a high temperature phase obtained by calcining and milling, the easiest approach to decrease particle size is to prolong the duration of milling. Unfortunately, the particle size of α-TCP does not decrease further than a few micrometers with our present equipment (Retsch RM100 Mortar Grinder) [9]. Upon further grinding, powder amorphization happens (Camire et al., 2005; Gbureck et al., 2003) and could bring potential contamination from the grinder. Therefore, only "middle" (refers to fine powder throughout the whole study) and "large" (refers to coarse powder throughout the whole study) α-TCP powders were used and their particle sizes distribution were measured by means of laser diffraction, after dispersion in ethanol in an ultrasonic bath. The mean particle sizes are 6 μm and 14 μm for the fine and coarse powders, respectively; this will allow us to investigate the influence of initial particle size on cement properties. Fig. 2-2 shows the morphology of the fine α-TCP particles.

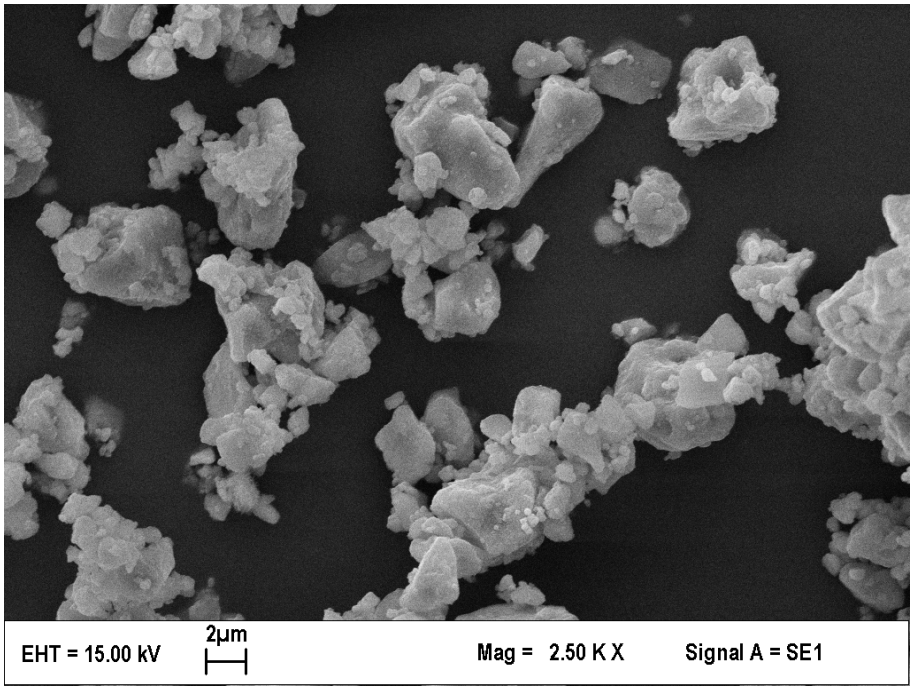

Fig. 2-2 SEM micrograph of fine α-TCP particles

[9] Actually we also tried to decrease the particle size by using high energy ball milling (Pulverisette 6, Fritch Gmbh) for different times (30 min, 60 min and 120 min). However, this method could not bring noticeable changes in particle size as measured by means of laser diffraction. Moreover, the compressive strength of cylindrical specimens prepared using the above three α-TCP powders were not significantly different from each other and from that of specimens fabricated using α-TCP powder milled with the present equipment (Retsch RM100 Mortar Grinder).

2.1.2 Recrystallization of mannitol

Macropores are critical for bone ingrowth in CPC. For this reason, water-soluble, rod-like mannitol particles were used to create macropores in the cement. However, the particles of commercial mannitol ($CH_2OH(CH(OH)_4)CH_2OH$)(Sigma) were usually too small to create macropores of desirable size, so it was recrystallized for both size regulation and purification. Mannitol was dissolved and saturated in 100 mL of a 80/20 (V/V) water/ethanol solution at 70 °C, filtered and then slowly cooled to 40 °C and incubated in a homothermal bath for 24 h. After this, the recrystallized mannitol was dried and passed through sieves with an opening of 400 μm (top sieve) and 200 μm (bottom sieve) (Tajima et al., 2006; Xu et al., 2001; Debra Vazquez 2010). The morphologies of the pristine mannitol powder and of recrystallised mannitol are shown in Fig. 2-3. From these micrographs, we could observe that the sizes of mannitol particles are significantly increased after recrystallization.

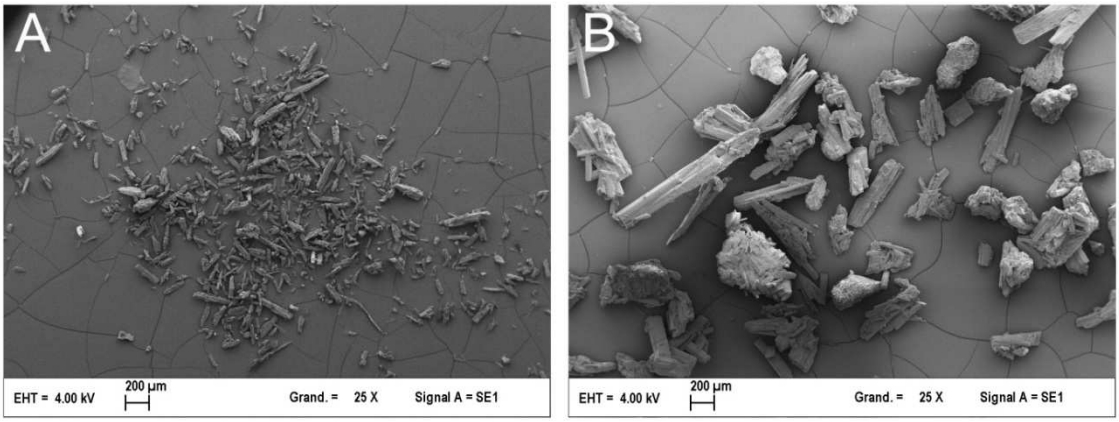

Fig. 2-3 SEM micrographs of mannitol particles (A) before and (B) after recrystallization.

2.1.3 Preparation of CPC

Cements made of apatite (CDHA) have been fabricated through the hydrolysis of α-TCP, which proceeds as follows (Bohner, 2007; TenHuisen et al., 1998)

$$3\ \alpha\text{-}Ca_3(PO_4)_2 + H_2O \rightarrow Ca_9(HPO_4)(PO_4)_5OH \qquad (2\text{-}2)$$

To achieve this, specimens using fine or coarse α-TCP powders have been fabricated. In both powders, 2 wt.% of precipitated CDHA was added as a seed for subsequent crystallisation of apatite in cements; the mixture of α-TCP and precipitated CDHA

constituted the “solid phase” of all cement pastes. An aqueous solution of 2.5 wt.% of disodium hydrogen phosphate (Na_2HPO_4) was used as the liquid phase[10]. Na_2HPO_4 was used because it was shown to accelerate cement setting (Montufar et al., 2010). CPC paste was prepared by manually mixing the liquid phase and the solid phase in a mortar for around 1 min and then the resulting paste was used for assessment of both handling properties and mechanical properties. For the latter, the paste was packed into cylindrical moulds (diameter = 6 mm, height = 12 mm) or into rhombohedral Teflon moulds of $36 \times 8 \times 8$ mm^3 using a spatula. Before packing, the paste was vibrated so as to remove as many air bubbles as possible. The mould containing the paste was kept in a small chamber with 100% relative humidity at 37 °C for 20 minutes, then immersed in 100 mL of a saline solution (0.9 wt.% sodium chloride) and incubated in a homothermal oven at 37 °C for five days. Macroporous specimens fabricated using recrystallized mannitol particles as porogen were made with the fine powder. The fabrication procedure of these macroporous specimens was the same as the one to fabricate the specimens with fine and coarse powders except that after preparation of the CPC paste, mannitol particles were added into the paste and mixed homogeneously using a spatula.

Two series of experiments were conducted to investigate the effect of various parameters (particle size, L/P ratio, amount and morphology of porosity including macropores, measurement in dry or wet condition) on the mechanical properties of CPC (results will be presented in Chapter 3 and Chapter 4).

The specimens which will be used in Chapter 3 were made using fine or coarse α-TCP powders. For convenience, the specimens prepared with fine and coarse α-TCP powder are coded as Cement F and Cement C respectively. Five specimens were made for each L/P ratio. The L/P ratios of Cement F are 0.30, 0.35, 0.40, 0.45 and 0.50, expressed by default in mL/g throughout the thesis. In contrast, the L/P ratios of Cement C are 0.30, 0.40, 0.50 and 0.60. Specimens using recrystallized mannitol as porogen are made with the fine powder. The recrystallized mannitol particles are mixed with the fine α-TCP at the following mannitol / (mannitol+fine α-TCP) mass fractions: 10%, 20%, 30%, 40% and 50%. A fixed L/P ratio of 0.35 is used, due to a rather good moldability. The total amount of liquid phase in the paste is determined from the total weight of powders (α-TCP + mannitol). Five specimens are made for each mannitol fraction for a total of 25

[10] The aqueous solution of 2.5 wt.% of Na_2HPO_4 is used as the liquid phase throughout the thesis except in Chapter 5 in which the liquid phase is a solution of cellulose ethers. The specific method of preparing solutions of cellulose ethers will be detailed in that chapter.

specimens.

The study conducted in Chapter 4 is partly an extension of the study in Chapter 3; this will be discussed and explained later. In Chapter 4, Cement F are prepared and the L/P ratio is extended from the range of 0.3-0.5 to 0.25-0.6. Twelve specimens are prepared for each L/P ratio for a total of 96 specimens. Moreover, specimens using recrystallized mannitol as porogen are also made with the fine powder. Five mannitol / (mannitol+fine α-TCP) mass fractions are chosen: 10%, 20%, 30%, 40% and 50%. A fixed L/P ratio of 0.35 is used. Twenty-four specimens are prepared for each mannitol fraction for a total of 120 specimens. Table 2-2 shows the experimental design of the studies in Chapter 3 and Chapter 4 with various factors and levels. Furthermore, since the method of preparing the liquid phase of CPC in Chapter 5 is much different from that of other chapters, for convenience, the experimental design of Chapter 5 will be detailed there.

Table 2-1 Experimental design in Chapter 3 and Chapter 4 with different variables and levels

		Factors			
	Code	Particle size of α-TCP powder	L/P Ratio (mL/g)	Mass fraction of mannitol (wt%)	Testing under dry/wet condition
Chapter 3	Cement C	Coarse	0.30, 0.40, 0.50, 0.60	0	Dry
	Cement F	Fine	0.30, 0.35, 0.40, 0.45, 0.50	0	Dry
	Macro-CPC	Fine	0.35	10, 20, 30, 40, 50	Dry
Chapter 4	Cement F	Fine	0.25, 0.30, 0.35, 0.40, 0.45, 0.50, 0.55, 0.60	0	Wet
	Macro-CPC	Fine	0.35	10, 20, 30, 40, 50	Wet
	Macro-CPC	Fine	0.35	10, 20, 30, 40, 50	Dry

2.2 Determination of density and porosity

CPC is intrinsically microporous. The porosity of CPC significantly influences its biological and mechanical properties. For this reason, it is critical to characterize and quantify the porosity (micropores left by water and macropores created by porogen).

Fig. 2-4 shows the morphologies of micropores in Cement F and macropores created by recrystallized mannitol particles.

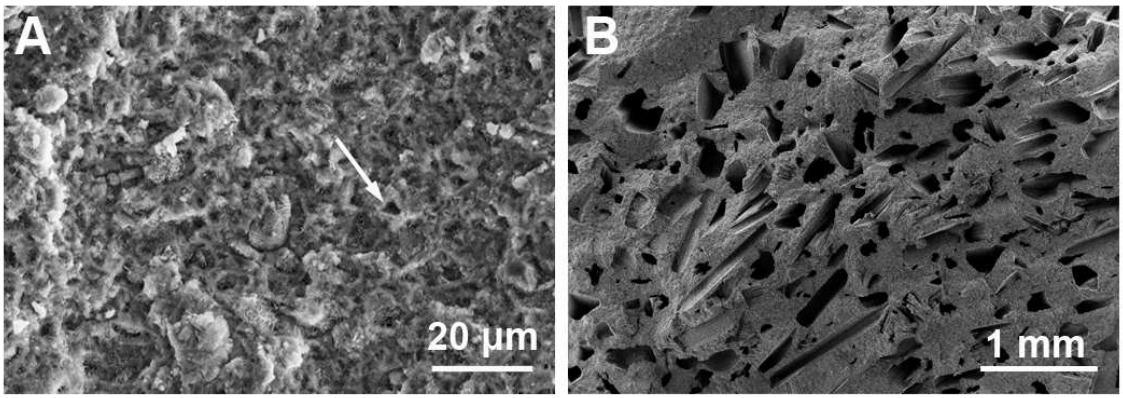

Fig. 2-4 SEM micrographs of (A) micropores in Cement F (white arrow points to micropore) and (B) macropores produced after dissolution of mannitol crystals

After drying in a homothermal oven for several days (about seven days) until there is no more weight loss[11], the total porosity of the specimens are measured by gravimetry according to the equation:

$$p_{total} = 1 - \frac{\rho}{\rho_{CDHA}} \tag{2-3}$$

where ρ_{CDHA} is the density of fully dense CDHA (2.79 g.cm^{-3}) (Monma et al, 1981) and ρ is the apparent density of the specimen measured by dividing its weight by its volume. The volume of the rhombohedral specimens was calculated from their dimensions, measured with a micrometer, with each linear dimension being the average of three locations along the specimen, following a procedure described previously (Zhang et al., 2006). Six specimens are measured to calculate the mean porosity and its standard deviation.

For macroporous specimens fabricated with mannitol as a porogen, it is assumed in the first instance that the microporosity of the cement "matrix" between macropores is

[11] The efficiency of this drying procedure and its consequences will be discussed in Chapter 4. This drying process is used throughout the thesis. Moreover, the order of the drying process is reversed for the specimens measured in different conditions. Specifically, specimens measured in dry condition are dried before the measurement of mechanical properties. In contrast, specimens measured in wet condition are dried after the measurement of mechanical properties.

independent of the mannitol mass fraction, because specimens are all fabricated with the same L/P ratio (0.35). Thus microporosity is defined as:

$$p_{micro} = \frac{V_{micro}}{V_{total-s} - V_{macro}} \tag{2-4}$$

with $V_{total\text{-}s}$, V_{micro} and V_{macro} being respectively the total volume of the specimen, the microporous volume and the macroporous volume. Furthermore, macroporosity is defined as the ratio between V_{macro} and $V_{total\text{-}s}$. These definitions yield a relationship between total, micro- and macroporosities, which can be deduced in the following steps:

First, we can get

$$V_{total} = V_{micro} + V_{macro} \tag{2-5}$$

where V_{total} is the total volume of porosity in the specimens. Then by dividing both sides of equation (2-5) by $V_{total\text{-}s}$, we can further get

$$p_{macro} = \frac{V_{macro}}{V_{total-s}} = \frac{V_{total} - V_{micro}}{V_{total-s}} \tag{2-6}$$

By combing equation (2-4) and (2-6), we can get the relation between total, micro- and macroporosities:

$$p_{macro} = \frac{p_{total} - p_{micro}}{1 - p_{micro}} \tag{2-7}$$

which is equivalent to a previously reported method (Xu et al., 2005) used to estimate macroporosity from the measurement of total porosity of macroporous specimens and of the microporosity of cements without macropores but prepared with the same L/P ratio. The validity of this hypothesis will be discussed in Chapter 3.

Indeed, in addition to the aforementioned method, a direct measurement based on quantitative image analysis on polished cross-sections (Friel, 1992) was also used to determine the macroporosity of the CPC. After measurement of mechanical properties in bending[12] , cubic blocks (8 × 8 × 8 mm^3) cut out from 36 × 8 × 8 mm^3 bars were

[12] The measurement of mechanical properties will be detailed in section 2.5.

impregnated under vacuum with an epoxy resin (EpoFix Kit, Struers, Denmark), followed by aging at room temperature for 12 h. After this process, the blocks were polished with SiC papers down to grade P4000. Then the polished surfaces were coated with carbon and observed with SEM (Leo 1450VP) using a back-scatter electron detector. Fig. 2-5 shows the morphology of the cross-section of a CPC with 50% mannitol.

Finally, the SEM micrographs of macroporous CPC were analysed and the volume of macroporosity were quantified by means of software Leica Qwin V3, based on the different contrasts of epoxy resin (dark areas) and CPC (bright areas).

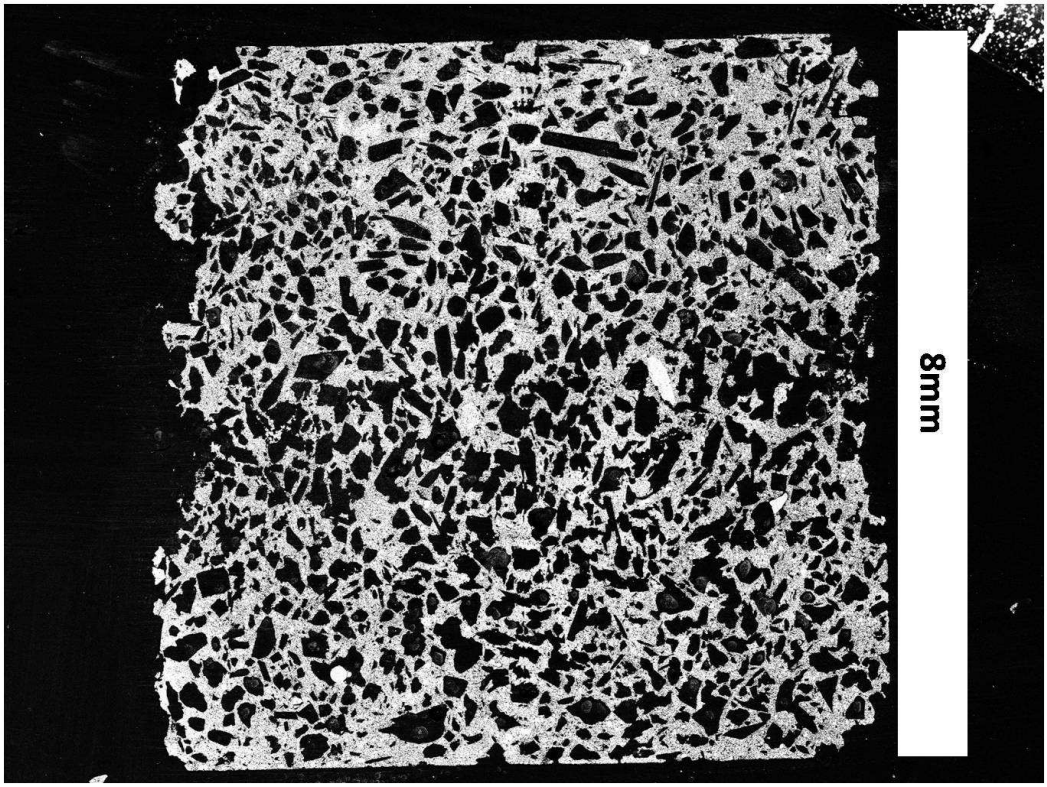

Fig. 2-5 SEM micrograph (back-scatter electron) of macroporous CPC (50% mannitol) impregnated with epoxy resin.

2.3 Phase and microstructure characterization

The compositions of hardened CPC specimens were analyzed by X-ray diffraction (XRD, X'pert pro, PANalytical, Netherlands) using Cu Kα radiation (40 kV, 40 mA) in a continuous scanning mode. The diffraction angle 2θ was varied from 10° to 80° at a scanning speed of 0.017°/s. Moreover, infrared absorption spectra were recorded by Fourier transform infrared spectroscopy (FTIR; Magna-IR 550, Nicolet Co., USA) in the

4000~400 cm^{-1} range. Finally, fracture surfaces of CPC specimens were observed by a scanning electron microscope (SEM; Merlin, Carl Zeiss, Germany).

2.4 Evaluation of handling properties

Handling properties[13] (injectability, cohesion, anti-washout, and both initial and final setting times of CPC have been evaluated. The procedures for examining the above mentioned handling properties are detailed in the following sections.

2.4.1 Injectability

The injectability of the CPC was tested following the method reported in a previous study (Khairoun et al., 1998), using a 5 mL syringe, which is fitted with an orifice of 1.2 mm inner diameter. CPC paste was prepared and immediately packed into the syringe. Before the test, trapped air bubbles between the orifice and the gasket of the syringe plunger were eliminated by manually shifting the plunger. Six minutes after mixing the cement powder and liquid, the syringe was pressed via a multifunction testing machine (TAHD plus, Stable Micro Systems, UK). The CPC paste was extruded from the syringe at a speed of 15 mm/min until a maximum force of 100 N was achieved; the force during injection was recorded. The injectability was judged as the mass of the paste extruded from the syringe divided by the original mass of the paste inside the syringe (Khairoun et al., 1998). The tests were performed at 25 °C with 50% relative humidity. Each measurement was carried out in triplicate.

2.4.2 Cohesion and anti-washout ability

The cohesion time was measured with a specially designed method (Chen et al., 2009), consisting in putting the newly prepared CPC paste in early contact with saline solution and visual inspection for cohesion or disintegration. The cohesion time was recorded when there were no visible particles released from the CPC paste.

For the measurement of anti-washout ability, the newly prepared CPC paste was manually shaped into a ball and placed into the saline solution (Xu et al., 2004B). The specimen was considered washout-proof if there is no visible surface abrasion from the

[13] The evaluation of handling properties of CPC is mainly demonstrated in Chapter 5 although setting time is also examined in Chapter 3.

CPC ball by hand scrubbing it in saline solution. Each measurement was carried out in triplicate.

2.4.3 Setting time

The setting time of the CPC was measured using Gillmore needles (H-3150, Humboldt Mfg. Co. USA) according to ASTM C266 standard. After the newly prepared CPC paste was packed into a stainless-steel mold. A light needle (113.4 g in weight and 2.12 mm in diameter) was vertically and lightly loaded to the surface of the cement. The cement was considered initially set when the light needle could not mark the cement surface with a complete circular impression for the first time. Furthermore, to verify the initial set, two additional penetration measurements on different areas of the cement surface were obtained within 90 s of the first “initial set” measurement. Final setting time was recorded with a heavy needle (453.6 g in weight and 1.06 mm in diameter) following the same procedure as for determination of initial setting time. The measurement of setting time was conducted with 100% relative humidity at 37 °C.

2.5 Measurement of mechanical properties

Mechanical properties (Young’s modulus, flexural strength, fracture toughness and compressive strength) of CPC have been measured. The procedures for measuring the aforementioned mechanical properties are detailed in the following sections.

2.5.1 Young’s modulus

A standard three-point bending test with a span of 32 mm was used to measure the Young’s modulus of CPC at a crosshead speed of 0.1 mm/min on a computer-controlled universal testing machine. Before the test, all the 36 mm × 8 mm surfaces of the specimen were slightly polished by using SiC paper of grade P1200. Moreover, special care was taken to ensure that the loading roller was properly aligned on the sample surface to prevent off-axial load. Specimen deflection was measured using a Linear Variable Differential Transformer (LVDT), with a precision of less than a micrometer. The LVDT was directly linked to the upper roller on the one hand, and to one of the lower rollers on the other hand, to ensure that the deflection is measured as close as possible to the specimen. The test was conducted until the specimen was broken, and both loading force,

F, and specimen deflection, d, were recorded. The measurement was conducted in air at a relative humidity between 40% and 55% at room temperature (20 °C-25 °C), and this condition was used throughout the study for all the measurement of mechanical properties. The schema for the measurement of Young's modulus is shown in Fig. 2-6.

After measurement, the Young's modulus (E) of CPC is calculated according to:

$$E = S.\frac{L^3}{4BW^3} \quad (2\text{-}8)$$

where S is the stiffness, S = ΔF/Δd (expressed in N/m), i.e. the slope of the linear-elastic portion of the loading curve.

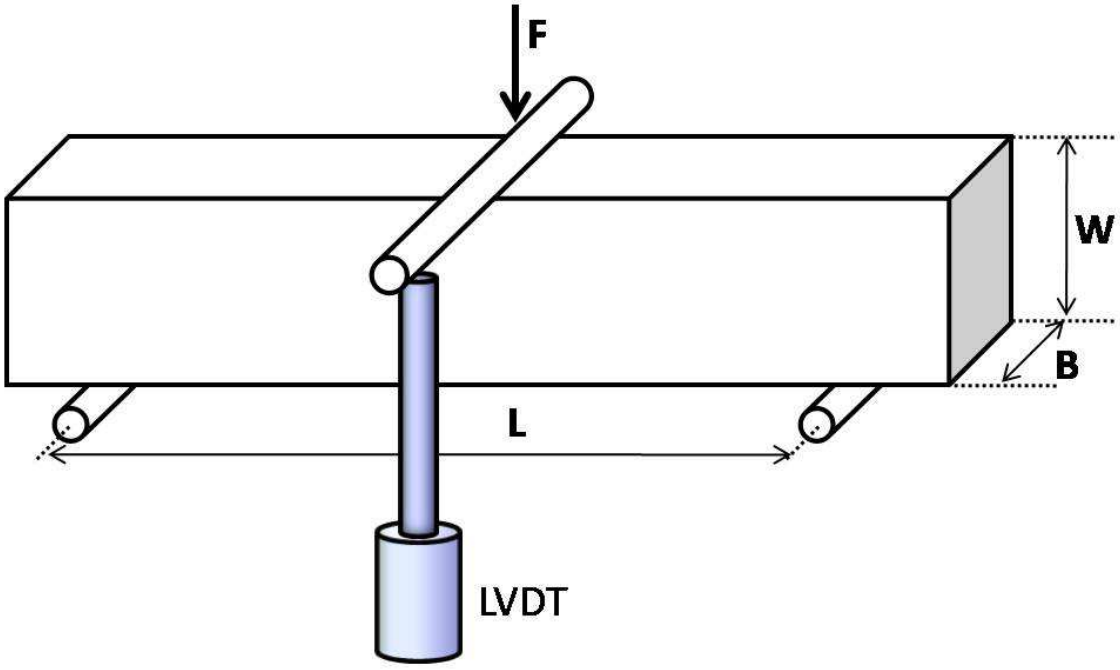

Fig. 2-6 Schematic diagram for the measurement of Young's modulus of CPC. L (32 mm), span between two supports; B (8 mm) and W (8 mm), width and height of the specimen respectively. LVDT is affixed to the mounting and is in contact with the loading roller.

2.5.2 Flexural strength

The bending setup for the measurement of flexural stength of CPC is the same as for determining the Young's modulus. For this reason, after the measurement of the latter property, the former property can be calculated concomitantly using the following equation:

$$\sigma_f = \frac{3F_{\max}L}{2BW^2} \tag{2-9}$$

where F_{max} is the maximal (i.e. breaking) force during bending.

2.5.3 Fracture toughness

At present, a number of techniques have been demonstrated, which all aim at determining the fracture toughness of different materials. Moreover, these techniques can be divided into two groups. One group of them consist of fracture mechanics using large cracks (notches) and in some cases secondarily induced precracks: the single-edge-notched-bend (SENB), and its two derivatives, the single-edge pre-cracked-beam (SEPB) and the single-edge-V-notched-beam (SEVNB), double cantilever beam (DCB) and chevron-notched (CN) beam. The other group is based on the sharp-indenter approach, introducing diagnostic microcracks by Vickers or Knoop indentation: indentation fracture (IF) and indentation strength (IS). Among these techniques, the CN beam fracture toughness method has the advantage of not requiring precracking of the sample to produce an atomically sharp crack and not needing to measure the actual crack length, and has been used extensively for brittle materials testing, where precracking is extremely difficult (Morgan et al., 1997). For this reason, in this study, the fracture toughness of CPC is measured on CN specimens following a procedure described by Dlouhy et al. (1994), using the same bending setup as for the Young's modulus. The schema for the measurement of fracture toughness and the cross-section of specimen after measurement are shown in Fig. 2-7.

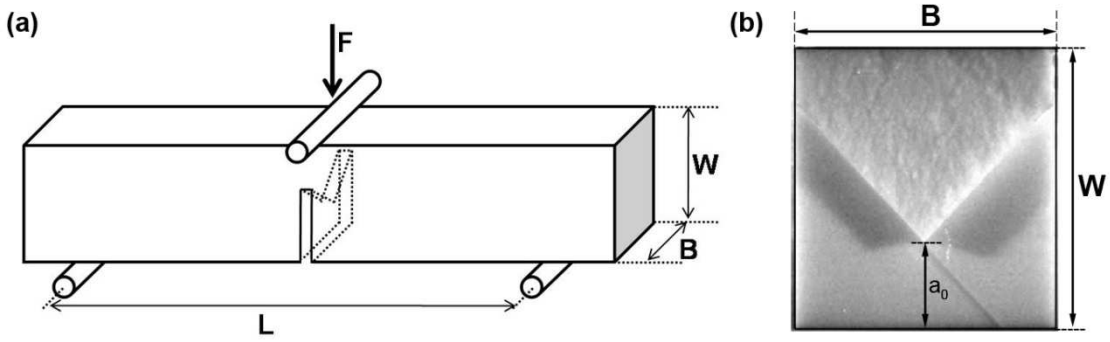

Fig. 2-7 (a) Schematic diagram for the measurement of fracture toughness, (b) cross-section of a broken CPC specimen, showing the initial notch depth, a_0.

The fracture toughness of CPC is calculated with the following equation:

$$K_{1C} = \frac{Y^*_{\min} F_{\max}}{BW^{1/2}} \tag{2-10}$$

where Y^*_{min} is the minimum value of the geometrical factor Y^* depending mainly on the shape of the plane defect on which fracture initiates (Dlouhy et al., 1994). To obtain it, the theoretical evolution of Y^* as a function of crack extension is computed, and its minimum, Y^*_{min}, is calculated numerically.

2.5.4 Compressive strength

After measurement of the Young's modulus, bending strength and fracture toughness, specimens of approximately 16 × 8 × 8 mm^3, cut out from 36 × 8 × 8 mm^3 bars, are used to measure compressive strength. It is worth mentioning that appropriate aspect ratio and specimen dimensions are critical to get correct strength values. On the one hand, an aspect ratio lower than one and small specimen dimensions can often yield an overestimated strength (Barralet et al., 2003; Metsger et al., 1999). On the other hand, if the aspect ratio is too large, it can result in an undesirable bending of the specimen, also called buckling (Wang et al., 2003). In this study, the aspect ratio of the specimen is two, which has been extensively used in the community of biomaterials. The tests are performed with a loading speed of 0.5 mm/ min on the same machine. During the test of compressive strength, a single sheet of thin cardboard was inserted between the loading plates and the specimen to reduce the high contact stresses at the loading lines, compensate for any surface irregularities of the specimen in contact with the loading plates and lead to a uniform load distribution. The compressive strength of CPC is calculated using the equation below:

$$\sigma_r = \frac{F_{\max}}{BW} \tag{2-11}$$

2.6 Experimental design of the thesis

Finally, in order to better understand the thesis, a flow chart (Fig. 2-8) has been drawn as follows to illustrate the fabrication routes for CPC with different parameters, and the

corresponding mechanical tests (evaluation of handling properties for composite CPC) conducted on each.

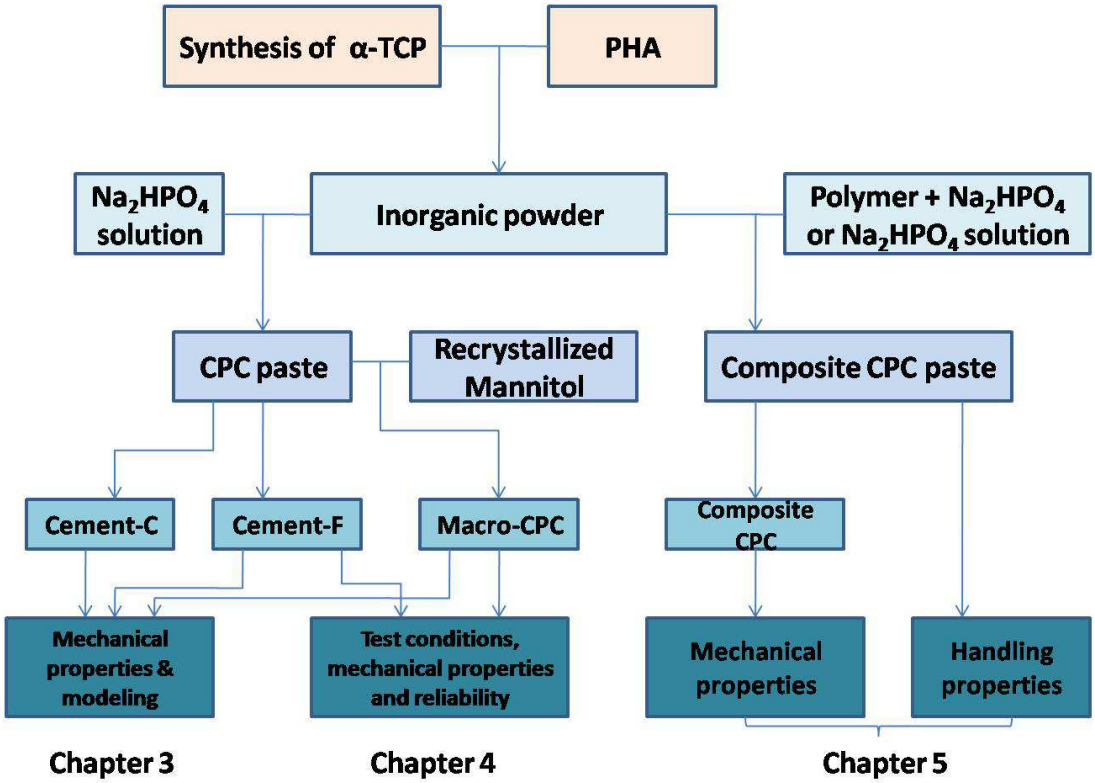

Fig. 2-8 Flow chart showing experimental design of the thesis.

Chapter 3 Influence of microporosity and macroporosity on the mechanical properties of CPC

As reviewed in the first chapter, there is a consensus in the biomaterial community that CPC is still too weak to be used in load-bearing places. For this reason, lots of works have been focused on mechanical properties, and their evaluation is still necessary in the development of CPC. However, most of them were examined using strength tests such as compressive strength and diametrical tensile strength. In contrast, few studies mentioned fracture toughness which is one of the real limitations for CPC, rather than strength per se. Moreover, as reviewed in Chapter 1, despite numerous works on it, there is a lack of a systematical study on the mechanical properties of CPC. There is also nearly nothing on the evolution of mechanical properties with microporosity and macroporosity considered separately, as well as on its modeling which is generally considered to be a useful tool not only for a better understanding of the mechanical behavior but also to help in the design of materials with desirable mechanical properties. For these reasons, in this chapter we will investigate the influence of microposity (controlled by the L/P ratio) and macroporosity (generated by the dissolution of recrystallized mannitol particles) on the mechanical properties (Young's modulus, fracture toughness and compressive strength), and describe them with models as functions of microporosity and macroporosity. In addition, before describing the above-mentioned work, a preliminary kinetics study based on the same CPC system will be presented, which is critical for the preparation of CPC specimens and for the comparison of their measured mechanical properties.

3.1 Kinetics study of α-TCP based CPC

3.1.1 Setting time of CPC

Setting time (initial and final) of CPC is a very important parameter for its surgical application. Its clinical meaning is that the cement paste should be implanted before initial setting and that the wound can be closed after final setting. Moreover, the cement should not be deformed between initial and final setting times because during this period any deformation could cause cracks (Dorozhkin, 2008; Driessens et al., 1998). In general,

CPC should set slowly enough to provide sufficient time for surgeons to perform implantation but fast enough to prevent delaying the operation (Dorozhkin, 2008). Although this chapter mainly focuses on mechanical properties, it is still necessary to gain some knowledge on the setting behavior of the present CPC system, which is critical for the preparation of CPC specimens with the minimum possible defects. The initial and final setting times of CPC prepared with fine and coarse powders, as well as by adding different amounts of mannitol, were measured (Fig. 3-1).

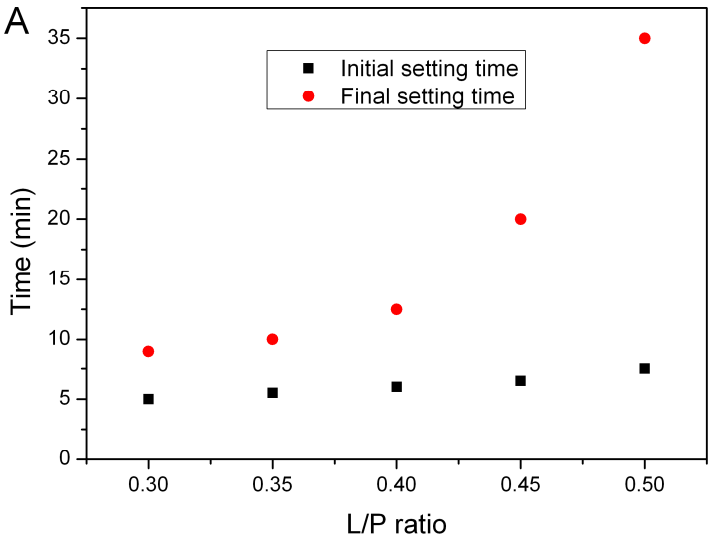

Fig. 3-1A Initial and final setting times of Cement F

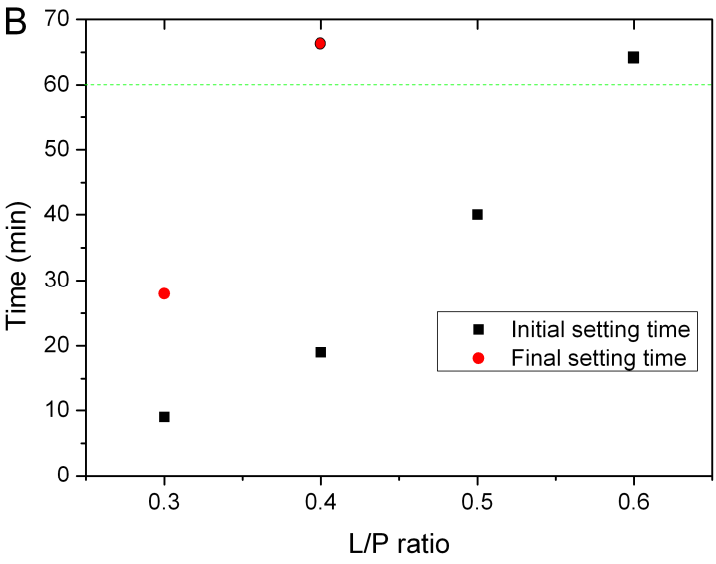

Fig. 3-1B Initial and final setting times of Cement C. The green dashed line indicates that above the line the setting times are longer than 60 minutes and will not be shown or shown as a symbolic setting time rather than an actual one.

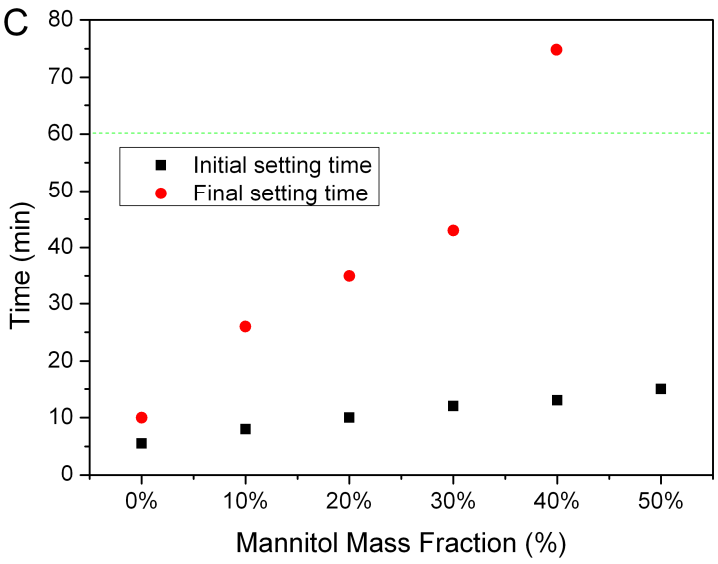

Fig. 3-1C Initial and final setting times of CPC with different amounts of mannitol. The green dashed line has the same meaning as in Fig. 3-1B.

Fig. 3-1A (and B) shows that both initial and final setting times of Cement F (and Cement C) increase with increasing L/P ratio. This is simply due to the fact that with increasing L/P ratio, the distance between initial α-TCP particles increases. This modifies the interaction between α-TCP particles, and then delays the formation of the entangled network of apatite crystals which is responsible for the mechanical properties of CPC, therefore prolonging the setting time. It can also be observed that at the same L/P ratio, a reduction of particle size results in a substantial decrease of both initial and final setting times (Cement F sets faster than Cement C). This behavior can be explained by considering the different interactions occurring in the cement paste. In fact, it should be kept in mind that, generally speaking, both the chemical reaction that is taking place, and physical attractive forces between the cement particles, contribute to setting. In the case of Cement F, owing to its higher specific area, the dissolution reaction takes place at a much faster rate. Furthermore, the smaller the particles the stronger the electrostatic attractive forces are (Ginebra et al., 2004). For the CPC with mannitol, both initial setting time and final setting time increase with increasing amount of incorporated mannitol particles. Before explaining this, it is worth reminding that in the case of CPC with mannitol the total amount of liquid in the paste was determined from the total weight of powders (α-TCP + mannitol). Then the results can be explained in terms of liquid availability: when the amount of mannitol added increases, there is less α-TCP available for the dissolution reaction, which increases the actual liquid to α-TCP ratio and thus

prolongs the setting time, as in the case of Cement F and Cement C.

3.1.2 Evolution of mechanical properties with hardening time

From Chapter 1, it appears that one of the main weaknesses of the existing literature is the lack of a comprehensive and systematic comparative study of the relations between processing, microstructure and mechanical properties of CPC. To address this issue and for the purpose of comparison, proper experimental parameters such as hardening time or specimen dimensions throughout the whole study should be deliberately chosen and then fixed. For the hardening time, a kinetic study on the development of compressive strength as a function of time up to 35 days has been performed. Fine α-TCP was selected due to a faster reaction rate as shown in section 3.1.1. Cylindrical CPC specimens with a L/P of 0.35 have been prepared and immersed in a saline solution for different times to provoke hardening. After hardening and drying, their compressive strength and corresponding porosities were measured (Fig. 3-2).

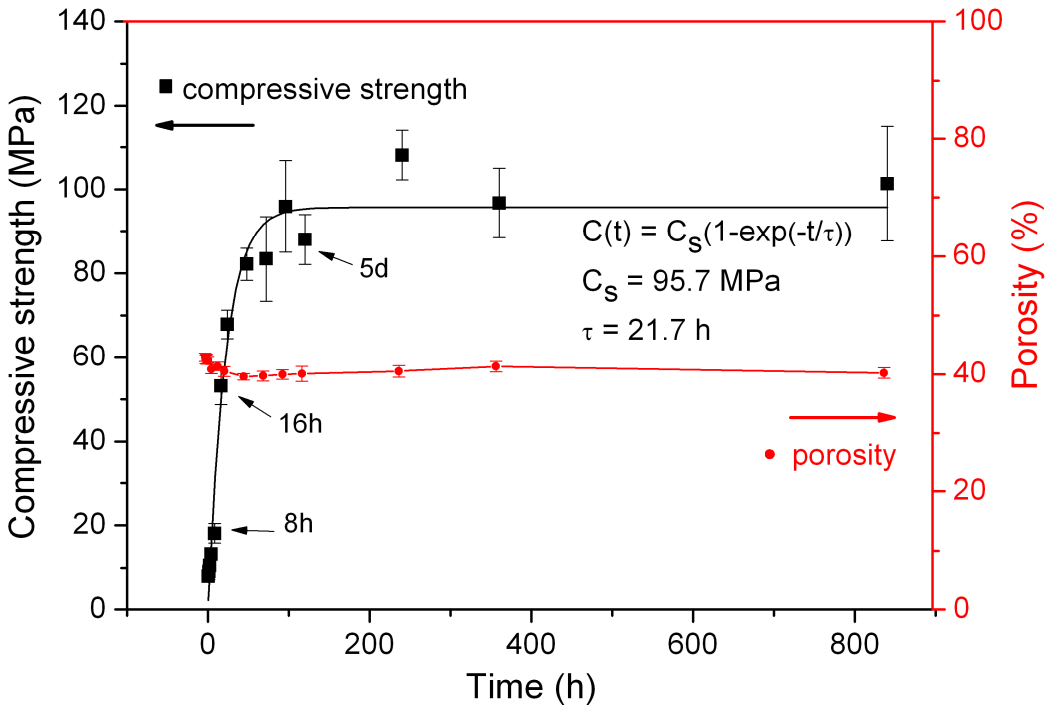

Fig. 3-2 Evolution of compressive strength and porosity of CPC with hardening time. Each point represents the mean of six specimens ± one standard deviation.

From Fig. 3-2, it is observed that the compressive strength of Cement F slowly increases in the initial 8 h, reaching a strength value of 18 MPa. In contrast, the value

jumps to 53 MPa in the following 8 h. Four days after the preparation, it further increases to 95 MPa and then maintains a similar level during the whole hardening time. Furthermore, in order to better understand this kinetics, the evolution of strength value with the hardening time was fitted with an exponential function (Ginebra et al., 2004), as shown in Fig. 3-2. In the function, C_s represents the compressive strength at saturation and τ is a time constant which indicates the time when the CPC can reach 63% of C_s. The smaller the time constant, the faster the reaction rate. Unlike the development of strength, porosity remains almost the same (around 40%) during the whole hardening process, which is due to the fact that the same mass of solids is kept in a nearly constant volume. After measuring porosity and strength, CPC was examined by means of XRD (Fig. 3-3) to determine the phases in presence.

From the figure, we can monitor the evolution of phase composition (disappearance of α-TCP and formation of CDHA) as a function of hardening time. Furthermore, the above evolution of phase composition can be quantitatively described by plotting an indicative reaction ratio R, which was calculated on the basis of the peak intensity of α-TCP as a function of hardening time (Fig. 3-4). Similar to Fig. 3-2, the degree of reaction R with the hardening time can be fitted with an exponential function but with slightly different parameters. In the present case, R_s represents the reaction ratio at saturation and τ is a time constant which indicates the time when the CPC can reach 63% of R_s. The smaller the time constant, the faster the reaction rate. In addition, it is important to note that the calculation of R is based on the peak intensity variation of a main peak (30.72^o) of α-TCP, which is just a rough estimation. However, the trend calculated from the estimation is very obvious and thus can help to understand the strength evolution.

Finally, after comparison between Fig. 3-2 and Fig. 3-4, a relation could be established between strength development and phase evolution by considering the origin of the strength of CPC. As a first approximation, it can be described by a straight line as shown in Fig. 3-5. This shows a strong correlation between strength and degree of reaction (the strength of CPC globally increases with increasing R). During hardening, α-TCP progressively reacts with water, and an entangled network of apatite crystals is formed, which is responsible for the mechanical properties. With time, α-TCP further disappears, apatite crystals continue growing and the network of crystals becomes more and more entangled, so the cement becomes stronger.

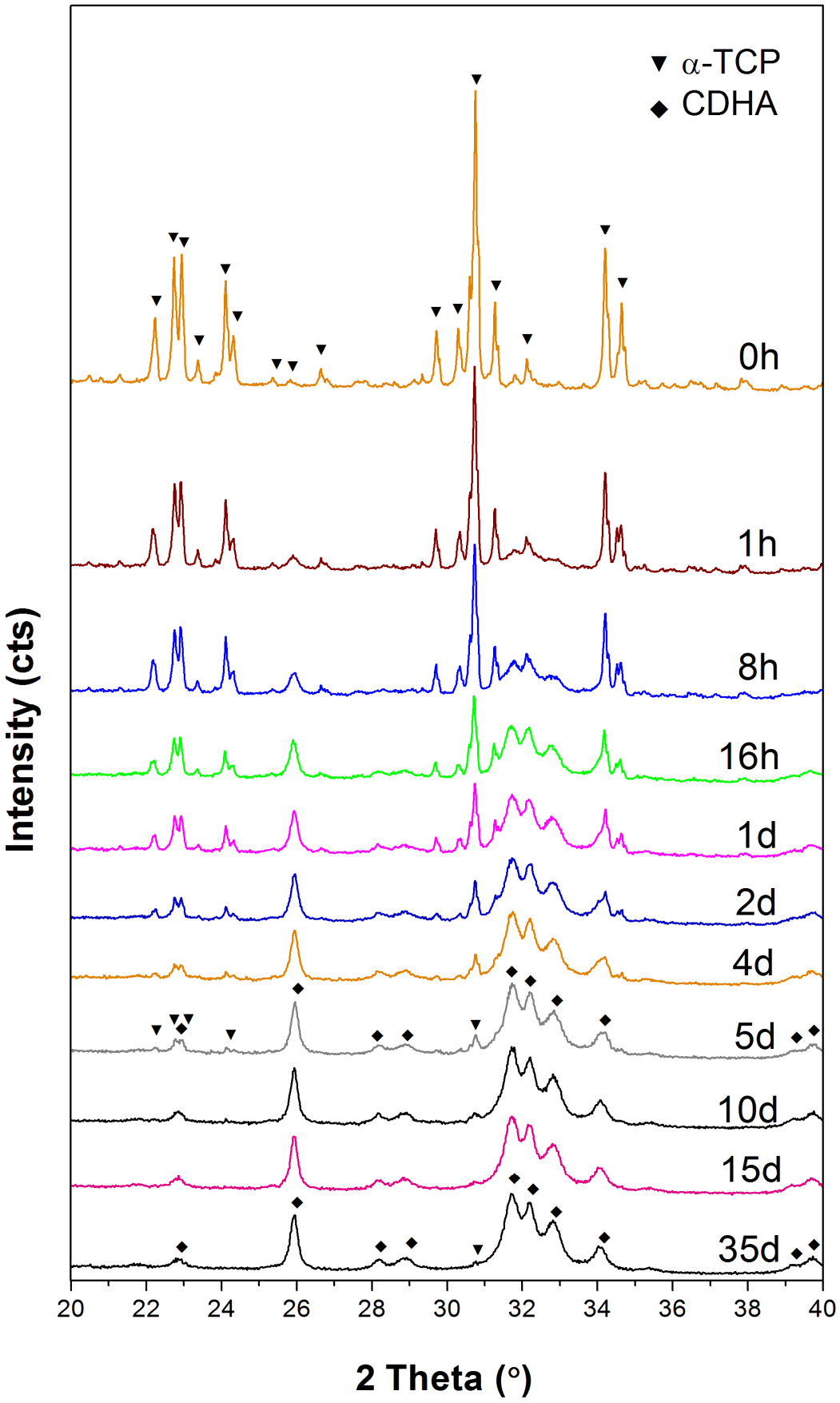

Fig. 3-3 XRD diagram of Cement F after different hardening times

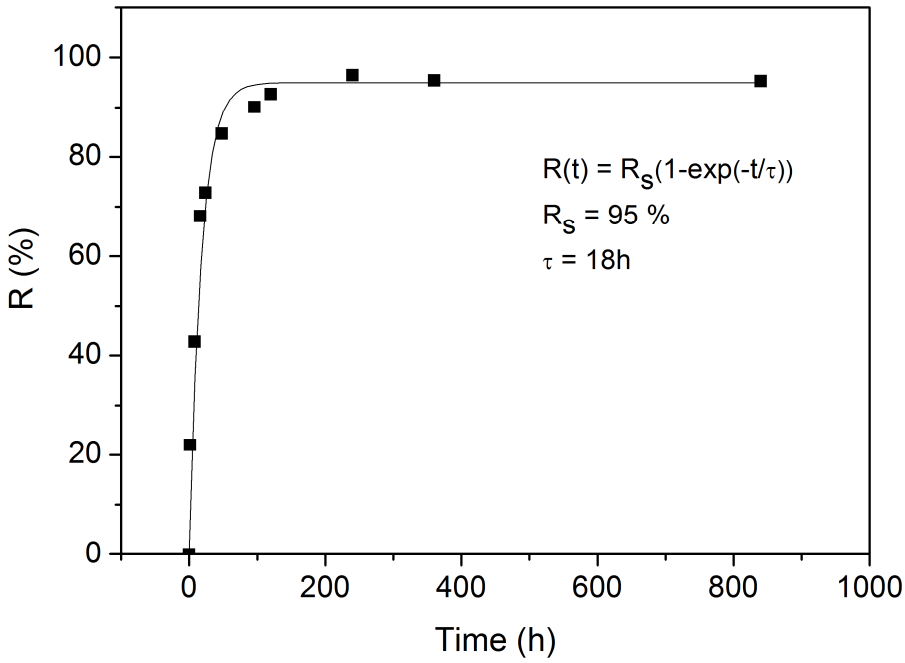

Fig. 3-4 Degree of reaction (R) as a function of hardening time

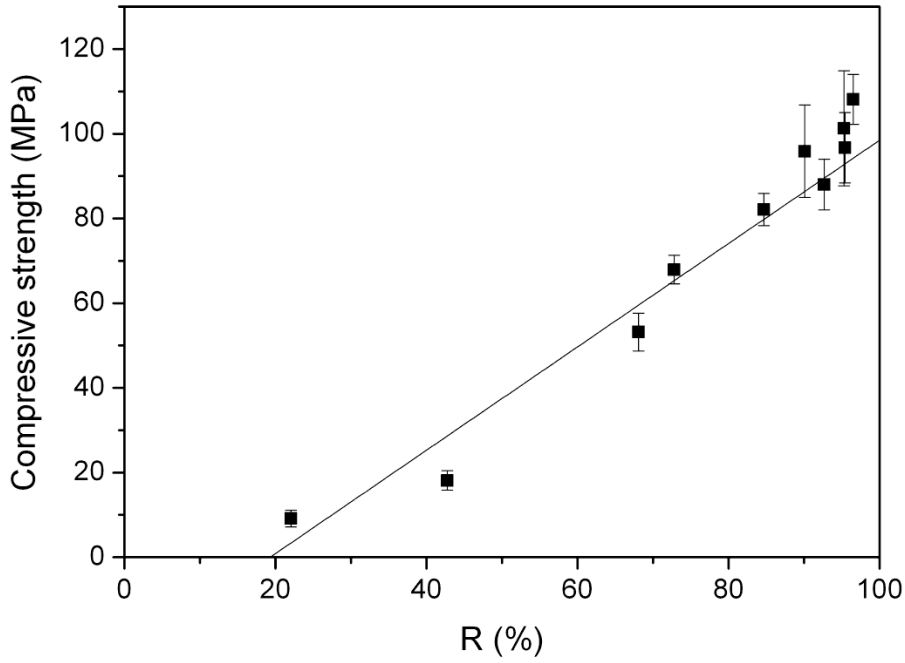

Fig. 3-5 Compressive strength as a function of degree of reaction R

In the present study, the presence of CDHA can be clearly detected after 8 h (see Fig. 3-3), corresponding to a degree of reaction R of only 42%, which could explain the concomitant low strength (18 MPa). Eight hours later, the amount of formed CDHA noticeably increases, related to a degree of reaction R of 68%, and this is consistent with the significantly increased strength value (53 MPa) measured at the same time. Five days

following the preparation, CDHA is already the predominant phase with a degree of reaction R of 92% although some unreacted α-TCP can still be observed (the influence of unreacted α-TCP on mechanical properties will be discussed later). In our study, five days is considered to be sufficient to ensure hardening in terms of measured strength values which are quite stable during the rest of hardening if the errors are taken into account, and in terms of the amount of unreacted α-TCP. In general, we always want to avoid residual reactant (unreacted α-TCP in our case) in the final reaction product, but this seems to be rather difficult within five days in our case. However a longer time, on the one hand, does not bring any noticeable changes in microstructure and properties (Ginebra et al., 2004), and on the other hand would cause our experiments to last too long. Five days of hardening can therefore be considered as an optimal compromise.

3.2 "Microstructure" and mechanical properties of microporous CPC

3.2.1 Influence of microporosity on Cement F

3.2.1.1 Porosity of Cement F

The porosity of Cement F with different L/P ratios is plotted in Fig. 3-6.

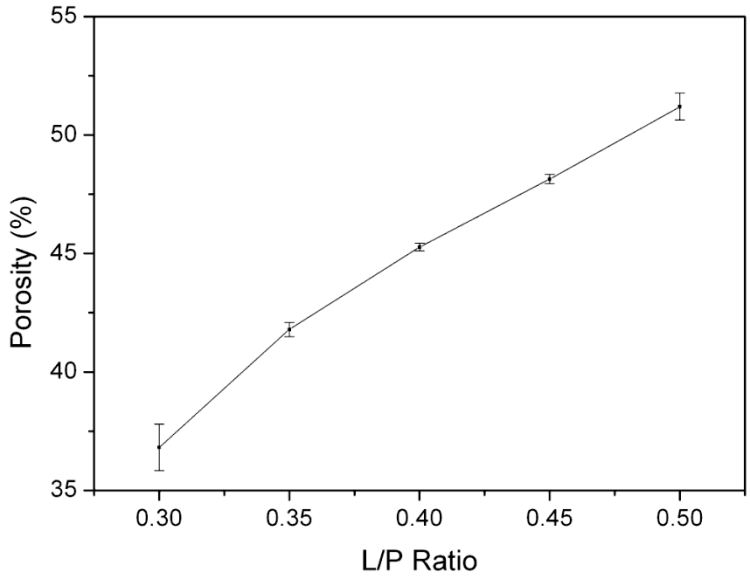

Fig. 3-6 Porosity of Cement F as a function of the L/P ratio. Each point represents the mean of five specimens ± one standard deviation.

As expected, the total porosity of Cement F increases with an increase in the L/P ratio, ranging from 36% to 51%. This is due to the higher proportion of liquid in the constant volume of the mold. Furthermore, it should be reminded that our assessment of porosity is based on the theoretical density of pure CDHA (2.79 g/cm^3, Monma et al, 1981). Nevertheless, this could be somewhat different when some unreacted α-TCP is present in the final composition. However, the latter has a theoretical density of 2.86 g/cm^3; so that the detected amounts of unreacted α-TCP (see Fig. 3-8 below) may not influence the calculated porosity by more than 1%. This principle will also be used in the following sections to evaluate the total porosity of Cement C and macroporous CPC. The intrinsic porosity (Fig. 3-7) of CPC comprises two types of voids: inter-crystallite voids and voids between aggregates (Espanol et al. 2009), which are usually smaller than 10 μm and beneficial for impregnation of biological fluids.

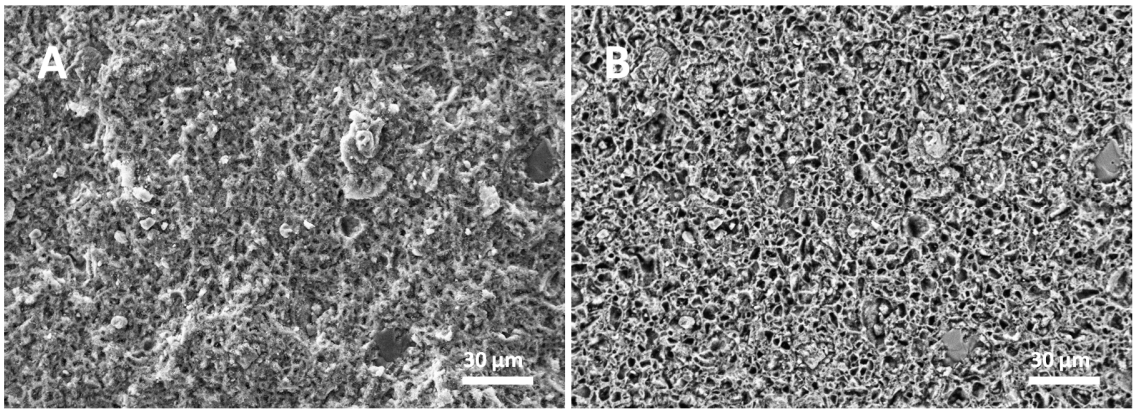

Fig. 3-7 SEM micrographs of micropores in Cement F: (A) secondary electrons imaging, (B)back-scattered electrons imaging of the same area as (A), showing the morphology and size of micropores.

3.2.1.2 Phase and microstructural features of Cement F

The XRD patterns of Cement F prepared with different L/P ratios are shown in Fig. 3-8. The first XRD pattern corresponds to the pristine α-TCP powder, in which no β-TCP is observed. These patterns are consistent with the finding of section 3.1.2. After five days of hardening, it is observed that most of the fine α-TCP powder mixed with different L/P ratios has reacted with water and has transformed into CDHA. Similarly, some unreacted α-TCP can still be detected, but the amount of the unreacted α-TCP globally decreases with the increase of the L/P ratio, as can be seen by observing the intensity of the main peak of α-TCP (the large peak at 30.7° on the 0.30 and 0.35 diagrams, a small peak on

the 0.40 diagram and even smaller peaks on the 0.45 and 0.50 ones).

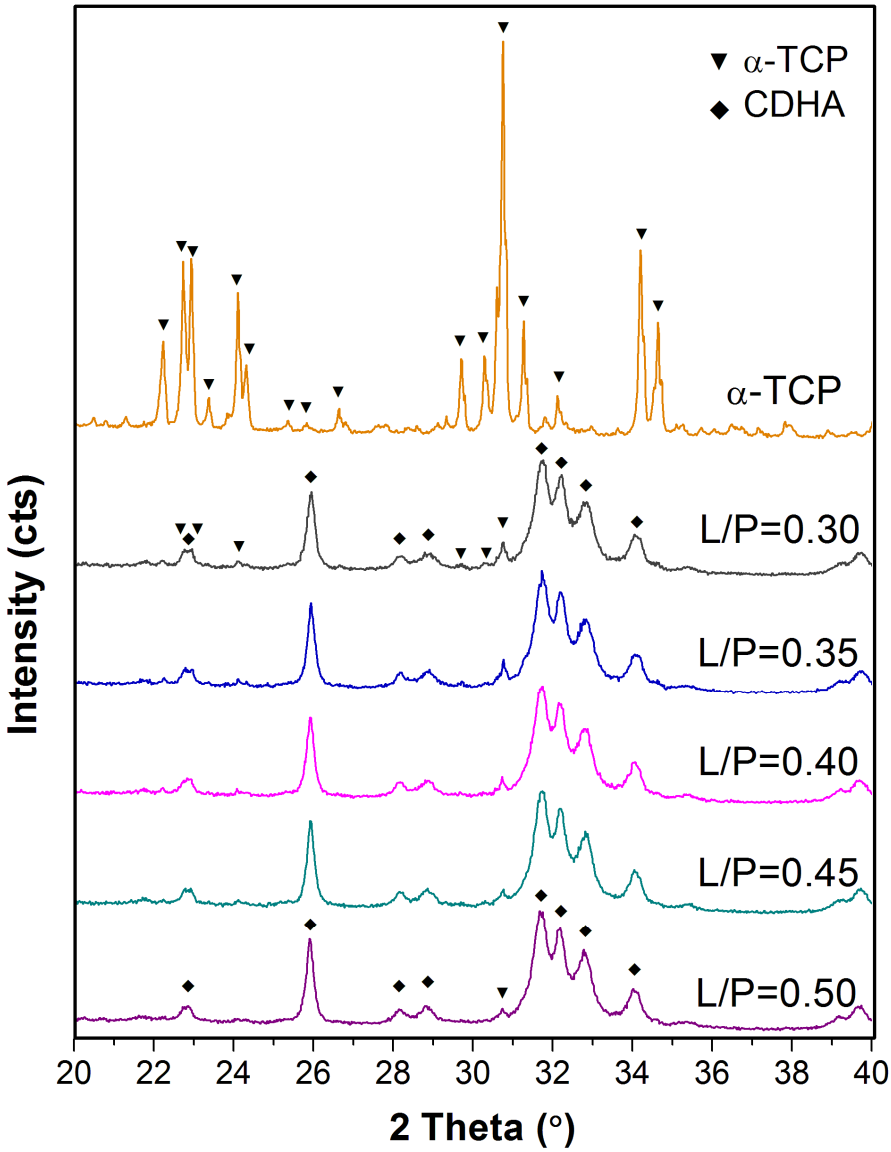

Fig. 3-8 XRD patterns of Cement F prepared with different L/P ratios.

Two hypotheses can be formulated to explain this trend. One can be stated in light of liquid availability: when the L/P ratio increases there is more liquid available for the dissolution reaction, which could end in less unreacted α-TCP in the final cement. The other explanation could be based on "geometric" features: when the L/P ratio increases, porosity increases (see Fig. 3-6), leaving more open voids for the saline solution to flow inside the material and react with α-TCP, causing a decrease in the amount of unreacted α-TCP.

The fracture surfaces of Cement F with two different L/P ratios as observed by SEM are shown in Fig. 3-9.

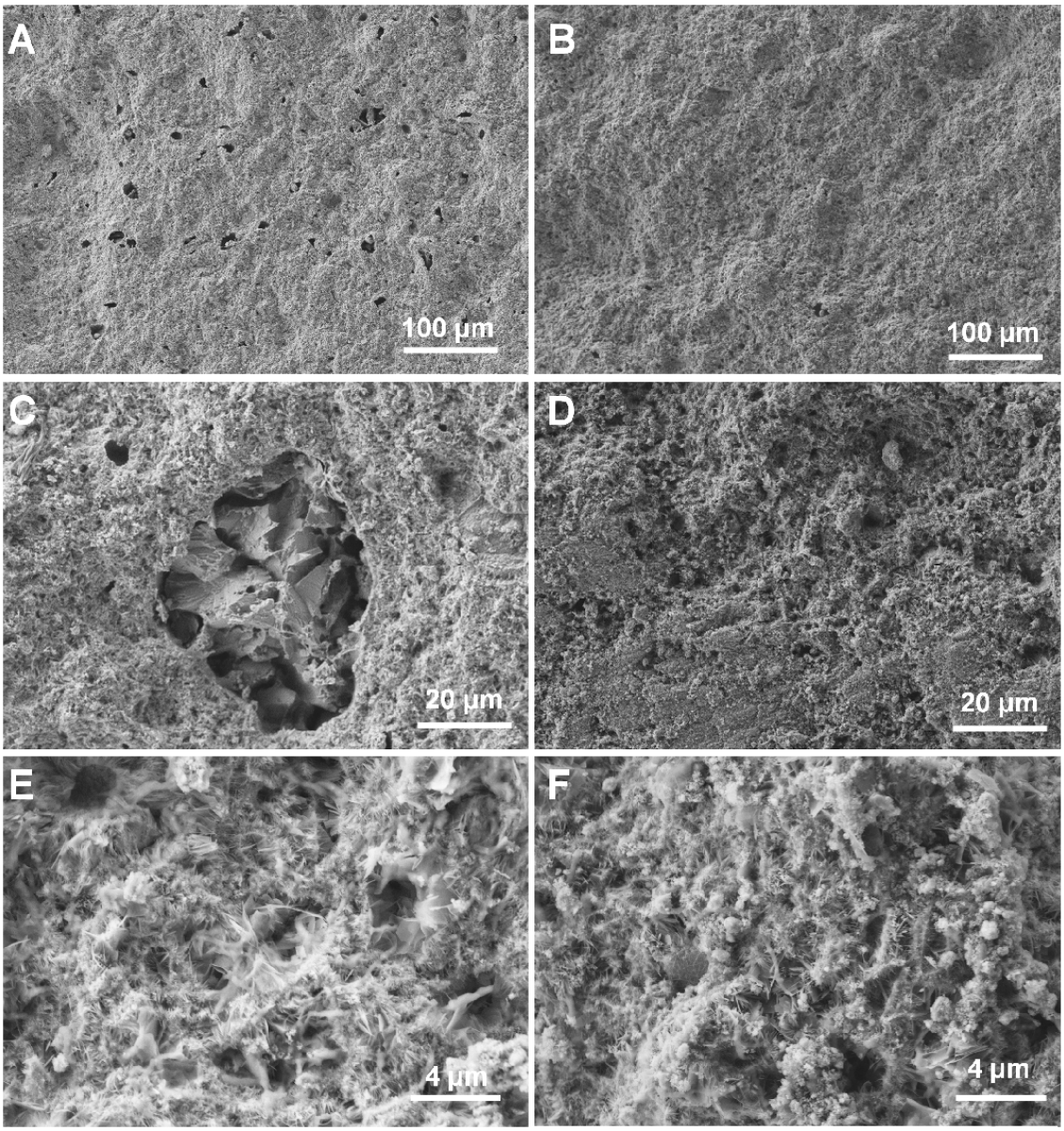

Fig. 3-9 SEM micrographs of Cement F fracture surfaces: (A), (C), (E) Cement F prepared with L/P ratio 0.30; (B), (D), (F) Cement F prepared with L/P ratio 0.40.

Fig. 3-9A shows some voids of tens of micrometers randomly distributed on the surface of Cement F with a L/P ratio of 0.30 at a magnification of 200×. At a higher magnification (Fig. 3-9C), particle clusters composed of unreacted α-TCP[14] can be found inside the void but apparently separated from the surrounding apatite matrix. This finding

[14] There is no direct evidence to prove that these particle clusters are unreacted α-TCP, which has the same chemical constituents as the surrounding matrix, and cannot be distinguished with our equipment. However, as shown in Fig. 3-8, the α-TCP synthesized is very pure and there is a noticeable difference, between Cements F prepared with L/P of 0.30 and 0.40, in the results of XRD (Fig. 3.8) and SEM (Fig. 3.9 A, B, C, D), which in all strongly indicates the presence of unreacted α-TCP. Additionally, the morphology of these particle clusters shown in Fig. 3-9C is similar to that of pristine α-TCP (Fig. 2-2), which can further support this hypothesis.

is consistent with the result of XRD (Fig. 3-8), further verifying the existence of unreacted α-TCP in the final composition of Cement F prepared using the same L/P ratio. On the contrary, no such large voids can be seen on the surface of Cement F with L/P ratio of 0.4 at the magnification of 200× (Fig. 3-9B). Furthermore, no unreacted α-TCP can be observed on the same surface at a higher magnification (Fig. 3-9D). This is probably due to the small amount of unreacted α-TCP for this L/P ratio, which is very difficult to be observed by means of SEM. Despite this difference, the morphology and size of the formed apatite crystals, which are mainly needle-like and at nanometer or submicron level, of the two Cements F using L/P of 0.3 (Fig. 3-9E) and L/P of 0.4 (Fig. 3-9F) seem to be similar.

3.2.1.3 Mechanical properties of Cement F

Mechanical properties (Young's modulus, E, fracture toughness, K_{IC} and compressive strength, σ_r) of Cement F prepared using different L/P ratios are shown in Fig. 3-10. Each value is the mean of five measurements with the error bar showing one standard deviation. The solid curve in each figure is a power law fitting of the measured data, and the corresponding equation in the figure shows the relationship between each mechanical property and porosity. This modeling part will be discussed later. As expected, all the above measured mechanical properties decrease with the increase of porosity. Indeed, it is well known that porosity has a great influence on the mechanical properties of materials. The porosity dependence of elastic modulus and strength of materials has been widely studied (see for instance Barralet et al., 2002; Gibson, 1985; Hing et al., 1999; Liu, 1997; Rodriguez-Lorenzo et al., 2002; Tancret et al., 2006; Zhang et al., 2006;).

In order to better understand the physical phenomena and help in the design of materials with desirable mechanical properties, many different models have been put forward to describe the evolution with porosity of mechanical properties of materials. In the present situation, we have deliberately selected a model with a small number of parameters: given the usual scatter in the measurement of mechanical properties of brittle materials, models with two parameters are generally sufficient.

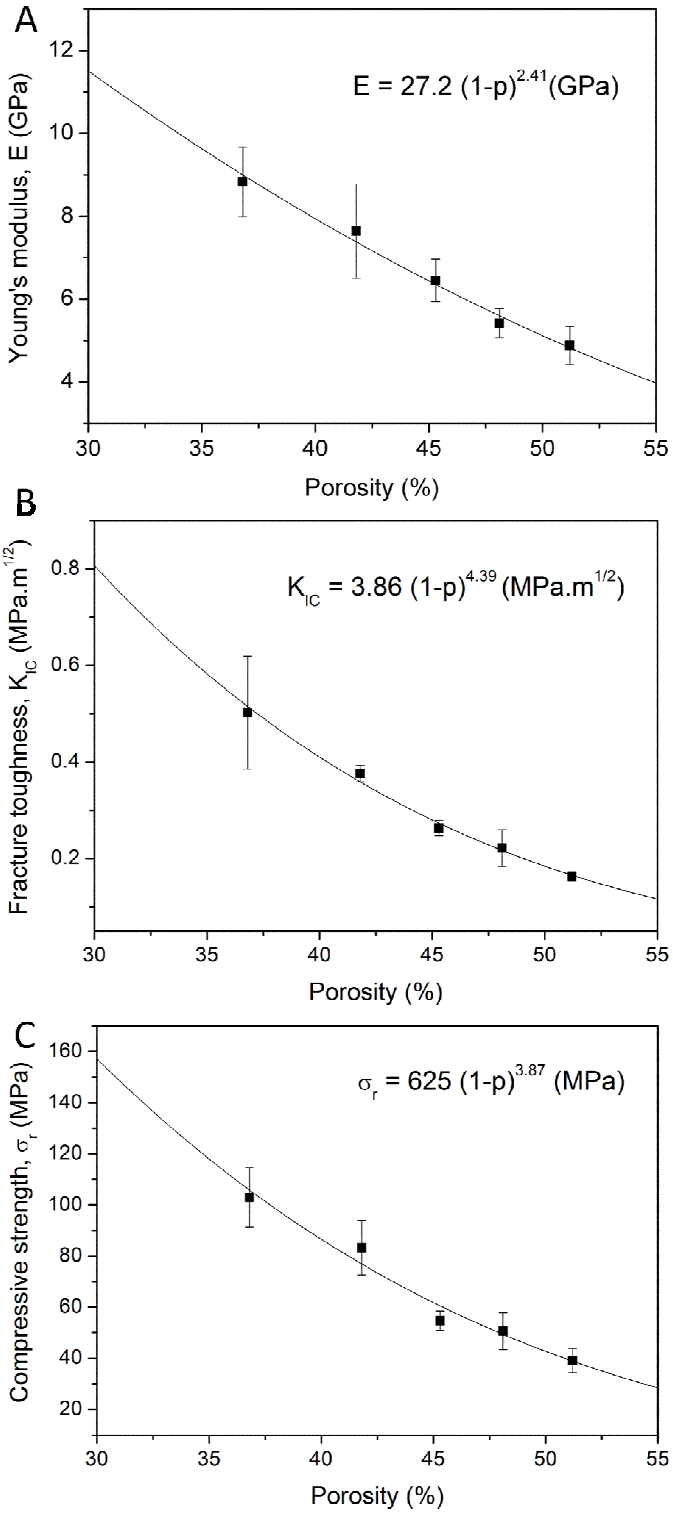

Fig. 3-10 Evolution of Young's modulus (A), fracture toughness (B) and compressive strength (C) as a function of porosity. Each point represents the mean of five specimens ± one standard deviation.

According to this requirement, both power law:

$$X = X_0.(1-p)^a \qquad (3\text{-}1)$$

and exponential law:

$$X = X_0.e^{-bp} \quad (3\text{-}2)$$

which are two of the most often used models, seem to work very well on this point. In these two equations, X is a selected mechanical property of a porous material, X_0 is the same property of the fully dense material, p is the porosity of the material, and both a and b are constants related to pore characteristics.

However, with further comparison, the first one seems to be more suitable in our present study. The first reason is that theoretically it predicts that when porosity p = 1 (or density is zero), X = 0, which must be fulfilled in all cases, while it is not the case for the exponential law; the use of the latter should therefore be restricted to low porosities (Rice 1996). Furthermore, the present microstructures, composed of thin entangled needle-like and/or plate-like crystals at the microporosity scale, and/or of "isolated" macropores (discussed in section 3.3), are similar to those of cellular materials, in which cells can be either closed ("isolated" pores) or open (typical of "trabecular" structures). These latter structures have been extensively studied by Gibson and Ashby (1982, 1985 and 1999), proposing models based on power laws to describe porosity-mechanical properties relationships. Finally, basing on the power law model proposed by Wagh et al., (1991, 1993), and later corrected by Arató (1996) and Tancret et al. (1997), Tancret et al., (2006) further developed the models and successfully applied them to macroporous BCP ceramics. From a scientific point of view, there is also a need to try and confirm the validity of the models in CPC. Therefore, according to the above reasons, a power law (Eq. 3-1) rather than an exponential law (Eq. 3-2) is chosen throughout the study to describe the evolution with porosity of mechanical properties of CPC.

In the present study, the modeling of mechanical properties with porosity can be conducted in two steps. The first one is to confirm the validity of a power law model to fit the measured data. By fitting equation (3-1) to the measured properties, the best fits obtained are shown in Fig. 3-10. All the measured data can be fitted rather well, with a coefficient of determination R^2 = 0.97, 0.99 and 0.96, for Young's modulus, fracture toughness and compressive strength respectively, which strongly supports the validity of power law models. The regressions for the three mechanical properties result in the following relationships:

$$E = 27.2.(1-p)^{2.41}\ \text{GPa} \tag{3-3}$$

$$K_{IC} = 3.86.(1-p)^{4.39}\ \text{MPa.m}^{1/2} \tag{3-4}$$

$$\sigma_r = 625.(1-p)^{3.87}\ \text{MPa} \tag{3-5}$$

The above three equations may be used as predictive models for the corresponding mechanical properties. However, the coefficients of these equations are property-specific; therefore, from a theoretical point of view, it would be more meaningful if an inter-relationship could be established between them, as initially proposed by Wagh et al (1993). This demand guides the work of modeling to its second step. In previous reports (Tancret et al., 2006; Pecqueux et al., 2010), the authors developed series of models and applied them to microporous BCP ceramics, proposing that the same function can be used to describe the three relative mechanical properties, X/X_0 (Young's modulus, fracture toughness and compressive strength). The derivation of the common function has been reviewed in the section 1.5.3. Nevertheless, for the purpose of better understanding, it is still worth recalling the hypotheses required during the derivation of a common function i.e., in the present case, of a common exponent in the power law: constancy of fracture mechanisms over the whole range of porosity and constancy in the critical flaw size. In the case of Cement F, it was, however, impossible to fit the three curves with the same value of a. A fitting of all three curves, using the same exponent, is nevertheless shown in Fig. 3-11.

Apparently, a common exponent value of a = 4.13 can only be found for fracture toughness and compressive strength, but not for Young's modulus. The solid curves in Fig. 3-11B and C represent such a fitting of fracture toughness and compressive strength, with K_{IC0} = 3.31 $MP.m^{1/2}$ and σ_{r0} = 730 MPa respectively. The solid curve in Fig. 3-11A shows the "virtual" evolution of Young's modulus using the same value of a as for fracture toughness and compressive strength, and for a matched value of E_0 = 84 GPa. If the trend seems to be justifiable for high porosities (i.e. high L/P ratios), there is an obvious overestimation for low porosities (i.e. low L/P ratios: 0.3 and 0.35).

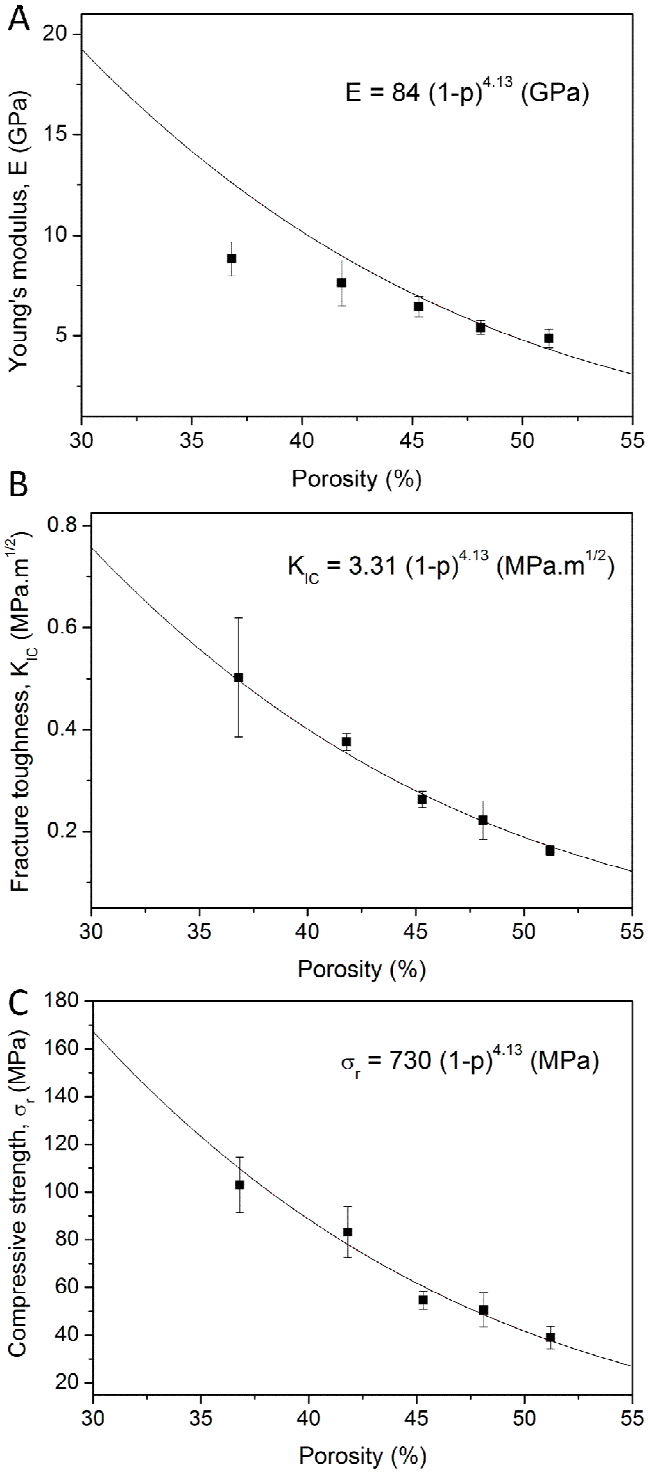

Fig. 3-11 Evolution of Young's modulus (A), fracture toughness (B) and compressive strength (C) as a function of porosity. Each point represents the mean of five specimens ± one standard deviation.

This could be explained if the unreacted α-TCP is taken into account. In fact, as shown in Fig. 3-8, unreacted α-TCP could be detected with XRD, especially for L/P ratios of 0.30 and 0.35. Moreover, by means of SEM, it was observed that the unreacted α-TCP particles were separated from the CDHA matrix by empty spaces which can be compared

to “cracks” (Fig. 3-9C), or at least to zones without cohesion. The more unreacted α-TCP left, the more “cracks” the Cement F matrix contains, provoking a decrease in Young’s modulus and the observed deviation from the curve. Nevertheless, this “microcracking” does not seem to influence toughness, which agrees with reported cases in other multi-cracked materials (Tancret et al., 2001), or with the famous case of aluminum titanate, which shows a toughness similar to that of alumina but a ten times lower Young’s modulus due to serious microcracking.

Furthermore, from the microstructural point of view (i.e. microcracks), the influence of unreacted α-TCP on the mechanical properties of CPC seems to be similar to that of β-TCP on the mechanical properties of some BCP ceramics although the specific effect is different. For the latter, β-TCP, in most cases, is proved to be detrimental to the strength of ceramics due to the introduction of microcracks during a change in volume accompanying the reversible phase transformation (β-TCP to and from α-TCP) that can take place during sintering (Wagoner Johnson et al., 2011). In comparison, as discussed above, the negative effect of unreacted α-TCP crystals could be attributed to the “microcracks” between them and the CDHA matrix. Finally, the extrapolated values (E_0 = 84 GPa, σ_{r0} = 730 MPa) can be compared to reported measurement on dense sintered hydroxyapatite which has a E_0 = 117 GPa and σ_{r0} = 800 MPa (De With, et al., 1981). Therefore the present results for CPC do not seem to be abnormal although the microstructure is very different from that of ceramics. Moreover, although the extrapolated values for the mechanical properties of “dense CPC” agree well with published results, it is here important to note that such “virtual” values might not be reachable for real dense CPC, as the fracture mechanisms may change when porosity is reduced (this will be discussed in Chapter 4), and above all because it is impossible to produce a dense CPC. Nevertheless, the role of modeling is still interesting, as it is a useful way to explain and understand experimental observations.

3.2.2 Influence of microporosity on Cement C

3.2.2.1 Porosity of Cement C

The porosity of Cement C prepared with different L/P ratios is plotted in Fig. 3-12. Similar to Cement F, the total porosity of Cement C increases with increasing L/P ratio, ranging from 38% to 52%. This can also be attributed to the higher proportion of liquid phase in the constant volume of the mold. Moreover, when compared to Cement F, the

total porosity of Cement C is significantly lower at the same L/P ratio (except for a L/P ratio of 0.3); this is probably due to the different mass of paste loaded per mold. Indeed, with the same paste volume the fine powder, which has a larger specific surface area, requires more liquid to be wetted, thus reducing the actual amount of powder in the mold, and vice versa. Furthermore, this could also be related to different particle morphologies, hence to different packing abilities of the grains in the pastes.

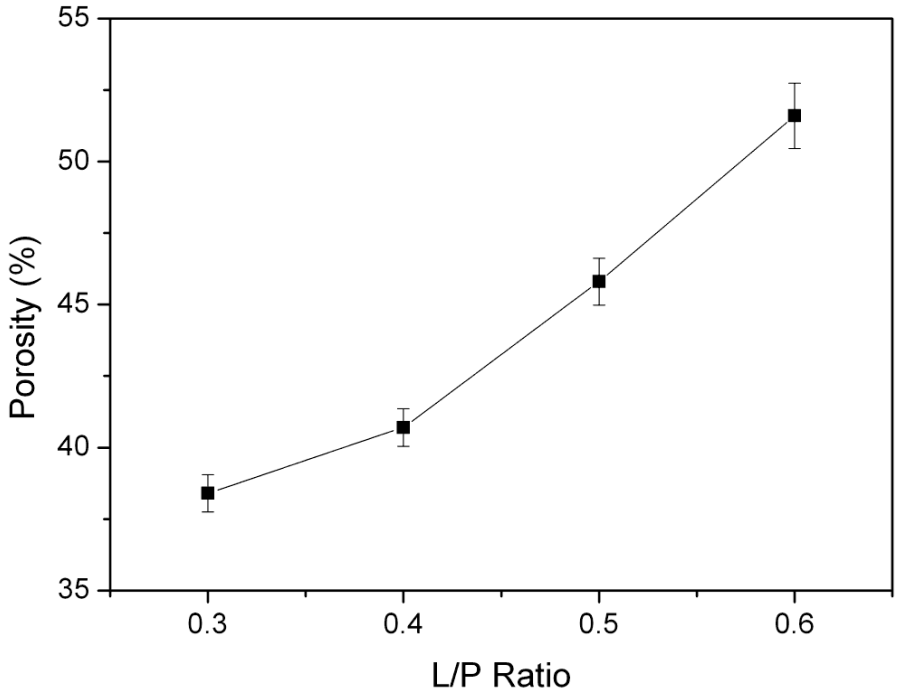

Fig. 3-12 Porosity of Cement C as a function of the L/P ratio. Each point represents the mean of five specimens ± one standard deviation.

3.2.2.2 Phase and microstructural features of Cement C

The XRD patterns of Cement C prepared with different L/P ratios are shown in Fig. 3-13. For easy comparison, the top pattern corresponds to the initial α-TCP powder, and just below is the pattern of the cement prepared with the fine powder with a L/P ratio of 0.3. In comparison with the cement prepared from the fine powder, it can be observed that the coarse α-TCP powder has transformed into CDHA with a great deal of unreacted α-TCP as evidenced by the obvious peaks of α-TCP. This can be interpreted by a simple size effect, that it is more difficult to completely dissolve large particles than to dissolve small ones (different kinetics). Moreover, similar to Cement F, the amount of unreacted α-TCP gets lower with the increasing L/P ratio, and this can also be explained by the same hypotheses as those proposed for Cement F (see 3.2.1.2).

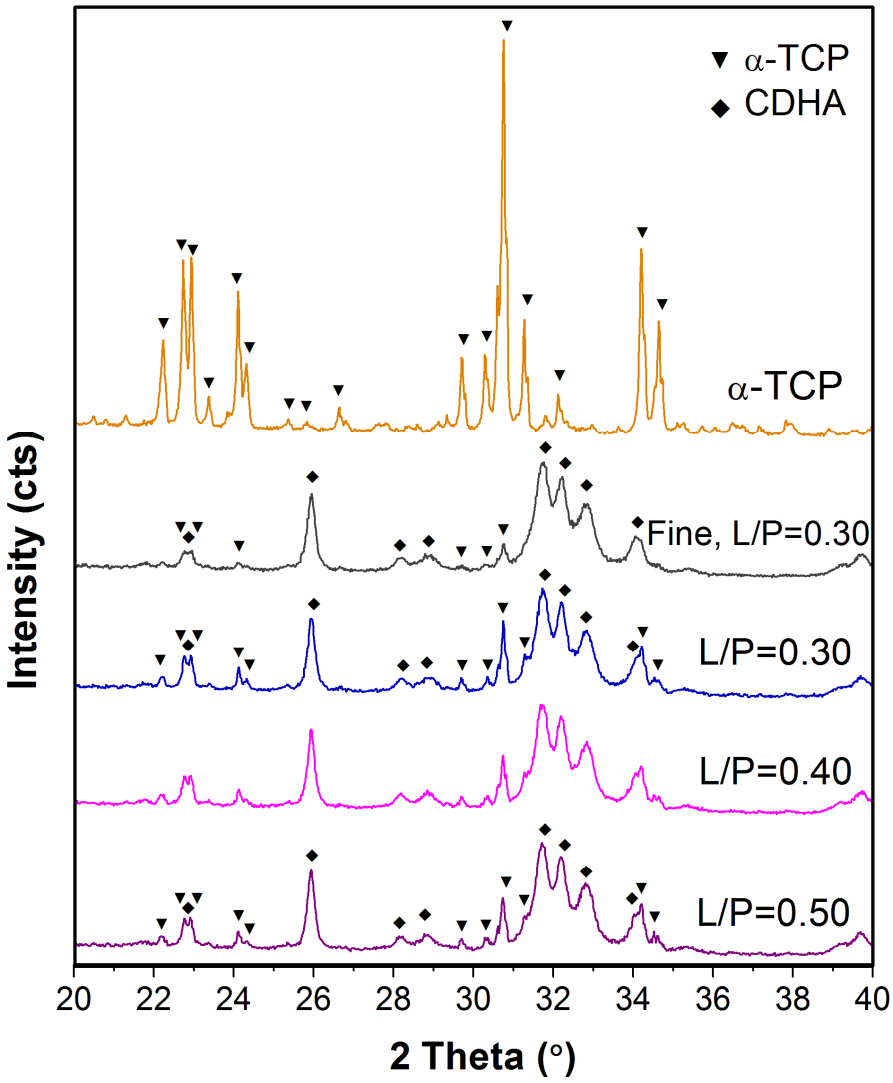

Fig. 3-13 XRD patterns of Cement C prepared with different L/P ratios

The fracture surfaces of Cement C prepared with two different L/P ratios, as observed by SEM, are shown in Fig. 3-14. Unreacted α-TCP can be seen on the fracture surface of the Cement C with a L/P ratio of 0.3 at a magnification of 250× (Fig. 3-14A). Similarly, some unreacted α-TCP can also be observed in the Cement C with a L/P ratio of 0.5, but with much less quantity (Fig. 3-14B). Both of the above SEM observations are consistent with the result of XRD that the lower the L/P ratio, the more unreacted α-TCP (Fig. 3-13). At a higher magnification of 2500×, no matter the L/P ratio (0.3, Fig. 3-14C; 0.5, Fig. 3-14D), it is very easy to find some cracks along the edge of unreacted α-TCP particles, separating them from the surrounding CDHA matrix and indicating a weak link between the unreacted α-TCP and CDHA crystals. This finding is also similar to the observation of Cement F prepared with a L/P ratio of 0.3 (Fig. 3-9C).

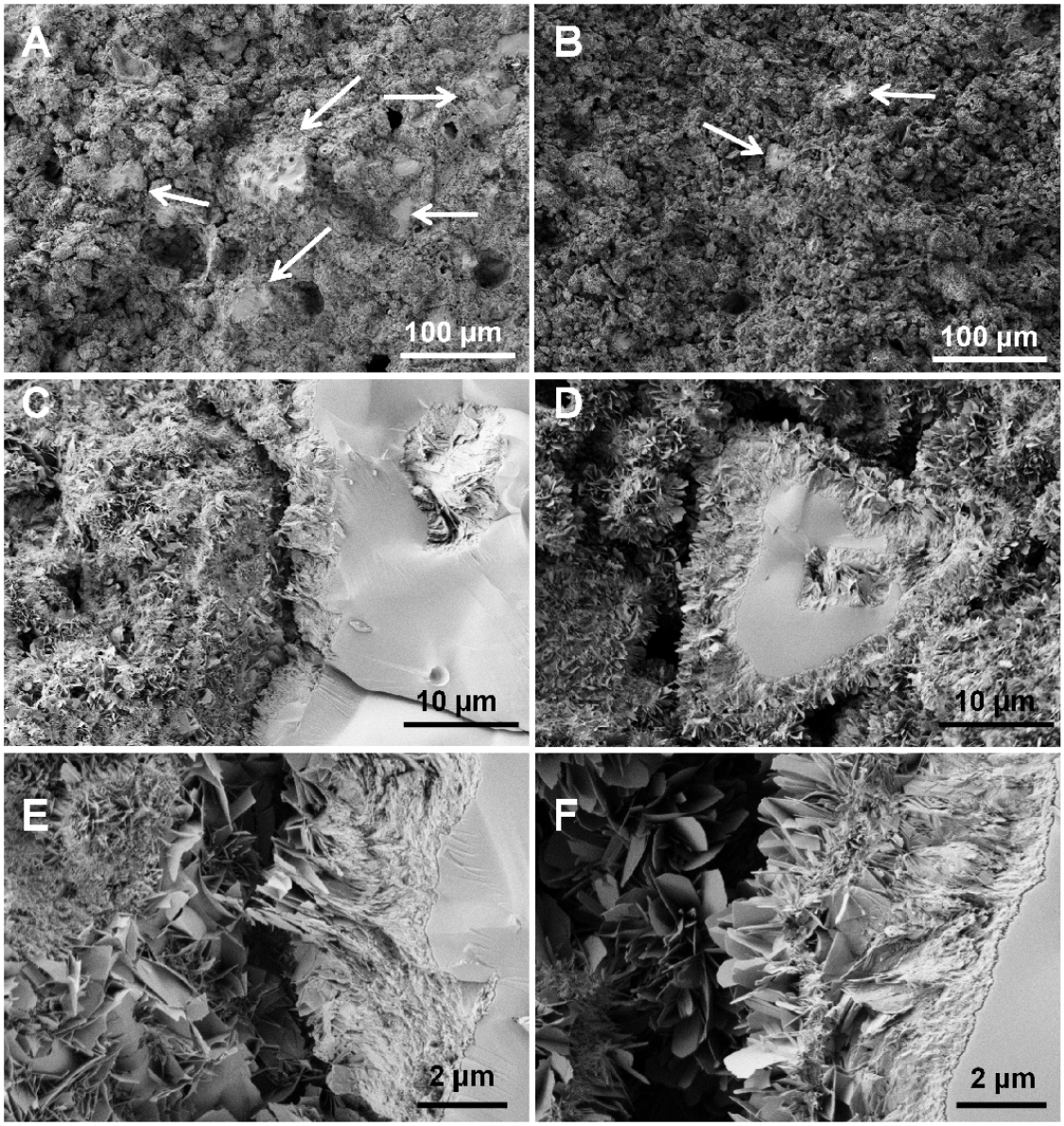

Fig. 3-14 SEM micrographs of Cement C fracture surfaces: (A), (C), (E) Cement C prepared with L/P ratio 0.30; (B), (D), (F) Cement C prepared with L/P ratio 0.50. The white arrows in (A) and (B) point to unreacted α-TCP.

Moreover, the morphology and size of the formed apatite crystals of the two Cements C with different L/P ratios were examined at a magnification of 10 000×. No noticeable difference can be seen between the two Cements C, neither in the crystal shape, which is mostly plate-like, nor in size, which is at nanometer or submicron scale. In addition, the formed apatite crystals of Cement C are larger than those of Cement F (Fig. 3-9E, F). This can be explained by the higher degree of supersaturation achieved by the dissolution of the powder with a higher specific area. In fact, a higher supersaturation in the solution helps the formation of crystalline nuclei, resulting in the precipitation of

more crystals. When the supersaturation is lower, less nuclei precipitate and crystal growth is favoured (Espanol et al., 2009; Ginebra et al., 2004).

Fig. 3-14E and F also clearly reveal the process of apatite crystals formation from α-TCP particles: layers of several micrometers of nano-sized/submicron-sized, plated-like apatite crystals are attached to the unreacted α-TCP particle with a gradual densification of the apatite crystals from the outside layer towards the inside layer.

3.2.2.3 Mechanical properties of Cement C

Mechanical properties (Young's modulus, E, fracture toughness, K_{IC}, and compressive strength, σ_r) of Cements C prepared with different L/P ratios are plotted in Fig. 3-15.

Each value is the mean of five measurements with the error bar showing one standard deviation. As expected, all the above measured mechanical properties decrease with increasing porosity. Moreover, like Cement F, in order to better explain and understand experimental observation, a power law is also used to describe the evolution with porosity of mechanical properties of Cement C. However, as discussed in the case of Cement F (3.2.1.3), it is firstly necessary to test the validity of the power law on the measured data. The best fits of equation (3-1) to the data are shown in Fig. 3-15.

As can be seen, all the measured data can be fitted rather well, with $R^2 = 0.98$, 0.99 and 0.97, for Young's modulus, fracture toughness and compressive strength respectively, which supports the validity of the power law model in the case of Cement C. The regressions for the three mechanical properties result in the following relationships:

$$E = 16.4.(1-p)^{2.93}\ \text{GPa} \tag{3-6}$$

$$K_{IC} = 2.34.(1-p)^{3.79}\ \text{MPa.m}^{1/2} \tag{3-7}$$

$$\sigma_r = 469.(1-p)^{4.89}\ \text{MPa} \tag{3-8}$$

Like Cement F, although the coefficients of the above three equations are property-specific, these equations can still be used as predictive models for the mechanical properties of Cement C.

After confirming the validity of the power law in the case of Cement C, which can be of practical interest, it is also desirable, from a theoretical point of view, to try to establish, between the three measured mechanical properties, an inter-relationship where the same

coefficient “a” can be used in the equations for Young’s modulus, fracture toughness and compressive strength.

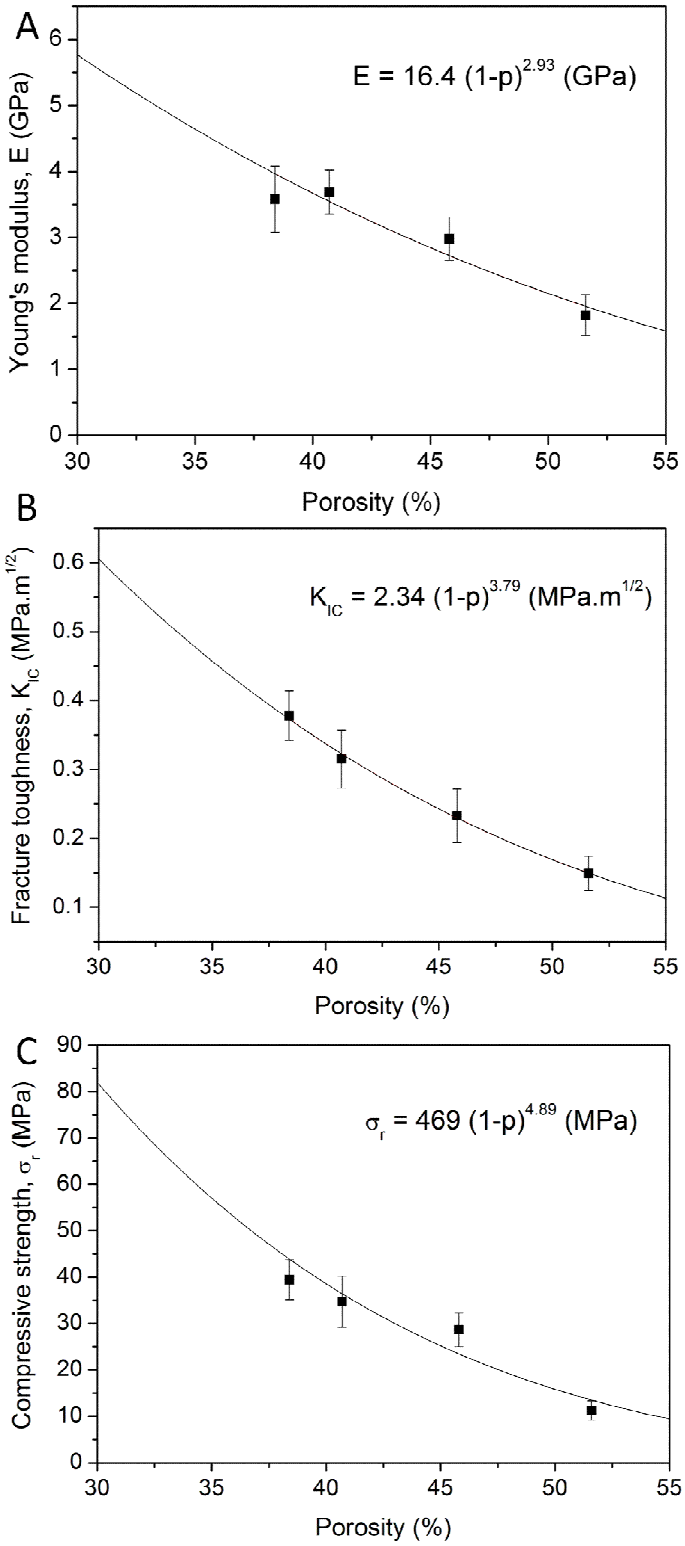

Fig. 3-15 Evolution of Young’s modulus (A) fracture toughness (B) and compressive strength (C) as a function of porosity for Cement C. Each point represents the mean of five specimens ± one standard deviation.

Unlike Cement F, all three properties can be described in Cement C with the same exponent a = 3.77 (Fig. 3-16), although the effect of "microcracking" on stiffness due to the presence of unreacted α-TCP can also be observed (Fig. 3-16A, Fig. 3-14). Indeed, all the cements prepared with the coarse powder contain prominent amounts of unreacted α-TCP (Fig. 3-13), and are therefore more "microcracked" than Cement F, which is consistent with the previous observation on Cement F: unreacted α-TCP reduces the Young's modulus through microcracking; this can therefore partly explain why the value of E_0 = 26.9 GPa for Cement C is only one third of E_0 = 84 GPa of Cement F. In addition, the data point for a L/P ratio of 0.30 appears significantly lower than what can be expected from the fitted curve; this is also consistent with a higher degree of "microcracking", associated to a higher fraction of unreacted α-TCP (Fig. 3-13).

The inter-relationship also gives K_{IC0} = 2.31 MPa.m$^{1/2}$ for Cement C, which is lower than that (3.31 MPa.m$^{1/2}$) of Cement F. This can be explained by considering the origin of fracture toughness (crack resistance ability) in CPC. In fact, without considering extrinsic toughening mechanisms such as fiber bridging and crack deflection (Launey et al., 2009; Ritchie, 2011), CPC is naturally brittle and its crack resistance ability mainly derives from the entangled apatite crystals. In the case of Cement C, it contains more plate-like, large apatite crystals than Cement F. In contrast, Cement F has more needle-like, smaller apatite crystals. The smaller the apatite crystals, the more the contact points, which may contribute to the higher fracture toughness of Cement F. Similar phenomenon has also been observed on other materials (Tancret et al., 2003). Moreover, this denser entanglement of apatite crystals in Cement F might also account for its higher Young's modulus than Cement C, in addition to the aforementioned mechanism. Finally, a strength value of σ_{r0} = 245 MPa could be derived for Cement C from the inter-relationship, which is much lower than that (730 MPa) of Cement F. Such a large difference in strength cannot be explained by toughness values alone, indicating a larger critical flaw size than in Cement F; this is consistent with a coarser microstructure, that additionally contains many "cracks".

This result appears different from a previous study (Espanol et al., 2009) where the strength of Cement F and C are rather similar, but the investigated particle sizes are quite different: 6 and 14 μm in our study, and 2.8 and 5.2 μm in the reported study. In the latter case, the particle sizes are smaller and might not directly influence the critical flaw size, whereas in our study both the coarser microstructure and the presence of "cracks" can play roles in the fracture initiation.

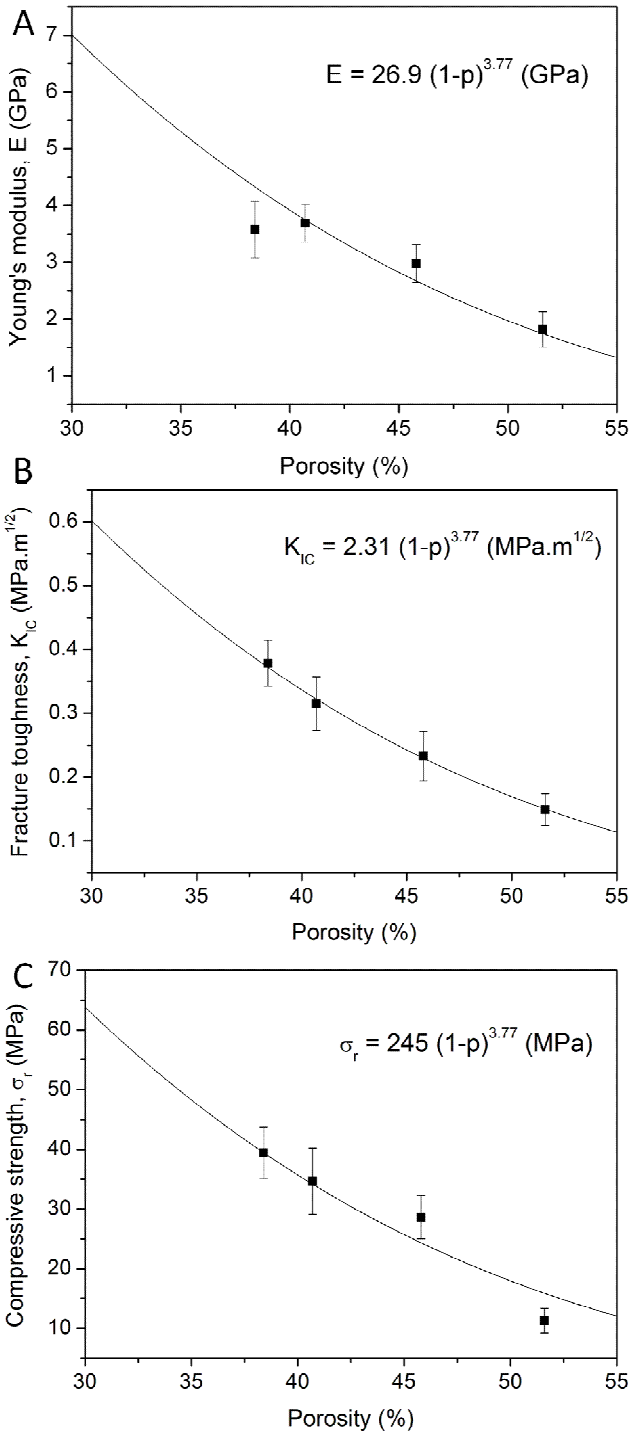

Fig. 3-16 Evolution of Young's modulus (A), fracture toughness (B) and compressive strength (C) as a function of porosity for Cement C. Each point represents the mean of five specimens ± one standard deviation.

3.3 "Microstructure" and mechanical properties of macroporous CPC

3.3.1 Porosity of Macro CPC

Before showing the results, it is worth restating that macroporous specimens were fabricated by adding, to the cement paste, mannitol particles as a porogen which is subsequently dissolved during the setting and hardening process. Because it was not possible to systematically map many couples of mannitol mass fractions and L/P ratios, it was chosen to fix a total L/P ratio, defined as the ratio between the amount of liquid and the total mass of solid phases (α-TCP + mannitol), and then to make the mannitol mass fraction vary. As a first approximation, and as explained in Chapter 2, it was assumed that the microporosity would be constant. This allowed calculating an estimate of macroporosity from the measurement of total porosity, using equation (2-7) of Chapter 2. Nevertheless, there is no physical reason why microporosity should be constant, and hence why this calculated macroporosity should be correct. As described in Chapter 2, the real macroporosity has been determined experimentally by image analysis on some specimens. Both calculated and measured macroporosities are presented on Fig. 3-17, showing that the macroporosity was initially overestimated.

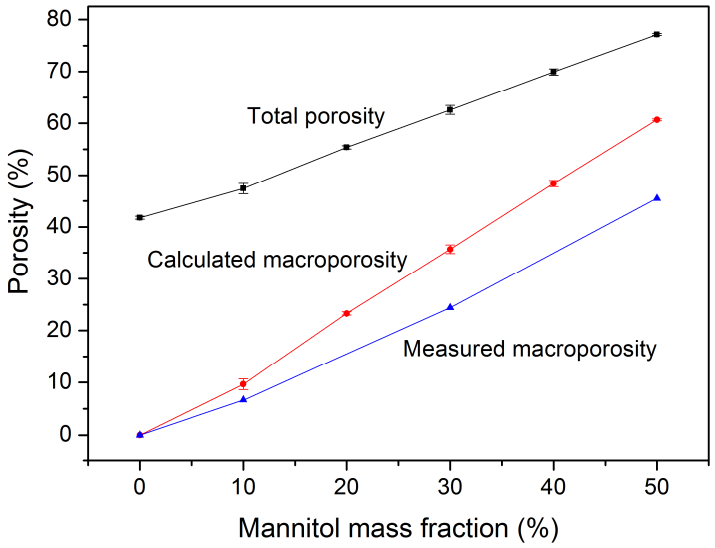

Fig. 3-17 Total porosity, calculated macroporosity and measured macroporosity of Macro CPC as a function of the mannitol mass fraction. For the former two, each point represents the mean of five specimens ± one standard deviation.

In what follows, only the macroporosity coming from measurements will be considered, and when necessary it will be estimated by linear interpolation of measurements, which corresponds to the blue solid lines on Fig. 3-17.

The consequence of this difference between calculated and measured macroporosities is that microporosity must not be independent of the mannitol mass fraction as initially approximated, and hence must not be independent of macroporosity. Indeed, reversing equation (2-7) yields:

$$p_{micro} = \frac{p_{total} - p_{macro}}{1 - p_{macro}} \tag{3-9}$$

The evolution of microporosity, calculated with equation (3-9) using the measured total porosity and the measured (or interpolated) macroporosity, is shown on Fig. 3-18. The horizontal line is the value that would have been obtained with the initial assumption that microporosity is independent of the mannitol mass fraction and of macroporosity; the difference is obvious.

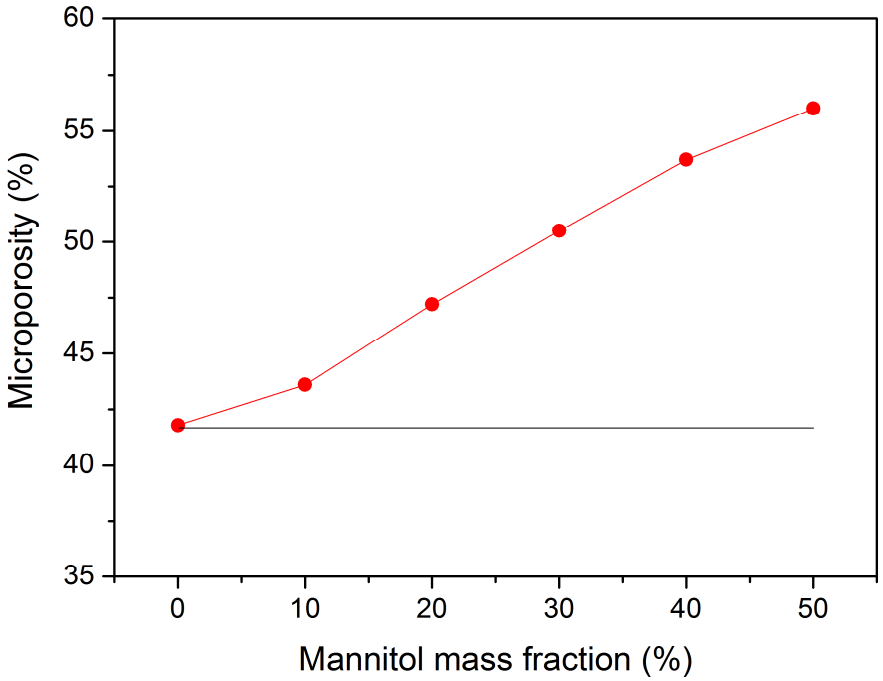

Fig. 3-18 The red dots and line represent the microporosity, calculated from measured total porosity and measured (or interpolated) macroporosity, as a function of mannitol mass fraction. The horizontal line represents microporosity which is assumed to be independent of mannitol mass fraction and used for the initial estimation of macroporosity.

3.3.2 Phase and microstructural features of Macro CPC

The XRD patterns of Macro CPC prepared with different mass fractions of mannitol are shown in Fig. 3-19.

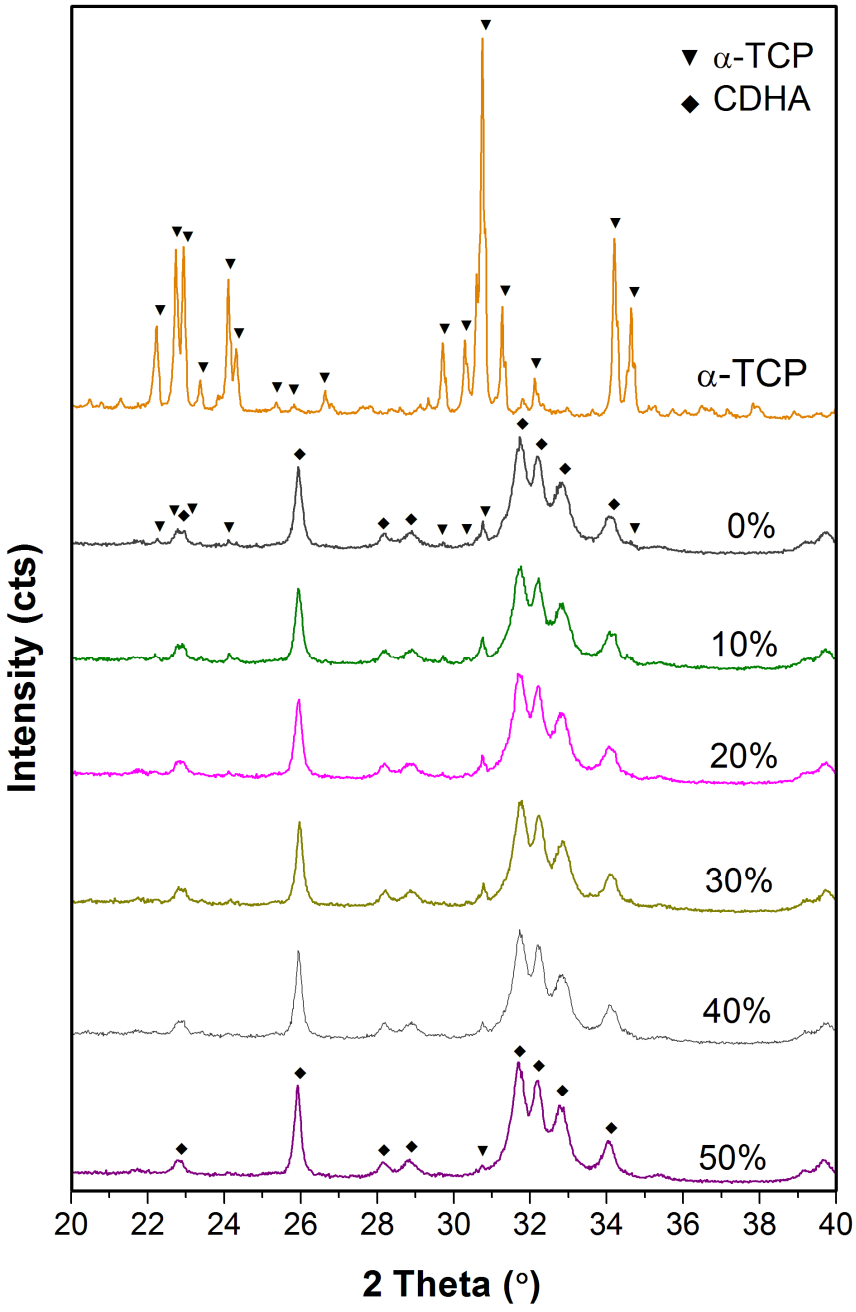

Fig. 3-19 XRD patterns of Macro CPC prepared with different amounts of mannitol.

For easy comparison, the first pattern is the pristine α-TCP powder. Below that is the pattern of CPC without adding mannitol, which is the same as Cement F with a L/P ratio of 0.35. The XRD patterns of Macro CPC with different mannitol mass fractions are

similar to that of Cement F, indicating that the addition of mannitol does not affect the hydration reaction of α-TCP. The reaction products are also poorly crystalline CDHA, which is consistent with previously reported observations (Shimogoryo et al., 2009). Furthermore, similar to Cement F, the peaks of unreacted α-TCP can also be found in these patterns, but the intensity of the major peaks of the unreacted α-TCP decrease with increasing mannitol mass fractions.

Once more, two hypotheses can be proposed to explain this. First, the total amount of water in the paste being determined from the total weight of powders (α-TCP + mannitol), it may occur that more water becomes available for reaction with α-TCP when the mannitol mass fraction is increased, corresponding to an increase of the effective L/P ratio of the mineral part of the cement. The observed trend would then agree with the results of Fig. 3-6. The second hypothesis is, as for the fine powder, based on "geometry": when the mannitol mass fraction increases, macroporosity left by its dissolution increases and therefore the permeability of the material increases, allowing water to flow more easily inside the material and improving its contact with α-TCP, enhancing the chemical reaction and leading to less unreacted α-TCP.

The fracture surfaces of Macro CPC as observed by SEM are shown in Fig. 3-20. As expected, no macropores are found in the CPC with 0% mannitol (Fig. 3-20A). On the contrary, some macropores from mannitol dissolution and of hundreds of micrometers appear to be well-formed in the shapes of the entrapped mannitol particles and are randomly distributed on the surface of CPC with 10% mannitol (Fig. 3-20B). As mannitol mass fraction increases (30%, Fig. 3-20C; 50%, Fig. 3-20D), more macropores are observed on the surface of CPC, with different orientations indicating that the mannitol particles are well mixed and homogeneously distributed during the preparation of specimens. In addition, no noticeable difference is observed in macropore size or shape between the samples with different mannitol mass fractions.

Fig. 3-20E shows, at a high magnification, the details of an irregularly shaped macropore which is probably created by the dissolution of several connected mannitol particles. Finally, the microstructure of the Macro CPC matrix was examined (Fig. 3-20F). No noticeable differences can be found between the latter and Cement F in both the morphology and size of the formed apatite crystals, indicating that the addition of mannitol does not affect the formation and growth of CDHA crystals (Shimogoryo et al., 2009).

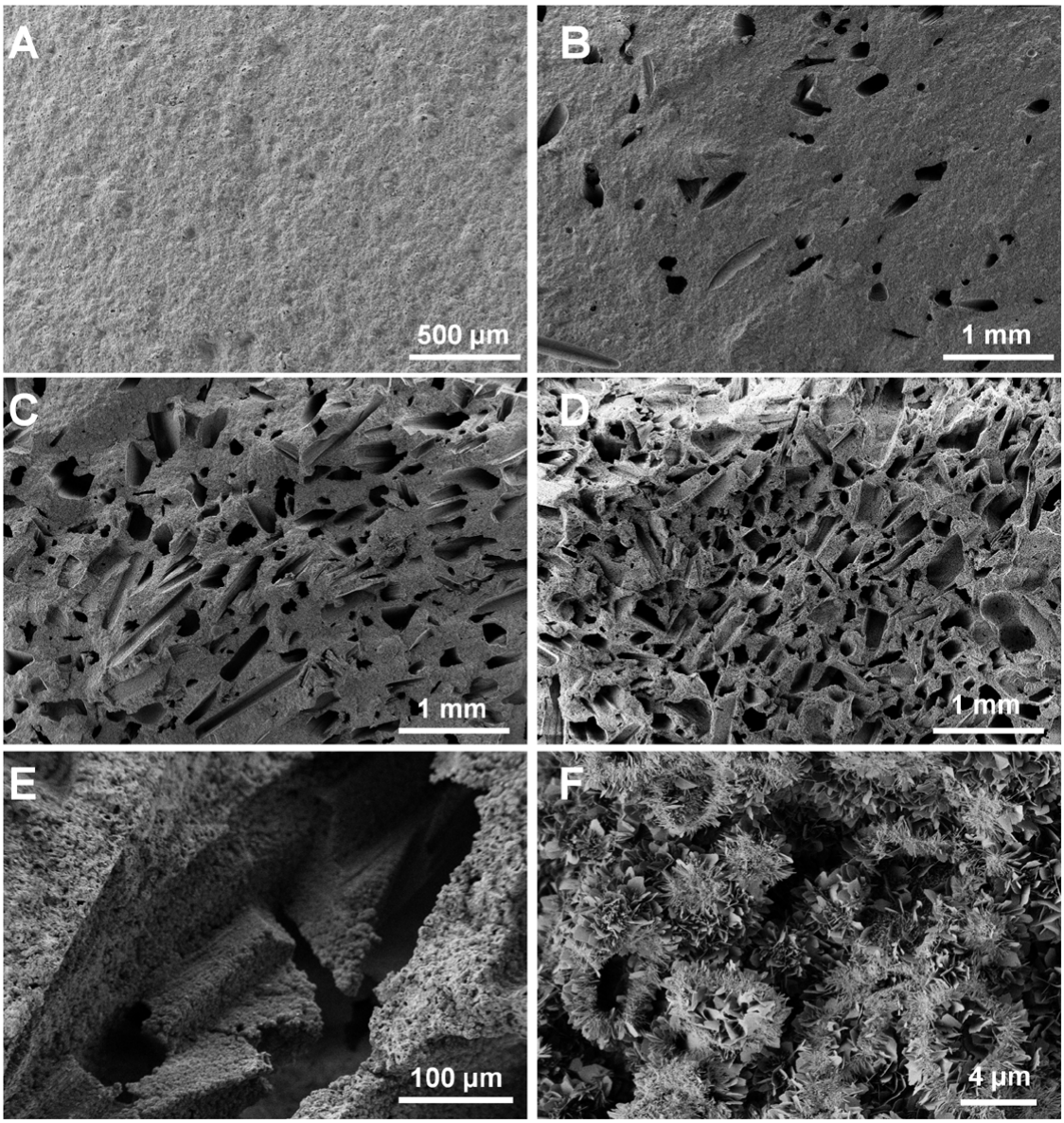

Fig. 3-20 SEM micrographs of Macro CPC fracture surfaces: (A) CPC with 0% mannitol showing no macropores; (B) CPC with 10% mannitol; (C) CPC with 30% mannitol; (D) CPC with 50% mannitol; (E) CPC with 40% mannitol showing details of macropores; (F) microstructure of the Macro CPC matrix at a high magnification.

3.3.3 Mechanical properties of Macro CPC

Mechanical properties (Young's modulus, E, fracture toughness, K_{IC} and compressive strength, σ_r) of Macro CPC with different mannitol mass fractions are shown in Fig. 3-21. Each value is the mean of five measurements with the error bar showing one standard deviation.

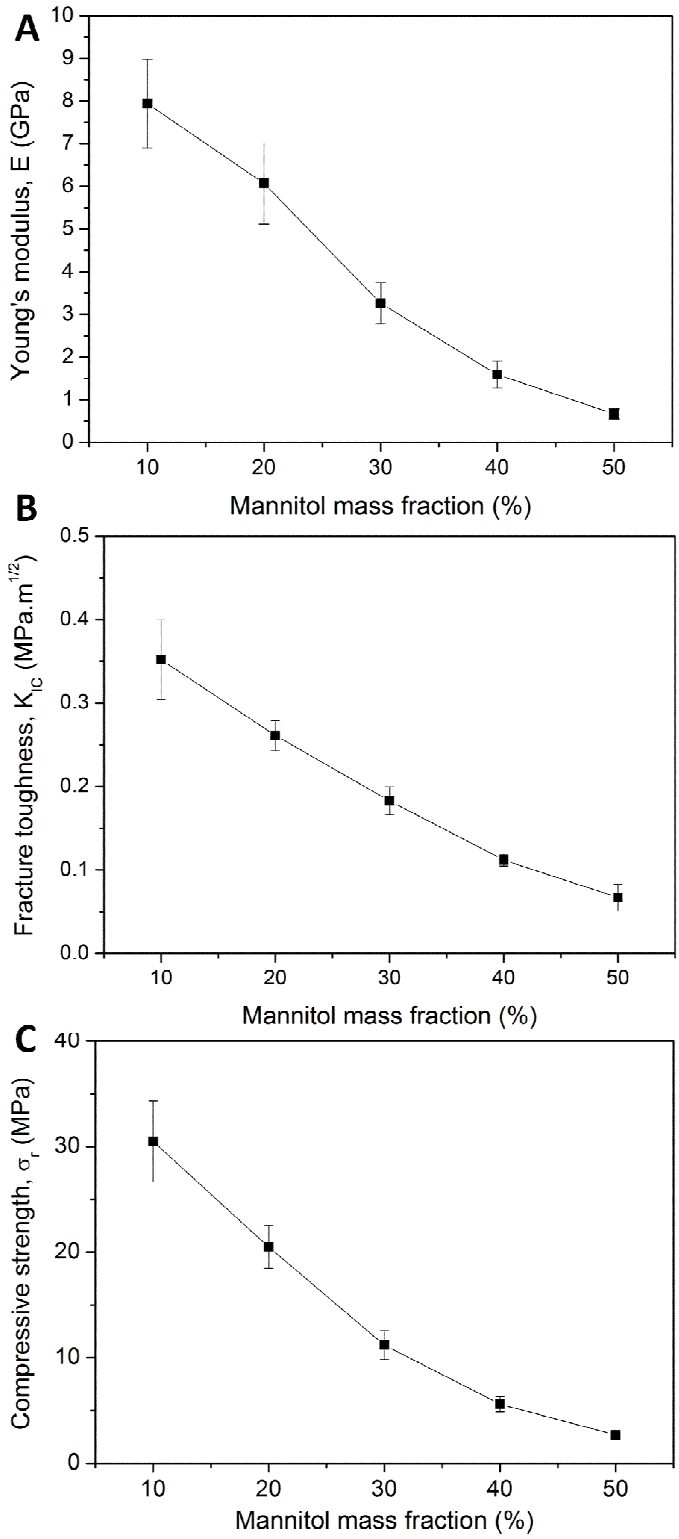

Fig. 3-21 Mechanical properties of Macro CPC as a function of mannitol mass fraction. Each point represents the mean of five specimens ± one standard deviation.

As expected, all the measured mechanical properties decrease with increasing macroporosity (mannitol mass fraction). Similar to Cement F and Cement C, for a better understanding of experimental observation, a power law will be applied to try to describe

the evolution with macroporosity of mechanical properties of Macro CPC, and it can be expressed using the following expression:

$$X = X_m.(1-p_{macro})^c \quad (3\text{-}9)$$

where p_{macro} is the measured macroporosity of Macro CPC, and c is a parameter related to pore characteristics. Moreover, it is important to note that here X_m does not correspond to the dense material, but to the properties of similar materials without macropores (e.g. Cement F with intrinsic microporosity). In other words, X_m is supposed to be the (virtual) mechanical property of the microporous matrix between macropores.

However, the formulation of equation (3-9) cannot be directly used in the case of Macro CPC to model its mechanical properties because X_m is not a constant but a function of microporosity. Indeed, as shown in Fig. 3-18, the microporosity of the cement matrix between macropores increases with the increasing mannitol mass fraction; as a consequence X_m must vary concomitantly.

For this reason, the effect of microporosity of the cement matrix should be taken into account simultaneously, as discussed in section 3.2.1.3 and expressed as:

$$X_m = X_0.(1-p_{micro})^a \quad (3\text{-}10)$$

where p_{micro} is the intrinsic microporosity of the matrix. Combining the last two equations, this gives:

$$X = X_0.(1-p_{micro})^a.(1-p_{macro})^c \quad (3\text{-}11)$$

in which the effect of macropores and micropores are considered separately. This constitutes a new model describing the mechanical properties of CPC being both microporous and macroporous, although the model construction, i.e. combining different models for microporosity and macroporosity taken separately, is equivalent to what had been proposed in the case of BCP ceramics, with however different equations (Tancret et al. 2006, Pecqueux et al., 2009, 2010). However, in the present case, because microporosity and macroporosity are not independent, it is not possible to infer simultaneously the values of a and c from the data. Therefore, it will be assumed that the dependence of mechanical properties on microporosity are similar in Cement F and

Macro CPC, so that the value of "a" can be taken equal to the one determined during the study on Cement F (a = 4.13). Then the equation 3-11, in conjunction with a = 4.13, is used to model the mechanical properties of Macro CPC and to check the possibility of using a common exponent "c".

In addition, because macroporosity and microporosity are interdependent, plotting mechanical properties as a function of the solely macroporosity would not represent any physical trend. For this reason, another method is used to display the results by plotting the measured values as a function of the calculated ones (Fig. 3-22).

Good fits can be obtained, giving the following relationships:

$$E = 96.6.(1-p_{micro})^{4.13}.(1-p_{macro})^{1.55} \quad \text{GPa} \tag{3-12}$$

$$K_{IC} = 4.47.(1-p_{micro})^{4.13}.(1-p_{macro})^{1.55} \quad \text{MPa.m}^{1/2} \tag{3-13}$$

$$\sigma_r = 400.(1-p_{micro})^{4.13}.(1-p_{macro})^{2.5} \quad \text{MPa} \tag{3-14}$$

As shown in Fig. 3-22, a good agreement is obtained for all the mechanical properties studied between the measured and the calculated values. In addition, the determined reference values for Young's modulus and fracture toughness are 96.6 GPa and 4.47 MPa.m$^{1/2}$, which are also comparable to that of Cement F, confirming the validity of proposed equation 3-11 being used in the case of Macro CPC. Furthermore, as noted in equations 3-12, 13 and 14, a common exponent c = 1.55 can only be used for Young's modulus and toughness, but not for compressive strength whose "c" is 2.5. This finding is consistent with a recent study focusing on macroporous BCP ceramics (Pecqueux et al., 2010), where the exponent in the power law associated to compressive strength was also higher than those of the Young's modulus and toughness, the latter two being identical. This feature had been related to an increase in the critical flaw size as a function of macroporosity, and explained as follows.

When there was only a limited number of macropores in the specimen, macropores were widely dispersed in the material (as in the case of CPC, see Fig. 3-20B) and did not interact strongly with each other. When macroporosity increased, the average distance between nearby macropores decreased, and their associated stress concentration fields started to interact.

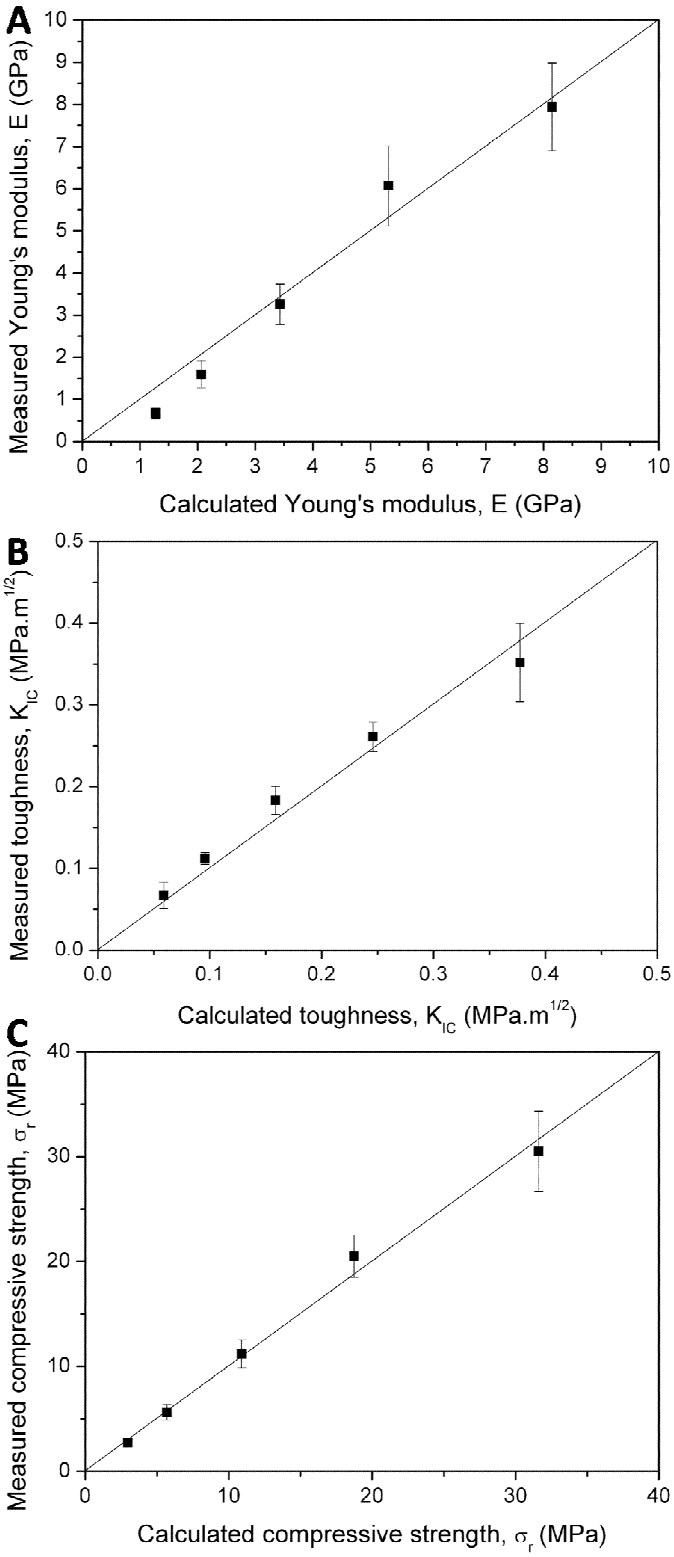

Fig. 3-22 Comparison between measured and calculated values for (A) Young's modulus, (B) fracture toughness and (C) compressive strength. Each point represents the mean of 5 specimens ± one standard deviation.

Moreover, from a statistical viewpoint related to the total number of macropores, there was an increasing probability to find groups of macropores in some areas. During

compression loading, these groups of macropores could become critical flaws through subcritical microcrack growth and linking before reaching the peak stress, acting as new enlarged critical flaws instead of single macropores. As macroporosity increased, these groups of macropores would statistically become larger, which was therefore associated with an increasing critical flaw size. This has been suggested to occur in other macroporous ceramics (Pernot et al. 1999). The role of such groups of macropores on fracture initiation has also been investigated by Cannillo et al. (2004), using finite element simulation, in model microstructures in two dimensions. This study has shown that in the case of groups of macropores, subcritical cracks would form during compression loading, progressively linking the pores in the loading direction. It is therefore possible that a similar mechanism acts in Macro CPC.

As for the reported BCP ceramics, in the case of our cements the above hypothesis can be further evidenced by plotting the quantity $(K_{IC}/\sigma_r)^2$, which is proportional to the critical flaw size[15], as a function of macroporosity (Fig. 3-23).

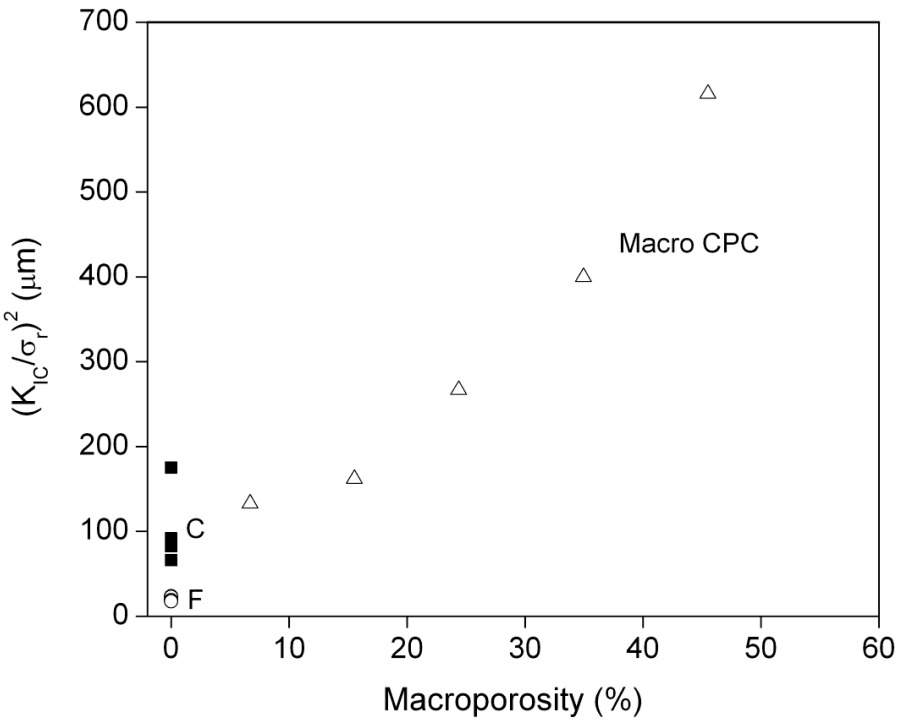

Fig. 3-23 Variation of $(K_{IC}/\sigma_r)^2$ as a function of macroporosity, for Cement C, Cement F and Macro CPC.

As shown in Fig. 3-23, the range of critical flaw size is roughly constant for cements

[15] As reviewed in chapter 1, fracture toughness K_{IC} can be expressed as $K_{IC} = Y\sigma_r c^{1/2}$ (see P25). From K_{IC} and σ_r, we can further deduce $Y^2c = (K_{IC}/\sigma_r)^2$, which is therefore proportional to the critical flaw size c.

prepared without macropores (Cement F on the one hand and Cement C on the other hand, the latter having a somewhat larger critical flaw size, due to its coarser microstructure as discussed in 3.2.2.3). In contrast, the critical flaw size of Macro CPC pronouncedly increases with the increasing macroporosity, which is similar to the observation in macroporous BCP ceramics (Pecqueux et al., 2010), and supports the hypothesis proposed previously.

Therefore, the initial hypothesis for the derivation of a common exponent "c", that the critical flaw is always of the same size, is not effective for Macro CPC ; this can explain the different exponents fitted for fracture toughness and compressive strength (equations 3-13 and 3-14). Similarly, the roughly constant critical flaw sizes for Cement F or Cement C are consistent with the fact that common exponents can be used to fit both fracture toughness and compressive strength (Cement F, Fig. 3-11; Cement C, Fig. 3-16).

However, it would be useful to further test such hypotheses by other means. The first one would be a direct observation of fracture mechanisms in situ, but this is an extremely difficult task in brittle materials, which can become even more complex in highly porous media. Another possibility is to push forward the mechanical analysis, by evaluating the values of critical flaws and comparing them to the actual microstructures.

In fact, compression fracture in brittle materials, and in particular in porous brittle materials, can proceed through the catastrophic propagation of a crack parallel to the applied stress, initiating from a critical flaw (Saimoto et al., 2003). But it can also, in some cases, occur by a progressive accumulation of stable damage (Sammis et al. 1986). In our case, sudden fracture occurs, as evidenced by the shape of the loading curves (Fig. 3-24A), and ends in a vertical splitting of the material (Fig. 3-24B), which is characteristic of a brittle fracture initiating on a critical flaw.

The scientific literature is rather rich about compression fracture in brittle materials, but in the case of initiation on a critical flaw, several sources indicate that crack propagation starts in mode II from defects of various natures. This is what Saimoto et al. (2003) proposed, who obtained a law of the form $K_C = Y.\sigma_r.C^{1/2}$, but involving K_{IIC} instead of K_{IC}. Besides, in the case of brittle materials with a low toughness (less than 5 $MPa.m^{1/2}$), it seems that the toughnesses in modes I and II are similar (Munz et al., 1999); thus as a first approximation we have $K_{IC} = K_{IIC,}$ and the equation $K_{IC} = Y.\sigma_r.C^{1/2}$ can still be applied. It should be noted, however, that the geometricl factor, Y, associated to the critical flaw does not have the same value under tension (mode I) and under shear (mode II), the latter stress state occurring during compression fracture. The geometrical

factor Y is smaller for compression fracture than for tensile fracture (Ashby et al., 2008; Saimoto et al., 2003). According to the calculations of Saimoto et al. for a fracture in mode II without friction between the crack faces, which should be the case for a fracture initiating from a pore, the factor Y is equal to half of the one associated to a flaw having the same shape but loaded in mode I. For instance, starting from the value of Y associated to a plane circular crack in mode I ($Y = 2/\sqrt{\pi}$), we obtain $Y = 1/\sqrt{\pi}$. Then, assuming that K_{IIC} is equal to K_{IC} (Munz et al., 1999), the calculation of the critical flaw size in our less macroporous CPC gives a radius C ≈ 420 µm for the critical flaw, and a diameter of ~ 840 µm, which is of the same order as the size of the largest macropores (see Fig. 3-20). It should be noted that the calculation of Saimoto et al. suggests that the ratio between compressive and tensile strengths should always be close to two, which is actually observed in the Macro CPC of the present study (see Chapter 4).

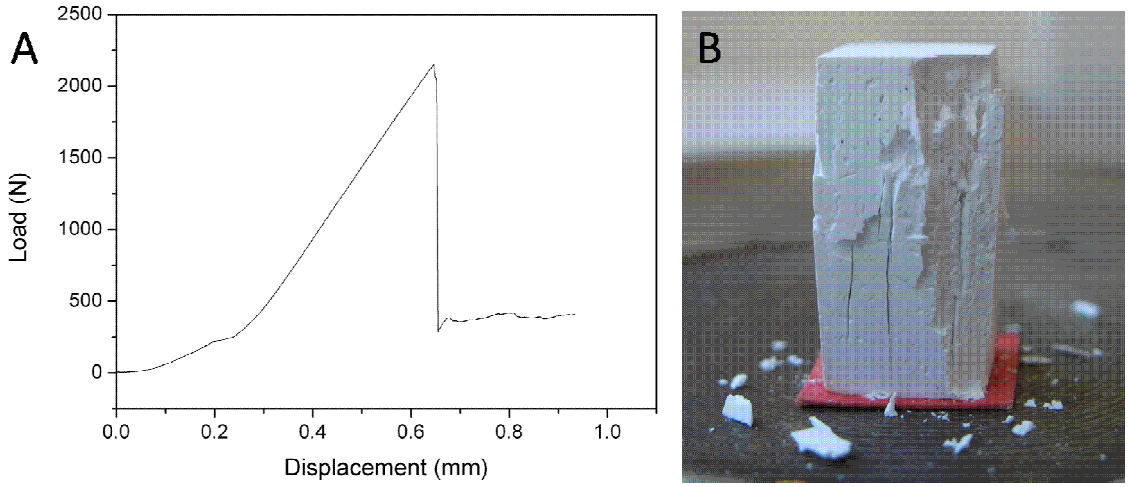

Fig. 3-24 (A) Load versus displacement curve of Macro CPC (10% mannitol) under compression at a displacement rate of 0.5 mm/min; (B) similar sample as A, showing several vertical splitting after compression test.

The increase in the critical flaw size with macroporosity can then be explained with the same hypothesis as Pecqueux et al. (2010), as already mentioned earlier. The question whether this mechanism could also happen during tensile loading (or in bending) in Macro CPC should therefore be raised. Indeed, stable crack growth most often remains a feature of compression loading (Sammis et al., 1986, Cannillo et al. 2004), although such effects have also been evidenced in some porous brittle materials in bending (Merkert et al., 1998; Pernot et al., 1999).

3.4 Chapter conclusion and perspectives

To the best of our knowledge, for the first time three mechanical properties (Young's modulus, fracture toughness and compressive strength) have been measured on CPC prepared with up to five different L/P ratios, two different particle sizes and five different levels of macroporosity. For a better understanding of the experimental observation, a power law has been used to describe all the mechanical properties of the CPC as a function of microporosity or macroporosity.

Unreacted α-TCP can be detected by means of XRD and SEM, especially in the cements prepared with a coarse α-TCP powder. These α-TCP particles show weak links with the CDHA matrix and are usually surrounded by "spaces" separating them from the surrounding matrix, such spaces being comparable to "microcracks". The latter can provoke a decrease in Young's modulus, but do not seem to influence fracture toughness.

The particle size of pristine α-TCP has a strong effect on the microstructure of its final reaction product (CDHA). The larger the starting α-TCP particle, the coarser the microstructure of CDHA, which in the end results in a larger critical flaw size. In the case of Macro CPC, the critical flaw size is of the order of that of the largest macropores for low macroporosities, and then increases monotonically with increasing macroporosity. This indicates that the critical flaw is a macropore or, as previously suggested in macroporous BCP ceramics (Pecqueux et al. 2010), a group of macropores where subcritical crack growth occurs during loading before catastrophic failure.

Despite the above important conclusions, there is still a need for further investigation. First, it would be appealing to extend the range of the investigated microporosity, which is still quite narrow. Second, measuring the flexural strength may bring extra information about the role of microstructural elements like macropores as critical flaws. Especially, the proposed mechanism of subcritical crack growth and macropore interaction may not be suitable for a tensile stress state. Moreover, all the measurements of mechanical properties in this study were conducted in dry condition, which is however different from the *in vivo* wet environment where CPC are implanted. Thus, it will be more meaningful to measure the mechanical properties of CPC in wet condition. Finally, it is generally considered that mechanical reliability is a critical issue for a safe application of brittle materials, so that a study of fracture statistics would also be of interest. All of these issues will be further investigated in Chapter 4.

Chapter 4 Influence of fabrication and test conditions on the mechanical properties and reliability of CPC

In the last chapter, mechanical properties including Young's modulus, fracture toughness and compressive strength have been systematically investigated on CPC prepared by using different L/P ratios, particle sizes and amounts of macroporosity.

However, for experimental simplicity, all the measurements in the study were conducted in dry conditions, which is different from the *in vivo* wet environment where CPC are implanted. Because some mechanical properties of dense apatite have been reported to depend strongly on water and humidity (Benaqqa et al., 2005), in view of practical applications it would be more meaningful to measure mechanical properties of CPC in wet conditions. Moreover, the range of the microporosity studied is still narrow and, in spite of the experimental difficulty to produce CPC with either a high L/P ratio (a very fluid paste which tends to sediment) or a low L/P ratio (a very dry paste difficult to shape), it would be useful to further extend it if a complete description of the trend is desired. In addition, the discussion in the last chapter has raised the need to study the tensile (or bending) strength of macroporous cements, on the basis of the observed increase in critical flaw size with macroporosity in the case of compression fracture. Therefore, bending experiments will also be conducted to investigate this particular point, among others. Besides, it is widely accepted that strength reliability is more suitable for evaluation or design of brittle materials rather than the mean strength, but this method is nevertheless rarely used in CPC which is also intrinsically brittle. All of these issues will be explored in the present chapter in the case of CPC prepared with a fine powder (like Cement F in chapter 3). Finally, because the specimens of the present study are going to be measured in a simulated *in vivo* environment (e.g. in a saline solution), but some of the measurements (e.g. fracture toughness or flexural strength) are experimentally difficult to be implemented in such a way (this will be explained later), a pre-experiment is initially conducted to explore the possibility of doing the test with a simple but reliable manner.

4.1 Pre-experiment

4.1.1 Influence of test condition on compressive strength

A specific setup was used for the pre-experiment (Fig. 4-1).

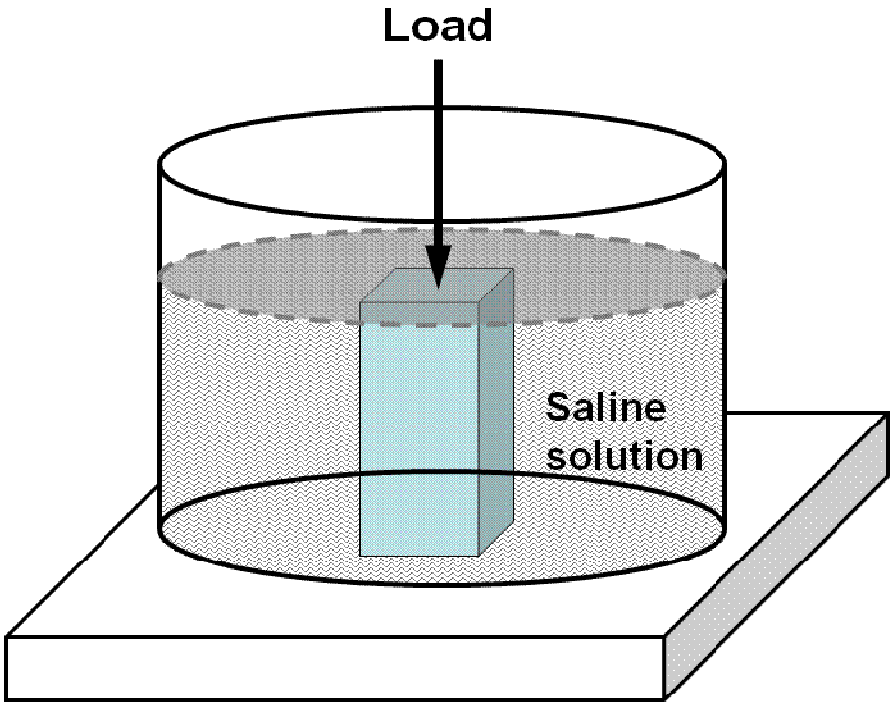

Fig. 4.1 Experimental setup for the measurement of compressive strength in saline solution

Indeed, it is easy to measure compressive strength of CPC specimens in a saline solution (Fig. 4-1). However, things become more complex for bend testing due to the fact that precisely positioning the rhombohedral bar and an extensometer is a necessary premise for accurate measurement of flexural strength or Young's modulus, which is nevertheless difficult to be completed in a container filled with a saline solution. For this reason, it would be preferable if our bending experiments could be conducted in wet condition but out of the saline solution, i.e. for instance in air but immediately after taking the specimens out of the solution. To check whether this procedure would yield, or not, a difference in the measured properties, a preliminary and comparative experiment was performed in the simpler case of compression. Compressive strength was tested on cylindrical specimens immersed in the saline solution. In contrast, identical specimens were also measured in the air (20 ^{o}C, 50% relative humidity) immediately after being taken out of the saline solution. The latter test was completed within one minute. No

statistically significant difference can be found between them (Fig. 4-2). The above experiment indicates that reliable results, which are similar to those measured in a saline solution, can be obtained if the mechanical tests can be completed in air within a short period (e.g. one minute) after the specimens are taken out of the solution. Thus, this testing procedure will be used throughout the rest of this manuscript for all the specimens measured in wet conditions.

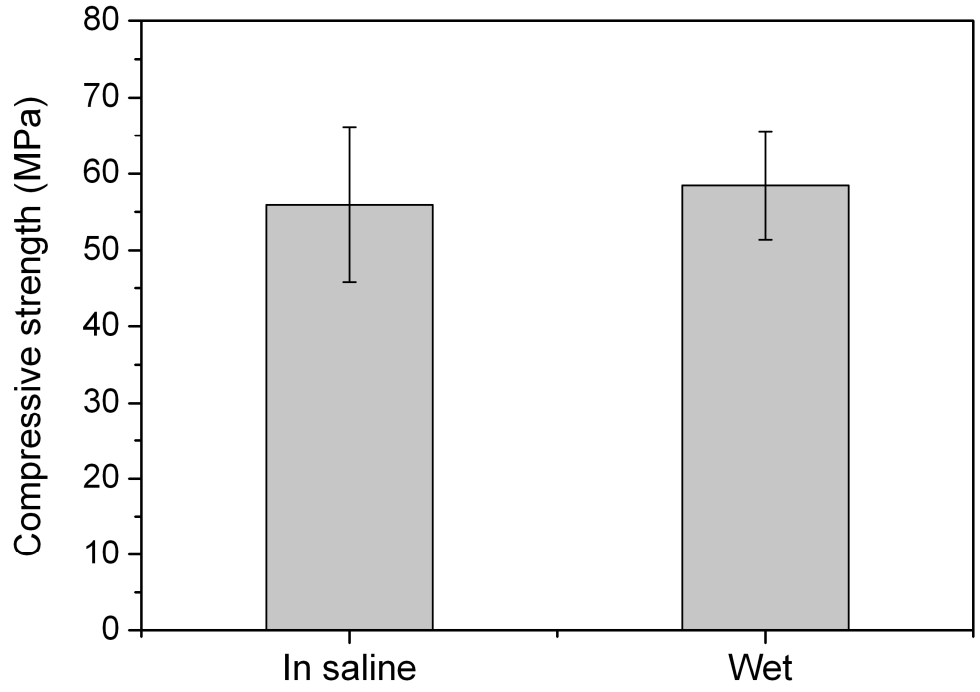

Fig. 4-2 Compressive strength of cylindrical specimens measured in different conditions. L/P = 0.35. Each value is the mean of twelve measurements ± one standard deviation.

4.1.2 Influence of immersion time on compressive strength

Another pre-experiment was also conducted to investigate the effect of immersion time on the compressive strength of CPC. Doing this experiment is of practical interest for our own work. In fact, many specimens were needed and prepared for the present study (twelve rhombohedral specimens for each L/P ratio, i.e. 96 specimens for a total of eight different L/P ratios). Due to this, all the specimens could not be prepared within a short time (e.g. one day). Moreover, after the measurement of fracture toughness and Young's modulus, the halves of the original bars were further polished for the measurement of compressive strength (e.g. twenty specimens for each L/P ratio, i.e. 160 specimens for a total of eight different L/P ratios). All the specimens were measured within a short period so as to reduce experimental errors, which means that some specimens have to be stored,

after complete hardening, in a saline solution at room temperature[16] for different times until the measurements are made. Thus, it is necessary to know if this additional immersion could affect the mechanical properties. To this end, compressive strength was tested on cylindrical specimens that were hardened at 37 °C for five days followed by a storage in a saline solution at room temperature for different periods. No statistically significant differences can be found for these specimens despite a very slight decrease of the mean strength value with the increasing immersion time (Fig. 4-3).

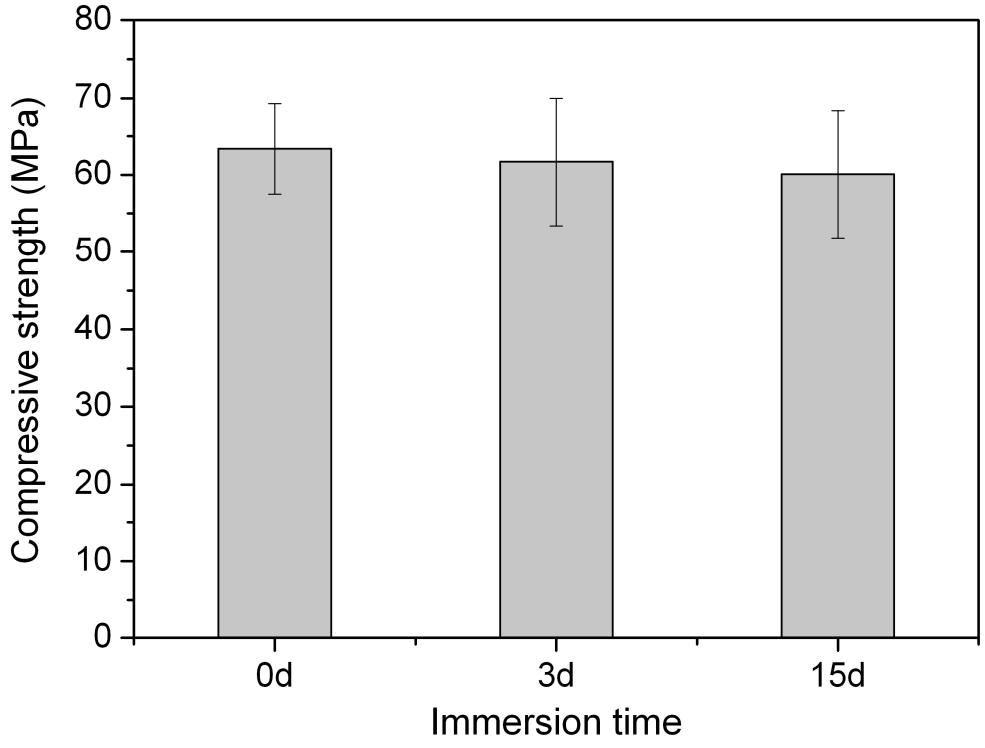

Fig. 4-3 Compressive strengths of cylindrical specimens as a function of immersion time. L/P = 0.35. Each value is the mean of twelve measurements ± one standard deviation.

Besides, it is worth mentioning that it was not necessary to store the CPC specimens in a saline solution at room temperature in all the cases, and this only happened when large amounts of specimens had to be prepared. The maximum strorage time that was used in the following study was five days, indicating that this parameter should have no significant influence on results.

[16] As already stated, the CPC specimens are hardened in a saline solution at 37 °C for five days. After this, the specimens have to be stored in a saline solution at a lower temperature to avoid any possible further transformation.

4.2 Mechanical properties and strength reliability of microporous CPC measured in wet conditions

4.2.1 Porosity and phase evolution

The porosity of the CPC was measured (Fig. 4-4). As shown previously, the porosity of cements increases with the increase of the L/P ratio. This is due to the higher proportion of liquid in the constant volume of the mold. Moreover, compared to the Cement F prepared in the last chapter, the range of the porosity of the cements prepared here is extended by nearly 62%.

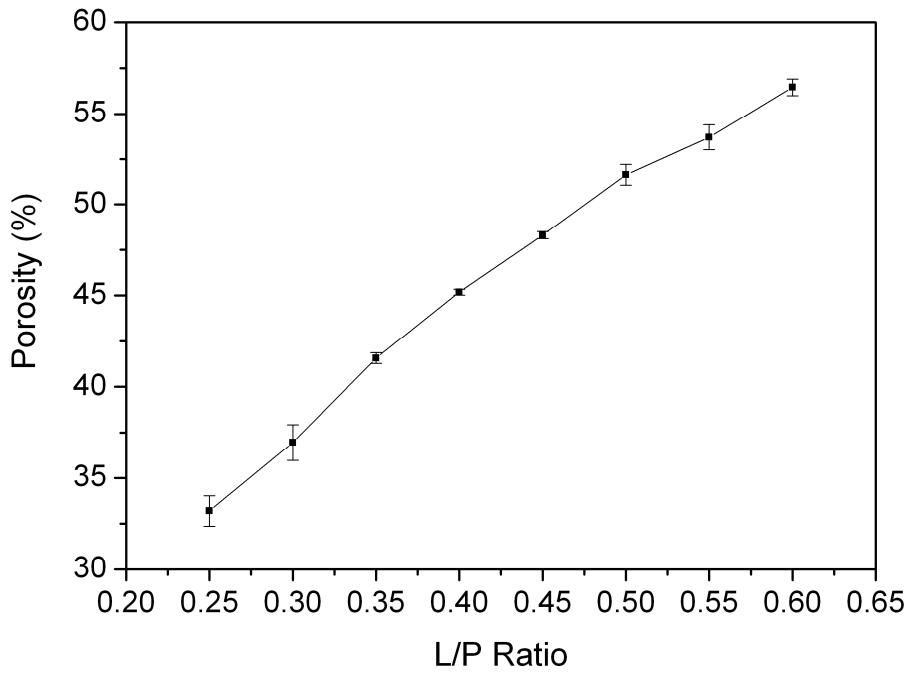

Fig. 4-4 Porosity of CPC as a function of the L/P ratio. Each point represents the mean of six specimens ± one standard deviation.

The final phases of the present CPC with different L/P ratios were examined by using XRD. The XRD patterns of the CPC are very similar to those shown in Fig. 3-8, thus they are not shown again. However, it is still worth reminding that most of the α-TCP powder mixed with different L/P ratios in the study has reacted to form CDHA. Besides, some unreacted α-TCP can also be detected, but the amount of unreacted α-TCP globally decreases with the increase of the L/P ratio.

4.2.2 Mechanical properties of CPC measured in wet conditions

Mechanical properties (Young's modulus, fracture toughness, compressive strength and flexural strength) of CPC prepared with different L/P ratios were measured in wet conditions (Fig. 4-5).

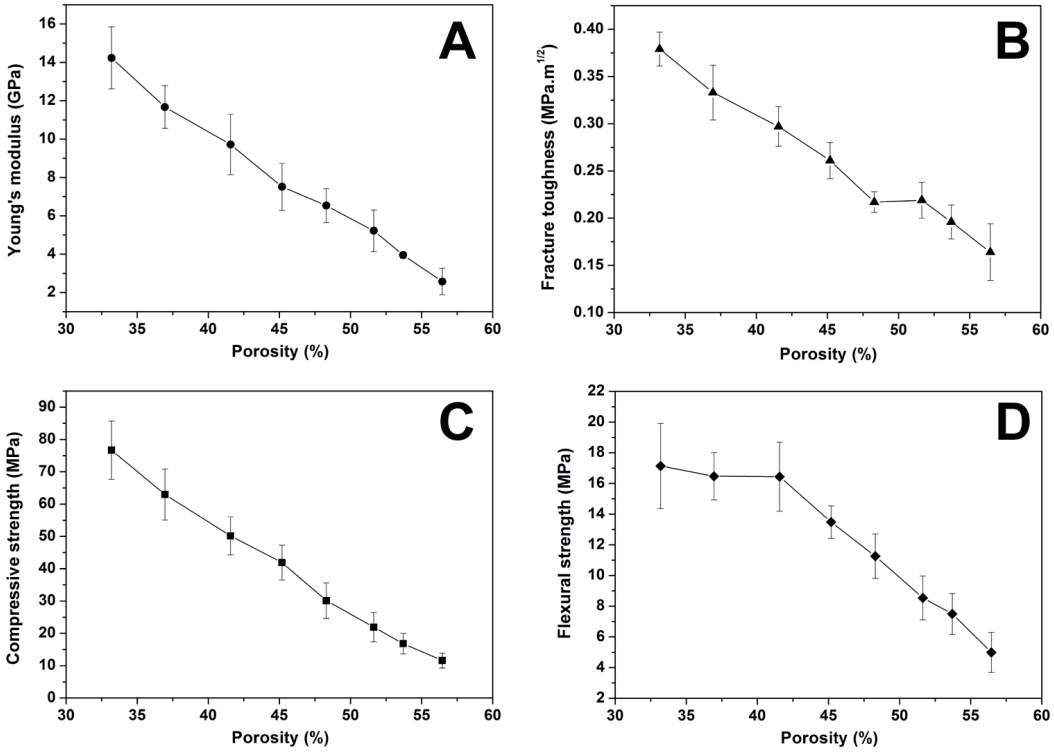

Fig. 4-5 Evolution of Young's modulus (A), fracture toughness (B), compressive strength (C) and flexural strength (D) of CPC as a function of porosity. In graphs A, B, D, each point represents the mean of six specimens ± one standard deviation. In graph C, each point represents the mean of twenty specimens ± one standard deviation (except the porosity of 53%, where there are nineteen specimens).

Similar to CPC measured in dry conditions (Fig. 3-10), all the above measured mechanical properties decrease globally with the increasing porosity.

In Chapter 3, models based on a power law were used to fit and to explain mechanical properties. This strategy was also initially tried in the present study. However, fitting does not work well for all the mechanical properties in the whole range of porosity studied. This might be explained in two aspects. First, as shown in Fig. 4-4, the porosity range of CPC has been significantly extended (+62%); thus it is likely that one simple model is not enough to describe the mechanical properties in the whole range of porosity, which has also been reported for other materials (Rice, 1998). An explanation for this could be a

change in deformation and/or fracture mechanisms with porosity, especially for very high or very low L/P ratios where the cement pastes become respectively very fluid or very dry, and may induce the presence of defects which are different from those present in the intermediate range of porosity. Second, an assumption, which is based on constant fracture strain for the transfer of the stored elastic energy to fracture energy, has been raised for the models used in Chapter 3 (Tancret et al., 2006). However, this assumption might be ineffective in wet CPC due to the existence of water which may affect the surface energy during fracture (Benaqqa et al., 2005). For these reasons, modeling of mechanical properties will not be discussed here, and our interest will be focused on the effect of different testing conditions (wet and dry) on the mechanical properties of CPC.

The mechanical properties measured in wet condition are compared with those measured in dry condition. Before showing the results, it is worth noting that in general it is difficult to make direct comparisons between mechanical properties measured in different studies, due to the differences in formulations (or batches), porosities, pore sizes, geometries of specimens, instruments, testing conditions and even operators. Thus, meaningful comparisons can only be made between mechanical properties of specimens prepared with similar conditions.

The Young's modulus measured in wet and dry conditions is compared (Fig. 4-6), for the L/P ratios where both measurements are available.

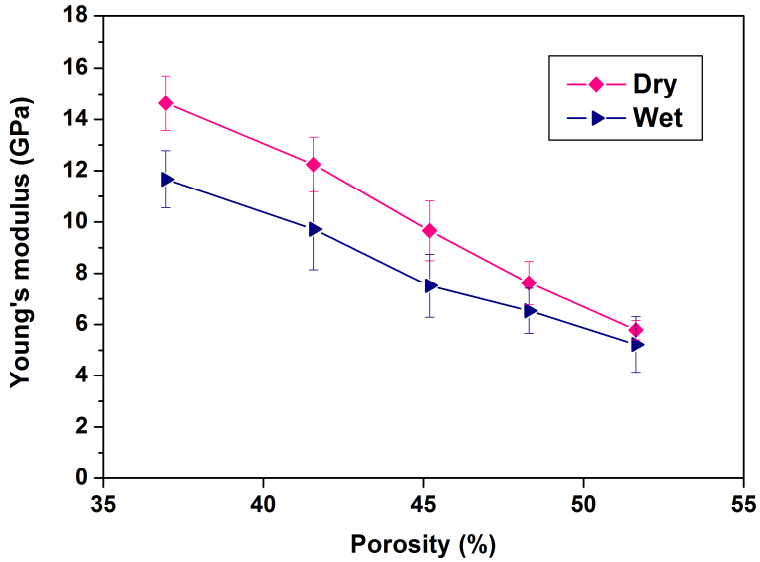

Fig. 4-6 Young's modulus of CPC measured in dry and wet conditions as a function of porosity. Young's modulus measured in wet condition is extracted from Fig. 4-5A. Each point represents the mean of six specimens ± one standard deviation.

As can be seen, the Young's modulus measured in dry conditions is higher than that measured in wet conditions, but the difference between both Young's moduli decreases with increasing porosity, although these two effects remain unexplained. Moreover, it is worth noting that the Young's modulus measured in dry condition is somewhat higher than that shown in Chapter 3 (Fig. 3-10), mainly coming from the fact that they are two different batches.

Fracture toughness measured in wet conditions is also compared with that measured in dry conditions. In general, the former is lower than the corresponding latter one (Fig. 4-5B, Fig. 3-10B). The detrimental effect of water on fracture toughness has also been found in hydroxyapatite ceramics, and it is mainly due to the decreased surface energy on crack surface in the presence of water (Benaqqa et al., 2005). The influence of water on fracture toughness of CPC is further investigated in the present study. Fracture toughness was measured on CPC prepared with three L/P ratios (0.3, 0.35 and 0.4) and dried at different temperatures (37 ^{o}C or 65 ^{o}C) for different periods (Fig. 4-7).

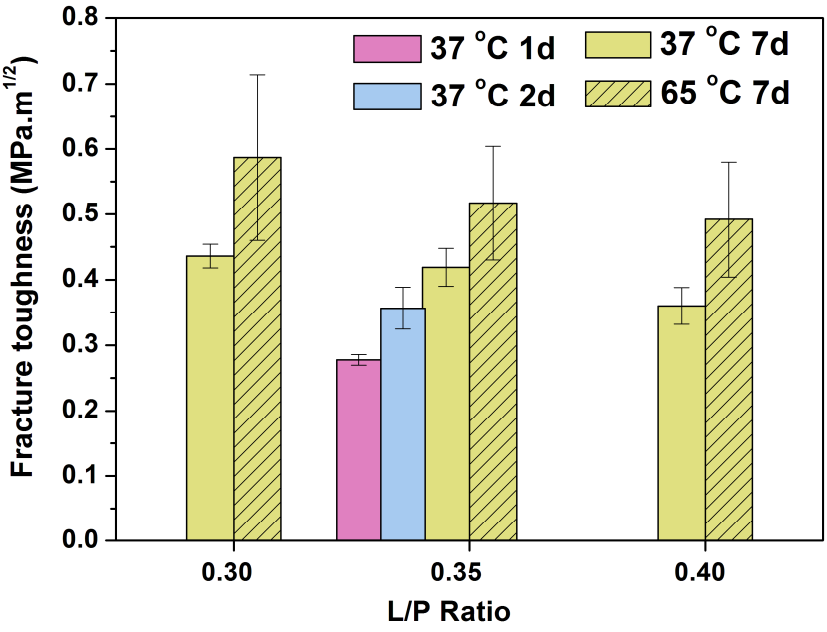

Fig. 4-7 Fracture toughness of CPC with different L/P ratios after drying at different temperatures for different periods. Each point represents the mean of three specimens ± one standard deviation.

It was found that drying at 37 ^{o}C or 65 ^{o}C for seven days was sufficient for CPC specimens to reach a constant weight at each drying temperature. As expected, for each condition (dried seven days at 37 °C or 65 °C) the fracture toughness decreases with increasing L/P ratio (porosity). Moreover, the fracture toughness is higher for each CPC

dried at 65 °C than at 37 °C despite nearly the same porosities (this point will be discussed later). It is also apparent that the fracture toughness of CPC with a L/P ratio of 0.35 increases with the increasing drying time at 37 °C. According to the role of water on fracture toughness of apatite mentioned previously, all the above results may therefore be attributed to the influence of different amounts of water existing in the cement. The more water present in the cement, the smaller the fracture toughness.

A thermogravimetric (TG) test was further performed on CPC with a L/P of 0.35 to verify the previous assumption that fracture toughness of CPC is related to the water existing in the cement (Fig. 4-8). The TG test was performed after the specimen has been dried in 37 ^{o}C for seven days.

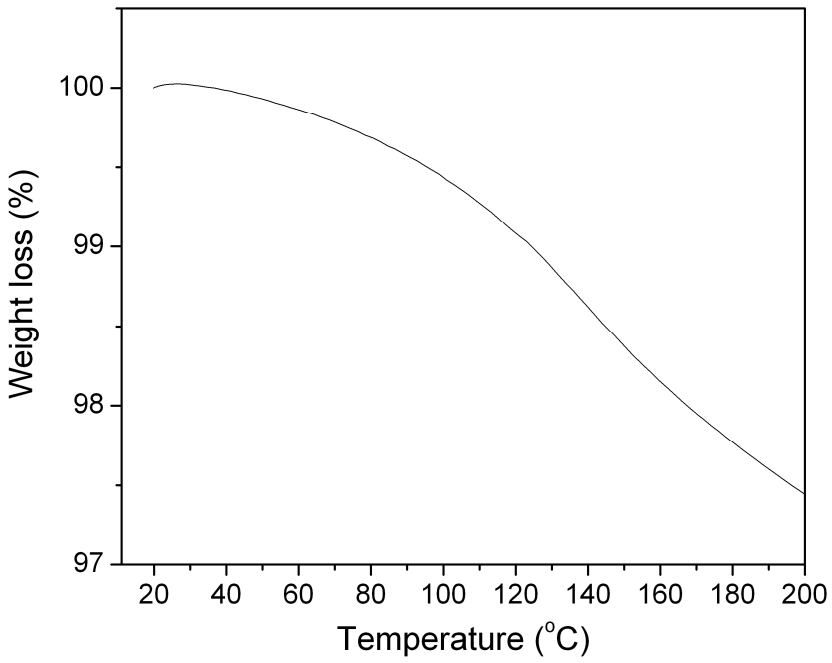

Fig. 4-8 Weight loss of CPC as a function of temperature by means of TG with a heating rate of 5 ^{o}C / min. L/P = 0.35, the specimen was tested after being dried at 37 ^{o}C for seven days.

As can be seen, despite the previous long drying time at 37 °C, a very slight weight loss of water can still be observed (Fig. 4-8), which might explain the different toughness values of CPC even after being dried for seven days (Fig. 4-7). In addition, it is important to note that although the above results indicate a significant effect of water on the fracture toughness of CPC, the approach is too simple and further investigation would still be necessary to explore the detailed fracture mechanisms of CPC and their dependence on the presence of water (or other liquids). Finally, it is worth noting that the existence of water, which is thought to be a detrimental factor to the fracture toughness of CPC in the

present study, appears to be a critical component of cortical bone to maintain its fracture toughness (Nyman et al., 2006).

Compressive strength measured in wet conditions is compared with that measured in dry conditions. The former is apparently lower than the corresponding latter one (Fig. 4-5C, Fig. 3-10C). Moreover, similar trends are also observed in flexural strength measured in different conditions (Fig. 4-9).

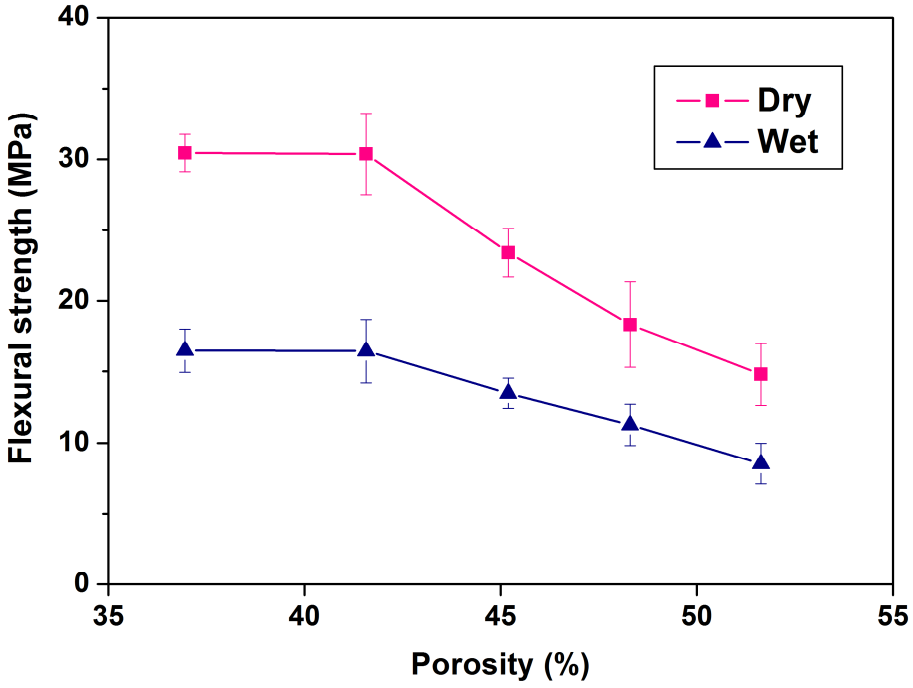

Fig. 4-9 Flexural strength of CPC measured in dry and wet conditions as a function of porosity. Each point represents the mean of six specimens ± one standard deviation.

The inferior flexural strength in the presence of high moisture (water) has been reported in alumina ceramics, which is mainly attributed to sub-critical crack growth related to a stress-assisted chemical reaction at the tip of cracks between ceramic constituents and environmental constituents (especially moisture) (Cho et al., 2000, 2003). In the present case, the lower flexural and compressive strengths measured in wet conditions is mainly attributed to the corresponding lower fracture toughness which is actually the intrinsic property of materials and determines its strengths if the critical flaw is unchanged.

4.2.3 Reliability of CPC measured in wet condition

As discussed previously, CPC is intrinsically brittle, thus it is susceptible to fracture under stress on critical flaws that are either inherent to the materials themselves or introduced during processing. However, since it is impossible to predetermine the size, location and distribution of the most critical flaws, the strength of a number of nominally identical standard CPC specimens can never be determined reliably from average fracture strengths. For this reason, a strength reliability description rather than the mean strength seems to be more suitable for evaluation or design of brittle materials.

The reliability of CPC was analyzed by means of Weibull statistics (Weibull, 1939, 1951). The compressive strength data for the groups of twenty nominally identical CPC specimens of approximately 8 × 8 × 16 mm^3, cut out from the 8 × 8 × 36 mm^3 bars, were ranked in ascending order and a Weibull analysis was performed on the resultant data using the Weibull probability function, as shown in the equation 4-1. Moreover, in order to better understand the calculation procedures of Weibull modulus, it is worth remembering and explaining the Weibull probability function as follows:

$$P_f = 1 - \exp\left[-\left(\frac{\sigma_r}{\sigma_0}\right)^m\right] \tag{4-1}$$

P_f is the probability of failure, which varies from 0 to 1 and is estimated from

$$P_f = \left(\frac{n}{N^* + 1}\right) \tag{4-2}$$

where N^* is the total number of specimens and n is the ranking number of the specimens being ranked in ascending order. σ_r is the compressive strength, σ_0 is a normalizing parameter determined from the stress at which 1/e of the population survives and m is called the Weibull modulus; the meaning of the latter will be discussed later. The equation 4-1 can be further simplified using logarithms to the form:

$$\ln\ln\left(\frac{1}{1-P_f}\right) = m\ln(\sigma_r) - m\ln(\sigma_0) \tag{4-3}$$

where the intercept at the ordinate is m $\ln(\sigma_0)$ and the slope is m, the Weibull modulus.

The Weibull modulus, m, is a dimensionless number used to characterize the variability in measured strength of components made from brittle materials, which arises from the presence of flaws having a distribution in size and orientation (Karageorgiou et al., 2005). A high value of m indicates a sharp distribution of strength data while a low value represents a large scatter. It should be noted, however, that the Weibull model is based on an empirical description of the probability of failure of individual volume elements of the material (i.e. not relying on fracture mechanics), and as such cannot be considered a physically sound model. Nevertheless, because of its practical applicability, it has become the most widely used model to describe fracture statistics in brittle materials.

The logarithmic Weibull plots calculated by means of the equation 4-3 for the compression specimens of CPC prepared with different L/P ratios are shown, and the Weibull modulus for each CPC was determined (Fig. 4-10). As can be seen, there exists a jump in the Weibull modulus values of CPC for a L/P ratio between 0.4 and 0.45. Specifically, the Weibull moduli for CPC with L/P ratios between 0.25 and 0.4 are all between 8 and 9, which are pronouncedly higher than those for CPC with L/P ratios between 0.45 and 0.6 which are all between 5 and 6.

In order to better explain the above results, the quantity $(K_{IC}/\sigma_r)^2$, which is proportional to the mean critical flaw size on which fracture initiates, is plotted as a function of the L/P ratio. Moreover, for the purpose of better understanding, the Weibull modulus determined for each L/P ratio is marked above each corresponding data point (Fig. 4-11). As seen, the critical flaw size of CPC increases with the increase of the L/P ratio; moreover there is an obvious turning point for critical flaw size between L/P ratios of 0.4 and 0.45, where the critical flaw size begins to increase very fast. Interestingly, the turning point in the critical flaw size and the jump in the Weibull modulus coincide.

In fact, when the L/P ratio increases, pore size and pore interconnectivity increase, which could explain a mild increase in critical flaw size, as observed for L/P ratios up to 0.4. Meanwhile, the statistical dispersion of strength, linked to the statistical dispersion of flaws, remains rather sharp, maybe just because small defects are statistically more abundant, therefore introducing more determinism in strength.

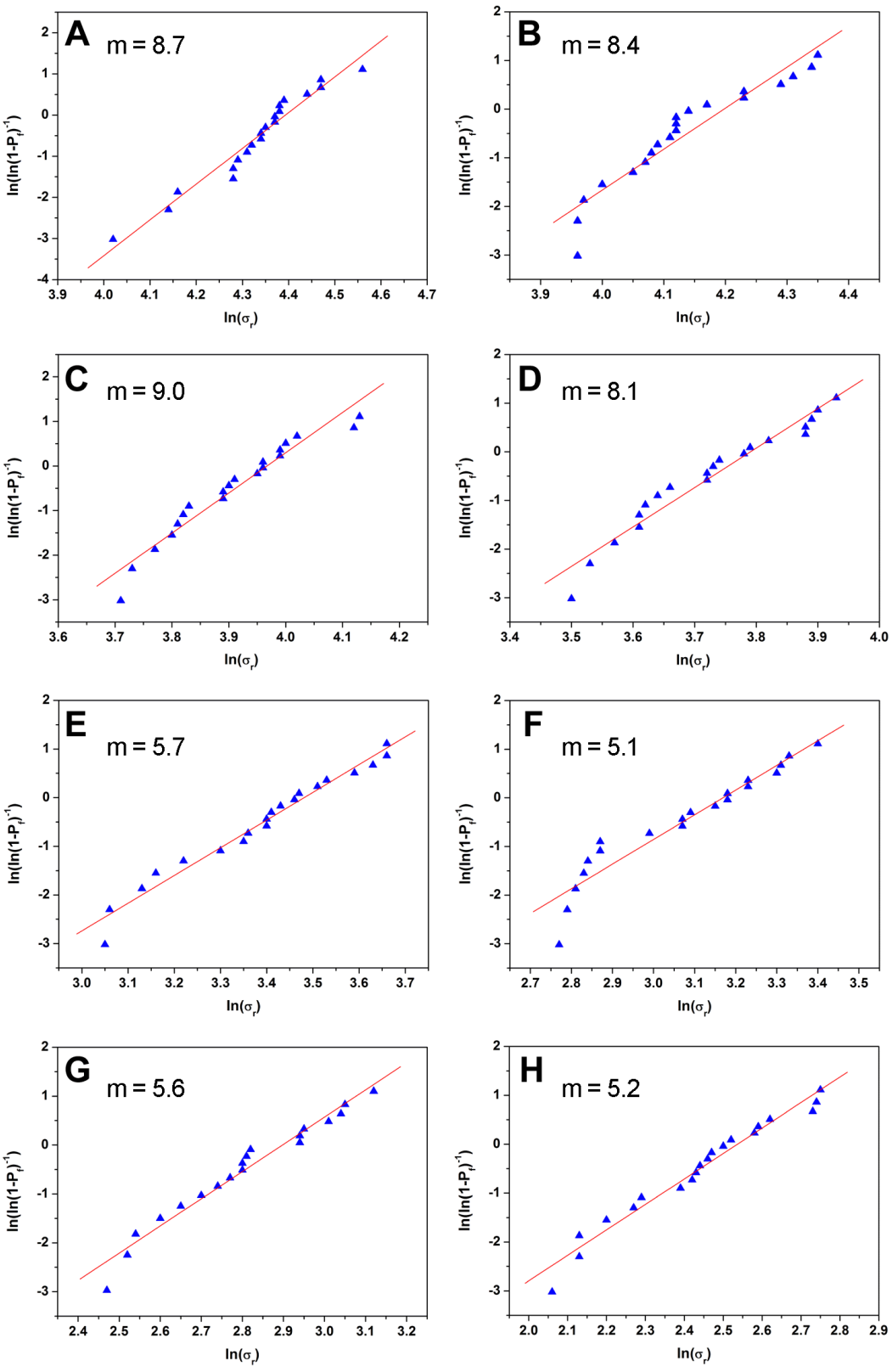

Fig. 4-10 Weibull logarithmic plots for CPC with different L/P ratios. (A) 0.25; (B) 0.3; (C) 0.35; (D) 0.4; (E) 0.45; (F) 0.5; (G) 0.55; (H) 0.6. The slope of the red line gives the Weibull modulus, m. There are twenty specimens in each L/P ratio (except L/P = 0.55 where there are nineteen specimens)

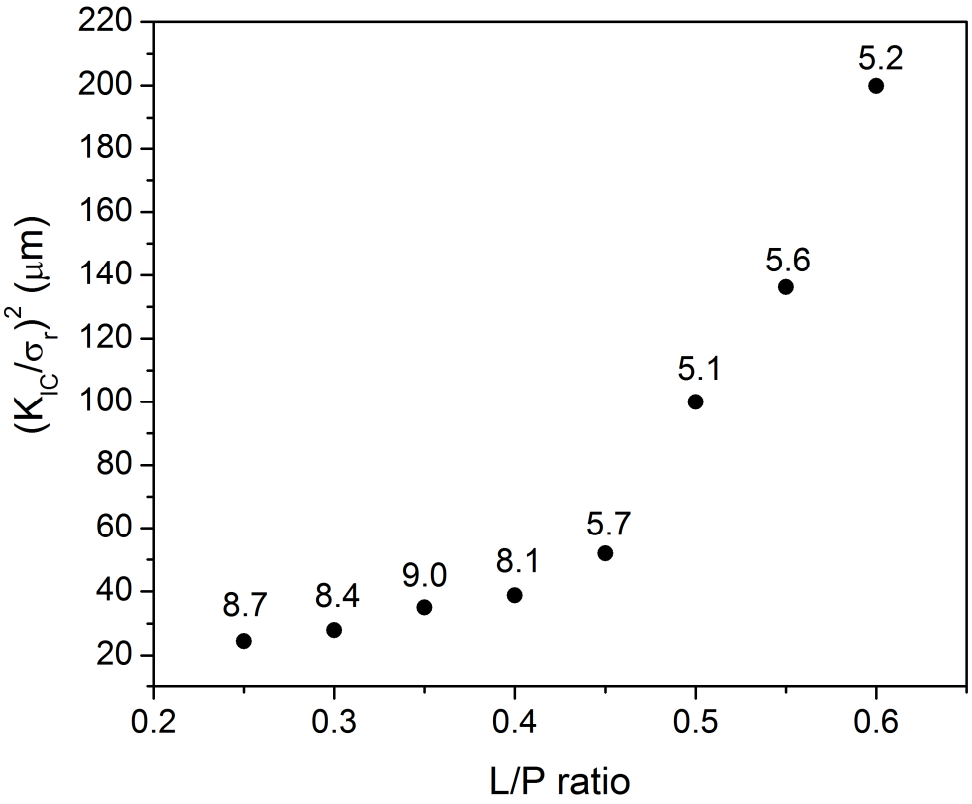

Fig. 4-11 Variation of $(K_{IC}/\sigma_r)^2$ as a function of the L/P ratio. The number above each data point is the Weibull modulus for each L/P ratio.

However, when the L/P ratio increases beyond 0.4, the paste becomes more and more "fluid" during processing, and air bubbles can be easily trapped in the cement paste, and act as larger critical flaws. Even though a vibrating table has been used to attempt and remove as many bubbles as possible, more air bubbles would be likely to be trapped in the paste when the L/P ratio increases, whereas it is rather easy to remove air in the driest pastes through densification by vibration or by manual pressing. As a result, because the probability of finding large air bubbles in the paste increases with the L/P ratio (0.45 and above), the measured mean critical flaw size also begins to increase very fast. In addition, only a small amount of air bubbles is likely to be trapped in each specimen, thus bubble trapping has a strong statistical character, which could explain why the statistical distribution of critical flaw size, and therefore of strength, becomes wider, through a lower Weibull modulus, when the L/P ratio passes the threshold where easy bubble trapping starts (around 0.4 or 0.45).

SEM pictures of CPC with L/P ratios beside the turning point are shown in Fig. 4-12. A small round pore, which is a typical character of an entrapped air bubble, can be observed in the CPC with a L/P ratio of 0.4 (Fig. 4-12A). In contrast, more round pores of larger

sizes can be found in the CPC with a L/P ratio of 0.45 (Fig. 4-12B), relating to a lower strength and Weibull modulus. This SEM observation is consistent with our previous explanations.

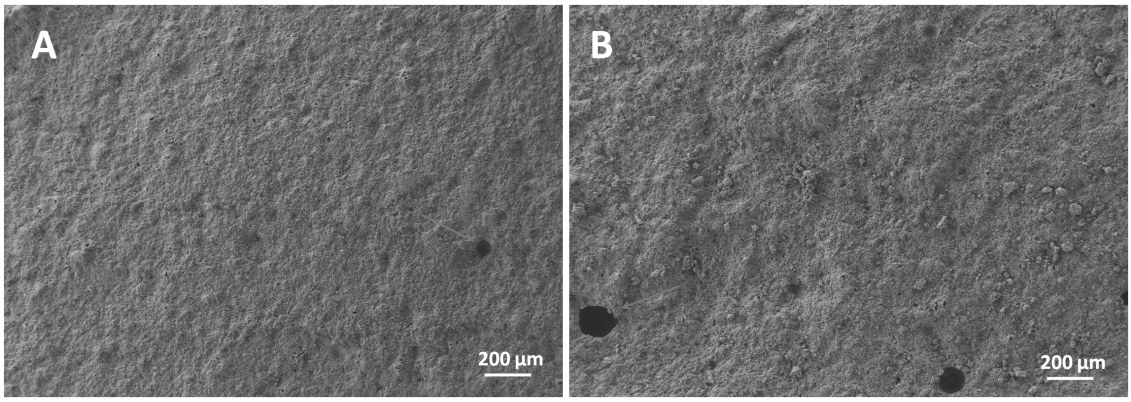

Fig. 4-12 SEM micrographs of Cement F: (A) L/P = 0.4; (B) 0.45, showing entrapped air bubbles.

4.3 Mechanical properties and strength reliability of macroporous CPC

4.3.1 Mechanical properties of macroporous CPC tested in different conditions

The mechanical properties (Young's modulus, fracture toughness, compressive strength and flexural strength) were measured on macroporous CPC in wet and dry conditions (Fig. 4-13).

As expected, all the mechanical properties decrease with the increase of macroporosity regardless of the testing conditions. Moreover, similar to microporous CPC, the mechanical properties measured in wet condition are generally lower than those measured in dry condition, but the differences between them tend to decrease with increasing macroporosity. The lower mechanical properties measured in wet conditions for macroporous CPC could be attributed to the detrimental effect of water existing in the CPC, as discussed previously.

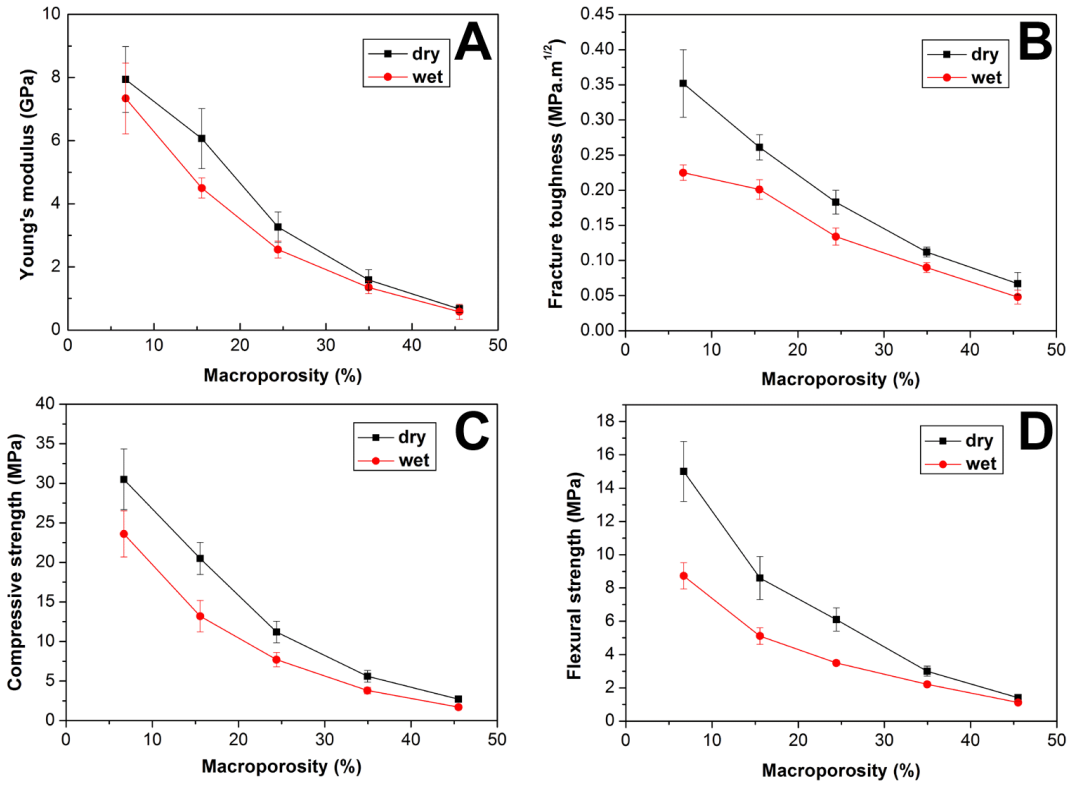

Fig. 4-13 (A) Young's modulus, (B) fracture toughness, (C) compressive strength and (D) flexural strength measured in wet and dry conditions, as a function of macroporosity. In graphs A, B, D, each point represents the mean of six specimens ± one standard deviation. In graph C, each point represents the mean of seventeen-to-nineteen specimens ± one standard deviation.

Moreover, in the last chapter, an increase in critical flaw size as a function of macroporosity was observed on the macroporous CPC suffering compression loading (this has also been observed here, and will be presented later). This enlarged critical flaw, compared to single macropores, are attributed to subcritical microcrack growth and linking between macropores before reaching the peak stress (Pecqueux et al., 2010). This stable crack growth often happens in compression loading (Sammis et al., 1986, Cannillo et al. 2004), although such effects have also been seen in some porous brittle materials in bending (Merkert et al., 1998; Pernot et al., 1999). Thus it will be of great interest to study if such stable crack growth could also happen during tensile loading (or in bending) in our macroporous CPC. To this end, similar to the procedure conducted in Chapter 3, the quantity $(K_{IC}/\sigma_f)^2$ (σ_f is the flexural strength of macroporous CPC), which is proportional to the critical flaw size on which fracture initiates, is plotted as a function of macroporosity (Fig. 4-14). Moreover, in order to avoid the interference caused by water as shown previously, only flexural strength measured in dry conditions was used.

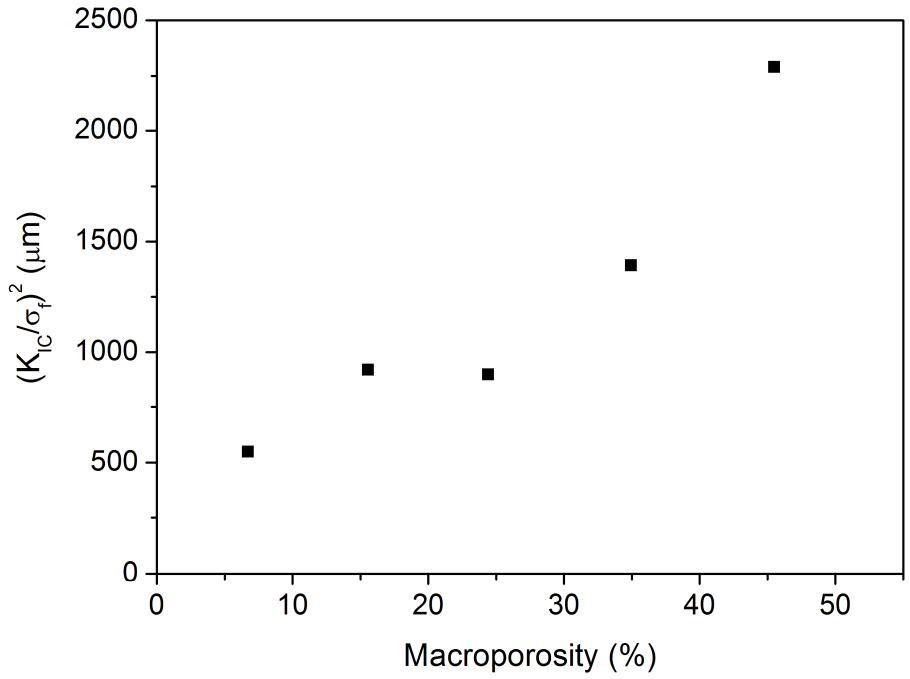

Fig. 4-14 Variation of $(K_{IC}/\sigma_f)^2$ for macroporous CPC as a function of macroporosity

The critical flaw size calculated from flexural strength globally and pronouncedly increases with the increasing macroporosity, which is similar to our previous observation on the critical flaw size calculated from compressive strength. However, it must be noted that the quantity plotted is not the critical flaw size itself, but is proportional to it, with the proportionality factor depending on the shape and orientation of flaws and on the cracking mode (Saimoto et al., 2003), so that it is normal that the values plotted on Fig. 4-14 in the case of bending are very different from those plotted on Fig. 3-23 in the case of compression. Indeed, the geometrical factor Y is larger for tensile fracture than for compression fracture (Ashby et al., 2008; Saimoto et al., 2003). According to the calculation of Saimoto et al., the geometrical factor Y for tensile fracture is twice that for compression fracture, which can explain that in the present study the bending strengths are typically two times smaller than the compressive strengths, if the critical flaw sizes are similar, according to:

$$\sigma_{fracture} = \frac{K_{IC}}{Y\sqrt{c}} \tag{4-4}$$

Above all, the trend is obvious that the critical flaw size calculated from flexural strength globally increases with increasing macroporosity, indicating that stable crack growth may also happen during tensile loading in the macroporous CPC.

4.3.2 Reliability of macroporous CPC tested in different conditions

The reliability of macroporous CPC was analyzed by means of Weibull statistics. Similar to microporous CPC, the logarithmic Weibull plots for the compression specimens of macroporous CPC prepared with different mass fractions of mannitol and measured in different conditions are shown (Fig. 4-15, wet condition; Fig. 4-16, dry condition), and the Weibull modulus for each macroporous CPC was calculated.

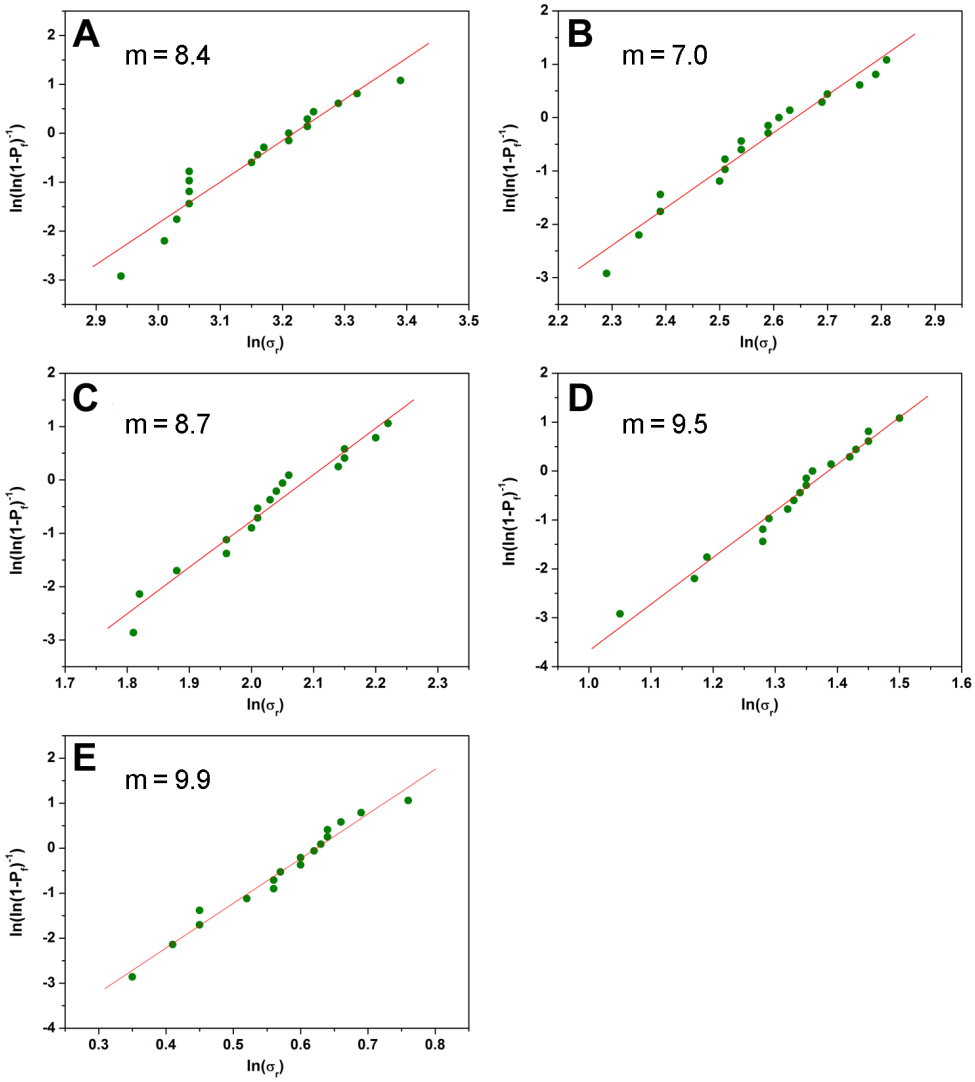

Fig. 4-15 Weibull logarithmic plots for macroporous CPC with different mass fractions of mannitol (A) 10%; (B) 20%; (C) 30%; (D) 40%; (E) 50%. The slope of the red line gives the Weibull modulus, m. Specimens were measured in wet conditions. There are seventeen or eighteen specimens for each mass fraction.

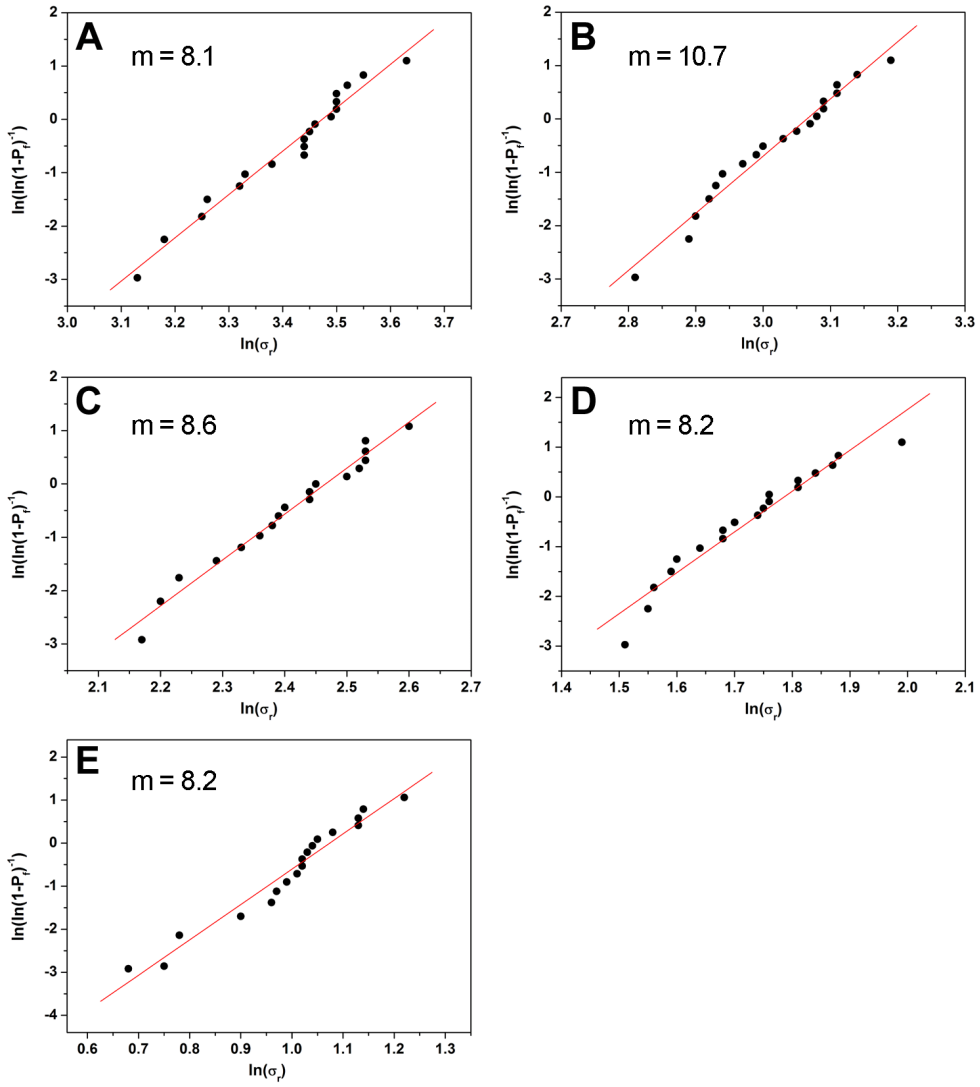

Fig. 4-16 Weibull logarithmic plots for macroporous CPC with different mass fractions of mannitol (A) 10%; (B) 20%; (C) 30%; (D) 40%; (E) 50%. The slope of the red line gives the Weibull modulus, m. Specimens were measured in dry conditions. There are eighteen-nineteen specimens for each mass fraction.

Moreover, similar to microporous CPC, the quantity $(K_{IC}/\sigma_r)^2$ (σ_r is the compressive strength) for macroporous CPC under different testing conditions is plotted as a function of macroporosity. In addition, for the purpose of clarity, the calculated Weibull modulus for each macroporosity is marked above or below each corresponding data point of the same color (Fig. 4-17).

As can be seen, regardless of different testing conditions, the critical flaw size of macroporous CPC increases with the increase of macroporosity. This result is consistent with that obtained in Chapter 3. Besides, the critical flaw sizes calculated from wet measurements are generally larger than those calculated from dry measurements, which

seems at first contradictory with the fact that despite different test conditions, the macroporous CPC were prepared using the same methods, so that the actual critical flaw size, if linked to microstructural features, should also be the same. The specific reason for this discrepancy is unclear, but may be due to two reasons: (i) mesurements of mechanical properties like toughness and strength are subject to errors, and the quantity plotted in Fig. 4-17 is the square of the ratios between them, so that the observed differences might just be due to uncertainties; (ii) the effect of water, which may amplify the calculated critical flaw, maybe because the assumed subcritical crack extension during loading could operate in a different manner, and to a larger extent, in a wet environment. Moreover, unlike the turning point seen in microporous CPC, the Weibull modulus for macroporous CPC is much less variable regardless of different testing conditions. This can be explained by the fact that, because macropores act as critical flaws, either alone or as interacting groups (Pecqueux et al., 2010), and because they are introduced in large numbers in each specimen, the strength becomes more "deterministic" (e.g. high Weibull modulus), as predicted by the "weak link" theory of fracture when the amount of flaws is large.

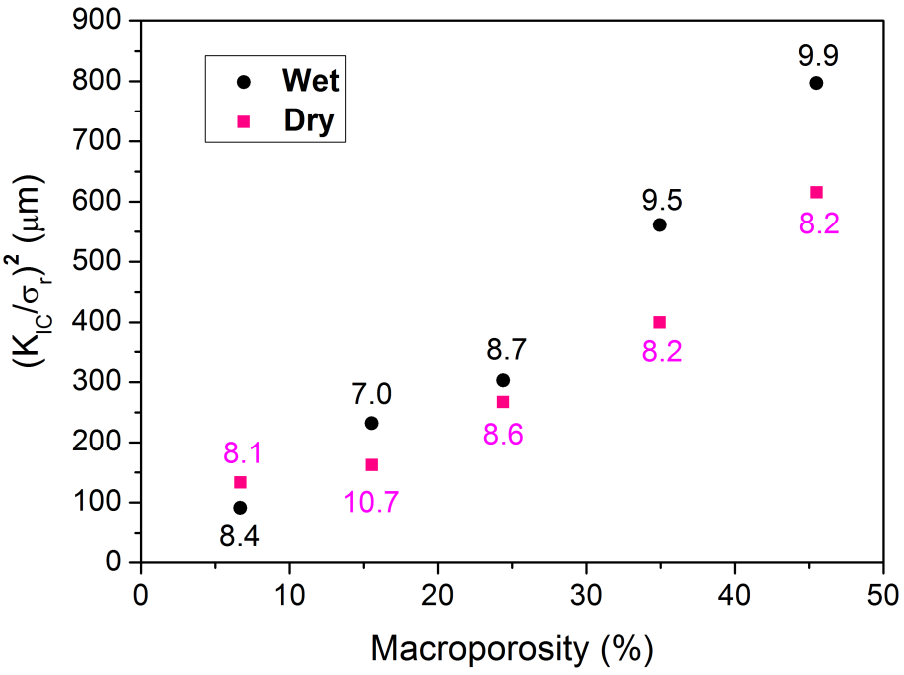

Fig. 4-17 Variation of $(K_{IC}/\sigma_r)^2$ as a function of macroporosity. The number corresponding to each data point of the same color is the Weibull modulus for each macroporosity.

Finally, the above measured mechanical properties of microporous CPC and macroporous CPC can be compared to reported mechanical properties of human cortical

or cancellous bone (Koester et al., 2008; Wagoner Johnson et al., 2011). If the Young's modulus of CPC is similar to that of cortical bone (several GPa), and normally higher than that of cancellous bone, both fracture toughness and strength of CPC are much lower than those of cortical bone, and comparable to those of cancellous bone.

4.4 Chapter conclusion

The mechanical properties of both microporous CPC and macroporous CPC decrease with the increase of porosity. The mechanical properties measured in wet conditions are generally lower than those measured in dry conditions. These mechanical properties measured in wet conditions were compared to those of human cancellous and cortical bone. However, only the Young's modulus for microporous CPC and compressive strength for macroporous CPC could match the properties of bone. Similar to compression fracture, stable crack growth also seems to happen during tensile loading in macroporous CPC. Fabrication process of CPC, particularly mixing of cement paste, may reduce the reliability of compressive strength of microporous CPC in high L/P ratios because of the unpredictable character of air bubbles trapped. On the contrary, the process of fabrication of CPC has less effect on the reliability of macroporous CPC with different amounts of macropores. The knowledge learned here should allow, in the end, to improve the reliability of the strength of CPC through a better control of microstructure.

Chapter 5 Handling and mechanical properties of composite CPC[17]

In the last two chapters, the mechanical properties (Young's modulus, fracture toughness, compressive strength, flexural strength and reliability) of CPC, which were prepared using different particle sizes and with different amounts of microporosity and macroporosity, have been investigated systematically. However, as stated in the literature, our CPC, without exception, is naturally brittle. Hence it is essential to develop new materials with optimized biological, handling and mechanical properties, which could particularly be less brittle and exhibit a kind of tolerance to damage.

To this end, various biopolymers, such as sodium alginate, HPMC (hydroxypropyl methylcellulose), MC (methylcellulose), hyaluronic acid, chitosan and modified starch have been used in the past as additives to produce composite materials. Among these polymers, cellulose ethers are of great interest from the cohesion point of view. They have been widely used as anti-washout admixtures in civil engineering to improve the cohesion and anti-washout performance of cement-based materials (e.g. Portland cement) (Khayat, 1998). Moreover, their positive effect to improve the toughness of Portland cement was also reported (Eden et al., 1985). Due to their good biocompatibility and biodegradability, these cellulose ethers are also used in biphasic calcium phosphate suspensions (Fatimi et al., 2010; Weiss et al., 1999) and various formulations of CPC for bone substitution (Cherng et al., 1997; Jyoti et al., 2010; Xu et al., 2004B), improving the workability of the bone substitutes. However, to the best of our knowledge, no systematic study is available until now on the effect of the addition of cellulose ethers, e.g. HPMC, MC or Si-HPMC (silanized HPMC), on both handling and mechanical properties of CPC, and in particular on fracture toughness and tolerance to damage. In recent studies (Ginebra, et al., 2007; Montufar, et al., 2010), some foaming agents have also been used to create macropores in composite CPC before its setting, which appears to be more attractive compared to the often used method of porogen dissolution occurring after the CPC has set. For this reason, Si-HPMC will be also attempted as an air-entraining agent to produce air bubbles due to its high viscosity and "self-setting" behavior, which may help to stabilize the bubbles. The obtained foam will be subsequently mixed with CPC

[17] This investigation has been performed as a joint work with Dr. Weizhen Liu

paste to prepare macroporous CPC. All of the above issues will be detailed in the present chapter, in an attempt to develop biomaterials with an improved overall performance for bone substitution. However, since the methods of preparing composite CPC with HPMC solutions, Si-HPMC solutions and foamed Si-HPMC solutions are quite different from each other, for convenience the experimental details for these studies will be described in the corresponding sections.

5.1 HPMC / MC composite CPC

In this section, the effect of cellulose ethers with different molecular weights and substitution levels on the handling and mechanical properties of CPC is systematically studied. Four different cellulose ethers (they will be presented later) are dissolved in deionized water together with Na_2HPO_4 as accelerator to get various liquids, which are then used as cement liquid phases and mixed with α-TCP. Their influence on the handling properties (e.g. injectability, cohesion time, anti-washout performance and initial and final setting times) and on the mechanical properties of the resulting composite CPC is then investigated. The mechanical properties of the specimens were measured in wet conditions.

5.1.1 Preparation of cement liquid phases

Four cellulose ether products, namely A15, E4M, K4M and K15M (METHOCEL, Dow Chemical) were used in this study (Table 5-1).

Table 5-1 Typical products of METHOCEL Cellulose Ether

Product name	MeO (%) [a]	HPO (%) [a]	viscosity range [a] 2%, 20 °C (mPa·s)	Molecular weight range ($g.mol^{-1}$) [b]
A15	30	0	12 - 18	46 000 - 50 000
E4M	29	8.5	3 000 - 5 600	320 000 - 380 000
K4M	22	8.1	3 000 - 5 600	320 000 - 380 000
K15M	22	8.1	11 250 - 21 000	480 000 - 540 000

[a] The parameters are acquired from product supplier (Dow Chemical). MeO and HPO columns indicate the levels of substitution in methoxy (MeO = $-OCH_3$) and hydroxypropyl (HPO = $-OCH_2CH(OH)CH_3$) groups. [b] These molecular weights were measured by Keary (2001)

The first letter of the product designation represents the chemistry of the cellulose ether. “A” means methylcellulose products; “E” and “K” represent hydroxypropyl methylcellulose products. The number and/or letter following the first letter indicates the viscosity of a 2% aqueous solution, which depends mainly on the molecular weight of the polymer.

Different amounts of A15, E4M, K4M or K15M polymer powders were dissolved in a 2.5% Na_2HPO_4 solution to get the corresponding cement liquid phases. These polymer powders are soluble in cold water but insoluble in hot water. When the polymer powders are mixed in cold water, however, lumping usually happens due to the incomplete wetting of individual powder particles. Thus a method called “hot/cold” technique was applied here, taking advantage of the insolubility of cellulose ethers in hot water. Specifically, the polymer powder was first mixed with the Na_2HPO_4 solution at 80 °C and dispersed by stirring thoroughly until all the particles were completely wetted and evenly dispersed. Then the solution was cooled and transferred into a refrigerator to reach a lower temperature at which the polymer becomes water soluble and starts to hydrate. After that, the solution was further stirred at room temperature for three days until hydration was complete.

A fixed L/P ratio of 0.45 mL/g was used for the preparation of cement pastes, but the polymer content in the cement was varied by using different amounts of polymer in the liquid phase. The different materials prepared are showed in Table 5-2.

Table 5-2 Concentration of cellulose ether additives in solution for CPC preparation

Mass fraction, by mass of solid phase	0.25 %	0.50 %	0.75%	1.00%	1.25%	1.50%	2.00%
A15 (w/v%)[a]		1.12		2.23		3.34	4.45
E4M (w/v%)	0.56	1.12	1.67	2.23	2.78		
K4M (w/v%)	0.56	1.12	1.67	2.23	2.78		
K15M (w/v%)	0.56	1.12	1.67				

[a] 1 w/v% = 10 g/L

The numbers in the first row represent the proportion of polymer in the final cement without taking water into account, i.e. the weight percentage of polymer with repect to the sum polymer + inorganic solid. The numbers in the other rows represent the amounts of polymer in the liquid phase solutions allowing to get the target mass fractions indicated in

the first row. Moreover, polymer solutions, prepared with E4M, K4M and K15M above certain concentrations, could not be used for viscosity reasons, since highly viscous solutions cannot be applied to fabricate homogenous and workable cement pastes.

5.1.2 Handling properties of composite CPC with cellulose ethers

Handing properties including injectability, cohesion (anti-washout) and setting time were measured on CPC composites prepared by using different cellulose ethers. Before showing the results, it is important to explain the behaviors of cellulose ethers in water. These behaviors can be classified in three categories (Khayat, 1995, 1998):

(1) Adsorption. The long-chain polymer molecules adhere to the periphery of water molecules, thus adsorbing and fixing the water and thereby expanding. This increases the viscosity of the water and that of the cement-based product.

(2) Association. Molecules in nearby polymer chains can develop attractive forces, thus further blocking the motion of water, causing a gel formation and an increase in viscosity.

(3) Intertwining. In static conditions or at low rates of shear, and especially at high concentrations, the polymer chains can intertwine and entangle, resulting in an increased viscosity.

All these actions occur simultaneously in the cellulose ether solution and in the cement-based system, contributing to an increase of viscosity. The above modes of action in aqueous solution can help to explain and understand experimental results.

5.1.2.1 Injectability

Before explaining the results, it is worth mentioning the definition of the injectability of a cement paste. Indeed, at present, there is no common definition in the biocement community about the meaning of injectability. In most cases, injectability has been related to the injection force that has to be applied to a syringe so as to deliver the cement paste, regardless of its quality, homogeneity or quantity (Khairoun et al., 1998; Wang et al., 2006). However, this definition appears not to measure the injectability of a paste, but rather its ease of injection, which is strongly dependent on the injection system (e.g. type of syringe, injection speed) (Bohner, 2010B; Bohner et al., 2005A). Moreover, the definition does not consider the quality of the extruded paste in which phase separation (also called filter-pressing and will be discussed later) may happen, probably causing a deviation of the actual composition of the extruded paste from the initial one.

Furthermore, due to this deviation, it also becomes unclear whether the setting, mechanical and biological behaviors of the extruded cement are still clinically acceptable (Dorozhkin, 2008). Therefore, it is imperative to redefine the meaning of injectability in which all these aforementioned problems can be eliminated. To this end, the injectability of a paste is defined here as its capacity to stay homogeneous during injection, independently of the injection force (Bohner et al., 2005A).

To get a good injectability, i.e. a homogeneous paste, it is important to understand the mechanisms limiting the injectability of a cement paste. According to Bohner et al. (2005A; 2010B), when the cement paste (e.g. a mixture of powder and liquid) is submitted to a pressure gradient, the liquid may flow faster than the solid, causing a regional change of the paste composition. In detail, the paste present in the zone of the highest pressure (e.g. close to the plunger of the syringe) may become so depleted in liquid that the powder-liquid mixture in this region becomes a wet powder rather than a paste. In contrast, the paste in the zone of the lowest pressure (e.g. at the cannula tip) is enriched in liquid. With time, the volume of the region depleted in liquid (wet powder) increases during injection, finally getting to the tip of the syringe and plugging it (Bohner, 2010B; Bohner et al., 2005A). The phenomenon is generally called filter-pressing (or phase separation or liquid phase migration), which is mostly believed to be the mechanism underlying the limited injectablity of a cement paste and has been proved by Habit et al (2008).

As reviewed previously, many methods have been used to reduce or to eliminate filter-pressing in order to improve the injectability of cement pastes (Andrianjatovo et al., 1995; Burguera et al., 2006; Ishikawa, 2003; Khairoun et al., 1998). Among these methods, the most adequate and applicable one is to increase the viscosity of the liquid phase since it is the only method[18] that can improve the injectablity of cement pastes and at the same time does not compromise neither the cohesion nor the anti-washout performance (Bohner et al., 2005A).

The same strategy has been applied in this study to try and enhance the injectability by mixing the cement powder with viscous cellulose solutions. Specifically, the increased

[18] In fact, using a cement powder with a smaller average particle size can also improve both injectability and cohesion of a cement paste. However, this method is difficult to apply since the particle size distribution of a cement paste changes continuously due to dissolution and precipitation. Thereby, using small particles may perhaps only improve temporarily/initially the injectability of the cement, but not for the whole injection process (Bohner et al., 2005A).

viscosity of a composite cement paste may effectively reduce or even prevent filter-pressing, thus significantly enhancing injectability.

The injectability of composite CPC is significantly improved by adding different amounts of cellulose ethers, as shown in Fig. 5-1. For instance, by adding only 0.25% of E4M, the injectability of the resulting paste can be increased by 75%.

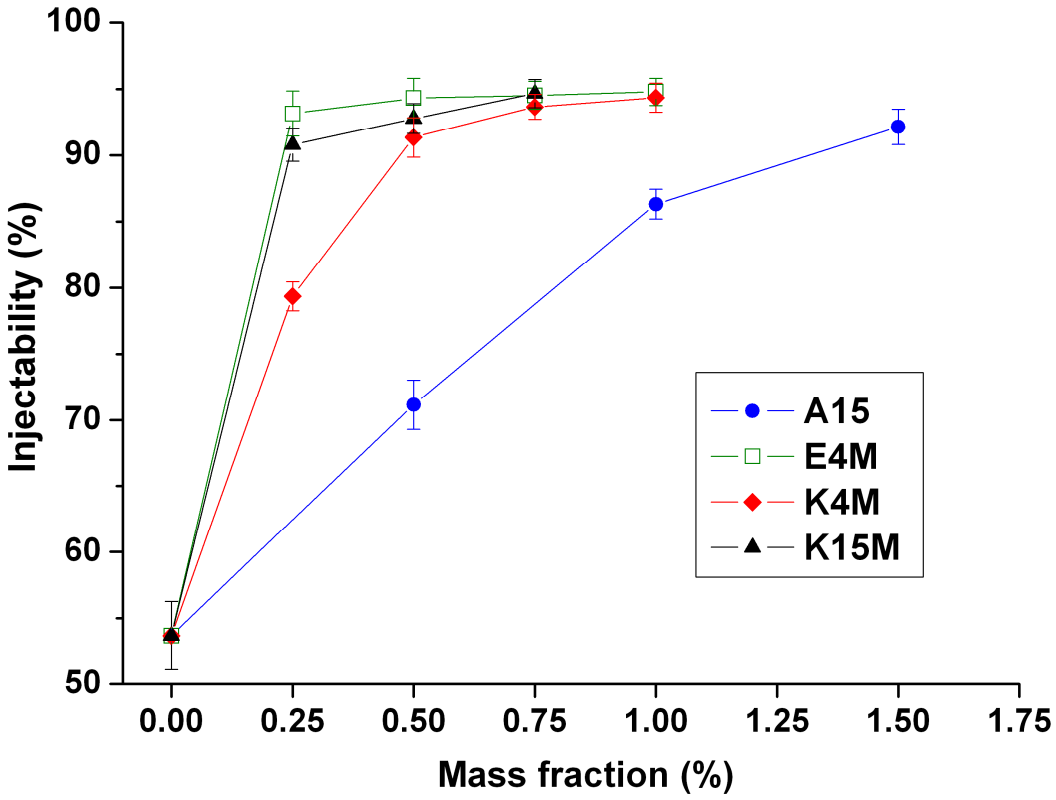

Fig. 5-1 Injectability of the paste with different contents of additives at L/P = 0.45 mL/g, 6 min after starting the mixing of liquid and powder. Each value is the mean of three measurements ± one standard deviation.

The viscosity of a composite cement paste is dependent on the viscosity of the cellulose solution which is roughly proportional to its molecular weight and concentration. Therefore, the larger the molecular weight or concentration of cellulose ether added, the higher the viscosity of the resulting cellulose solution, and the higher the viscosity of the composite cement paste. According to the above discussion, the injectability of composite cement pastes prepared with various cellulose solutions at the same concentration (e.g. 0.25%) should be ranked in the following ascending order: A15 < E4M ≈ K4M < K15M. However, interestingly, the composite cement prepared by adding the E4M solution (with a similar viscosity to K4M) appears to demonstrate the

best injectability, as shown in Fig. 5-1.

This discrepancy can be explained by analyzing the rheological properties of the composite cement pastes. In general, aqueous polymer solutions (e.g. cellulose ether solutions in this case) are non-Newtonian fluids and exhibit a pseudoplastic flow behavior, or shear thinning (Holmberg et al., 2002). The systems (here refers to CPC) modified with viscous polymer solutions generally also exhibit pseudoplasticity (Khayay, 1998; Wang et al., 2007). Moreover, the pseudoplasticity increases with increasing molecular weight or concentration. When submitted to a certain shear rate, due to their pseudoplastic behavior, the apparent viscosities of all the composite cement pastes would decrease, but in different extents, owing to the mixed cellulose solutions of various molecular weights. As for E4M, since it has a smaller molecular weight than K15M, its pseudoplasticity is less important (Dow chemical, 2002), although the same rule should apply to K4M. However, as listed in Table 5-1, E4M has a higher degree of substitution of MeO and HPO groups than K4M and K15M, which may result in a stronger steric effect, thereby further reducing its pseudoplastic behavior. According to the above two factors, it is possible that under a certain shear rate the apparent viscosity of the composite cement paste prepared with E4M solution at 0.25% is higher than that of the composite cement paste prepared with K4M solution at the same concentration, and even higher than that of the composite cement paste prepared with K15M solution at the same concentration, therefore resulting in a better injectability (Fig. 5-1). Furthermore, with increasing concentration, the apparent viscosities of composite cement pastes (E4M, K4M and K15M) continues increasing to a certain level so that all the cement paste can be extruded[19] (e.g. E4M and K4M at 1%).

In addition, the extrusion curves during injection are recorded, which can further verify previous results and explanations (Fig. 5-2). The extrusion curves are generally characterized by four more or less defined stages: (1) an overshoot followed by (2) a plateau, (3) a slow non-linearly increasing force and (4) finally a fast linearly increasing force until reaching the maximal extrusion force (e.g. 100 N in this study) (Fig. 5-2). The overshoot is related to yield stress (Baroud et al., 2005; Liu et al., 2006). Composite cement pastes have higher yield stresses than the control cement paste, which is mainly due to the extra force needed to overcome the internal resistance from entangled cellulose

[19] Actually, there is an upper limit to the injectability as measured by this method because even though the plunger reaches the end of the syringe, a small fixed amount of cement paste remains in the tip of the syringe. This can explain why the maximal injectability is around 95% (see Fig. 5-1).

molecules to initiate paste flow (Khayat, 1998). The plateau stage can be found in nearly all the composite cement pastes. During this stage, the extrusion force is almost constant, indicating that the composite cement pastes remain homogeneous and that little or even no filter-pressing happens due to the increased viscosity (Fig. 5-2). In contrast, the plateau disappears in the control cement paste and only stages 3 and 4 can be observed (Fig.5-2), implying that filter-pressing happens immediately after extrusion starts (Bohner et al., 2005A; Habib et al., 2008), which is related to a bad injectability (Fig. 5-4). Besides, different extents of filter-pressing (stage 3) can be also observed in composite cement pastes, depending on the molecular weight or concentration of cellulose ether solutions (Fig. 5-1, 5-2).

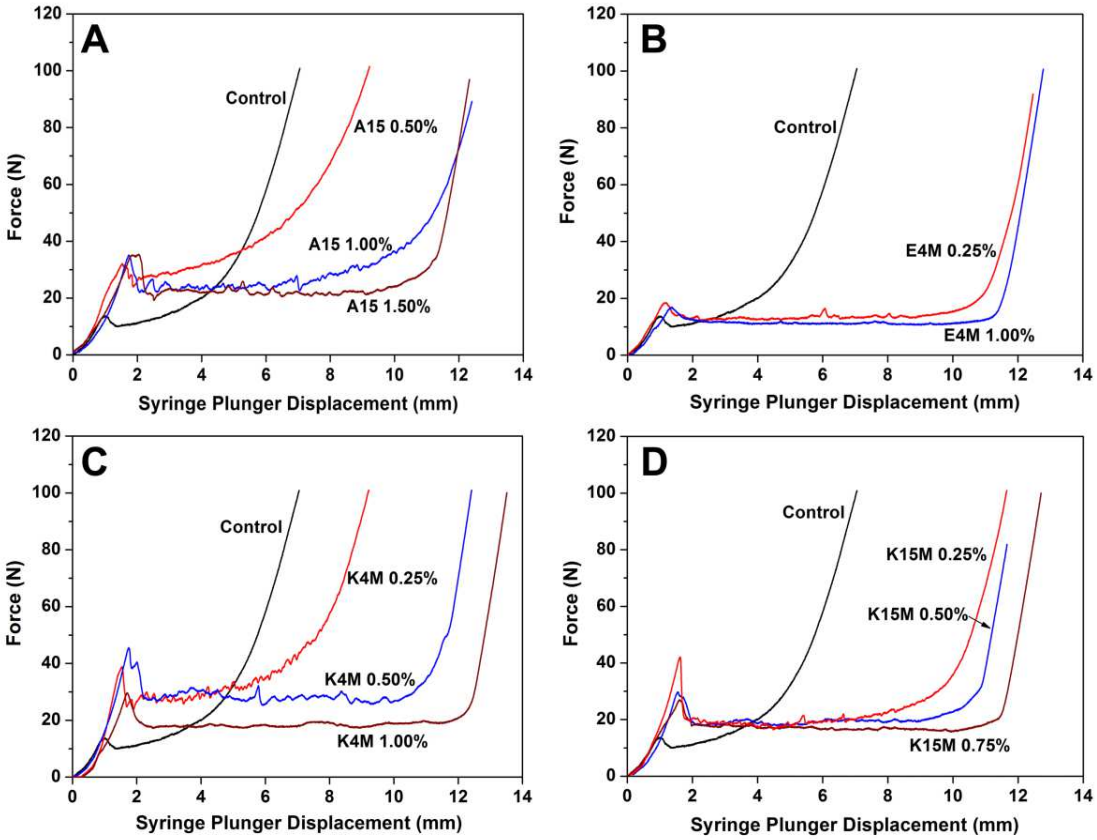

Fig. 5-2 Injection force curves during extrusion of the pastes with different mass fractions of additives, A) A15, B) E4M, C) K4M and D) K15M.

Generally, a cement paste starts being extruded from the syringe at the starting point of stage 2 and stops being extruded at the end of stage 3. Beyond stage 3, the cement behaves like a compact wet powder rather than like a paste, resulting in a rapidly and linearly increasing force. In fact, once extrusion force reaches stage 4, no matter how big the forces applied to the plunger, the paste is no longer amendable to injection.

Moreover, it is worth noting that the stage 4 mentioned above is only suitable for a cement which is not completely extruded. In the case of a cement extruded completely, the stage 4 is mainly related to the mechanical stiffness of the injection apparatus. Therefore, according to the above discussion, the injectability of composite cement pastes can also be qualitatively evaluated by the ratio of the volume injected during stage 2 (which is proportional to its length) over the total initial volume of the paste. The longer the stage 2, the better the injectability (Fig. 5-2), which can be achieved by using highly viscous cement liquids (Bohner et al., 2005A; Dorozhkin, 2008). Actually, if the apparent viscosity of the cement paste is high enough so that filter-pressing can be mostly avoided, a very small or even no stage 3 will be observed in the extrusion curve, meaning that the final steep increase in injection force is only due to the fact that full injection is reached, so that stage 2 has its maximum possible length, relating to an excellent injectability (Fig. 5-2B).

5.1.2.2 Cohesion and anti-washout performance

As expected, the addition of different cellulose ethers pronouncedly improves the cohesion and anti-washout performance of the composite CPC, by either using a cellulose ether additive with a high molecular weight or increasing the dosage of the additives (Fig. 5-3).

In previous studies regarding cement-based materials (Bohner, 2010B; Dorozhkin, 2008; Khayat, 1998), the improved cohesion and anti-washout have been mainly attributed to the improved rheological properties (e.g. viscosity) of the cement-polymer composite which is based on a viscous polymer solution. As expected, this conclusion should be also valid in the present CPC system. In this study, compared to the control (e.g. not composite) cement, the addition of HPMC or MC can increase the viscosity of the cement paste and therefore this increased viscosity should also play a key role on the improvement of cohesion and anti-washout performance. However, for a better understanding of this specific mechanism, it is worth firstly introducing how decohesion and washout of cement pastes happen in an aqueous solution. Basing on the definitions introduced previously, the cohesion of CPC can be viewed as an interaction between the CPC paste and the surrounding fluid. This interaction is mainly governed by the osmotic pressure (Bohner et al., 2006B), which is dependent on the difference in concentration of dissolved ions and molecules between the interstitial fluid of the cement paste and the surrounding liquid. If the total solute concentration in the solution is lower than in the

interstitial liquid, the flow from the solution into the cement will be larger than in the opposite direction. This flow enlarges the distance among cement particles and weakens their interaction, therefore resulting in decohesion of the cement (Bohner et al., 2006B). As for the washout of CPC, besides the above mentioned mechanism, a shearing force between the cement paste and the surrounding liquid further strengthens this behavior.

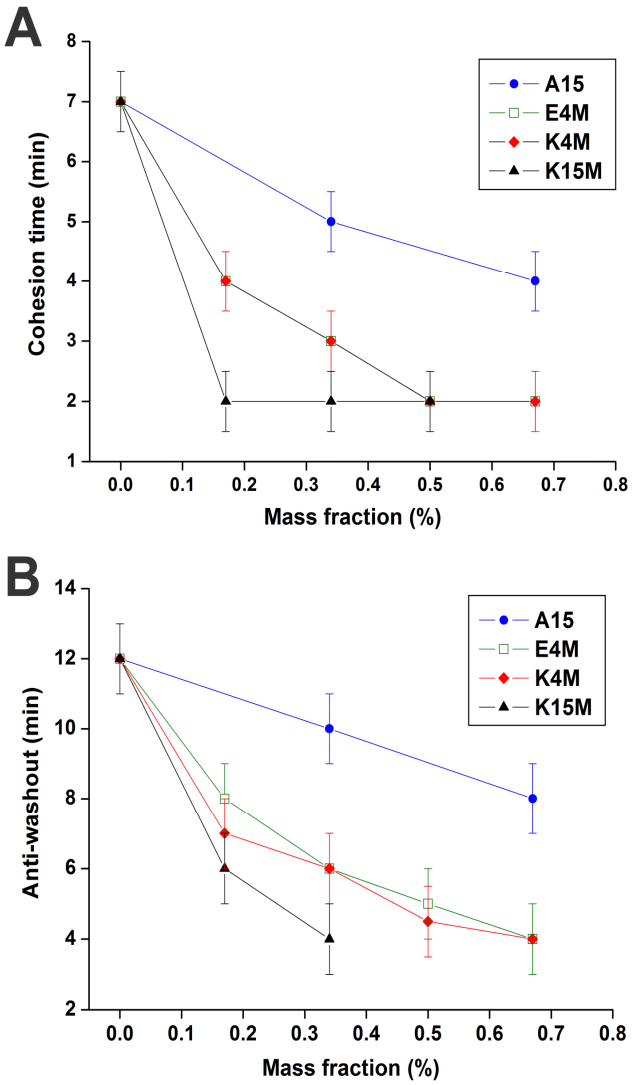

Fig. 5-3 (A) Cohesion time and (B) anti-washout performance of the cement pastes with different contents of additives (L/P = 0.30 mL/g). Each value is the mean of three measurements ± one standard deviation.

Thus, according to the above discussion, the specific process of how an increased viscosity helps to improve cohesion and anti-washout may be detailed as follows: (1) when immersed in a saline solution, the viscous cement paste may effectively reduce the influence of osmotic pressure and therefore well reduce its dilution or bleeding (Khayat, 1998), as evidenced by the consistent cement paste where no noticeable

swelling is observed; (2) the strong interaction within the polymer-coated cement grains due to the increased viscosity prohibits the release of the particles into the surrounding liquid. Both of the above two effects may contribute to the improved cohesion and anti-washout performance of CPC. So it can be also expected that the two effects will become more obvious by using a polymer solution prepared by adding cellulose ether of larger molecular weight or higher mass fraction, well explaining the observation in Fig. 5-3.

Besides, the addition of cellulose ethers to CPC also has an important meaning in surgery. In fact, for most CPCs, the difference between the cohesion time (without adding cohesion promoters) and initial setting time is small so that it is hardly possible to apply CPC clinically in an acceptable way without improvement of the properties (Khairoun et al., 1999). By using cellulose ethers, the cohesion time is significantly shortened, and at the same time setting time is prolonged (this point is discussed in 5.1.2.3), creating a certain period during which the CPC can be used safely.

5.1.2.3 Setting time

The initial and final setting times of CPC prepared by adding different amounts of cellulose ether additives are shown in Fig. 5-4.

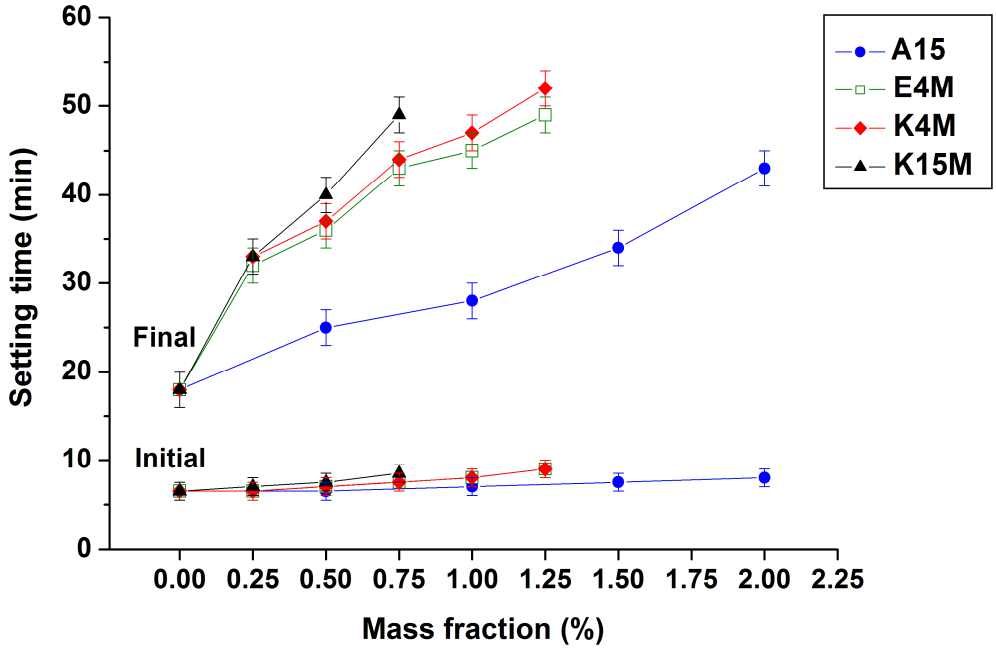

Fig. 5-4 Initial and final setting times of pastes prepared with different contents of four typical cellulose ethers (A15, E4M, K4M and K15M), with a L/P ratio of 0.45 mL/g. Each value is the mean of three measurements ± one standard deviation.

It is obvious that the initial setting times of the cements are only slightly delayed. In contrast, the final setting times of the cements are pronouncedly prolonged when the amount of additives increases.

As for the mechanism of delayed setting in composite CPC, it is considered to be similar to that in Portland cements (Weyer et al. 2005; Khayat, 1998). It is believed that cellulose ether macromolecules adsorb onto the cement grains or initial hydration product, forming a less permeable coating, and interfere with the dissolution of minerals, thereby influencing the rate of hydration and setting (Khayat, 1998; Khayat, et al., 1997; Pourchez, et al., 2010A). In the present CPC system, from an imaged viewpoint, the cellulose ether in the water can indeed be taken as a nano-sized mussy swelling "ball", which consists of long entangled polymer chains and fixes water inside. The nano-sized cellulose ether "balls" adsorb to the surface of micro-sized (6 μm) α-TCP, acting as "barriers" interfering with the dissolution of Ca^{2+} and PO_4^{3-} into water, therefore affecting the precipitation of apatite and prolonging the setting times. Thus it can be also speculated that the larger the molecule weight and the higher the concentration, the bigger the "balls" and the "barriers", the more difficult it is for the ions to permeate and precipitate. This mechanism can well explain the longer setting time for CPC composites prepared by adding cellulose ethers of large molecular weight or high mass fraction, as shown in Fig. 5-4. It must be noted that the above assumption does not take into account the influence of viscosity, which is usually expected to be an important factor controlling the diffussion of solutes. This is mainly due to the fact that the diffusivity of a small solute (Ca^{2+} and PO_4^{3-} in this case) in a polymeric solution is generally not severely affected by the macroscopic viscosity of the polymeric solution (Osmers et al., 1972). Moreover, the phases of the composite CPC were examined by XRD (Fig. 5-5).

Despite the observed retarding effect on setting, it is observed that after five days of hardening most of the α-TCP transforms into CDHA in the cement without or with cellulose ether additives and no noticeable difference is found among them, indicating that these additives do not inhibit the final formation of CDHA.

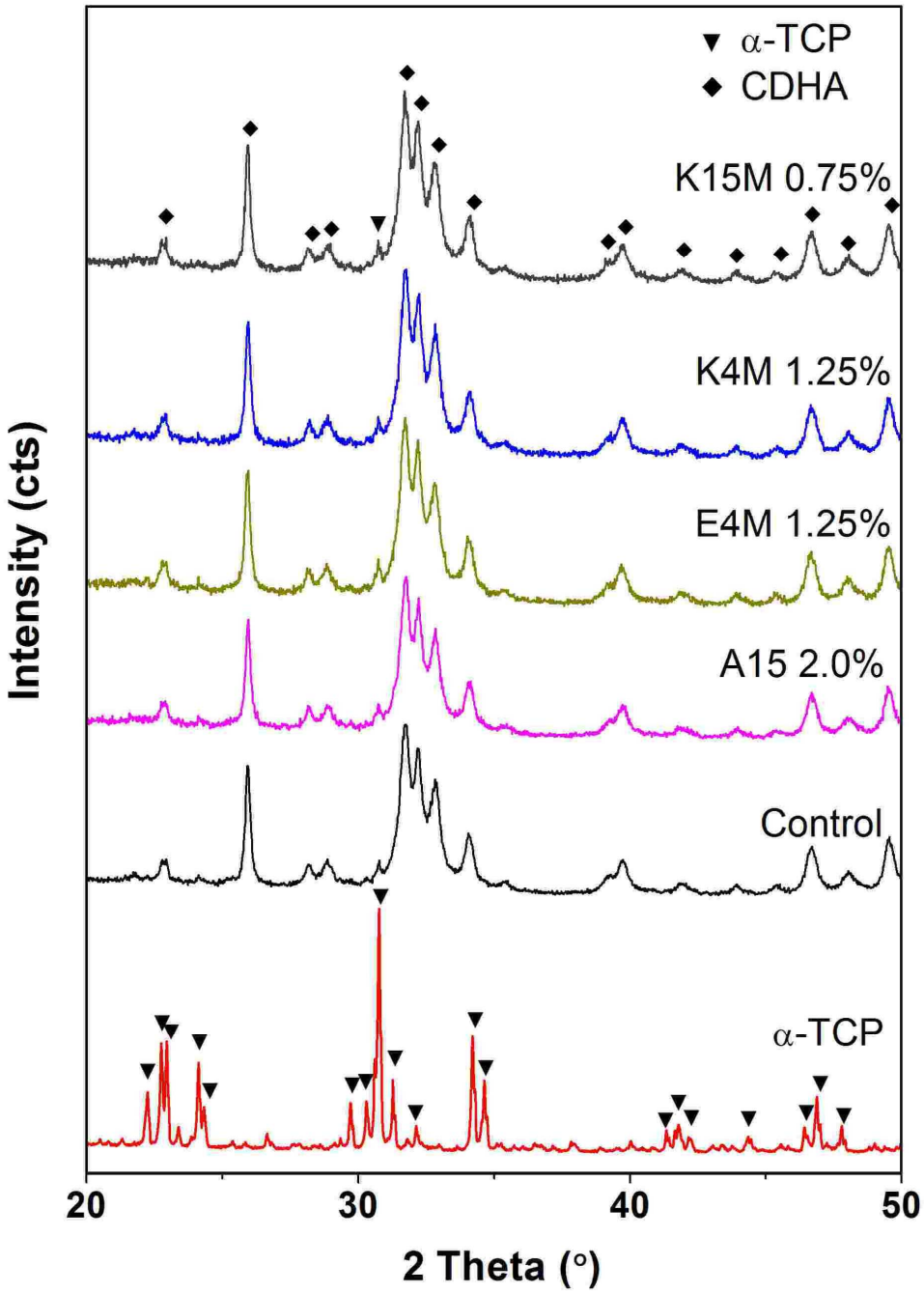

Fig. 5-5 XRD patterns of the α-TCP powder and its hardened products without or with different cellulose ether additives

5.1.3 Microstructure and mechanical properties

Both handling properties and mechanical properties are very important for surgical application of CPC. As demonstrated in 5.1.2, the cellulose ethers used in this study pronouncedly enhance handling properties such as injectability, cohesion and anti-washout. To examine whether these cellulose ethers influence mechanical properties, the fracture toughness and compressive strength of the composite cements prepared with

the cellulose ethers were measured[20]. Furthermore, since CPC is intrinsically porous and its porosity strongly influences mechanical properties, the porosity of these composite CPC was also measured. In the graphs of the following sub-sections, six samples were measured to calculate the mean of porosity and mechanical properties, with error bars showing one standard deviation.

5.1.3.1 Porosity

As shown in Fig. 5-6, compared to the control cement (mass fraction = 0%), the porosity of composite CPC with different cellulose ethers increases monotonically with the increasing mass fraction of each cellulose ether added.

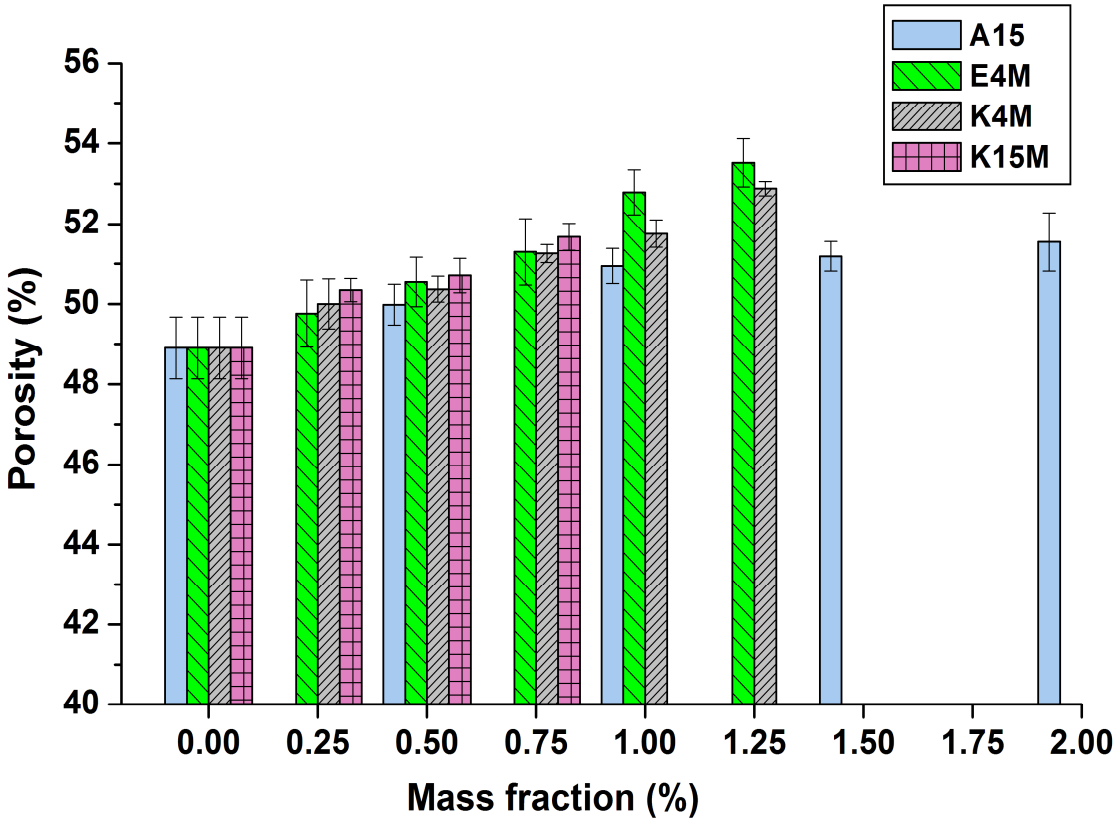

Fig. 5-6 Porosity of the CPC with different mass fractions of cellulose ether additives (L/P = 0.45 mL/g). Each value is the mean of six measurements ± one standard deviation.

This phenomenon can be explained by considering what happens during the mixing

[20] Indeed, besides fracture toughness and compressive strength, it is also of great interest to measure Young's modulus and flexural strength of the composite cements with HPMC / MC. However, because of the huge number (204) of rhombohedral specimens required for completing all the measurements, only the results of fracture toughness and compressive strength are available at the time of writing this manuscript.

process of the cement paste. Generally, due to the viscosity of the cement paste, a certain volume of air can be brought into the paste during the process of mixing the solid and the liquid phases. The SEM micrographs of fracture surfaces of CPC composite cements without and with different mass fractions of cellulose ethers (A15, E4M) at a magnification of 50× are shown in Fig. 5-7.

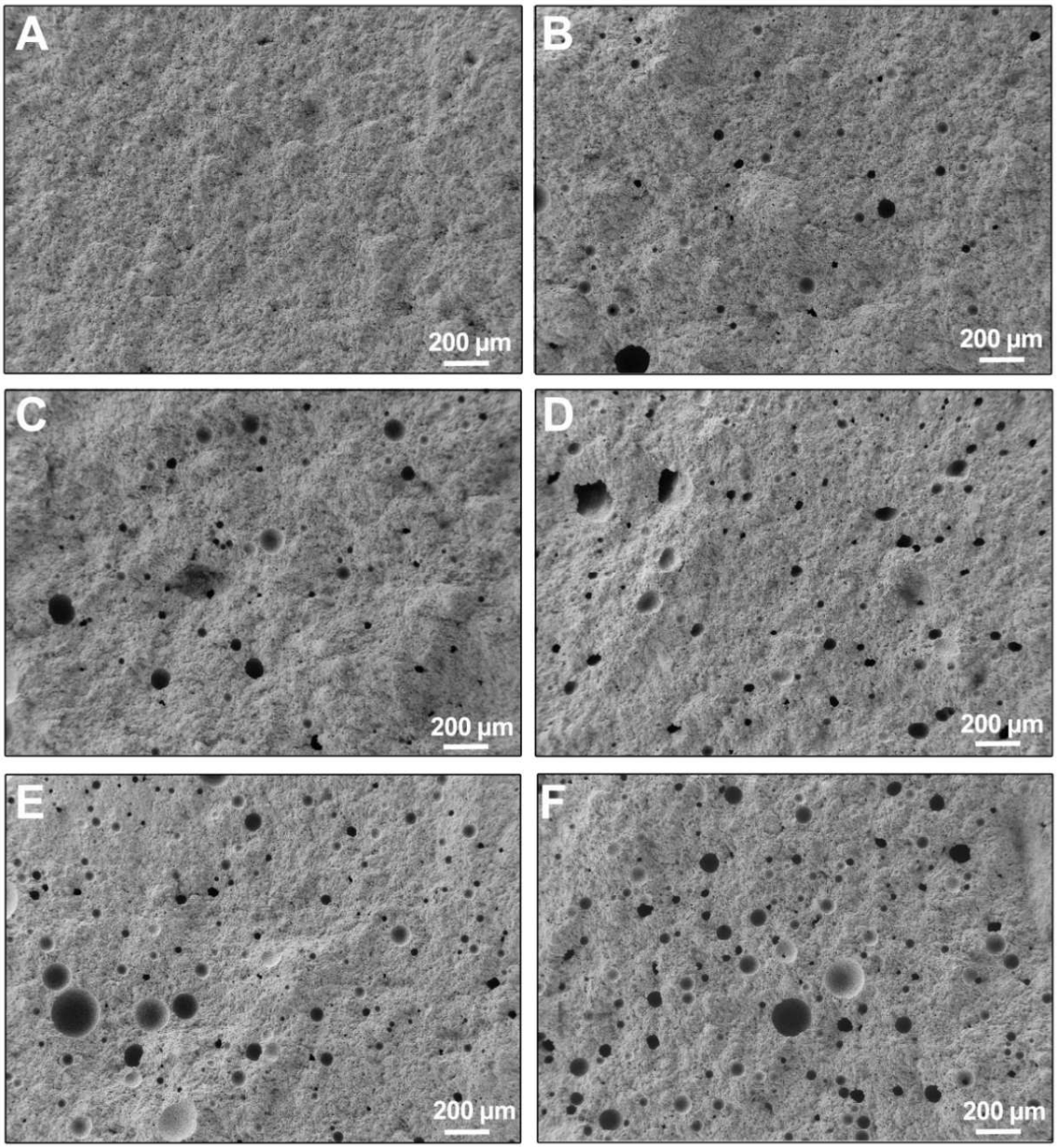

Fig. 5-7 SEM pictures of the fracture surface of CPC specimens with different mass fractions of additives under a magnification of 50× (A) Control, (B) with 0.5% of A15, (C) with 1.0% of A15, (D) with 2.0% of A15, (E) with 0.5% of E4M, (F) with 1.0% of E4M.

As can be seen, no entrained air bubbles can be observed in the control cement (Fig. 5-7A). However, once a cellulose ether is added, even with the lowest viscosity

(A15) and in a relatively small mass fraction (0.5%), some air bubbles of various sizes can be easily found (Fig. 5-7B). With the increasing mass fraction of A15, the amount of entrained air bubbles increases concomitantly (Fig. 5-7C, D). In addition, as expected, more air bubbles can be observed when a cellulose ether with a higher viscosity like E4M is used (Fig. 5-7E, F). The SEM observation is consistent with the porosity measurements presented in Fig. 5-6. In the literature review of Chapter 1, macropores (> 100 μm) were noted to be essential for cell migration into the implant (Hing et al., 1999). Therefore, from the osteoconductive point of view, these large entrained air bubbles may be considered as a positive factor.

The ability to form air bubbles and then to stabilize them is strongly dependent on the property of the cement liquid. In this study, the liquid solution used for the control cement has a high surface tension (similar to that of water) which is detrimental for the formation of air bubbles. Moreover, the liquid solution is very fluid (low viscosity) and therefore cannot help to stabilize the formed air bubbles, and also cannot prevent them from going up through the paste and breaking at the surface. In contrast, cellulose ethers, acting as surfactants (surface-active agents), can lower the surface tension of the liquid solution and thereby are helpful for the formation of air bubbles. Furthermore, as mentioned previously, cellulose ethers can increase the viscosity of the liquid solution, which is very useful for the stabilization of air bubbles and also prevents them from moving up and being eliminated at the surface. The more viscous the liquid solution, the more stable the entrapped air bubbles. The phenomenon that air bubbles are entrained during mechanical mixing and stabilized by cellulose ethers has also been observed in other cement-based materials (Jenni et al., 2005; Khayat, 1998; Pourchez et al., 2010B).

5.1.3.2 Fracture toughness

The fracture toughness of the composite cements with different cellulose ethers are shown in Fig. 5-8. The measured values of fracture toughness for the composite cements are generally higher than those of the control cement, although the difference is small and in most cases not significant given the overlapping error bars.

However, in order to better understand the influence of cellulose ethers on fracture toughness, it is interesting to plot the fracture toughness of composite cements as a function of total porosity (Fig. 5-9 A, C, E and G).

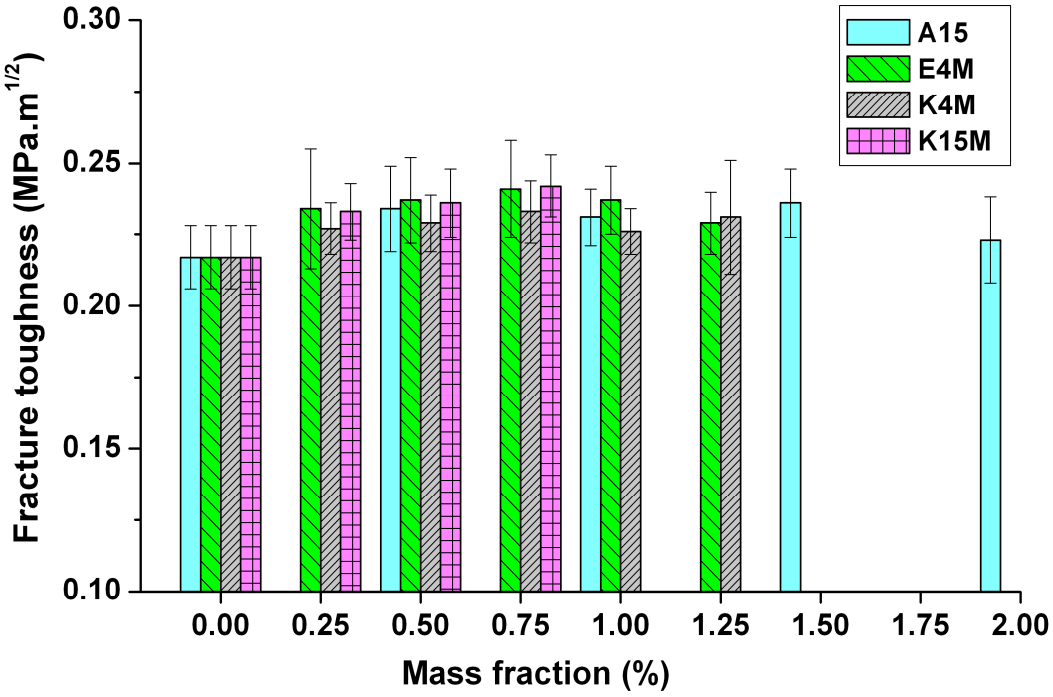

Fig. 5-8 Fracture toughness of composite CPC with different mass fractions of cellulose ethers additives (L/P = 0.45 mL/g). Each value is the mean of six measurements ± one standard deviation.

As can be seen, the fracture toughness of the composite cements remains constant or even increases with increasing porosity, which is nevertheless different from our previous result that fracture toughness decreases with the increase of porosity, indicating that the cellulose ethers have a toughening effect on CPC. However, this assumption only holds if the toughness of the composite cements is compared with that of control cements with the same porosities. Unfortunately, preparing control cements with exactly the same porosities as those of composite cements is practically impossible. For this reason, the curve of a mathematical model (as the models shown in Chapter 3) was adjusted to pass through the corresponding data point of control cement to assist the comparison (see Fig. 5-9A, C, E and G). A power law is chosen because it has been successfully used in previous studies to fit mechanical properties of CPC. As for the exponent m to be used, it is worth noting that the composite cements contain both micropores and macropores created by entrained air bubbles, but, because their macroporosity is difficult to be determined precisely, it is not suitable to choose directly the exponent m fitted for either microporous (about 4) or macroporous (about 2) control cements. For this reason, the average value (about 3) of the exponent m for the microporous and macroporous control cements was deliberately chosen here.

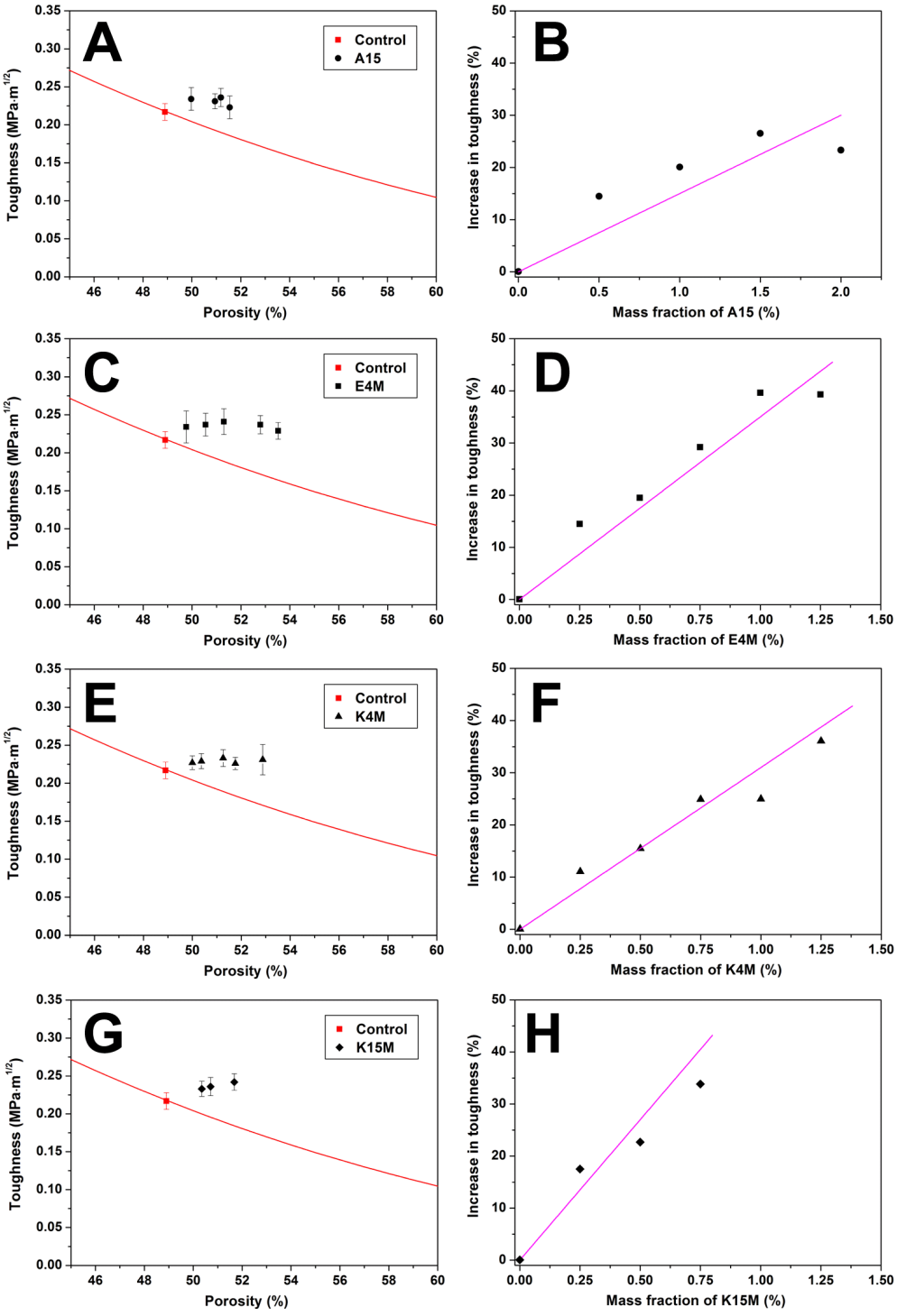

Fig. 5-9 Fracture toughness of composite cements (A) A15; (C) E4M; (E) K4M; (G) K15M as a function of porosity. The red curve crossing the data point of the control cement is representative of a mathematical model (power law in this case) assisting comparison of fracture toughness between composite and control cements with the same porosity. (B), (D), (F) and (H) show the relative increase of toughness as a function of the polymer mass fraction, compared to virtual control cements with identical porosities. The pink lines indicate schematically the increase in toughness of the composite cements. Each value is the mean of six measurements ± one standard deviation.

In fact, in the present study the power law associated with this exponent m has no physical meaning, but is just used as an indicative tool to show how fracture toughness evolves with porosity to assist the comparison between composite and control cements with the same porosity. This method (principle) will also be used in the following studies. As can be seen (Fig. 5-9A, C, E and G), the fracture toughness of all the composite cements is obviously higher than that of control cements with the same porosities. Furthermore, the relative increase in toughness of the composite cements (compared to "virtual" control cements with identical porosities) is plotted as a function of polymer mass fraction (Fig. 5-9B, D, F and H). The toughness increases continuously and strongly with the polymer mass fraction, indicating that the cellulose ether additives do have significant toughening effects on CPC. In addition, the data points of the relative increase of toughness can be globally described by straight lines. The slopes of the lines (related to the rate of increase in toughness) are plotted as a function of the molecular weights of the cellulose ethers (Fig. 5-10). As can be seen, the slopes globally increase with the increase of the molecular weight of the cellulose ethers, indicating that the latter also have a significant effect on the toughness of composite cement: with the same concentration of cellulose ethers, the higher the molecular weight, the faster the toughness increases.

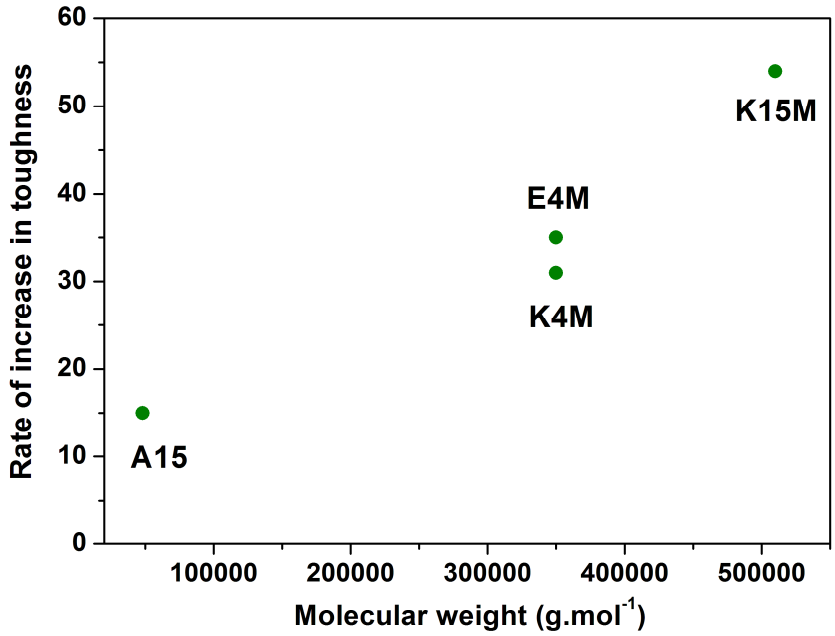

Fig. 5-10 Rate of increase in toughness of composite cements as a function of the molecular weight of cellulose ethers added.

The influences of various additives on the mechanical properties of CPC have been widely studied (Bermudez et al., 1993, 1994; Bohner et al., 2000; Brown et al., 1991; Durucan et al., 2002B; Fernandez et al., 1998). Among the additives, cement retarders, which may delay cement setting, are positively correlated with a higher strength (Barralet et al., 2004; Bohner et al., 2000; Durucan et al., 2002B; Fernandez et al., 1998; Ginebra et al., 2001; Marino et al., 2007). For instance, carboxylic acids (citric acid or glycolic acid) have been reported to initially retard cement setting but finally improve the strength. The strengthening mechanism is mainly attributed to the easier mixing of the cement and to the possibility to fabricate the cement with a reduced L/P ratio (resulting in a smaller porosity), thus ending in improved mechanical properties (Barralet et al., 2004; Marino et al., 2007). Methacrylamide, a derivative from 4-aminosalicylic acid, has also been noted to firstly hinder cement setting but to improve the strength in the end. Besides the reduced porosity, the reduced size of the precipitated crystals is regarded as the other factor leading to an enhanced strength (Ginebra et al., 2001). In the above research, the authors did not measure the fracture toughness, thus it is very hard to determine if the mentioned strengthening mechanisms could also improve the toughness of the cement.

As shown in Fig. 5-4 and Fig. 5-8, similarly, cellulose ethers initially retard the setting of composite cements but finally improve the fracture toughness. One may postulate that the above mentioned strengthening mechanisms are also suitable in this study. Nevertheless, experimental results seem to overthrow this speculation. For the first mechanism, inversely, the porosity of the composite cement is increased but not reduced (Fig. 5-6, 7). For the latter mechanism, no obvious difference can be observed in the crystal size and shape between control and composite cements (Fig. 5-11). This observation also indicates that although inhibiting the hydration of α-TCP at an early stage, the cellulose ethers do not influence the final formation of apatite crystals, which is consistent with the result of XRD (Fig. 5-5). Therefore, according to the above discussion, other toughening mechanisms should be proposed to account for the improved fracture toughness.

As reviewed previously, fracture toughness is defined as the ability of a material containing cracks or notches to resist crack propagation. Increasing fracture toughness can be achieved either by increasing the resistance of the microstructure ahead of the crack tip, or by reducing the effective stress intensity factor at the main crack tip, by crack bridging for instance, or even through both (Launey et al., 2009; Rödel, 1992; Steinbrech, 1992; Swain et al., 1984).

α-TCP particles have a median size of 6 μm. Because of milling process and the presence of humidity in the atmosphere, the small particles tend to stick together and form agglomerates. When mixed with α-TCP, cellulose ether molecules are adsorbed to the surface of the α-TCP particles. Due to their steric effect, the cellulose molecules can reduce the attractive Van der Waals force between the particles, thereby separating the particles and preventing them from forming agglomerates, resulting in a more homogeneous particle distribution in the paste (Burguera et al., 2006). Moreover, the homogenously distributed particles in the paste can be further stabilized by the increased viscosity of the composite cement paste. Therefore, it can be expected that the growth of apatite crystals from a homogeneous paste can finally form a uniform and optimized microstructure with fewer defects, resulting in an improved fracture toughness (Sarda et al., 2002).

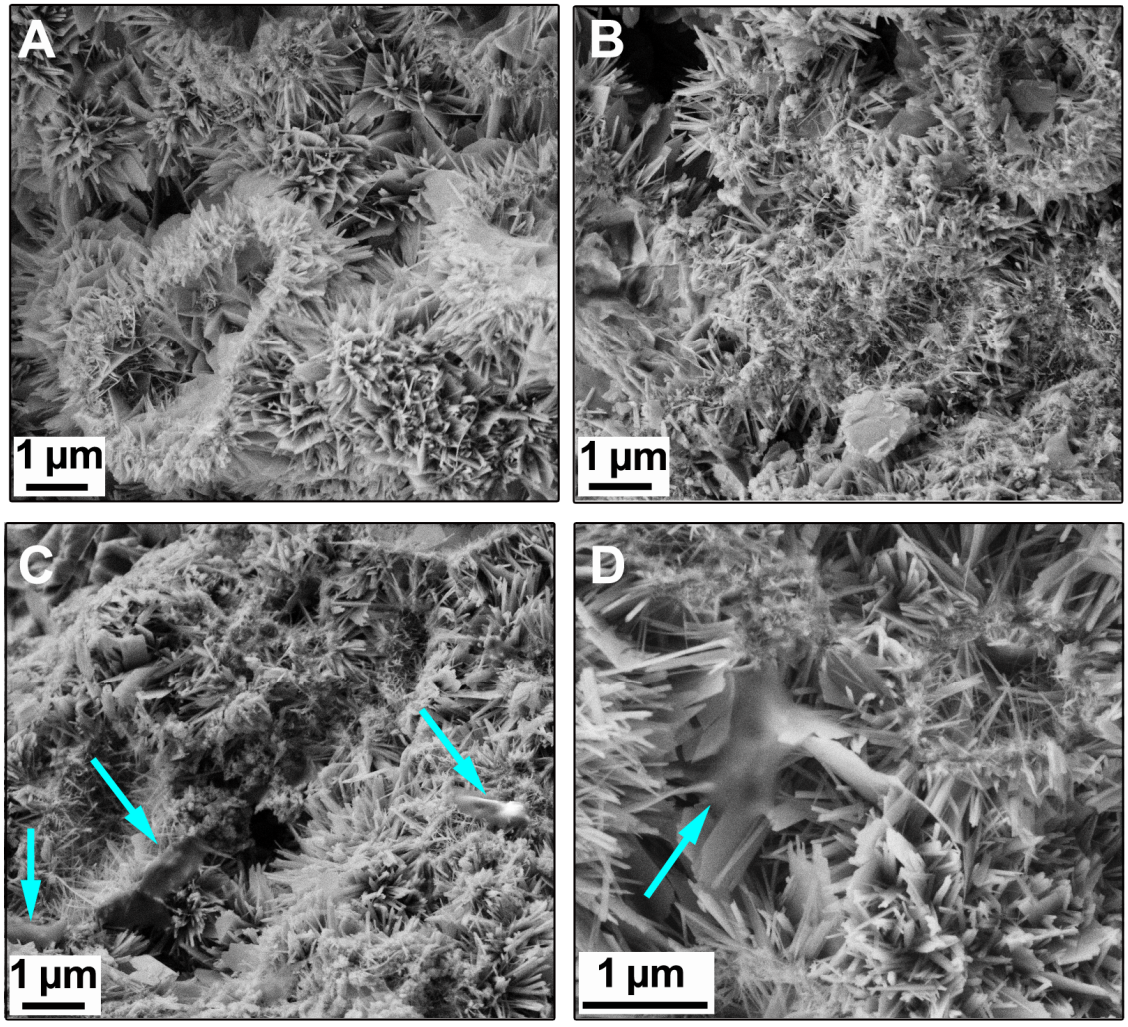

Fig. 5-11 SEM images of the fracture surface of CPC specimens (A) Control, (B) with 1.0% of A15, (C) with 1.0% of E4M, and (D) with 1.0% of K4M. The arrows indicate the polymer in the cement.

In addition, although the absorption bands of the cellulose ethers cannot be found in the FTIR spectra of the composite cements (Fig. 5-12), which may be due to the fact that the absorption bands of calcium phosphate components overlap the possible polymer absorptions bands (Weiss et al., 1997), some glue-like polymers, which may be derived from shrunk cellulose ethers after drying, can still be found sticking to neighboring apatite crystals (Fig. 5-11 C, D).

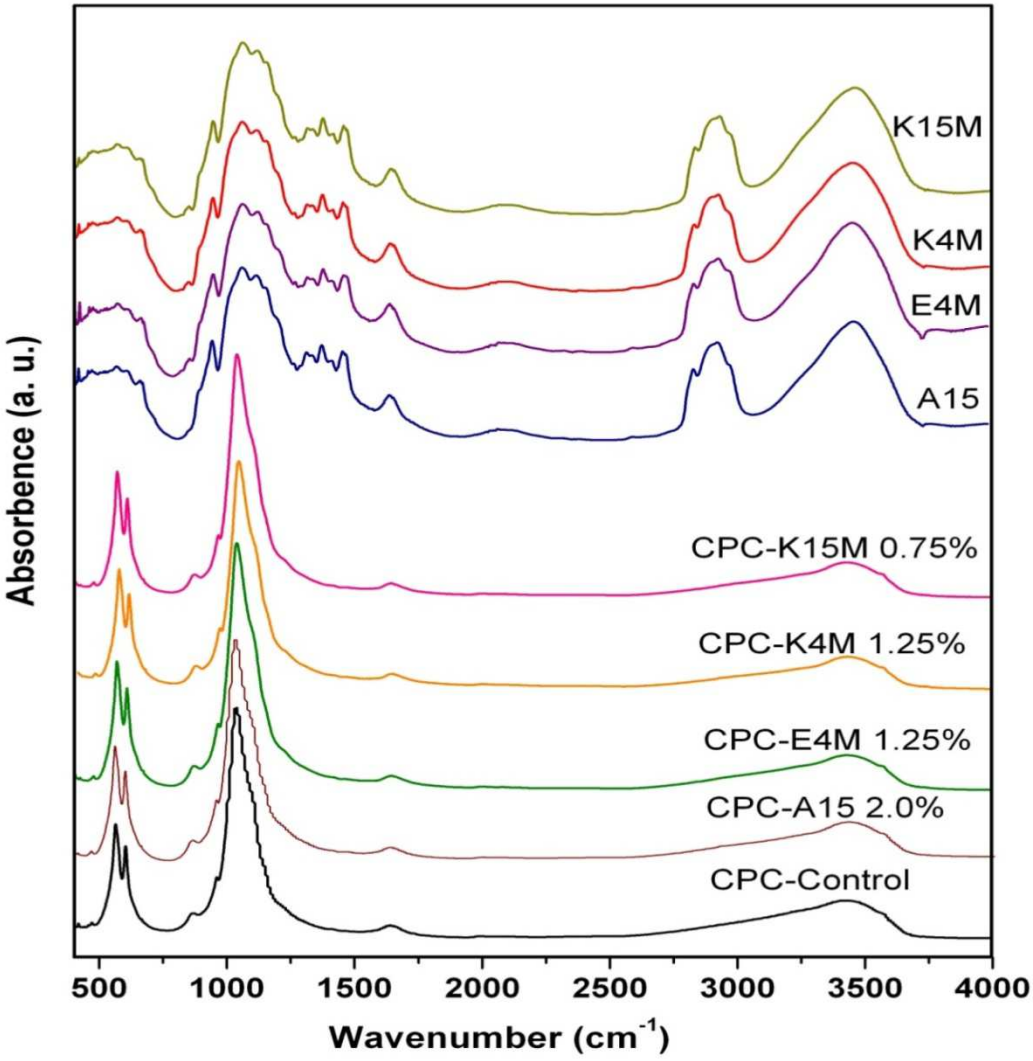

Fig. 5-12 FTIR spectra of the cellulose ethers additives and the composite CPC specimens. No visible difference can be found in the FTIR spectra of CPC specimens without or with different additives.

These polymers can help to alleviate the crack-driving force through crack bridging (linking cracks and consuming more energy through an elastic-plastic deformation), thereby further enhancing the fracture toughness (Launey et al., 2009). According to Ashby (1993), the increase in toughness due to crack bridging by plastically deforming

ligaments should be proportional both to the volume fraction and to the intrinsic strength of the reinforcing phase. The former effect has been evidenced in our composite cements (Fig. 5-9B, D, F and H), where the relative increase in toughness has been found to be proportional to the mass fraction of each polymer added; the latter effect would be consistent with the observation of Fig. 5-10, where the rate of increase in toughness has been found to depend on polymer molecular weight. Indeed, the strength of a polymer is usually, among others, linked to its molecular weight (Hallam et al., 1987). Thus, both the optimized microstructure with improved homogeneity and crack bridging by polymer ligaments may contribute to the enhanced fracture toughness of composite cements.

5.1.3.2 Compressive strength

Fig. 5-13 shows the compressive strength of the composite CPC prepared with different cellulose ether additives. The compressive strength of the CPC composite cements is in all cases lower than that of the control cement.

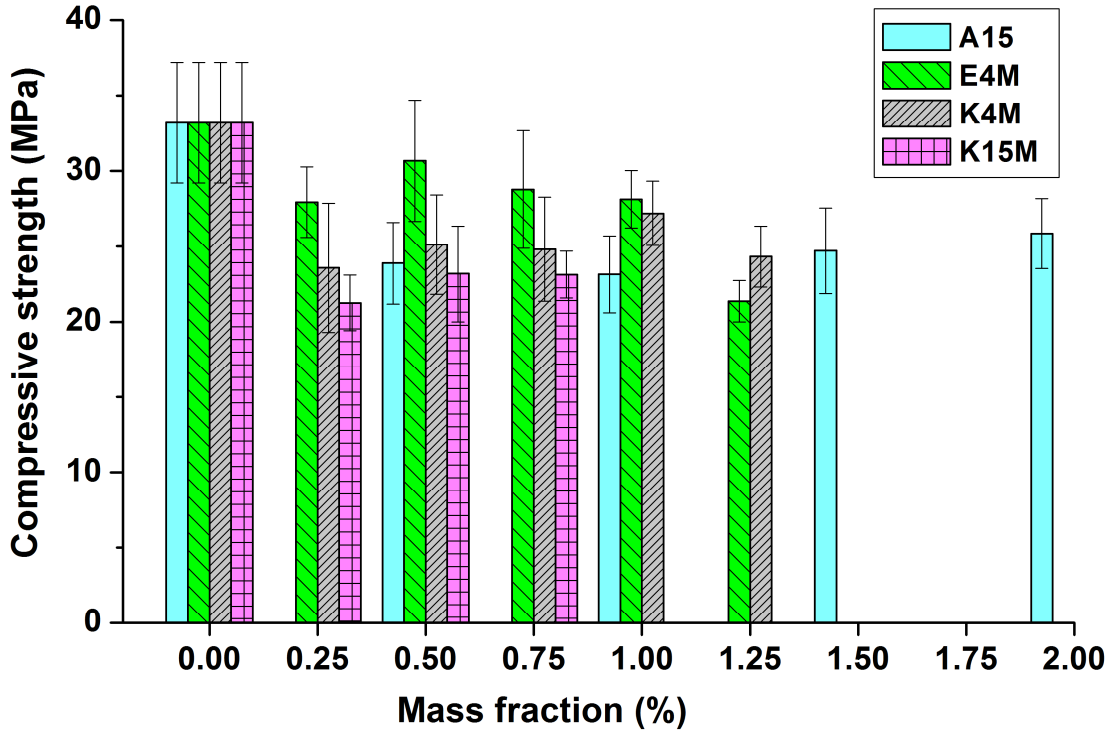

Fig. 5-13 Compressive strength of the composite CPC with different mass fractions of cellulose ether additives (L/P = 0.45 mL/g). Each value is the mean of six measurements ± one standard deviation.

In order to better understand the influence of cellulose ethers added on the compressive strength of composite cements, the latter was plotted as a function of porosity (Fig. 5-14A, C, E and G).

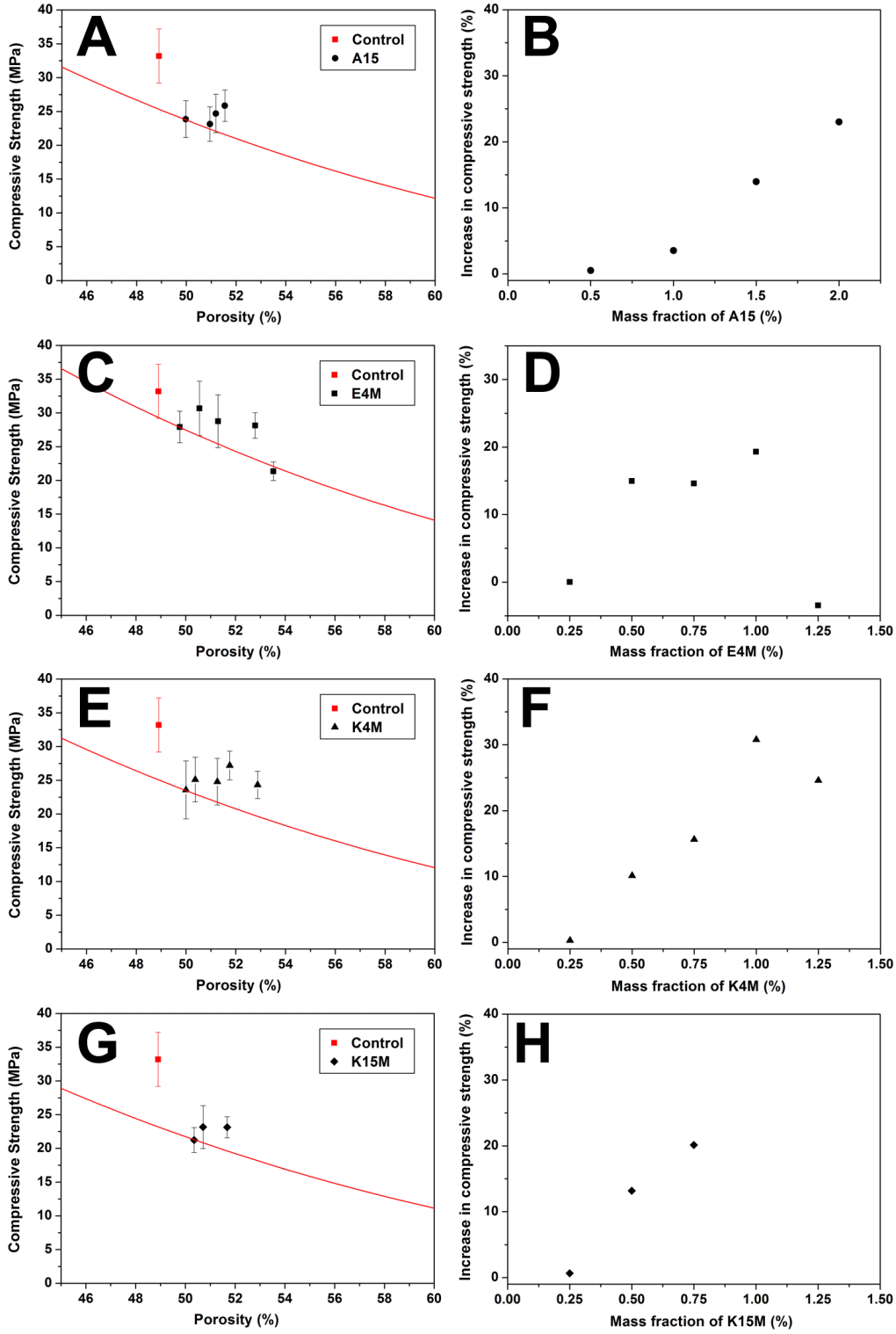

Fig. 5-14 Compressive strength of composite cements (A) A15; (C) E4M; (E) K4M; (G) K15M as function of porosity. (B), (D), (F) and (H) show the relative increase of strength of corresponding composite cements as a function of polymer mass fraction. The red curve crossing the first data point of composite cements is related to macroporous CPC and is representative of a mathematical model (power law in this case) assisting comparison of compressive strength between composite cements with identical porosities. Each value is the mean of six measurements ± one standard deviation.

As soon as the cellulose ethers are added, the strength of composite cements decreases sharply; this point will be discussed later. But once some polymer has been added, similar to fracture toughness, the strength generally remains constant or even increases with increasing porosity, which is also different from our previous result that strength decreases with the increase of porosity, indicating that the cellulose ethers may have a strengthening effect on CPC. Once more, this speculation can be proved only if the strength of the composite cements is compared with that of control cements with the same porosities. Thus, similar to the process conducted on fracture toughness, a power law with the same exponent m as that for fracture toughness was adjusted to pass through the first data point of each composite cement to assist the comparison (see Fig. 5-14A, C, E and G). The reason for choosing a power law and an exponent m with a specific value is similar to that for fracture toughness, as discussed previously.

The relative increase of the strength of the composite cements, compared to “virtual” cements with identical porosities, is plotted as a function of polymer mass fraction (Fig. 5-14B, D, F and H). In general, the relative increase in strength increases continuously and strongly with mass fraction, indicating that the cellulose ethers additives do have strengthening effects on CPC.

In fact, compressive strength is not an intrinsic property of the material, but depends both on the fracture toughness and on the shape and size of defects. Although cellulose ethers can improve the fracture toughness of the composite cements (see Fig. 5-9), which is beneficial for strength, the concomitant presence of large defects caused by entrained air bubbles (Fig. 5-6, 7) seems to counteract this bonus, resulting in a reduced compressive strength when compared to control cement without macropores (i.e. without polymer), as shown in Fig. 5-13 and 5-14. This reduced compressive strength due to entrapped air bubbles (or large defects) has also been observed in the macroporous CPC discussed previously (chapters 3 and 4), in other cement-based materials for civil engineering (Khayat, 1998), and in macroporous BCP ceramics (Pecqueux et al., 2010). However, when compared to macroporous “control” cements with the same porosity, the compressive strength of composite cements generally increases with increasing mass fraction, which may be attributed to the correspondingly increasing fracture toughness (Fig. 5-9).

Finally, the stress-displacement curves of the composite cements during compression tests are shown in Fig. 5-15. A small overshoot can be found at the beginning of the curve for all the tests, which is due to a clearance in the experimental setup. After the overshoot,

a linear increase of the stress followed by a steep drop can be observed for the control cement, corresponding to a typical brittle fracture (e.g. Fig. 5-15A, control). On the contrary, a less linear increase of the stress followed by a mild drop can be found for composite cements, indicating a less brittle failure, corresponding to a progressive microcracking / macrocracking of the material, which can be seen as a kind of tolerance to damage. These curves indicate a positive effect of cellulose ethers on the fracture behavior of composite cements (Fig. 5-9). This tolerance to damage is very interesting for biological applications, since the material, in case of an overload, will nevertheless retain some extent of mechanical integrity, in the sense that this will on the one hand prevent debris from escaping the implant site, and on the other hand allow the material to be able to withstand further (reduced) loading.

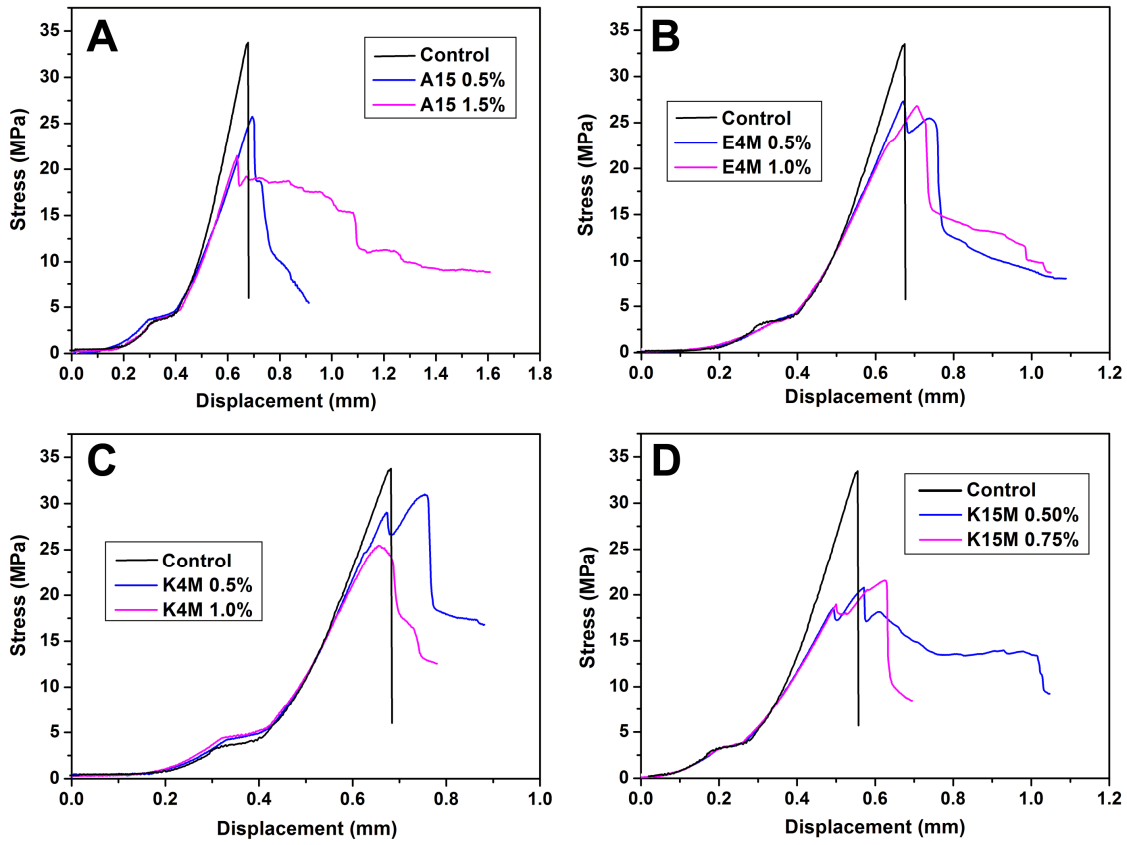

Fig. 5-15 Stress versus displacement curves of composite cements with different mass fractions of cellulose ether additives.

5.1.4 Section conclusion

In summary, the results of this study indicate that the addition of cellulose ethers (A15,

E4M, K4M and K15M) with different structural parameters modifies almost all performance aspects of the cements, including handling properties, porosity and mechanical properties.

Both molecular weight and substitution of HPMC/MC have a great influence on the injectability of CPC. The higher the viscosity of the HPMC solution, the better the injectability of the composite CPC paste. For different HPMC solutions with similar viscosity, the degree of substitution groups seems to play a great role. HPMC/MC seems to be an excellent option not only to improve injectability but also to improve cohesion and resistance to washout. In addition, HPMC/MC can prolong the setting time, especially the final setting time of composite cements. Only a small amount of HPMC/MC is needed to dramatically change all the handling properties of the cement pastes studied.

In spite of different molecular weights and/or substitutions, HPMC/MC all have a strong toughening effect, and this effect becomes more significant with the increase of the polymer mass fraction. However, as soon as small quantities of HPMC/MC are added, a sudden decrease of compressive strength is provoked by entrained air bubbles acting as critical flaws, but then the compressive strength generally tends to increase with increasing polymer mass fraction when compared to macroporous “control” cements with the same porosity, which may be attributed to a correspondingly increasing fracture toughness.

5.2 Si-HPMC composite CPC

In section 5.1, the influence of four different cellulose ethers on the handling and mechanical properties of α-TCP based CPC have been systematically investigated. The cellulose ethers studied manifest beneficial effects on cohesion, anti-washout, injectability, fracture toughness and tolerance to damage of the composite cements. However, despite a good cohesion, the composite CPC pastes with high L/P ratios are quite “fluid” and would probably tend to flow away from the place where they are implanted at the initial stage (see 5.2.2), indicating that an additive which can improve even more the handling and/or mechanical properties is still desirable.

Si-HPMC is synthesized through controllable grafting of silane into HPMC (Bourges et al., 2002). Similar to its precursor, HPMC, Si-HPMC is biocompatible and has been reported to be attractive for cartilage regeneration (Merceron et al., 2010). In addition, in solution it exhibits a high viscosity (Fatimi et al., 2008) and, as a “gel”, it presents a self-hardening behavior. Thus, it has been used for the second generation of injectable BCP bone substitutes (Daculsi et al., 2010A; Weiss et al., 2008), showing a significant advantage over the first generation by suppressing their long-term flow (Vinatier et al., 2009). Both the high viscosity and gelling of Si-HPMC could be interesting in view of preparing composite cements with possibly improved handling and mechanical properties.

However, to date this interesting cellulose ether has never been used in CPC. Given the above elements and what has been seen about the role of Si-HPMC in injectable BCP bone substitutes, it would thereby be very appealing to try and incorporate it to CPC.

In this section, similar to section 5.1, the effect of Si-HPMC on the handling (injectability, cohesion and setting time) and mechanical properties (Young’s modulus, fracture toughness, flexural and compressive strength) of the composite Si-HPMC CPC has been systematically investigated. All the mechanical properties were measured in wet conditions.

5.2.1 Preparation of Si-HPMC solution and cement liquid

The Si-HPMC powder was kindly provided by Dr. Pierre Weiss. The synthesis of Si-HPMC powder has been described in detail by Bourges et al. (2002). Briefly, it was produced by silane grafting on HPMC (Methocel®E4M) in NaOH solution, and

3-glycidoxypropyltrimethoxylane (3-GPTMS) was used as a silated agent.

For preparation of Si-HPMC solution, the Si-HPMC powder, which is insoluble in water, was dissolved in 0.2 M of NaOH solution at room temperature for 48 h. Subsequently, the Si-HPMC solutions were dialyzed against 3.8 L of NaOH solution (0.09 M) for 16 h and then against 4 L of NaOH solution (0.09 M) for another 2 h. The final pH value of the Si-HPMC solution was around 12.8. Si-HPMC solutions were prepared at different concentrations (2%, 3% and 4% w/v; here 1 w/v% = 10 g/L).

Si-HPMC solutions are stable in strong basic media (pH > 12.1). When the pH decreases, the gelation of Si-HPMC takes place, and the Si-HPMC solution is transformed into a hydrogel with a three-dimensional network of Si-HPMC chains (Fatimi et al. 2008, 2009). The gelation principle of the Si-HPMC is illustrated in Fig 5-16. Specifically, in a strong basic medium, the silane on the Si-HPMC chains is ionized into sodium silanolate (-SiO-Na^+). When the pH of the solution is below 12, the sodium silanolates transform into silanols (-SiOH), which is followed by condensation reactions and ends in the formation of a 3-D network of the polymer.

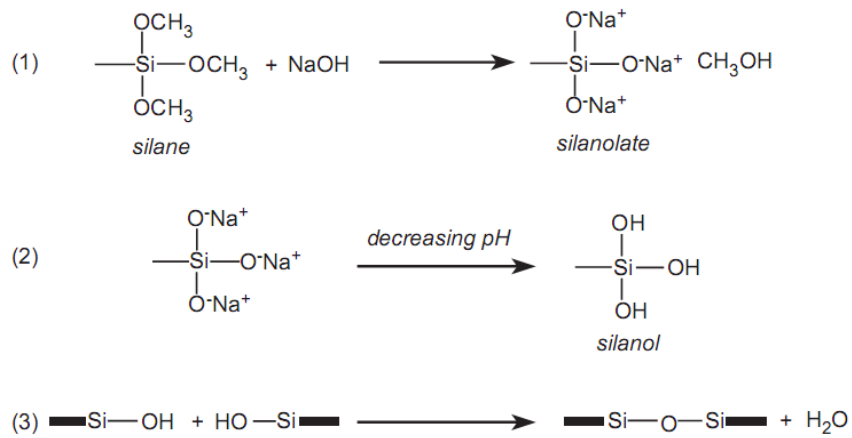

Fig. 5-16 The behavior of silane grafted on HPMC: (1) dissolution in basic solution with silanolate function formation, (2) transformation of silanolate into silanol by decreasing the pH, and (3) silanol condensation. Reprinted from Fatimi et al., (2008)

In this study, a solution of 30 wt% of NaH_2PO_4 was used as a buffer to initiate the gelation of Si-HPMC. Extemporaneously, the NaH_2PO_4 solution was mixed with the Si-HPMC solution in a syringe to obtain the cement liquid with a final pH ranging from 7 to 8. The gelation time of the cement liquid (Si-HPMC + NaH_2PO_4) was determined by a rheological method in oscillatory shear, which was carried out with a rotational rheometer (RheoStress 300, Germany) at 23 °C. The measurement of gelation time shows that the

gel point of Si-HPMC hydrogel in this formulation is about 30 min.

Si-HPMC composite cements were prepared with different L/P ratios and by using solutions of Si-HPMC at different concentrations, as shown in Table 5-3.

Table 5-3 Experiment series of Si-HPMC composite cements

Mass fraction (%) Si-HPMC / L/P[a]	2%	3%	4%
0.40		1.2	1.6
0.45		1.35	1.8
0.60	1.2		2.4
0.80			3.2
1.00	2.0		4.0

[a] Liquid volume (ml) = NaH_2PO_4 (ml) + Si-HPMC (ml)

The numbers in the first row represent the concentration of Si-HPMC in the polymer solution. The numbers in the other rows represent the corresponding proportion of Si-HPMC in the final cement without taking water into account.

5.2.2 Pre-experiment

Before showing the main content and results of this work, a preliminary experiment was done to visually demonstrate the excellent handling properties of the composite cements with Si-HPMC, as shown in Fig. 5-17 and 5-18. A control cement (without additive) (Fig. 5-17A), as well as composite cements with HPMC (E4M) (Fig. 5-17B) and with Si-HPMC (Fig. 5-17C) of 3% w/v were prepared with a L/P ratio of 1.0 and packed into rhombohedral molds, followed by immediate demolding. The control cement paste cannot maintain its cuboid shape and spreads over a large area of the glass plate (Fig. 5-17 D), due to a low viscosity (Fig. 5-17G). Similarly, the composite cement paste with E4M cannot keep its shape either but spreads a little less over the glass plate (Fig. 5-17 E), indicating a somewhat higher viscosity (Fig. 5-17H). The Si-HPMC composite cement paste, at the opposite, can preserve its cuboid shape without any noticeable defects (Fig. 5-17 F and I), due to a very high viscosity.

Moreover, the Si-HPMC composite cement paste exhibits a particular mechanical behavior at its early age, i.e. when demolded immediately after having been molded (Fig. 5-18).

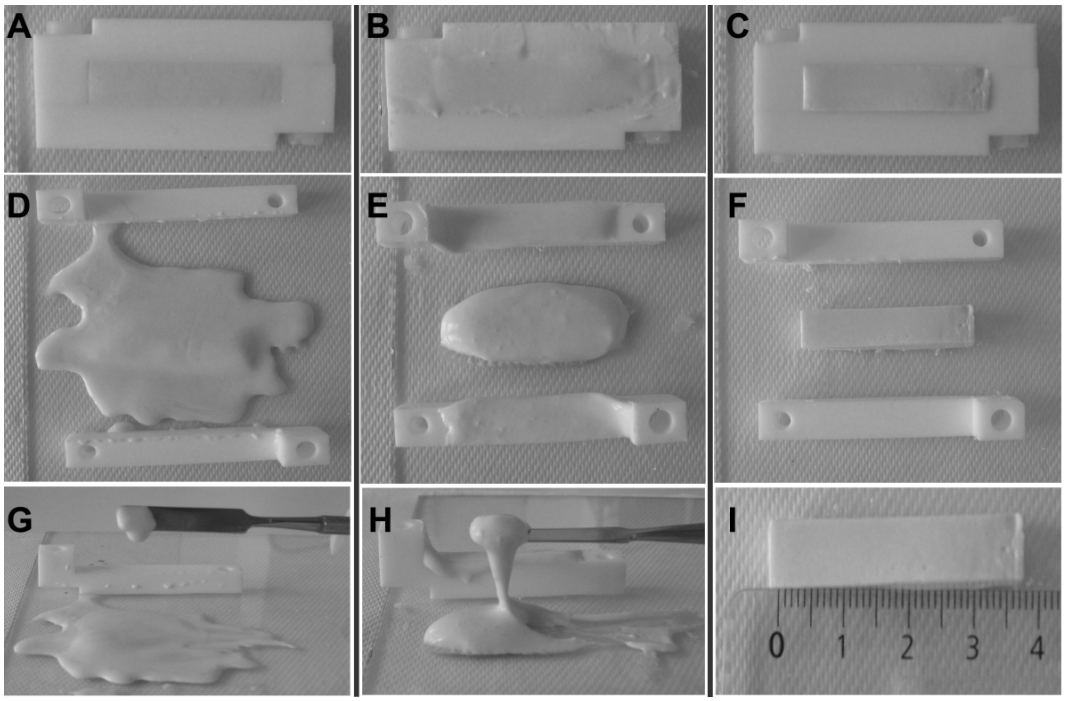

Fig. 5-17 Immediate demolding after the preparation of (A, D, G) the control cement; (B, E, H) the composite cement with HPMC; (C, F, I) the composite cement with Si-HPMC. L/P =1.0; the concentration of Si-HPMC in liquid phase is 3%.

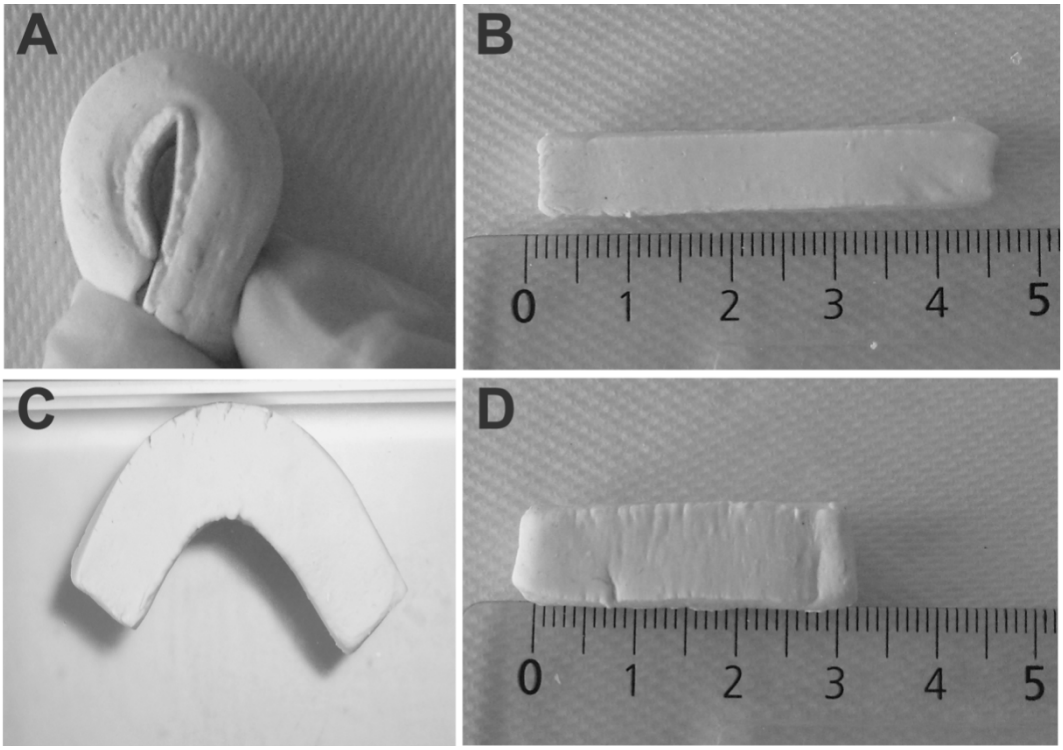

Fig. 5-18 Mechanical behavior of the composite CPC paste with Si-HPMC, demolded immediately after molding: (A) bending, (C) unloading after bending, (B) after stretching and (D) after compression. The initial length of the bar is 38 mm.

It can be bent extremely without breaking (Fig. 5-18 A). After unloading, the composite cement bar can still largely maintain the bent shape (Fig. 5-18 C). The phenomenon that the composite cement bar can preserve its shape after unloading has also been observed after stretching (Fig. 5-18 B) or compression (Fig. 5-18 D) of the bar, which is probably due to a large viscoelasticity.

As shown above, the Si-HPMC composite cement displays an appealing mechanical behavior at early age during which flowing of a cement paste with a high L/P ratio can also be avoided in the place implanted, whereas the paste remains easy to deform and able to adapt to complex shapes without damage, which will further attract us to exploiting its application as bone substitutes.

5.2.3 Handling properties of Si-HPMC composite CPC

5.2.3.1 Injectability

The injectability of the Si-HPMC composite cements at 4% with different L/P ratios and after various gelling times was measured, and the results are plotted in Fig. 5-19.

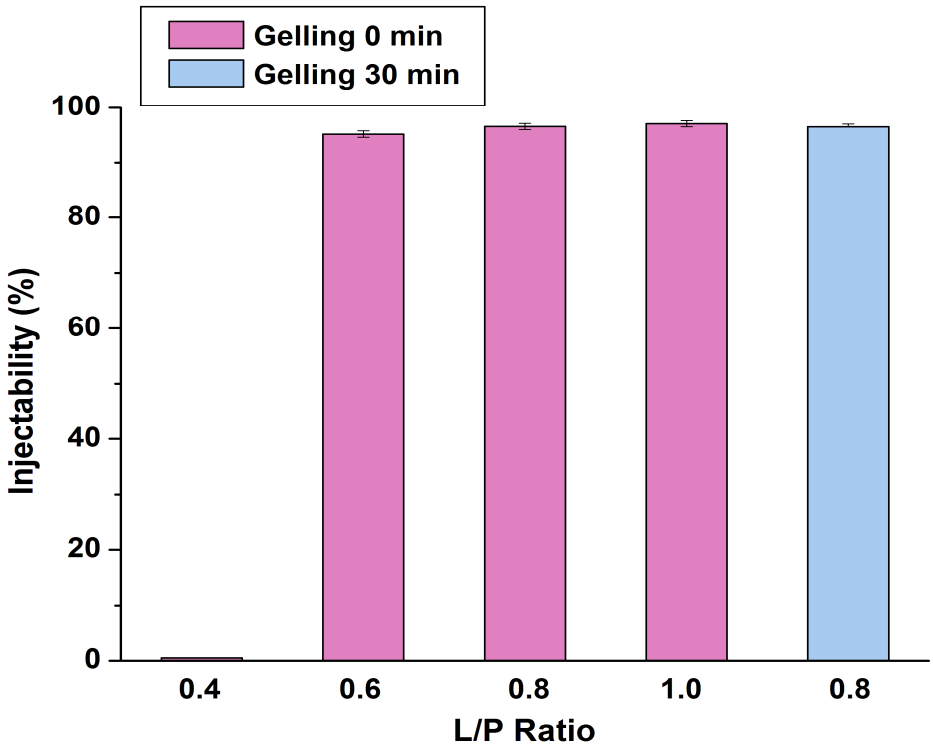

Fig. 5-19 Injectability of the Si-HPMC composite cement paste at 4% with different L/P ratios and gelling times, 4 min after starting the mixing of liquid and powder. Each value is the mean of three measurements ± one standard deviation.

The gelling time is the time during which the Si-HPMC solution has been let to gel before mixing with the inorganic powder. Surprisingly, the composite cement with a L/P ratio of 0.4 can hardly be injected. In contrast, all the composite cements prepared with higher L/P ratios can be extruded, reaching a maximal injectability of about 95%. It is worth reminding that the remaining 5% of paste is left in the syringe tip, so that 95% is actually the upper limit of the injectability measured by this method. For the L/P ratio of 0.8, a preliminary gelling time of 30 min does not affect injectability.

In section 5.1, the improved injectability of the HPMC or MC composite cements was attributed to the increased paste viscosity which can effectively alleviate and even prevent filter-pressing, which is considered to be the mechanism causing limited injectablity of cement pastes. The same strategy has been used here to improve the injectability of Si-HPMC composite cements. Indeed, under the present testing conditions, most of the control cements can also be extruded (the case of the L/P ratio of 0.4 will be discussed later). Therefore, as mentioned previously, increasing the viscosity of the cement paste seems to be a very good strategy to improve injectability. As shown in Fig. 5-20, except for the composite cement with a L/P of 0.4, the extrusion curves for composite cements with high L/P ratios are very similar to those of HPMC composite cements (Fig. 5-2).

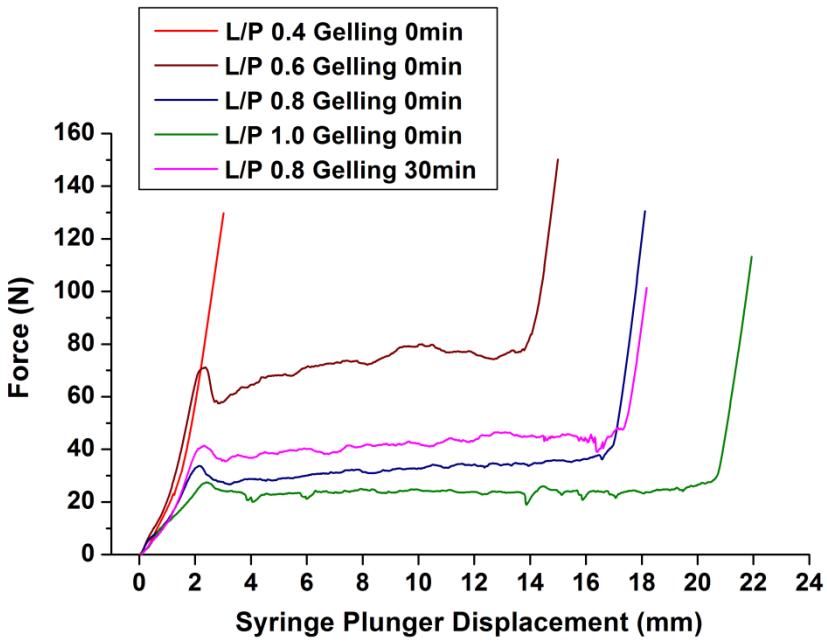

Fig. 5-20 Injection force curves during extrusion of the Si-HPMC composite cement pastes at 4% with different L/P ratios and gelling times.

The horizontal plateau is considered to be related to homogeneous injection of the

cement paste without filter-pressing, and the longer the plateau, the better the injectability. As in the case of HPMC and MC composite cements, a long horizontal plateau is also observed in the present composite cements with high L/P ratios (0.6, 0.8 and 1.0) and even after a gelling time of 30 min, relating to a very good injectability (Fig. 5-19). Moreover, the extrusion force at the plateau increases with a decrease of the L/P ratio, which is simply due to the correspondingly increasing viscosity of the cement paste. Besides, the extrusion force is higher for the cement paste with Si-HPMC gelled for 30 min than that without gelling. This can be mainly attributed to the extra force needed to break the formed hydrogel network. Finally, for the composite cement with a L/P ratio of 0.4, although the paste is very viscous, the extrusion force increases very fast without any plateau, relating to a bad injectability (actually it can hardly be injected) (Fig. 5-19). This result is contradictory to the definition of injectability in the present study that the higher the viscosity, the better the injectability. However, the bad injectability of the composite cement with a L/P ratio of 0.4 may be related to a very high yield point (i.e. the force necessary to initiate the paste flow), which could surpass the maximum extrusion force used in the present study (~ 100 N).

5.2.3.2 Cohesion

When injected into the saline solution immediately after preparation (< 3 minutes), the control cement paste disintegrates completely and particles sediment to the bottom of the flat beaker (Fig. 5-21A), whatever the L/P is (from 0.4 to 0.8). In contrast, the Si-HPMC composite cement pastes can maintain their injected noodle-like shape until hardening and no disintegration can be observed, indicating an outstanding cohesion (Fig. 5-21 B).

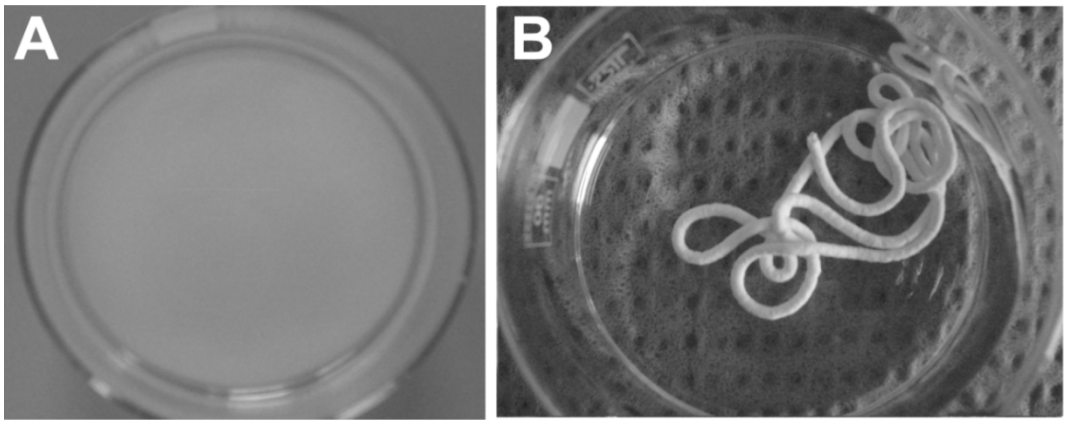

Fig. 5-21 Photos of the (A) control and (B) composite (3% Si-HPMC) cement pastes injected into a saline solution immediately after preparation (within 3 min). L/P=1.0

Similar to HPMC composite cements, the improved cohesion of Si-HPMC composite cements can be attributed to the increased paste viscosity which may on the one hand reduce the influence of osmotic pressure between the interstitial fluid of the cement paste and the surrounding liquid and on the other hand prohibit the release of particles into the surrounding liquid. Moreover, the latter mechanism may be further strengthened by the three-dimensional network of the Si-HPMC hydrogel.

5.2.3.3 Setting time

The initial and final setting times of CPC without or with 4% of Si-HPMC were measured in different L/P ratios (Fig. 5-22).

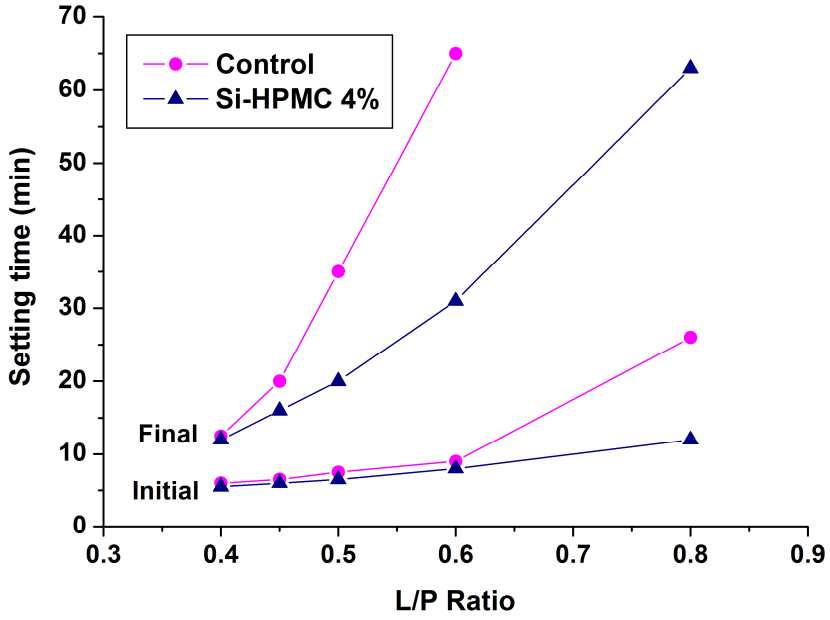

Fig. 5-22 Initial and final setting times of cements without or with Si-HPMC (4%) at different L/P ratios. The final setting time of control cement with L/P ratio 0.8 is much longer than 60 minutes and is not displayed.

Unlike HPMC which delays the setting of composite cement (Fig. 5-4), Si-HPMC appears to slightly shorten the initial setting of the composite cements with L/P ratios up to 0.6, but to significantly reduce it for a L/P ratio of 0.8. The phenomenon of shortening setting time becomes much more obvious with regard to the final setting times with increasing L/P ratios.

As for the mechanism of faster setting in the composite cement, it may be mainly attributed to the effect of gelation of Si-HPMC. In fact, like HPMC, Si-HPMC molecules would adsorb to the surface of α-TCP particles and hence would be expected to delay the

setting. However, meanwhile, Si-HPMC gels to form a hydrogel with a three-dimensional network of Si-HPMC chains due to the decreased pH caused by NaH_2PO_4. Thus it is very likely that the effect of gelation of Si-HPMC may counteract the influence of the delay of cement setting caused by polymer absorbing, and finally produce a stronger resistance which is related to an apparent faster setting. In addition, with increasing the L/P ratio to 0.8, the α-TCP particles in the control cement paste tend to sediment by gravity, leaving less α-TCP particles in the top of the paste, the latter therefore taking a longer time to form an entangled structure of apatite crystals resisting loading (it is reminded that setting times are measured by pressing needles onto the cement top surface). In contrast, due to the increased viscosity, the sedimentation of α-TCP particles in the composite cement paste can be avoided, resulting in a more homogeneous distribution of α-TCP particles, which may also contribute to a faster setting, especially in cements with the L/P ratio of 0.8 (Fig. 5-22).

After five days of hardening, the final phases of control and composite cements were examined by XRD (Fig. 5-23).

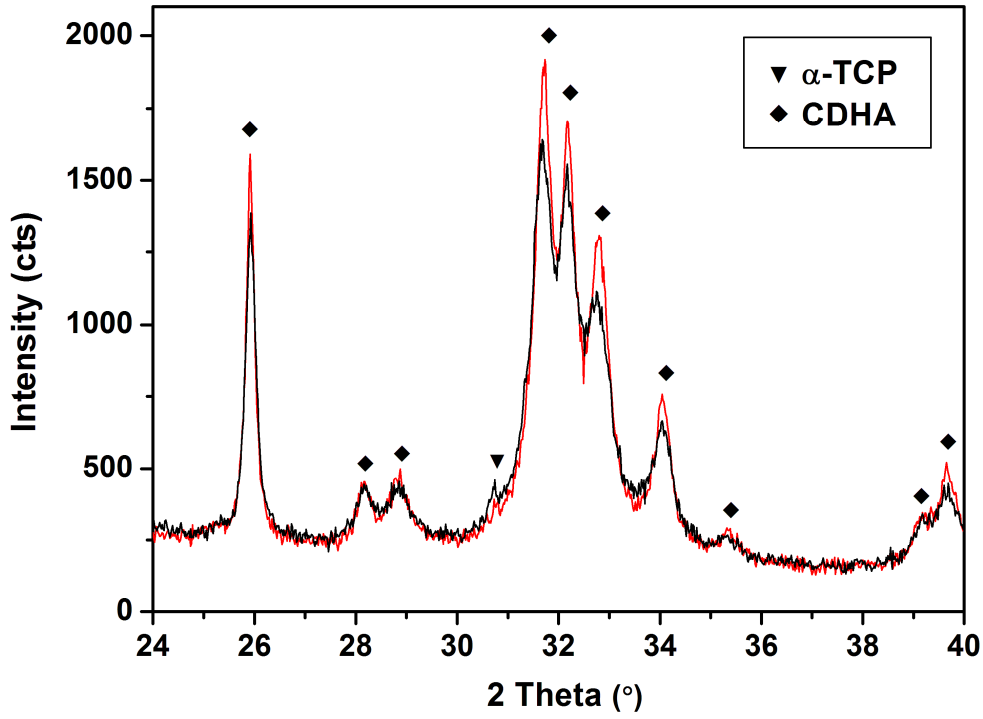

Fig. 5-23 XRD patterns of control cement and composite cement with HPMC-Si of 4%. L/P = 1. Red pattern refers to control cement. Black pattern represents Si-HPMC composite cement.

Similar to HPMC composite cements, most of the α-TCP in the Si-HPMC composite cements also transforms into CDHA. However, interestingly, despite the faster setting in

the early stage, the final formation of CDHA in the Si-HPMC composite cement seems to be retarded, as indicated by the lower intensity of the peaks of CDHA and higher intensity of the peaks of α-TCP. This may be due to the fact that the faster setting of composite cement with Si-HPMC in the initial stage mainly results from the effect of gelation of Si-HPMC. But, with time, Si-HPMC further gels to form a three-dimensional hydrogel network which interferes with the dissolution of Ca^{2+} and PO_4^{3-} into water, therefore affecting the final formation of CDHA. However, a more comprehensive kinetic study on the evolution of strength and microstructure of the composite cements would be necessary to prove these assumptions.

5.2.4 Microstructure and mechanical properties

As demonstrated in section 5.2.3, Si-HPMC significantly improves the handling properties such as injectability, cohesion and setting time. To examine whether Si-HPMC adversely influences mechanical properties, Young's modulus, fracture toughness and strength of the composite cements were measured. Besides, since CPC is intrinsically porous and its porosity strongly affects mechanical properties, and most probably also biological properties, the porosity of the composite CPC was also measured.

5.2.4.1 Porosity

As expected, the porosities of both control cements and composite cements increase with the increasing L/P ratios (Fig. 5-24A). Moreover, the porosity of the composite cements is higher than that of the control cements with the same L/P ratios, but the difference between the two porosities tends to decrease globally with increasing L/P ratio. Besides, the porosity of composite cements also increases with the increasing mass fraction of Si-HPMC added (Fig. 5-24B).

The increasing porosity with the increase of L/P ratios has been discussed in Chapter 3, and is mainly attributed to the higher proportion of liquid in the constant volume of the mold. In addition, similar to HPMC composite cements, the higher porosity of Si-HPMC composite cements than that of the corresponding control cements is believed to result from entrained air bubbles introduced during preparation (Jenni et al., 2005; Khayat, 1998; Pourchez et al., 2010B).

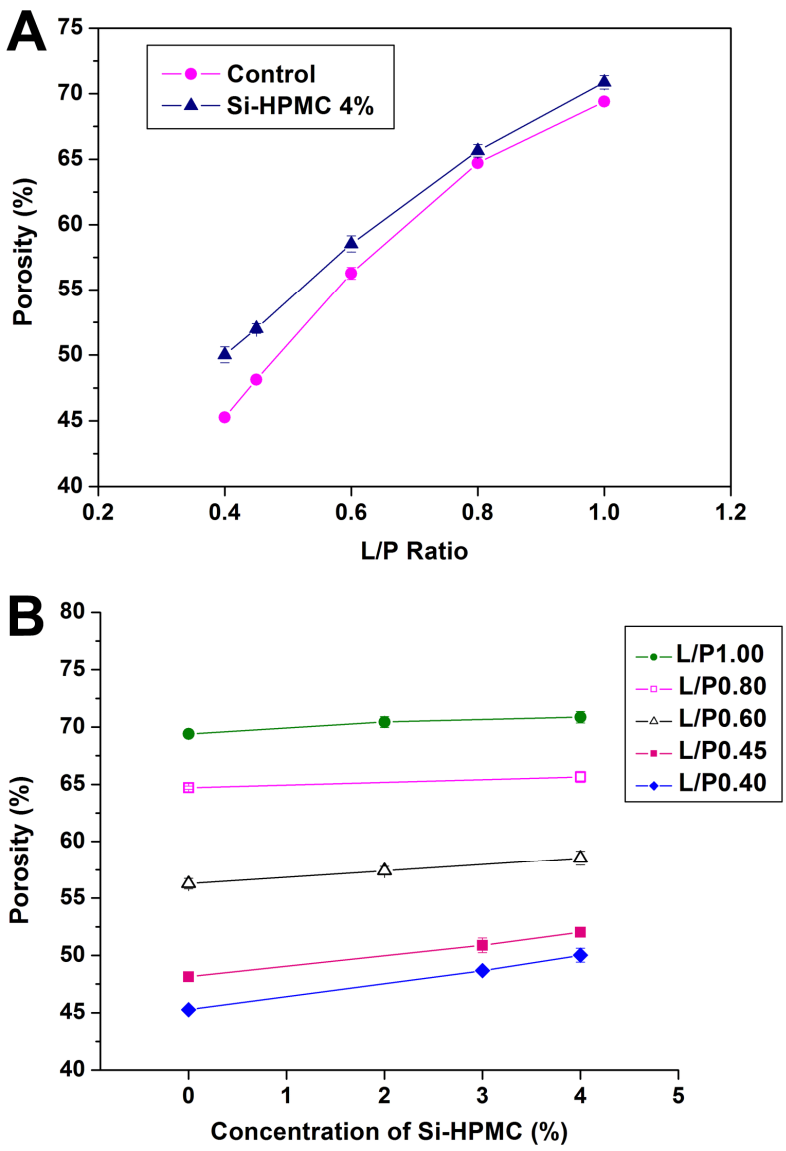

Fig. 5-24 Porosity of control cements and Si-HPMC composite cements as a function of (A) different L/P ratios (Si-HPMC 4%) or (B) different mass fractions of Si-HPMC. Each value is the mean of six measurements ± one standard deviation.

The SEM micrographs of fracture surfaces of control and Si-HPMC composite cements with different L/P ratios are shown in Fig. 5-25.

As can be seen, no entrained air bubbles can be observed in the control cement with a L/P ratio of 0.4 (Fig. 5-25A). In contrast, similar to HPMC composite cements (Fig. 5-7), once Si-HPMC is added, many air bubbles of various sizes can be easily found (Fig. 5-25B). With increasing L/P ratio (1.0), very few entrained air bubbles can be seen in the control cement, but the control cement matrix seems to become less dense (Fig. 5-25C), indicating a larger porosity. Meanwhile, compared to the Si-HPMC composite cement with a L/P ratio of 0.4, more macropores with a size larger than 100 μm can be

found in the Si-HPMC composite cement with a L/P ratio of 1.0, but no other noticeable difference can be observed between the two matrixes (Fig. 5-25D).

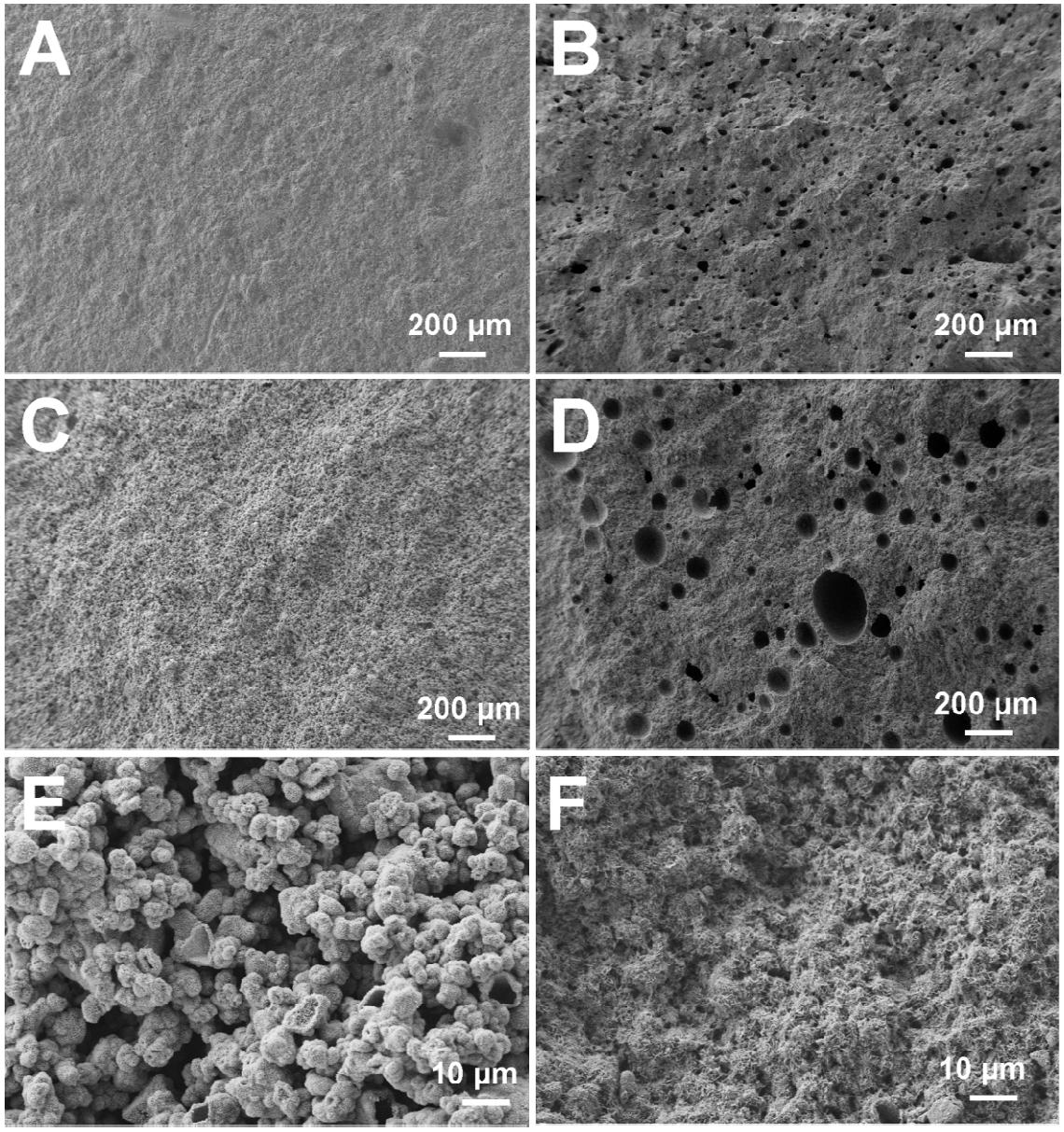

Fig. 5-25 SEM pictures of the fracture surfaces of control cements A) L/P = 0.4; C) L/P = 1.0; E) L/P = 1.0; and Si-HPMC (4%) composite cements B) L/P = 0.4; D) L/P = 1.0; F) L/P = 1.0. The pictures of A, B, C and D have the same magnification of 50 ×. The pictures of E and F have the same magnification of 1 000 ×.

The microstructure of control and Si-HPMC composite cements with L/P ratios of 1.0 is further examined at a higher magnification (1 000 ×). As for the control cement, large volume of voids can be observed between rather dense aggregates consisting of sphere-like clusters of apatite crystals (Fig. 5-25E). In contrast, no such voids can be seen in the Si-HPMC composite cement which is more compact and homogeneous

(Fig. 5-25F). The above SEM observations can therefore explain why the Si-HPMC composite cement with a L/P ratio of 1.0 has just a slightly higher total porosity than the control cement with the same L/P ratio (Fig. 5-24): while containing many macropores; it has a denser matrix.

5.2.4.2 Young's modulus

The Young's modulus[21] of the control and Si-HPMC composite cements prepared with different L/P ratios is plotted as a function of porosity (Fig. 5-26). The influence of porosity on the Young's modulus of CPC has been investigated in previous chapters. In the present study, the Young's modulus of both control and composite cements also decreases with increasing porosity (Fig. 5-26).

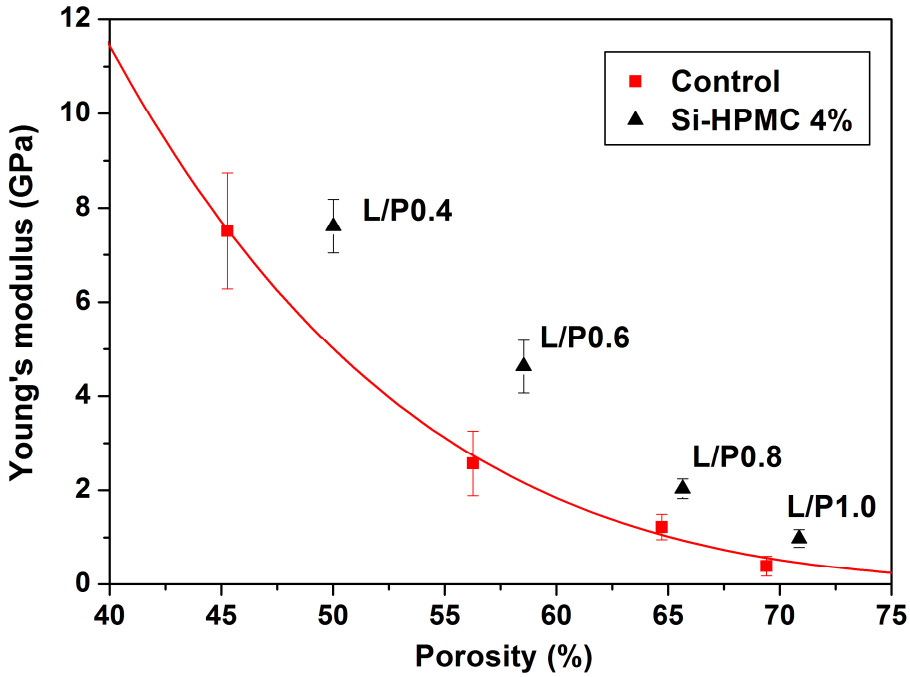

Fig. 5-26 Young's modulus of control cements and Si-HPMC composite cements as a function of porosity. The red curve is a fitting of Young's modulus of control cement as a function of porosity using a power law. Each value is the mean of six measurements ± one standard deviation

In order to study the effect of Si-HPMC on Young's modulus, it is therefore necessary to compare the Young's modulus of Si-HPMC composite cements with that of control cements with the same porosities. However, as mentioned previously, preparing a control cement with exactly the same porosity as that of a composite cement is practically

[21] Young's modulus and flexural strength were only measured on control cements and on composite cements prepared by using the Si-HPMC solution with a concentration of 4% at the time of writing this manuscript.

difficult. Thus, a power law was used to fit the Young's modulus of the control cement to assist the comparison (Fig. 5-26). Fitting of other mechanical properties will be also used in the following study. Moreover, it is worth mentioning that modeling of the mechanical properties of composite cements is not the main purpose of present study, but it is a useful tool to help to analyze and explain the results.

As can be seen, the Young's modulus of Si-HPMC composite cements is apparently higher than that of control cements with the same porosities. Furthermore, the relative increase of the Young's modulus of the composite cements is plotted as a function of the L/P ratio (Fig. 5-27). The relative increase of the Young's modulus increases continuously and strongly with the L/P ratio, implying that Si-HPMC pronouncedly improves the Young's modulus of CPC and this trend becomes more obvious in composite cements with high L/P ratios.

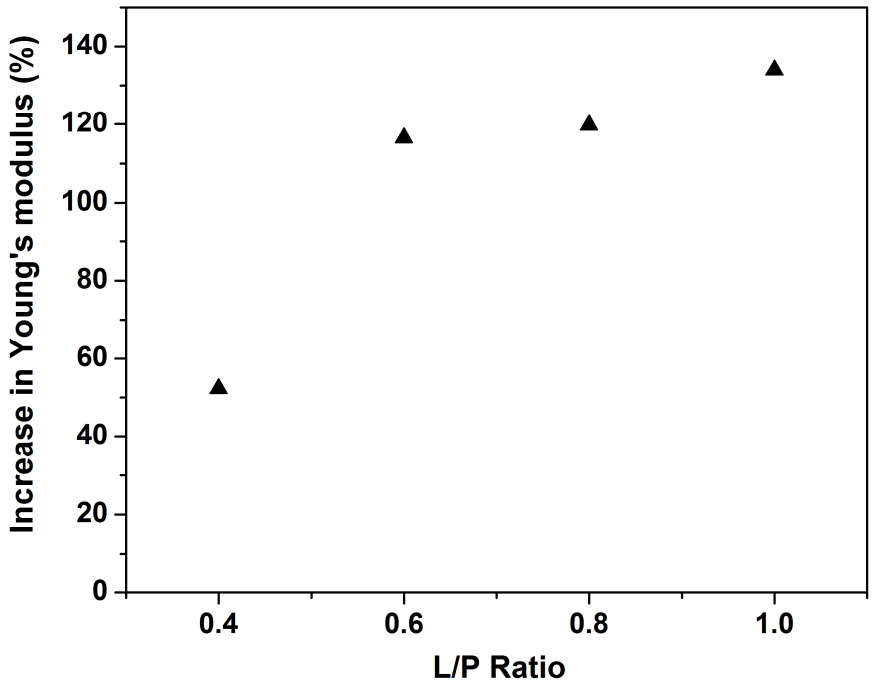

Fig. 5-27 Relative increase of Young's modulus of composite cements with 4% of Si-HPMC solution, as a function of L/P ratio.

This result seems to be contradictory to our previous result that the Young's modulus decreases with increasing porosity. The specific reason for this contradiction is unclear, but may be due to different microstructures resulting from the effect of Si-HPMC. For instance, the positive effect of a more homogeneous microporosity, as evidenced in Fig. 5-25 E and F, could surpass the negative effect of macropores due to air bubbles.

5.2.4.3 Fracture toughness

The fracture toughness was measured on the control and composite cements prepared with different L/P ratios and with Si-HPMC of different concentrations (Fig. 5-28). As expected, the fracture toughness is higher for both control and composite cements with low L/P ratios. In addition, the fracture toughness of composite cements increases with the increasing mass fraction of Si-HPMC added.

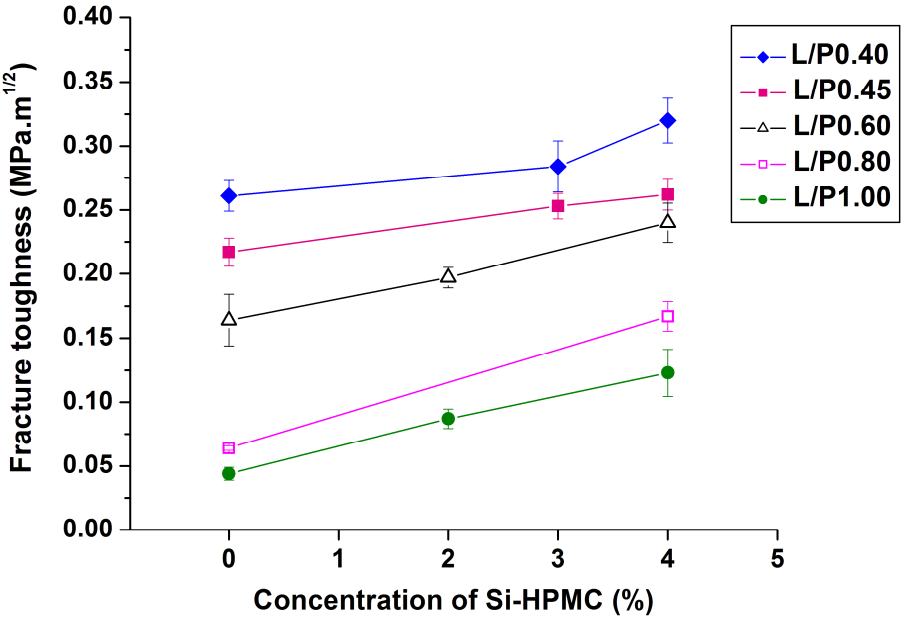

Fig. 5-28 Fracture toughness of control cements and Si-HPMC composite cements prepared with different L/P ratios, as a function of concentration of Si-HPMC. Each value is the mean of six measurements ± one standard deviation.

Similar to HPMC, in order to reveal the effect of Si-HPMC on fracture toughness, it is of great interest to plot the fracture toughness of Si-HPMC composite cements as a function of porosity (Fig. 5-29). As can be seen, the fracture toughness of the composite cements increases with increasing porosity whatever the L/P ratio is. This is different from our previous results that fracture toughness decreases with the increase of porosity, implying that Si-HPMC has a toughening effect on CPC. In order to prove this assumption, the toughness of the composite cements should be compared with that of control cements with the same porosities. Similarly, a power law was used to fit the fracture toughness of the control cements to assist the comparison (Fig. 5-29). The fracture toughness of all the composite cements is apparently higher than that of control cements with the same porosities.

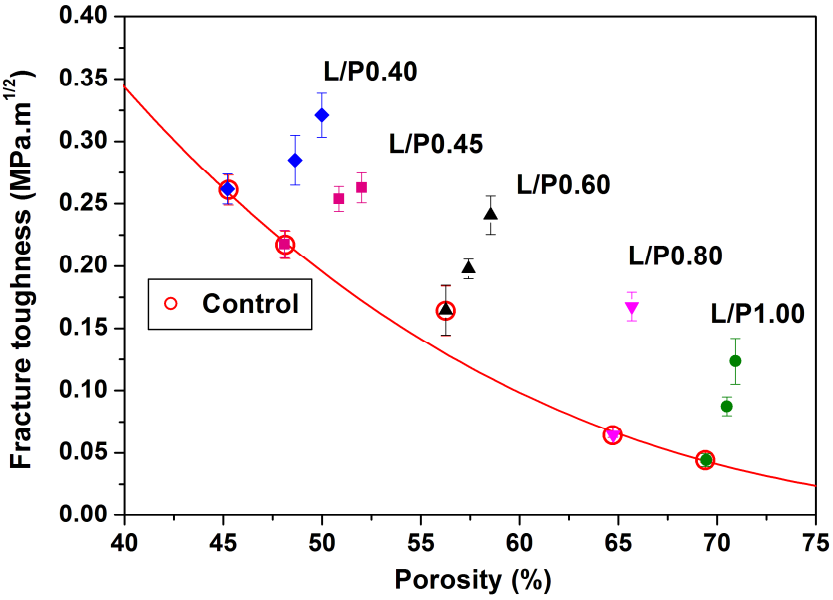

Fig. 5-29 Fracture toughness of control cements and Si-HPMC composite cements prepared with different L/P ratios, as a function of porosity. The marks with open circles around represent control cements with different L/P ratios. The red curve is a fitting of fracture toughness of control cement as a function of porosity using a power law. For each "color series" (i.e. for each L/P ratio), porosity is varied through different concentrations in Si-HPMC, as shown on Fig. 5-24 B). Each value is the mean of six measurements ± one standard deviation.

Besides, the relative increase in toughness of the composite cements with different concentrations of Si-HPMC is plotted as a function of the L/P ratio (Fig. 5-30).

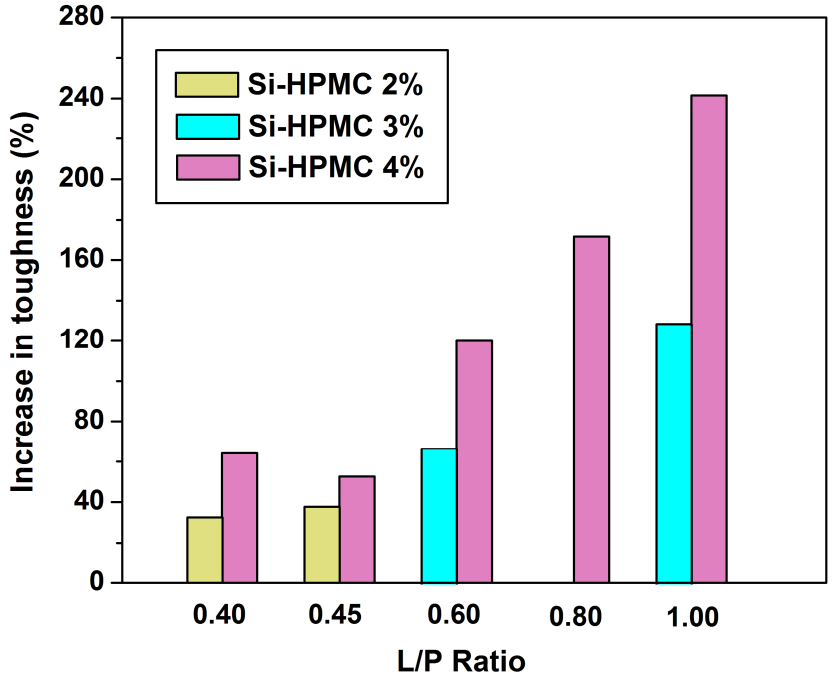

Fig. 5-30 Relative increase in fracture toughness of composite cements with different concentrations of Si-HPMC solution, as function of L/P ratio.

The relative increase in toughness increases significantly with polymer concentration, proving the hypothesis that Si-HPMC has toughening effects on CPC. Moreover, this toughening effect becomes more obvious in the composite cements with high L/P ratios.

A similar phenomenon has been observed in HPMC or MC composite cements (Fig. 5-9), and the improved fracture toughness has been attributed to a synergetic effect of a more homogeneous microstructure and of crack bridging by polymer ligaments. Because of the similarity between HPMC and Si-HPMC, it can be expected that the same toughening mechanisms operate in the Si-HPMC composite cements. Besides, it is worth noting that Si-HPMC can gel to form a three-dimensional hydrogel network, therefore an extra toughening from the cross-linked network might further improve the fracture toughness of Si-HPMC composite cements.

The fracture surfaces of control and Si-HPMC composite cements with different L/P ratios have been observed by SEM and are presented on Fig. 5-31 and 5-32.

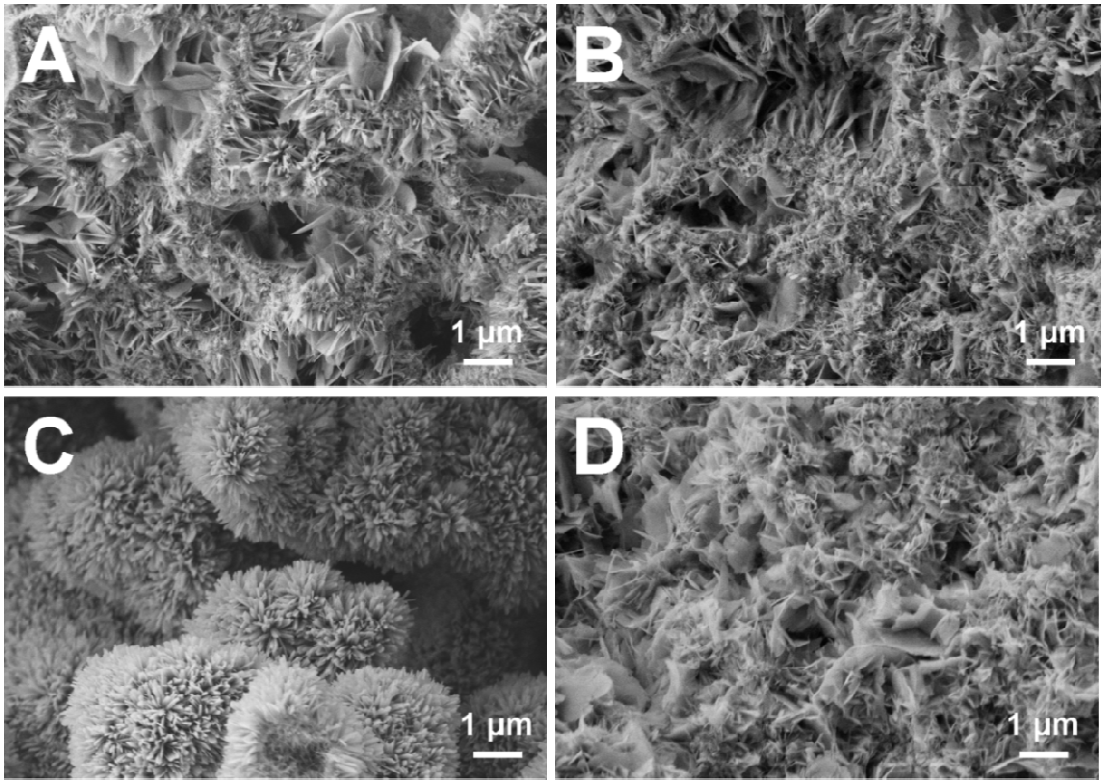

Fig. 5-31 SEM images of the fracture surfaces of control cements A) L/P = 0.4; C) L/P = 1.0 and Si-HPMC composite cements B) L/P = 0.4; D) L/P = 1.0 at magnification of 10 000 ×.

Fig. 5-31A shows the microstructure of the control cement with a L/P ratio of 0.4. As mentioned previously, needle-like and plate-like apatite crystals can be observed. Also, a similar structure can been found in the Si-HPMC composite cement with the same L/P

ratio (Fig. 5-31B). With increasing the L/P ratio (1.0), the microstructure of the control cement changes significantly, forming sphere-like apatite clusters consisting of numerous small and short needle-like crystals (Fig. 5-31C). Besides, these apatite clusters are inhomogeneously distributed in the cement matrix, with large voids between them. In contrast, the microstructure of the Si-HPMC composite cement with a L/P ratio of 1.0 remains similar to that of the Si-HPMC composite cement with a L/P ratio of 0.4 (Fig. 5-31D). The above SEM observations indicate that the viscous Si-HPMC solution can help to form a homogeneous cement matrix, probably partly contributing to the improved fracture toughness. The more homogenous matrix for composite cements may be responsible for a higher Young's modulus as compared to control cements, as shown in Fig. 5-26. Besides, the completely different microstructures of control cement in low (Fig. 5-31A) and high (Fig. 5-31C) L/P ratios may also account for the different extents of relative increase of fracture toughness of composite cements with different L/P ratios (Fig. 5-30).

In addition to the aforementioned toughening mechanism, similar to HPMC composite cements, some glue-like polymers, which may be derived from shrunk Si-HPMC hydrogels after drying, can be observed sticking to neighboring apatite crystals (Fig. 5-32); they may constitute crack bridging ligaments and also contribute to an increased toughness.

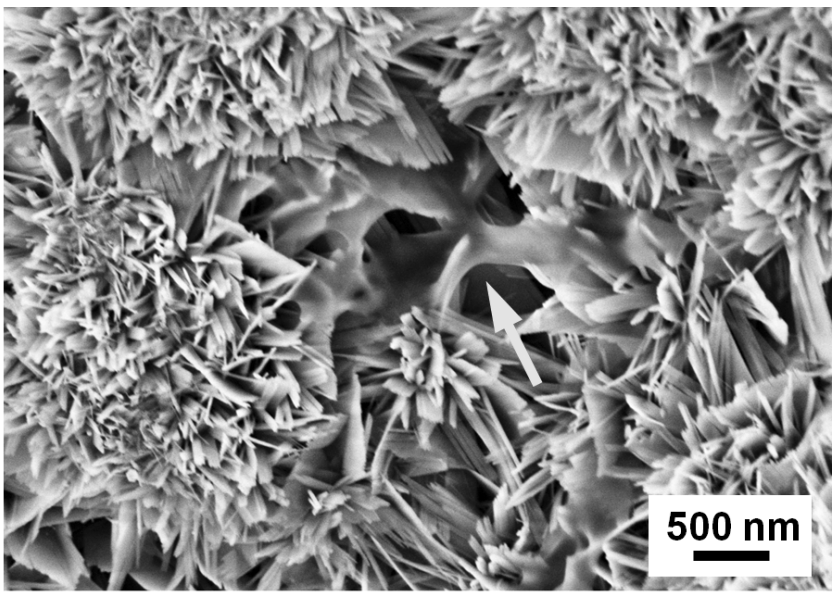

Fig. 5-32 SEM picture showing polymer in the Si-HPMC composite cement (arrow) with L/P = 0.6. The magnification of the picture is 20 000 ×.

Moreover, the composite cement was analyzed by FTIR, and increasing absorption bands which overlap that of control (water in the cement) and Si-HPMC (around 3400 cm^{-1}) could be found on the FTIR spectra (Fig. 5-33). Although the increases of absorption bands are much likely caused by water, it indirectly evidences the existence of Si-HPMC because before the FTIR analysis, the sample has been heated above 100 degrees, the remaining water can only come from the inner structure of Si-HPMC.

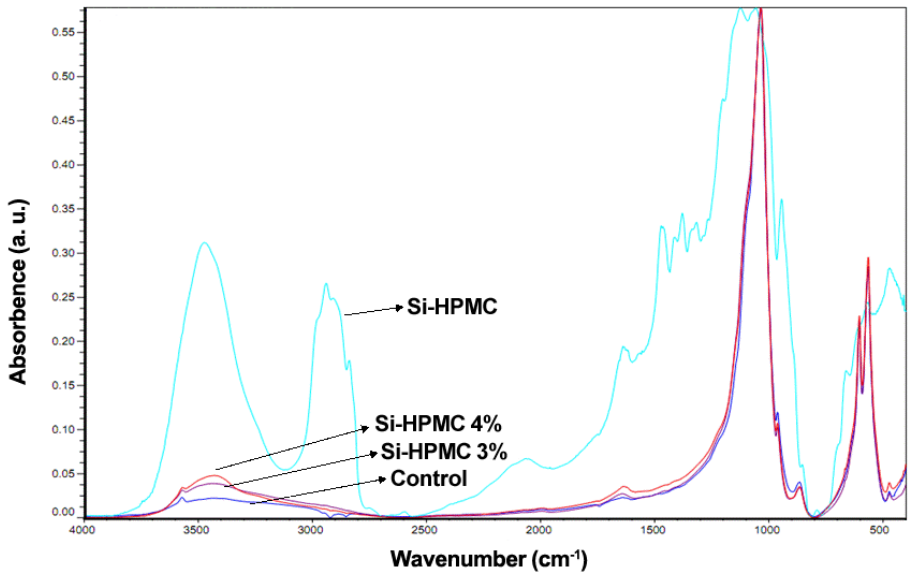

Fig. 5-33 FTIR spectra of control cement, Si-HPMC and Si-HPMC composite cements.

Thus, according to the above observations, both the optimized microstructure with improved homogeneity and crack bridging by polymer ligaments can contribute to the enhanced fracture toughness of Si-HPMC composite cements.

5.2.4.4 Flexural strength and compressive strength

The flexural strength of the control and Si-HPMC composite cements prepared with different L/P ratios is plotted as a function of porosity (Fig. 5-34). The influence of porosity on flexural strength of CPC has been studied previously, and it is generally harmful to the latter. Similarly, as shown in Fig. 5-34, flexural strength of both control and composite cements decreases with increasing porosity.

In order to investigate the influence of Si-HPMC on flexural strength, it is important to compare the flexural strength of Si-HPMC composite cements with that of control cements with the same porosities. To this end, as mentioned previously, it is necessary to use a power law to fit the flexural strength of the control cements to assist the comparison

(Fig. 5-34). As can be seen, except for the L/P ratio of 0.4, the flexural strength of Si-HPMC composite cements with other L/P ratios is obviously higher than that of control cements with the same porosities. In addition, the relative increase of the flexural strength of the composite cements, with respect to "virtual" control cements having identical porosities, is plotted as a function of the L/P ratio (Fig. 5-35).

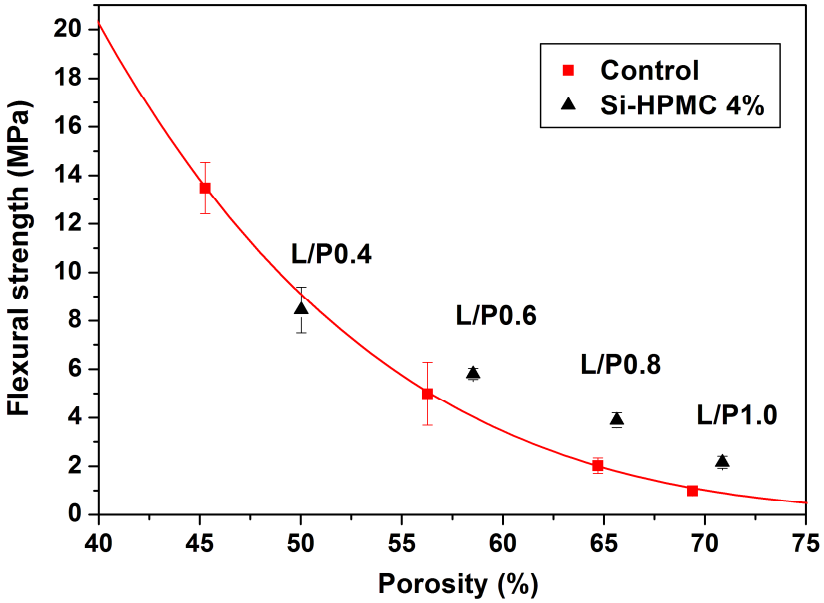

Fig. 5-34 Flexural strength of control cements and Si-HPMC composite cements as a function of porosity. The red curve is a fitting of flexural strength of control cements as a function of porosity using a power law. Each value is the mean of six measurements ± one standard deviation

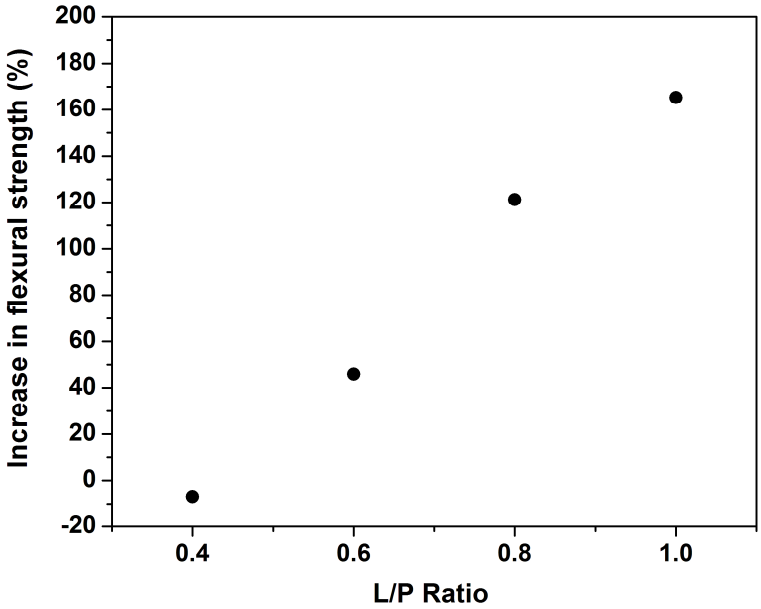

Fig. 5-35 Relative increase of flexural strength of composite cements with 4% of Si-HPMC solution, as a function of the L/P ratio.

The relative increase in flexural strength increases continuously and pronouncedly with increasing L/P ratio, indicating that Si-HPMC has a strengthening effect on CPC and this trend becomes more significant in composite cements with high L/P ratios. The strength of a material is dependent on the fracture toughness and on the size of the largest flaw in the material. Since the latter is detrimental to strength, this strengthening effect is mainly attributed to the correspondingly increasing fracture toughness (Fig. 5-30). Moreover, it is worth stating that the relative increase of flexural strength shown in Fig. 5-35 is based on microporous control cements where few macropores can be found. This character is much different from composite cements which contain numerous macropores provoked by entrained air bubbles (Fig. 5-25B, D). As a result, compared to the control cement with the same porosity, the lower flexural strength for the composite cement with a L/P ratio of 0.4 is only due to its large pores created by air bubbles, acting as critical flaws. Moreover, this also indicates that the relative increase of flexural strength of these composite cements is likely underestimated. However, despite this, the trend is still very obvious that Si-HPMC has a strong strengthening effect on the flexural strength of CPC.

The compressive strength was measured on the control and composite cements prepared with different L/P ratios and with Si-HPMC at different concentrations (Fig. 5-36).

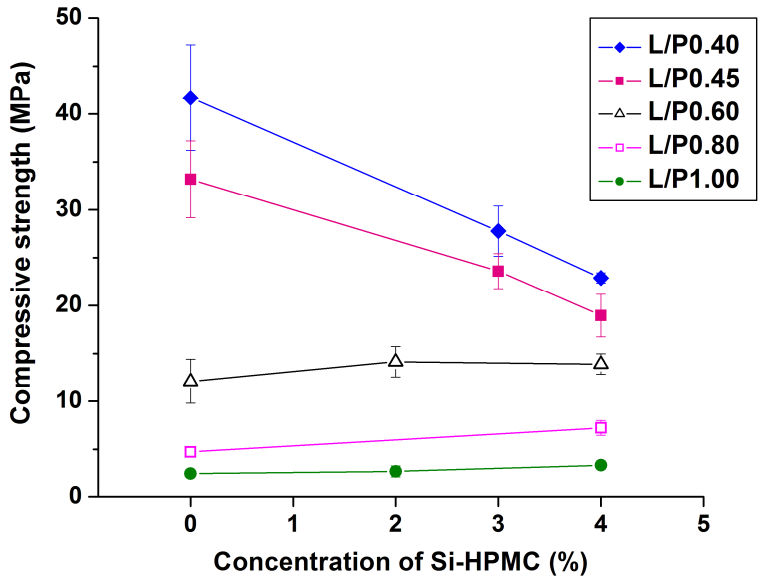

Fig. 5-36 Compressive strength of control cements and Si-HPMC composite cements prepared with different L/P ratios, as a function of concentration of Si-HPMC. Each value is the mean of six measurements ± one standard deviation.

As expected, the compressive strength is higher for both control and composite cements with low L/P ratios. Besides, the compressive strength of the composite cements with a L/P ratio of 0.4 or 0.45 decreases with the increasing concentration of Si-HPMC solution. In contrast, the compressive strength of the composite cements with L/P ratio of 0.6 or 1.0 remains constant or even slightly increases with the increasing concentration of Si-HPMC solution.

In order to explain the above results, the compressive strength of control and Si-HPMC composite cements is plotted as a function of porosity (Fig. 5-37).

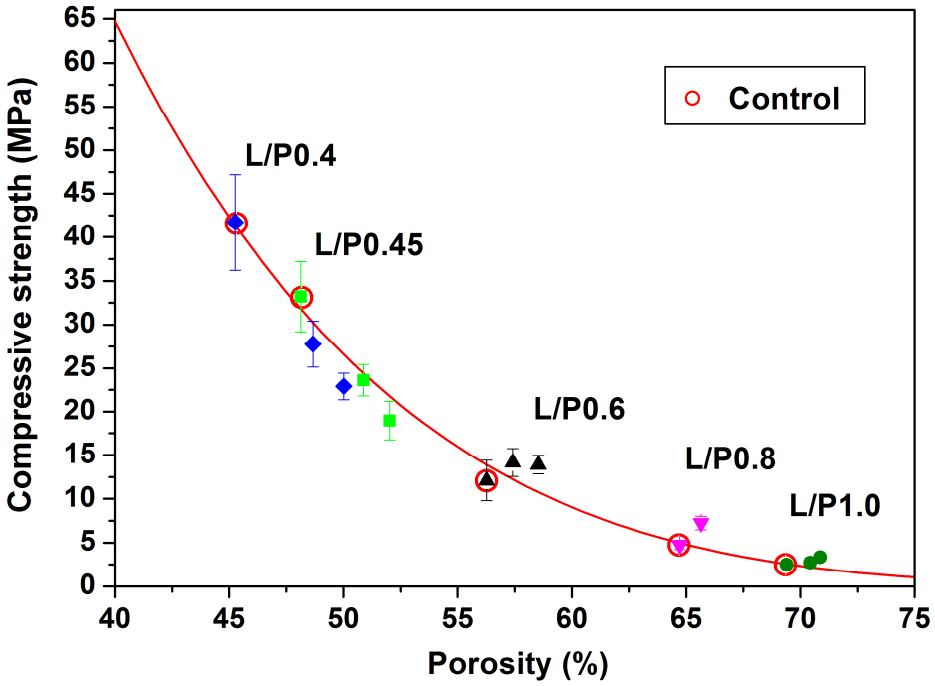

Fig. 5-37 Compressive strength of control cements and Si-HPMC composite cements prepared with different L/P ratios, as a function of porosity. The marks with open circles around represent control cements with different L/P ratios. The red curve is a fitting of compressive strength of control cements as a function of porosity using a power law. Each value is the mean of six measurements ± one standard deviation.

Two different trends can be observed. As for composite cements with L/P ratios of 0.4 or 0.45, the compressive strength decreases with the increase of porosity, which has been widely reported and is also observed in our previous studies. In contrast, for the composite cements with L/P ratios of 0.6 or 1.0, the compressive strength remains constant or even slightly increases with increasing porosity, indicating that Si-HPMC may also have a strengthening effect on compressive strength of CPC. Similarly, to verify this assumption, the compressive strength of Si-HPMC composite cements should be

compared to that of control cements with the same porosities. To reach this goal, a power law was used to fit the compressive strength of control cements to assist the comparison (Fig. 5-37). As can be seen, the compressive strength of the composite cements with L/P ratios of 0.4 or 0.45 is generally lower than that of control cements with the same porosity. On the contrary, the compressive strength of the composite cements with higher L/P ratios (0.6, 0.8 and 1.0) is higher than that of control cements with the same porosities. Moreover, the relative increase of the compressive strength of the composite cements with different concentrations of Si-HPMC is plotted as a function of the L/P ratio (Fig. 5-38).

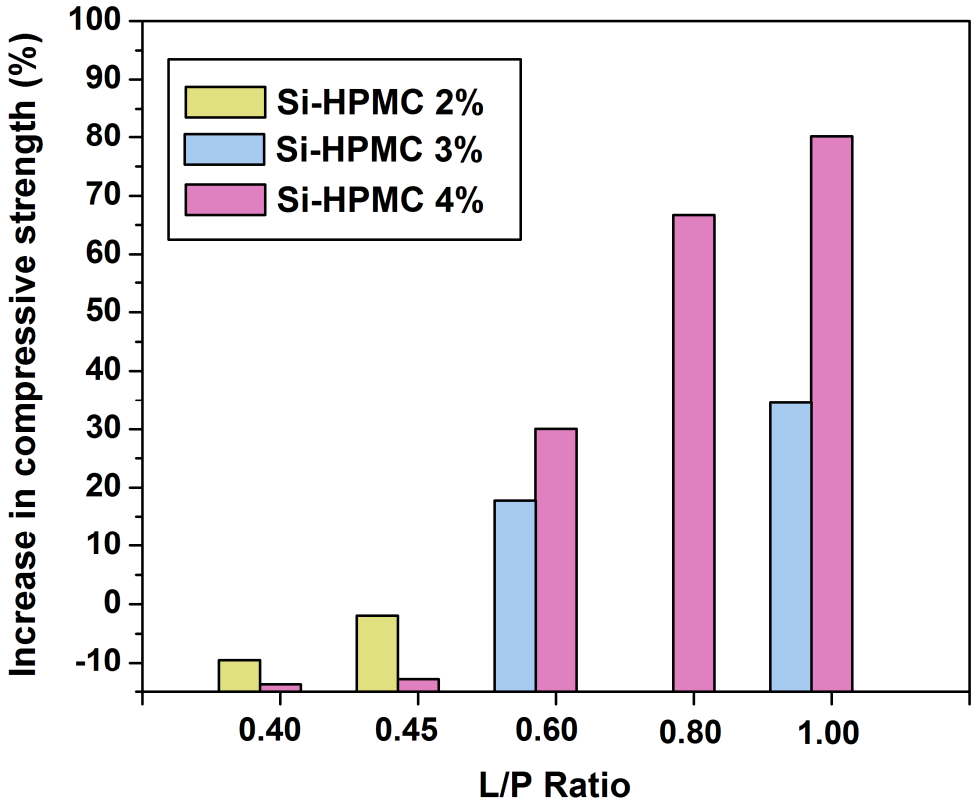

Fig. 5-38 Relative increase in compressive strength of composite cements with different concentrations of Si-HPMC solution, as a function of L/P ratio.

Similar to flexural strength, except for the composite cements with L/P ratios of 0.4 or 0.45, the relative increase in compressive strength increases strongly with polymer concentration, proving the assumption that Si-HPMC has strengthening effects on compressive strength of CPC. Moreover, this strengthening effect becomes more obvious in the composite cements with high L/P ratios. This strengthening effect is attributed to a correspondingly increasing fracture toughness. As for the composite cements with L/P

ratios of 0.4 and 0.45, the strengthening effect resulting from the increase of toughness should also contribute to an increasing strength. However, the large defects caused by concomitantly entrained air bubbles seems to counteract this benefit, especially because the increase in toughness is small for these L/P ratios (Fig. 5-30), resulting in a reduced compressive strength when compared to control cements without macropores (i.e. without polymer), as shown in Fig. 5-36 and 5-37.

Finally, some stress-displacement curves recorded during compression tests of control and Si-HPMC composite cements are shown in Fig. 5-39.

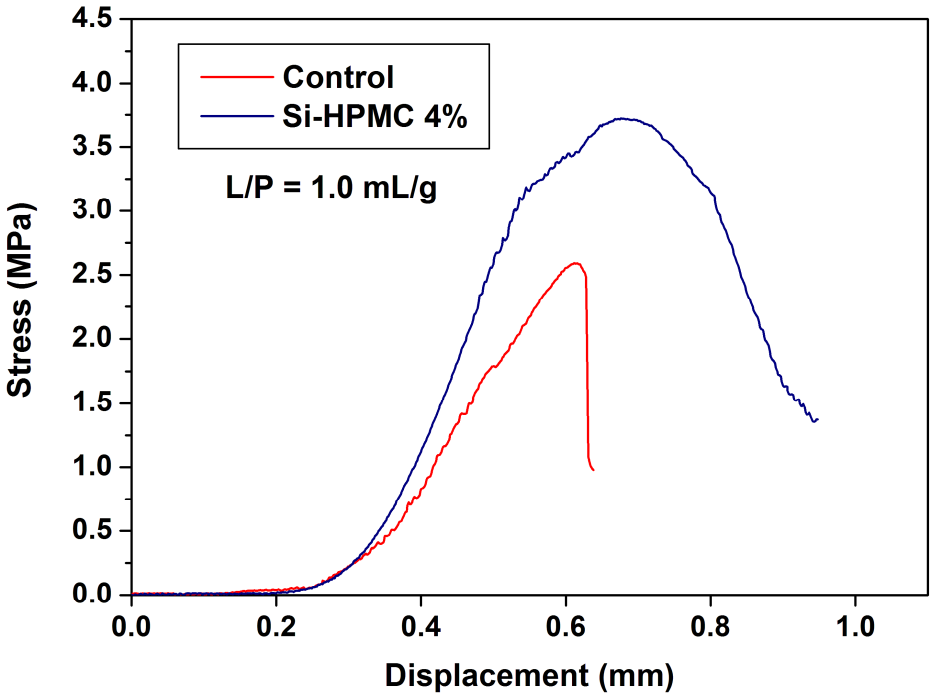

Fig. 5-39 Stress versus displacement curves of control and Si-HPMC composite cements. L/P = 1.0

An increase of the stress followed by a sharp drop can be seen for the control cement, which corresponds to a rather brittle fracture. In contrast, a less linear increase of the stress followed by a plateau and a final mild drop can be observed for the Si-HPMC composite cement with the same L/P ratio. The appearance of the plateau and the mild drop indicates a tolerance to damage, which is related to a non-brittle fracture. The curve of non-brittle failure of the Si-HPMC composite cement also demonstrates the positive effect of Si-HPMC on the fracture behavior (Fig. 5-29, 5-30).

5.2.5 Section conclusion

In this section, Si-HPMC hydrogel were used as the liquid phase to prepare CPC. The handling properties (injectability, cohesion and setting time) and mechanical properties (Young's modulus, fracture toughness, flexural and compressive strength) of the Si-HPMC have been systematically studied.

The addition of Si-HPMC changes all performance aspects of CPC. Si-HPMC significantly improves the injectability and cohesion of CPC. Moreover, unlike HPMC which delays the setting time, Si-HPMC reduces the setting time of CPC.

Si-HPMC seems to demonstrate a toughening effect on CPC, and this effect becomes more obvious with the increase of its mass fraction as well as in the CPC with a high L/P ratio.

5.3 Foamed Si-HPMC composite CPC

In section 5.2, the effect of Si-HPMC on the handling and mechanical properties of α-TCP based CPC have been systematically studied. Si-HPMC can improve all the handling properties studied such as injectability and cohesion, and shorten the setting time. Moreover, Si-HPMC can also improve the fracture toughness and provide the material with some extent of tolerance to damage, which are real limitations of inorganic CPC. In the study of section 5.2, it was observed that entrained air bubbles of various sizes could be found in the composite cements due to the effect of Si-HPMC added. On the one hand, these bubbles were found to be quite difficult to avoid, indicating that they are rather stable; and on the other hand their size, typically several tens of micrometers, is of the order of the size of macropores aimed at in calcium phosphates (Hing et al., 1999), in which bone cells can easily grow. It is therefore here proposed to exploit these features to entrain voluntarily a large number of air bubbles in Si-HPMC cements, to produce macroporous materials. Si-HPMC is thus preliminarily tried as an air-entraining agent to produce stable air bubbles, which will be further mixed with a CPC paste to prepare macroporous cements. The porosity, the handling properties (cohesion and injectability) and the mechanical properties[22] (compressive strength, flexural strength and Young's modulus) of the macroporous CPC have been investigated.

5.3.1 Preparation of Si-HPMC foams and foamed cements

The preparation process of Si-HPMC foams is similar to that of Si-HPMC hydrogels used in section 5.2. Specifically, according to the Table 5-4 which shows the formulation of the Si-HPMC foams and foamed cements, the Si-HPMC solution and the NaH_2PO_4 solution were initially sealed in two syringes of 5 mL. Then the desired volume of air was pumped into the syringe containing the NaH_2PO_4 solution (Fig. 5-40). Both syringes were then joined by a connector and the solutions and air were rapidly mixed by pushing the two plungers of the syringes several times and alternately in opposite directions for twenty seconds until a homogeneous Si-HPMC foam was formed (Fig. 5-40). The prepared Si-HPMC foam was then kept in a syringe for 15 min before the preparation of the foamed cement paste.

[22] Fracture toughness was not measured since the fracture force is too low to be determined precisely with our equipment.

Table 5-4 Formulation of the Si-HPMC foam and foamed cement specimens.

1	2	3	4	5	6	7	8
Powder (g)	Na_2HPO_4 2.5 wt.% (ml)	Si-HPMC solution [a] (ml)	NaH_2PO_4 30 wt.% (ml)	Hydrogel [b] (ml) =3+4	Total liquid volume (ml) =5+2	Total L/P ratio =6/1	Mass fraction of Si-HPMC in solid phase (%) [c]
4	1.40	0.917	0.083	1.00	2.40	0.60	0.9
3	1.05	1.238	0.113	1.35	2.40	0.80	1.6

[a] The concentration of Si-HPMC solution is 4% w/v. [b] The hydrogel is used for foaming with a $V_{air}/V_{hydrogel}$ ratio from 0 to 2.0. [c] The mass fraction of Si-HPMC in the solid phase is the proportion of Si-HPMC polymer in the final cement without taking water into account.

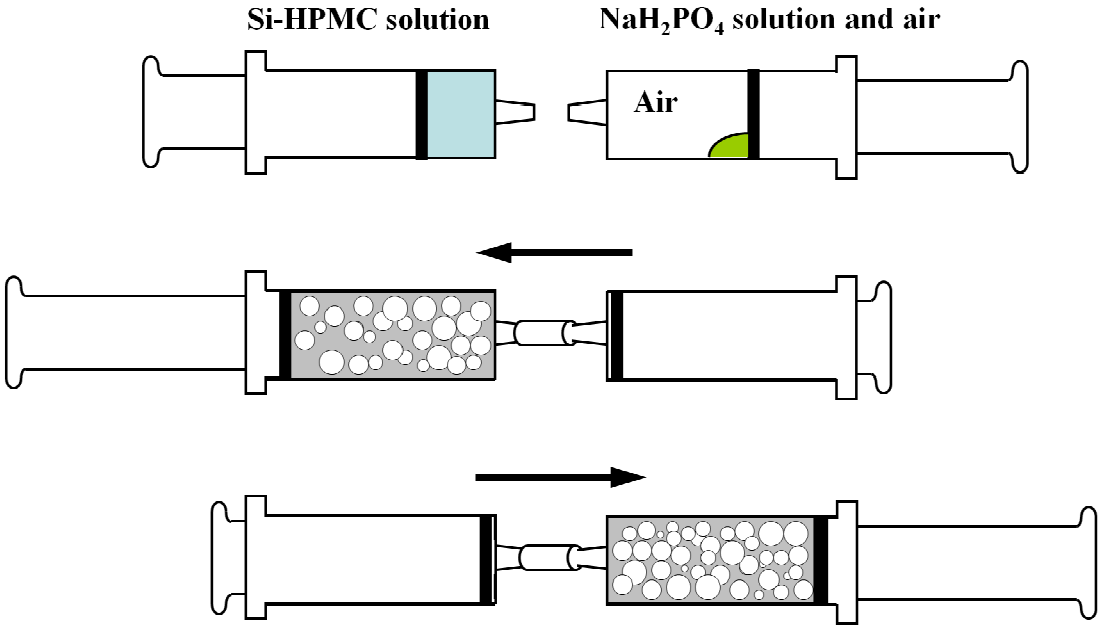

Fig. 5-40 Schemas showing the process of preparing Si-HPMC foam.

To prepare the cement paste, 2.5 wt% Na_2HPO_4 solution and α-TCP powder with 2 wt% CDHA were manually mixed in a mortar at a L/P ratio of 0.35 mL/g for 1 min, and then packed into a syringe of 5 mL followed by removing the entrained air. It is worth reminding that here the L/P ratio of 0.35, for the cement paste only, is calculated by dividing the number in column 2 of Table 5-4 by that in column 1, which is nevertheless different from the definition of the global L/P ratio of the final cement labeled in column 7. Subsequently, the pre-prepared Si-HPMC foam and cement paste were rapidly mixed for 30 seconds following the same procedure used for the preparation of the Si-HPMC foam (i.e. using two syringes and a connector) until a homogeneous foamed cement paste

was formed. For the purpose of clarity, the above process of preparing Si-HPMC foams and foamed cements is illustrated in Fig. 5-41.

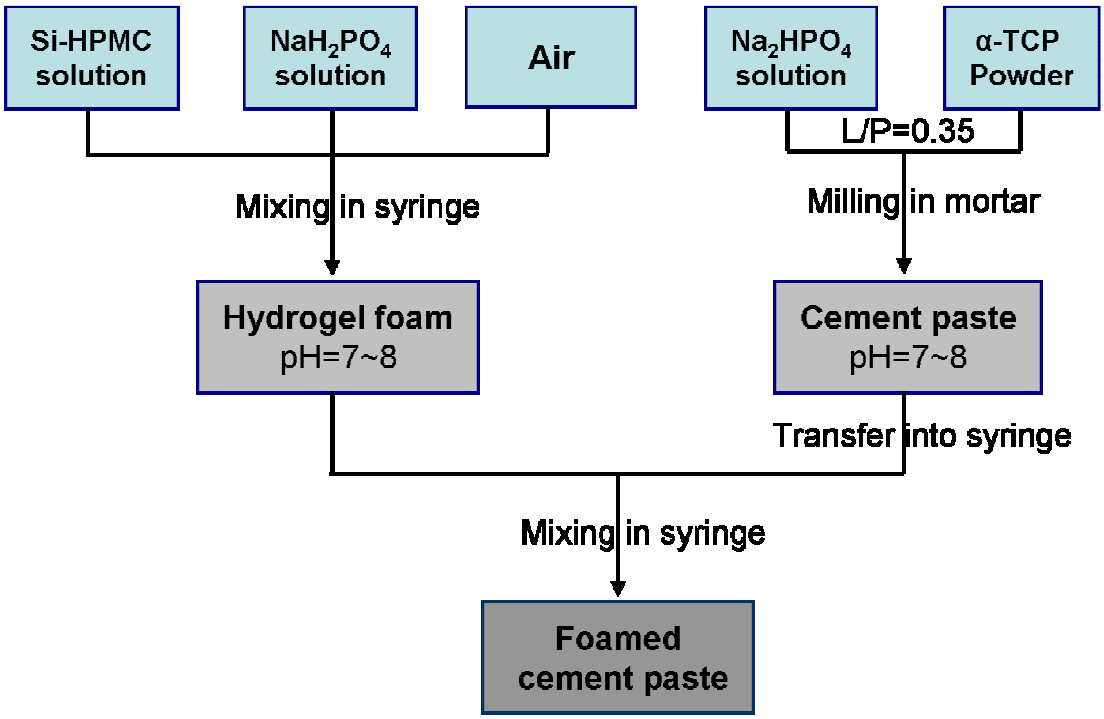

Fig. 5-41 Flow chart showing the process of preparing Si-HPMC foams and foamed cements

The prepared foamed cements were used for the evaluation of handing properties or used to prepare specimens for the measurement of porosity and mechanical properties. Cylindrical specimens were made for the measurement of compressive strength. Rhombohedral bars were made for the measurement of Young's modulus and flexural strength. All the mechanical properties were measured in wet conditions.

5.3.2 Handling properties of foamed Si-HPMC composite CPC

Only injectability and cohesion have been evaluated. Setting time is not included because the foamed cement is macroporous and it is therefore not possible to use the Gillmore needles to characterize its setting time.

5.3.2.1 Injectability

The injectability of the foamed Si-HPMC composite cements has been assessed and all the foamed cements studied can be extruded completely from the syringe (5% of the paste is left in the tip of the syringe; since all the foamed cements can be completely extruded, the graph of injectability is not shown here). Similar to HPMC or Si-HPMC composite

cements, the outstanding injectability of the foamed composite cements is due to the improved paste viscosity which can effectively reduce or even avoid filter-pressing. The extrusion curves during injection of the foamed cements are recorded, which is a useful tool to explain the extrusion process (Fig. 5-42).

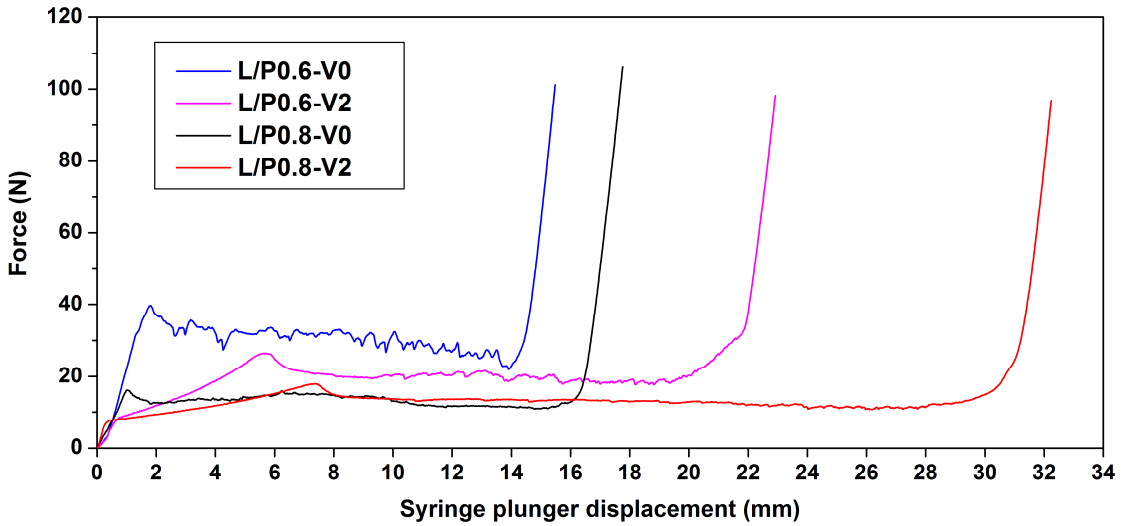

Fig. 5-42 Injection force curves during extrusion of the foamed Si-HPMC composite cement pastes at different L/P ratios and volume of air entrained. V0 and V2 is short for $V_{air}/V_{hydrogel}$ = 0 and 2.

In general, the extrusion curves of the foamed Si-HPMC composite cements are similar to those of non-foamed composite cements (see Fig. 5-5, 5-21). The slowly increasing overshoots for the foamed cements (e.g. see Fig. 5-32, L/P = 0.6, 0.8-V2) are mainly due to the entrained air bubbles which need to be pressed before the paste starts to flow. Plateaus can be observed for all the cements, indicating a homogeneous extrusion. Moreover, the plateau for the foamed cement is longer than that of the corresponding non-foamed cement, and this is simply due to the large volume of air bubbles which enlarges the total volume of the cement paste. Finally, the extrusion force at the plateau increases with the decreasing L/P ratio, which is simply due to the correspondingly increasing viscosity of the cement paste.

5.3.2.2 Cohesion

Even with a large amount of air bubbles, the foamed Si-HPMC composite cements still demonstrate an excellent cohesion. Indeed, when injected into a saline solution immediately after preparation (< 3 minutes), the foamed Si-HPMC composite cements paste can maintain their noodle-like shape until hardening, during which no

disintegration can be observed, indicating an outstanding cohesion (Fig. 5-43A). Moreover, because of the numerous air bubbles, the density of the foamed Si-HPMC composite cements is very low, thus the cements float in the saline solution (Fig. 5-43B) even after complete hardening.

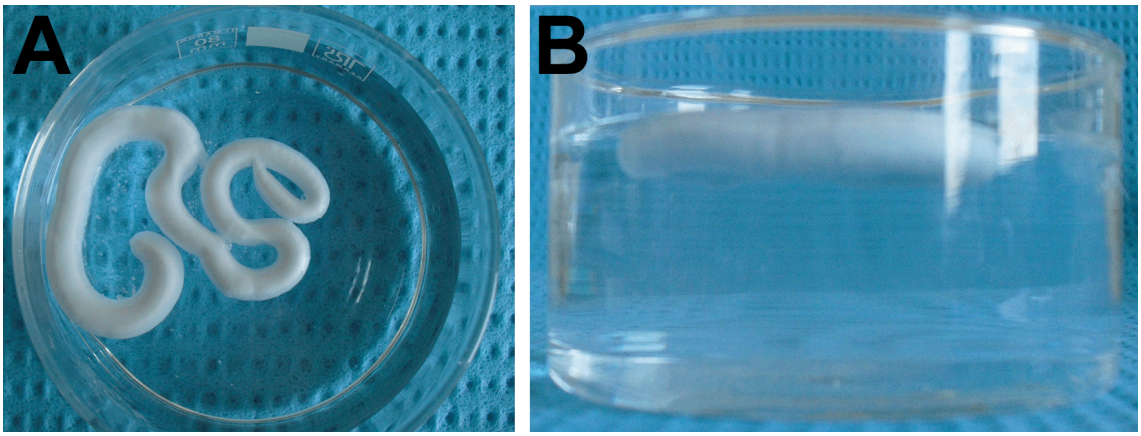

Fig. 5-43 Photos of a foamed Si-HPMC composite cement injected into a saline solution immediately after preparation (within 3 min), A) overhead view, no disintegration can be observed B) side view, showing the paste floating in the saline solution, indicating a low density (high porosity). L/P= 0.8, $V_{air}/V_{hydrogel}$ = 2.0

Like Si-HPMC composite cements, the strong cohesion of the foamed cements can be attributed to the enhanced paste viscosity and to the effect of the three-dimensional hydrogel network.

5.3.3 Microstructure and mechanical properties

5.3.3.1 Porosity

As expected, the total porosity of the foamed Si-HPMC composite cements increases with the increase of the volume of air introduced, and the total porosity of the foamed cement with a high L/P ratio is higher than that of the corresponding foamed cement with a lower L/P ratio (Fig. 5-44). The specific reason for the latter result has been explained previously in the case of other composite cements. Moreover, according to the process of how macropores are created in the present study, the macroporosity of the foamed cement can be primarily estimated by subtracting the total porosity of the corresponding cement, fabricated without air, from the total porosity of the foamed cement fabricated with air, using the equation 2-7 developed in Chapter 2.

Similarly, the macroporosity increases with the increase of the volume of air

introduced, and the macroporosity of the foamed cement with a L/P ratio of 0.8 is also higher than that of the corresponding foamed cement with a lower L/P ratio due to its larger volume of Si-HPMC hydrogel used for foaming (see the column 5 of Table 5-4).

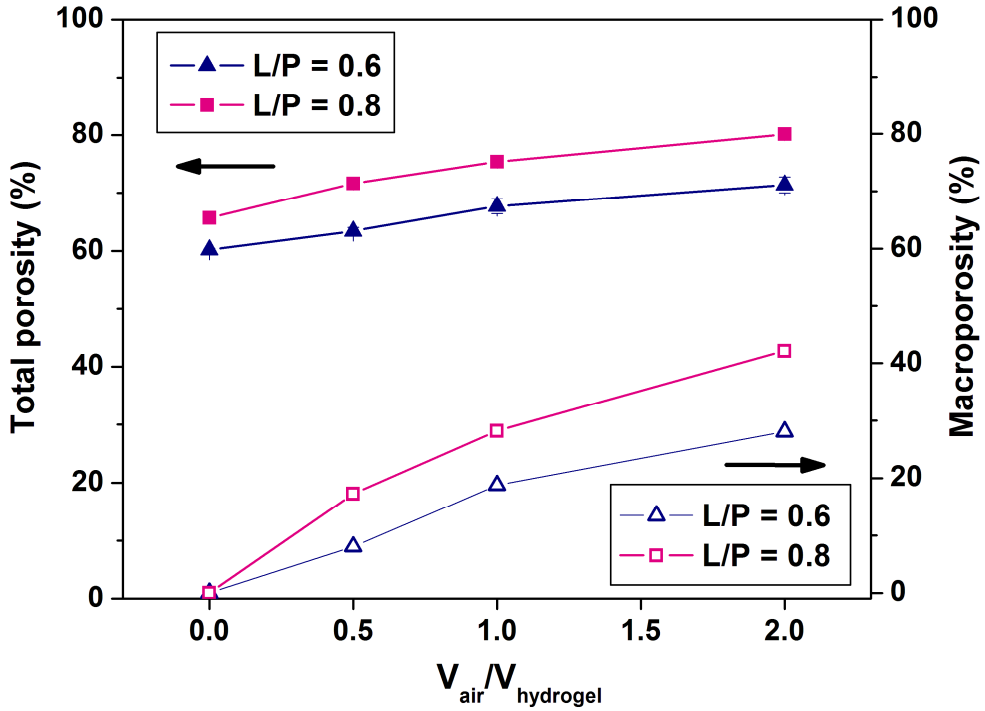

Fig. 5-44 Total porosity and estimated macroporosity of foamed Si-HPMC composite cements with different L/P ratios as a function of the volume of air bubbles introduced. Each value is the mean of six measurements ± one standard deviation.

The SEM micrographs of fracture surfaces of the foamed Si-HPMC composite cements are shown in Fig. 5-45. Numerous spherical macropores of various sizes are arbitrarily distributed in the foamed Si-HPMC composite cement with a L/P ratio of 0.8 and a $V_{air}/V_{hydrogel}$ ratio of one (Fig. 5-45A). With the increase of the $V_{air}/V_{hydrogel}$ ratio, many macropores with distorted shapes and larger sizes are observed (Fig. 5-45B). Moreover, at higher magnification, glue-like polymer, which is probably derived from shrunk Si-HPMC hydrogel after drying, can be found in the cement matrix between macropores (Fig. 5-45C), sticking to adjacent apatite crystals. Fig. 5-45D shows, at the surface of macropores, the morphology of the cement matrix, which is similar to that of the cement matrix between macropores. As mentioned previously, the polymers may contribute to higher mechanical properties, especially fracture toughness. In addition, a previous study on other cement formulations has pointed out the importance of maintaining macropores in the cement paste after injection (Ginebra et al., 2007). As seen

in Fig. 5-45, this issue does not seem to be a challenge for the present foamed Si-HPMC composite cement, further indicating the advantage of using Si-HPMC as an air-entraining agent in CPC.

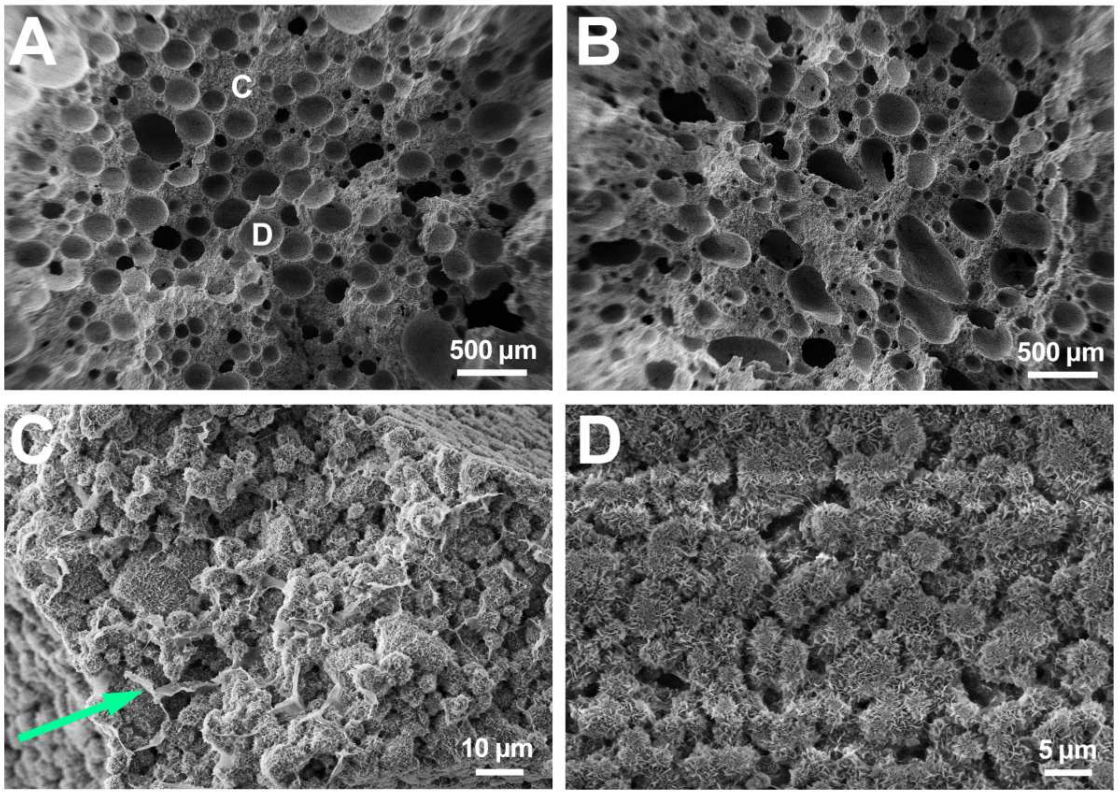

Fig. 5-45 SEM pictures of the fracture surfaces of the foamed Si-HPMC composite cements (A) L/P = 0.8, $V_{air}/V_{hydrogel}$ = 1; (B) L/P = 0.8, $V_{air}/V_{hydrogel}$ = 2; (C) cement matrix between air bubbles; (D) cement matrix inside an air bubble. Arrow in C points to shrunk Si-HPMC polymers sticking to apatite crystals.

The foamed Si-HPMC composite cements were examined by means of micro-computed tomography (CT) to preliminarily assess the sizes and distribution of the air bubbles introduced (Fig. 5-46 and 5-47). The minimal resolution of the CT is 7.5 µm, thus only pores larger than 7.5 µm can be seen in the pictures and measured by the analysis software. Only a few macropores can be found in the cross section of the foamed cement with a L/P ratio of 0.6 and a $V_{air}/V_{hydrogel}$ ratio of 0.5 (Fig. 5-46A). With increasing $V_{air}/V_{hydrogel}$ ratio, both the number and size of the macropores increase (Fig. 5-46B, C). In contrast, many macropores can be seen in the cross section of the foamed cement with a higher L/P ratio of 0.8 and a $V_{air}/V_{hydrogel}$ ratio of 0.5 (Fig. 5-46D). Besides, the number and size of the macropores increase significantly with the increase of $V_{air}/V_{hydrogel}$ (Fig. 5-46E, F).

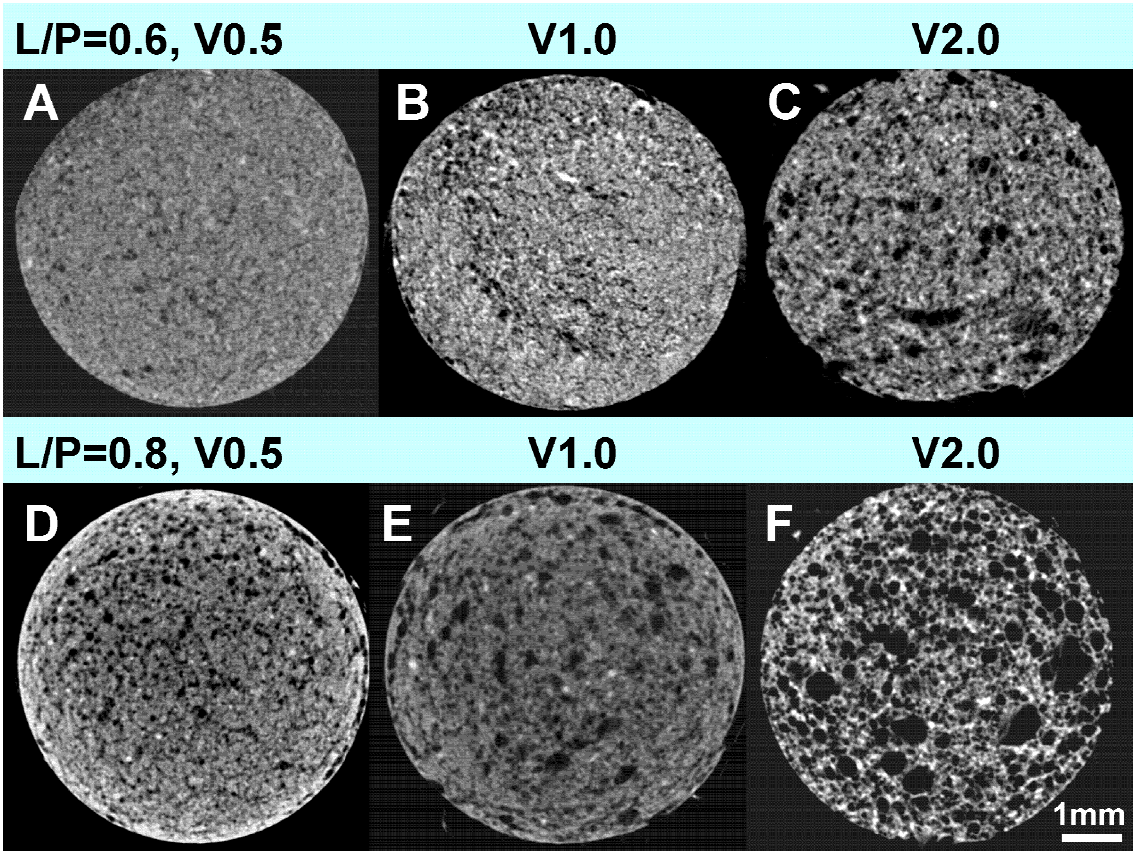

Fig. 5-46 CT Scanning of the cross sections of foamed Si-HPMC composite cements with different L/P ratios and volumes of air bubbles. The resolution of the CT is 7.5 μm.

Finally, the pore size distribution of the foamed Si-HPMC composite cements with different L/P ratios and volumes of air bubbles were calculated basing on the three-dimensional volume formed by combining all the cross sections scanned together (Fig. 5-47). For the foamed Si-HPMC composite cement with a L/P ratio of 0.6, the distribution mode corresponds to a pore size of around 50 μm, and this size tends to increase slightly with the increase of the $V_{air}/V_{hydrogel}$ ratio. Similar features have also been observed in the foamed Si-HPMC composite cement with a L/P ratio of 0.8. Moreover, pores with sizes over 300 μm can be found only in the cement with a L/P ratio of 0.8 and a $V_{air}/V_{hydrogel}$ ratio of two. All of the above observations are consistent with the results in Fig. 5-46.

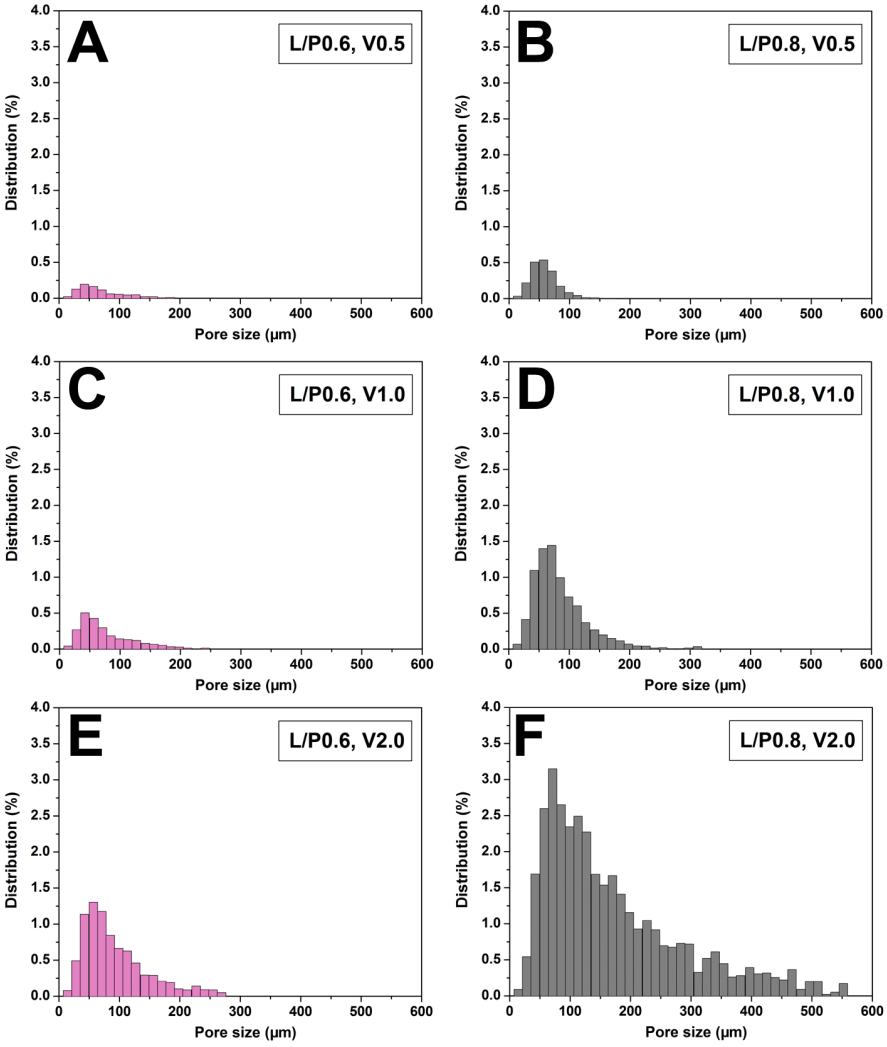

Fig. 5-47 Pore size distributions of the foamed Si-HPMC composite cements with different volumes of entrained air bubbles, tested by CT Scanning, A) L/P=0.6, B) L/P=0.8. V0.5, V1 and V2 are short for $V_{air}/V_{hydrogel}$ = 0.5, 1 and 2 respectively. The pore distribution on the vertical scale is based on the total volume of the specimen.

5.3.3.2 Mechanical properties

Before presenting the results, it is worth stating that the main purpose is to explore the possibility of using Si-HPMC as an air-entraining agent to produce macroporous cements. Mechanical properties do deserve some attention, but only preliminary results are available at the time of writing this manuscript. Moreover, as discussed previously, mechanical properties of CPC generally decrease with the increase of the porosity. Due to the high porosity of the foamed cements (Fig. 5-44), low mechanical properties are to be expected. Thus, in this section, only Young's modulus, flexural strength and compressive strength were measured to show how entrained air bubbles influence the mechanical

properties of the foamed Si-HPMC composite cements. Fracture toughness was not measured since the fracture force is too low to be determined precisely with our equipment.

As expected, all the mechanical properties measured decrease with the increase in macroporosity (Fig. 5-48).

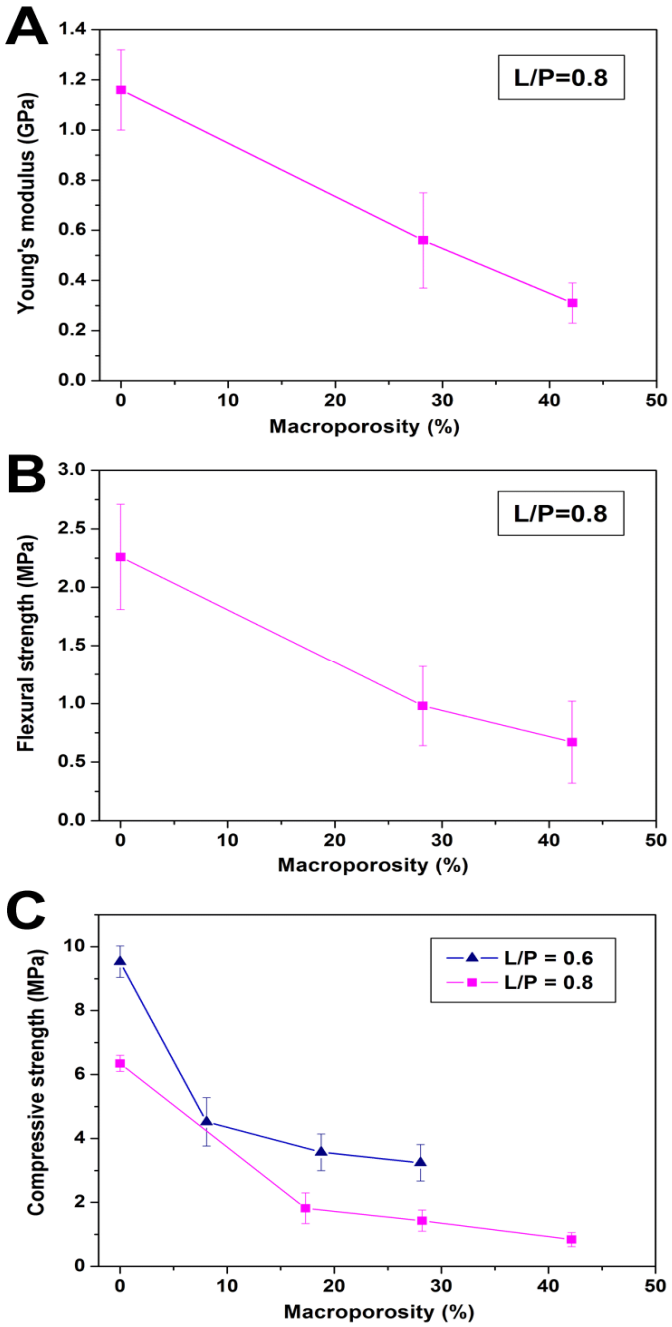

Fig. 5-48 (A) Young's modulus; (B) Flexural strength; and (C) Compressive strengths of foamed Si-HPMC composite cements as a function of macroporosity. For (A) and (B), each value is the mean of three measurements ± one standard deviation. For (C), measurements were conducted on cylindrical specimens, and each value is the mean of six measurements ± one standard deviation.

In most cases, there are not enough data points to be able to conclude on a trend, but in the case of the compressive strength and with a L/P ratio of 0.6, it seems that a sharp decrease can be found as soon as air bubbles are introduced. This phenomenon has also been observed in all the macroporous cements discussed previously. This is mainly attributed to the large air bubbles which act as critical flaws. Besides, the compressive strengths of the foamed cements with a L/P ratio of 0.6 are higher than those of the foamed cements with a L/P ratio of 0.8 due to their lower porosity. Finally, it is worth noting that although the mechanical properties of the foamed cements are very low, they are still comparable to those reported for spongy bone (Koester et al., 2008; Wagoner Johnson et al., 2011).

Finally, the stress-displacement curves recorded during compression tests of the foamed Si-HPMC composite cements with different amounts of air are shown in Fig. 5-49.

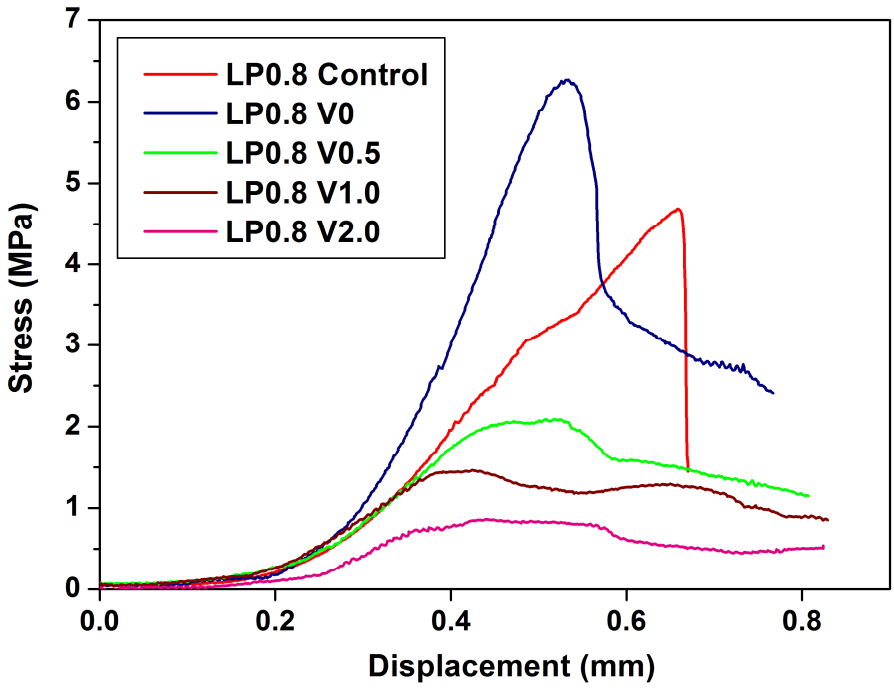

Fig. 5-49 Stress versus displacement curves of the control and foamed Si-HPMC composite cements with different amounts of air introduced. V0, V0.5, V1 and V2 are short for $V_{air}/V_{hydrogel}$ = 0, 0.5, 1 and 2 respectively.

A sharp drop of the loading stress can be observed for the control cement with a L/P ratio of 0.8, which is related to a brittle fracture. On the contrary, a mild drop of the loading stress can be found for the Si-HPMC composite cement with a $V_{air}/V_{hydrogel}$ ratio of 0 (no air bubbles), which can be seen as a kind of tolerance to damage. Furthermore,

the tolerance to damage becomes more obvious in the foamed Si-HPMC composite cements with different amounts of air introduced. These curves of non-brittle failure show the beneficial effect of Si-HPMC on the fracture behavior of the foamed Si-HPMC composite cements, which is also consistent with the HPMC/Si-HPMC composite cements discussed previously.

5.3.4 Section conclusion

In this study, stable Si-HPMC foams were prepared by mixing Si-HPMC hydrogel with air. These stable foams were further mixed with cement pastes to produce macroporous Si-HPMC composite cements.

These macroporous composite cements demonstrate excellent handling properties such as injectability and cohesion. Their mechanical properties (Young's modulus and compressive strength) are comparable to those of cancellous bone. Moreover, they also exhibit a kind of tolerance to damage, which is usually related to an improved fracture toughness. Given the main requirements reported for the application of CPC in surgery (macropores, handling properties and mechanical properties), the macroporous Si-HPMC composite cements developed in this study may represent appealing bone substitutes for cancellous bone.

Conclusions and perspectives

CPC with controllable microstructures (porosity, pore size, crystal shape (size)) were prepared, and their mechanical properties (Young's modulus, fracture toughness, compressive and flexural strength) were systematically investigated. Moreover, composite CPC were developed by using different cellulose ethers, and their handling and mechanical properties were studied. The main results of the research have already been described and discussed, but the most important features are here summarized.

Unreacted α-tricalcium phosphate (α-TCP) can be detected by means of XRD and SEM, for cements made with a low L/P ratio and as a general feature in the cements prepared with coarse α-TCP powder. These α-TCP particles exhibit weak links with the CDHA matrix and are usually surrounded by "spaces" separating them from the matrix, such spaces being comparable to "microcracks". The latter can provoke a decrease in Young's modulus, but do not seem to influence fracture toughness.

The particle size of pristine α-TCP has a strong effect on the microstructure of the final reaction product (CDHA). The larger the starting α-TCP particles, the coarser the microstructure of CDHA, which in the end results in a larger critical flaw size and hence in a reduced strength compared to cements made with a fine powder. In the case of macroporous CPC obtained using soluble mannitol particles as a porogen, the critical flaw size is of the order of that of the largest macropores for low macroporosities, and then increases monotonically with increasing macroporosity. The increasing critical flaw size is believed to be related to subcritical microcrack growth and linking between macropores before reaching the peak stress, as suggested in macroporous BCP ceramics (Pecqueux et al. 2010). Moreover, this stable crack growth seems to happen during both compression and tensile (flexural) loading in macroporous CPC. The evolution with both microporosity and macroporosity of most mechanical properties (Young's modulus, toughness and compressive strength) can be described with double-scale power-law models and when necessary interpreted by taking into account all the above-mentioned phenomena.

Test conditions (dry and wet) strongly affect the mechanical properties of CPC (microporous or macroporous). The mechanical properties measured in wet condition are generally lower than those measured in dry condition. The lower fracture properties measured in wet condition are mainly attributed to the presence of water which may

decrease the surface energy on crack surfaces.

The fabrication process of CPC, particularly the stage of mixing of the cement paste, may reduce the strength reliability of microporous CPC in high L/P ratios, due to the unpredictable character of a small number of large air bubbles trapped, acting as critical flaws with a strongly random size. In contrast, the fabrication process has less effect on the reliability of the macroporous CPC. Their reliability is high and constant with macroporosity, due to the presence of a large number of macropores of calibrated size, leading to a more deterministic critical flaw size.

Among the above properties measured in wet condition, only the Young's modulus for microporous CPC (Cement F) and compressive strength for macroporous CPC could suit the properties of cortical or cancellous bone.

The addition of cellulose ethers, HPMC/MC with different structural parameters and Si-HPMC with a three-dimensional network of polymer chains, modifies almost all performance aspects of CPC, including handling properties, porosity and mechanical properties.

Both the molecular weight and the substitution level of HPMC/MC have a great influence on the injectability of CPC. The higher the viscosity of the HPMC/MC solution, the better the injectability of the composite CPC paste. For different HPMC solutions with similar viscosities, the degree of substitution by MeO or HPO groups appears to play a great role. HPMC/MC seems to be an excellent option not only to improve injectability but also to improve cohesion and resistance to washout. In addition, HPMC/MC can prolong the setting time, especially the final setting time of composite cements. Similarly, the addition of Si-HPMC also significantly improves the injectability and cohesion of composite cement pastes. However, unlike HPMC/MC which delays the setting time, Si-HPMC reduces the apparent setting time of CPC, probably due to its "self-hardening" behavior during gelling. Only a small amount of HPMC/MC or Si-HPMC is needed to dramatically change all the handling properties of the cement pastes studied.

Both HPMC/MC and Si-HPMC have a strong toughening effect, and this effect becomes more significant in the composite cements with higher polymer mass fractions or molecular weight, or in the composite cements with high L/P ratios. This toughnening is attributed, among others, to crack bridging by plastically deforming polymer ligaments, and its extent is consistent with existing descriptions. Si-HPMC also improves the Young's modulus and toughness through a better homogeneity of the microporous structure. However, as soon as small quantities of HPMC/MC or Si-HPMC are added to

the cements, a sudden decrease of compressive strength is provoked by entrained air bubbles acting as critical flaws, but then the strength generally tends to increase with the polymer mass fraction when compared to macroporous "control" cements with the same porosity, which can be attributed to the correspondingly increasing fracture toughness. The addition of polymers also provide the materials with a certain extent of tolerance to damage, with a progressive deformation and cracking during loading instead of a brittle fracture; this may be interesting for biological applications, by preventing the release of debris in the body in the case of an overload.

Si-HPMC hydrogel seems to be a promising foaming agent for the preparation of macroporous CPC. The resulting macroporous CPC demonstrate excellent handling properties such as injectability and cohesion. Their mechanical properties (Young's modulus and compressive strength) are comparable to those of cancellous bone. Moreover, they also exhibit a kind of tolerance to damage, which is usually also related to an improved fracture toughness, although it has not been measured yet. Given the main requirements reported for the application of CPC in surgery (macropores, handling properties and mechanical properties), the macroporous Si-HPMC composite CPC developed in this study may represent appealing bone substitutes for cancellous bone.

Based on the above findings, especially the ones on the Si-HPMC macroporous composite cements, some further researches are therefore encouraged.

Strength reliability and fracture toughness are the real limitations for CPC. Thus it will be of great interest to investigate the reliability and fracture toughness of the Si-HPMC macroporous CPC, and if necessary, to try to improve them.

Si-HPMC was only primarily tried as foaming agent to produce macropores in CPC, but the amounts and sizes of these macropores were not well controlled and characterized. Therefore, it will be interesting for practical applications to develop a Si-HPMC macroporous CPC with controllable macropores and to better characterize them.

The next step of the whole study will be to investigate the *in vitro*/*in vivo* behavior of the Si-HPMC macroporous CPC, especially their effect on bone conductivity. For this purpose, an experimental formulation of Si-HPMC composite CPC is going to be implanted in rabbit femur for eight weeks to examine whether the Si-HPMC foamed macroporous CPC is efficient for cell colonization. Based on this result, a more complete biological study will or not be designed to measure the *in vitro*/*in vivo* safety and efficacy of Si-HPMC addition in big animals (e.g. pig, dog).

Résumé

Introduction et Chapitre 1: État des lieux et objectifs

L'os est un organe remarquable et rigide propre aux vertébrés, qui assure des fonctions importantes telles que le soutien structurel et la protection de divers organes du corps, la production de cellules sanguines et le stockage de minéraux pour le métabolisme (Hing 2004). Les os contiennent de nombreuses fissures, qui se forment et se développent sous l'effet de maladies ou des chargements mécaniques des activités quotidiennes. Cependant, l'os possède une propriété qui, jusqu'à présent, ne peut pas être obtenue dans les matériaux artificiels, malgré des progrès constants dans le domaine des matériaux « auto-réparants » (Cordier et al, 2008) : il est assez « intelligent » pour détecter et réparer les fissures avant qu'elles deviennent assez longues pour présenter un danger. Cette capacité d'auto-réparation de l'os, appelée remodelage, est contrôlée par deux types de cellules spécialisée: les ostéoclastes, qui résorbent l'os en libérant un acide puissant et des enzymes, et les ostéoblastes, qui fabriquent de l'os nouveau. Ces cellules sont regroupées en unités de base multicellulaires (UBM), qui créent des cavités d'environ 200 μm de diamètre se déplaçant à une vitesse de 40 μm par jour (Fig. 1-1) (Taylor et al, 2007). Bien que possédant cette nature fascinante, les os ne peuvent pas toujours prévenir la rupture catastrophique; par ailleurs les traumatismes, le vieillissement, les maladies (ostéoporose ou cancer) ou les anomalies congénitales touchent des millions de personnes à travers le Monde.

Les os possèdent une structure hiérarchique constituée de plusieurs niveaux différents (Fig. 1-2). D'un point de vue chimique, l'os comprend une matrice organique (32%), une partie minérale (43%) et de l'eau (25%) (Nyman et al., 2005). Les collagènes et les minéraux ont une grande influence sur les propriétés mécaniques de l'os : d'une part le collagène peut améliorer la ténacité, et d'autre part le minéral peut conférer résistance et rigidité. En outre, l'eau joue également un rôle important sur les propriétés mécaniques de l'os. La perte d'eau dans la phase collagène diminue la ténacité de l'os, et la perte d'eau liée à la phase minérale diminue à la fois la résistance et la ténacité des os (Nyman et al., 2006).

Comme mentionné ci-dessus, en dépit de la capacité d'auto-guérison, la fracture d'un os n'est pas toujours évitable. Afin de mieux comprendre comment la fissure se propage dans les os, la ténacité, K_C, aussi appelée facteur d'intensité de contrainte critique, est

utilisée pour décrire la résistance de l'os à la fissuration. Comme dans d'autres matériaux composites, la ténacité de l'os est plus grande que celle de ses constituants (organique et minéral). Par ailleurs, K_C n'est pas constante au cours de la propagation de fissure, mais augmente avec l'extension de fissure, ce qui est appelé un comportement de courbe R (« R » signifie « résistance », et une courbe R définit la résistance à la fissuration, ou ténacité, en fonction de l'extension de fissure, voir Fig. 1-3), et qui est dû à l'existence de phénomènes microscopiques que sont les mécanismes de renforcement (Nalla et al., 2005 ; Vashishth, 2004). Launey et Ritchie (2009) ont établi qu'il existait plusieurs mécanismes de renforcement dans l'os cortical, dont le pontage des fissures par des ligaments intacts (Nalla et al., 2005), la déviation de fissure (Peterlik et al., 2006), la microfissuration (Vashishth, 2004) et la viscoplasticité (Fantner 2005), qui peuvent être utilisés pour expliquer une courbe R croissante (Voir Fig. 1-4). Parmi eux, le pontage des fissures et la déviation de fissure sont les deux principaux mécanismes de renforcement.

De nos jours, en raison de maladies et d'événements traumatiques, près de trois millions de patients dans le Monde ont besoin de subir des opérations de greffage osseux chaque année. Actuellement, l'autogreffe est toujours considérée comme idéale, car les os prélevés sur les patients eux-mêmes contiennent des cellules vivantes et des facteurs de croissance. Toutefois, les prélèvements sont évidemment limités, ce qui interdit l'utilisation de cette technique pour des greffes de grande taille. Alternativement, l'allogreffe à partir d'une banque d'os issus de divers donneurs pourrait permettre de surmonter en partie cette limitation d'approvisionnement en os, mais après des traitements de stérilisation le greffon osseux perd ses facteurs biologiques et voit son efficacité affaiblie (Hing et al., 2005B). En raison des inconvénients ci-dessus, un large éventail de matériaux synthétiques, tels que les métaux, polymères, céramiques et ciments de phosphate de calcium, ont été proposés et développés comme substituts osseux ; leur approvisionnement n'est pas limité et ils permettent d'éviter toute contamination (Bohner 2010A). Ces substituts osseux synthétiques seront brièvement passés en revue.

Le polyméthacrylate de méthyle (PMMA) est un polymère synthétique qui a été largement utilisé dans la fixation de prothèses depuis 1960 (Charnley 1960). Néanmoins, le PMMA présente encore quelques lacunes bien connues, telles qu'une réaction exothermique lors de sa polymérisation qui peut causer une nécrose des tissus environnants, l'absence de pores d'une taille suffisante (macropores) pour permettre la croissance cellulaire, la libération de monomères n'ayant pas réagi et de faibles propriétés

mécaniques (Lewis, 1997).

Depuis leur première mention dans un document publié en 1971 (Blakeslee et al, 1971), les biocéramiques, qui peuvent être classées en deux familles (bioinerte et bioactive), sont utilisées comme substituts osseux depuis environ quarante ans. En outre, les céramiques bioactives, à base d'orthophosphates de calcium tels que le phosphate tricalcique (TCP), l'hydroxyapatite (HA) et le phosphate de calcium biphasique (BCP), ont été largement utilisés dans toutes les zones du squelette humain (Dorozhkin 2010). La plupart des études sur ces matériaux peuvent être classées en deux catégories principales: l'optimisation de la microstructure et l'obtention d'une activité chimique appropriée (Hing et al, 2005B). En ce qui concerne la microstructure, il est utile de mentionner que dans cette étude la microporosité se réfère à des pores de taille inférieure à 10 μm, alors que la macroporosité correspond à des pores de plus de 100 μm ; ce sont les définitions couramment rencontrées dans la communauté des biomatériaux. Les deux échelles de porosité (microporosité et macroporosité) jouent un rôle dans les substituts osseux. D'une part la microporosité permet l'imprégnation de l'implant par les fluides biologiques, et d'autre part la présence de macropores est considérée comme essentielle pour la migration des cellules (Hing et al., 1999). En dépit de leur large application, de nombreux défis subsistent pour les biocéramiques en termes de bioactivité et de propriétés mécaniques (résistance à la rupture, fiabilité), ces dernières ayant besoin d'être améliorées en vue d'applications dans des sites sollicités mécaniquement.

Les ciments de phosphate de calcium (CPC) sont des matériaux hautement biocompatibles qui sont progressivement remplacés par de l'os nouvellement formé in vivo. Depuis le premier brevet sur le CPC proposé par Brown et Chow en 1983 (Brown et al., 1983), beaucoup de CPC ayant des compositions différentes ont été étudiés et sont disponibles commercialement (Bohner et al., 2005B). Un CPC est produit par une réaction chimique entre deux phases, une poudre et un liquide qui, lorsqu'ils sont mélangés, forment une pâte qui durcit progressivement jusqu'à obtention d'un solide, ce qui est semblable aux ciments utilisés en génie civil. Le durcissement du ciment se fait à travers l'enchevêtrement de cristaux aciculaires ou en forme de plaques (Fig. 1-6). La chimie et la cinétique de prise des CPC seront détaillées ultérieurement. Actuellement, il y a seulement deux produits finaux possibles pour la réaction chimique de prise des CPC : la brushite (phosphate dicalcique dihydraté : DCPD) ou une apatite comme l'hydroxyapatite ou l'hydroxyapatite déficiente en calcium (CDHA) (Bohner 2007). Les CPC contiennent une microporosité intrinsèque interconnectée qui est utile pour

l'imprégnation par les fluides biologiques. Par ailleurs, comme pour d'autres substituts osseux, il serait également souhaitable de créer des macropores d'au moins quelques dizaines de micromètres dans les CPC pour favoriser la colonisation osseuse de l'implant. Toutefois, ces pores (micro ou macro) conduisent à de mauvaises propriétés mécaniques, notamment à une résistance à la rupture particulièrement faible et peu fiable, ce qui interdit l'utilisation des CPC dans des sites sollicités mécaniquement ; ils ont en cela encore besoin d'amélioration (Bohner 2010B). Ce point sera davantage détaillé dans la section 1.5. Outre des avantages tels qu'une biocompatibilité, une bioactivité et une ostéoconductivité élevées, les CPC possédent un avantage unique par rapport aux biocéramiques : ils peuvent être facilement manipulés et façonnés et, dans certains cas, être injectés dans la zone du défaut à combler, non seulement en évitant une intervention chirurgicale lourde, mais aussi en s'adaptant de manière intime à l'os environnant même pour des cavités de forme irrégulière. En outre, la composition finale des CPC est plus proche de celle des phosphates de calcium présents dans les tissus minéralisés que ne l'est celle des biocéramiques. Les CPC possèdent par ailleurs une surface spécifique élevée, présentant ainsi une (ré-)activité fortement améliorée et permettant des applications en ingénierie tissulaire ou un relargage simultané de substances médicamenteuses (Bohner 2001). Les avantages et les inconvénients des divers substituts de greffe osseuse sont résumés dans le tableau 1-2.

Malgré de nombreuses combinaisons possibles des ions calcium et phosphate dans les CPC, la chimie de la réaction de prise dans ces systèmes est toujours semblable et peut être expliquée et comprise en analysant la solubilité des composés impliqués (Chow, 2001). Le processus chimique au cours de la réaction de prise consiste principalement en deux mécanismes: dissolution et précipitation. Les forces motrices contrôlant la dissolution et la précipitation peuvent être interprétées en terme de concurrence entre le produit d'activité ionique d'un composé et son produit de solubilité. En particulier, un précipité tend à se dissoudre si son produit de solubilité est supérieur à l'activité des ions produits, et vice versa. Les produits de solubilité de certains phosphates de calcium, à différentes températures, sont présentés dans le tableau 1-3. En outre, la solubilité d'un composé peut être caractérisée de manière schématique l'aide d'un diagramme de phase de solubilité (Fig.1-7) (Chow 2009), qui décrit l'évolution de la solubilité d'un composé sous la forme du logarithme de la concentration totale en calcium en fonction du pH. Certains facteurs tels que le rapport Ca/P, la température (Fig.1-8) et la concentration en CO_3^{2-} sont considérés comme ayant un effet sur le diagramme de phase de solubilité

(Fernandez et al., 1999A).

Bien que le diagramme de phase de solubilité puisse être utilisé pour prédire le comportement thermodynamique des CPC, ils ne peut pas toujours expliquer le comportement de durcissement observé, et la cinétique doit également être prise en considération. Comprendre les mécanismes qui contrôlent le processus de formation des CPC aidera à avoir une connaissance approfondie de leurs cinétiques et à mieux contrôler leur microstructure, ce qui déterminera les différentes applications possibles. Actuellement, de nombreux substituts de type CPC sont basés sur l'hydrolyse d'une poudre de α-TCP, qui est aussi le matériau utilisé dans cette étude. Beaucoup de facteurs, tels que la taille des particules, la cristallinité, la température et la composition des réactifs (Bohner et al., 2009), influencent la cinétique de prise.

Malgré de nombreux avantages, les substituts osseux de type CPC présentent quelques inconvénients qui limitent leur application clinique potentielle. Parmi ces inconvénients, un temps de prise relativement long (le moment où le ciment peut résister à une certaine force appliquée) est un problème qui doit être traité. De manière générale, une pâte de ciment avec un temps de prise long pourrait causer des problèmes en raison de son incapacité à soutenir les efforts dans un bref délai. Par exemple, une réponse inflammatoire sévère s'est produite après qu'un CPC se soit désagrégé à l'intérieur et au voisinage du site d'emplantation (Ueyama et al., 2001). En outre, comme mentionné précédemment, l'un des avantages les plus importants des CPC par rapport aux biocéramiques est qu'ils n'ont pas besoin de pré-fabrication et peuvent être injectés avec une seringue. Cependant, dans la plupart des cas, un CPC seul (c'est-à-dire seulement constitué du mélange d'une poudre minérale et d'une solution saline) a une injectabilité plutôt mauvaise, ce qui est souvent la conséquence d'une séparation de phase entre le liquide et le solide à l'intérieur du dispositif d'injection. Par ailleurs, dans la plupart des cas, la pâte injectée a tendance à se disloquer lors d'un contact précoce avec le sang ou d'autres fluides physiologiques en raison de sa faible cohésion au jeune âge. Tous les inconvénients ci-dessus sont considérés comme des défis qui doivent être surmontés pour de larges applications des CPC. À cette fin, beaucoup de méthodes ont été utilisées pour améliorer ces propriétés de mise en œuvre.

Pour la plupart des applications biomédicales, les deux plus importantes propriétés des matériaux sont les propriétés mécaniques (« résistance ») et les propriétés chimiques (réactivité). Tout biomatériau possédant une grande réactivité mais une faible résistance sera inutile. Ainsi, les propriétés mécaniques et la réactivité doivent être prises en compte

dans l'élaboration d'un nouveau biomatériau. Les propriétés chimiques des CPC ont été discutées précédemment. En ce qui concerne les propriétés mécaniques, l'un des principaux paramètres les influençant est la porosité (en fait, la porosité influence aussi fortement l'activité biologique). L'étude qui suit portera sur les propriétés mécaniques des CPC et sur les modèles mécaniques décrivant leur dépendance vis-à-vis de la porosité.

Dans cette thèse, les propriétés mécaniques sont étudiées, y compris le module d'Young, la ténacité, la résistance à la compression et la résistance à la flexion. Le module d'Young (E), qui est l'un des modules d'élasticité, est une mesure de la rigidité d'un matériau élastique. La ténacité, K_{IC}, est une propriété qui est utilisée pour décrire la capacité d'un matériau contenant des défauts à résister à la propagation des fissures. Ces deux grandeurs sont des propriétés « intrinsèques » d'un matériau. La résistance (ou contrainte à la rupture) est la contrainte maximale qu'un matériau peut supporter avant que la rupture se produise. Elle peut être mesurée en compression ou en flexion. La contrainte à la rupture n'est pas une propriété intrinsèque du matériau, mais dépend de la ténacité et la taille des défauts présents dans le matériau.

Tel que mentionné précédemment, les biocéramiques ont été largement utilisées comme substituts osseux et de nombreux résultats ont été publiés à propos de leurs propriétés mécaniques. Par conséquent, il est intéressant d'examiner les propriétés mécaniques des biocéramiques avant d'examiner les propriétés mécaniques des CPC bien que leurs voies de fabrication soient différentes.

Les propriétés mécaniques des biocéramiques dépendent fortement des caractéristiques microstructurales telles que la porosité, la taille des grains ou la présence d'une seconde phase, mais les influences respectives de ces caractéristiques sont différentes, l'impact de la porosité sur les propriétés étant généralement plus grand que celui des autres paramètres. Les relations entre la microstructure et les propriétés mécaniques peuvent en partie être expliquées à travers le frittage, qui est le processus de consolidation à haute température des céramiques et qui peut produire une vaste gamme de microstructures. En principe, lors du frittage, les propriétés mécaniques augmentent avec la diminution de la porosité, mais diminuent avec l'augmentation de la taille des grains, en dépit de quelques exceptions (Rice et al., 1981A, 1981B), conduisant à un optimum variable en fonction de la microstructure (Fig. 1-9).

En général, la taille des pores, leur fraction volumique et leur forme (anisotropie) ont une influence significative sur les propriétés mécaniques des céramiques. Ces dernières

sont essentiellement de nature fragile ; elles sont donc sensibles aux défauts les plus critiques qui peuvent être des pores. Liu (1997) a fabriqué des céramiques HA poreuses avec diverses fractions de macropores de tailles différentes, en ajoutant du polyvinylbutyral (PVB) en tant que porogène; il a ensuite étudié leur résistance à la compression. Il a démontré que les échantillons renfermant de plus petits macropores présentaient une résistance plus élevée que ceux contenant de grands macropores. Néanmoins, la résistance semblait devenir insensible à la taille des macropores pour des niveaux élevés de porosité (Fig. 1-10). Les micropores sont également préjudiciables aux propriétés mécaniques des biocéramiques (Le Huec et al., 1995), et la microporosité est généralement contrôlée en effectuant des frittages à des températures différentes et pour diverses durées (Bignon et al., 2003 ; Milosevski et al., 1999 ; Thangamani et al., 2002).

L'influence de la porosité sur les propriétés mécaniques des biocéramiques a été largement étudiée, mais la plupart des études a porté sur l'effet de la porosité totale, ou sur celui de la macroporosité ou de la microporosité seules ; seulement quelques auteurs ont fait la distinction entre les deux types de porosité (Le Huec et al., 1995 ; Pecqueux et al., 2010 ; Tancret et al., 2006). Le Huec et al (1995) ont évalué les effets de la macroporosité (> 100 um, 6,5%-30% en volume) et de la microporosité (< 100 um, 20%-40% du volume total) sur la résistance à la compression de HA (Fig.1-11). Ce graphique montre que, sur la plage de porosité étudiée, un nombre infini de couples macroporosité-microporosité peut produire une valeur donnée de résistance à la compression. Pecqueux et al. (2010) ont préparé des biocéramiques BCP macroporeuses en faisant varier systématiquement la macroporosité et la microporosité, et ont étudié leurs propriétés mécaniques (module d'Young, ténacité et résistance à la compression) (Fig.1-12). Outre la fraction et la taille des pores, leur forme (isotropie ou anisotropie) influe sur les propriétés mécaniques. Hing et al (1999) ont trouvé que l'anisotropie avait un effet significatif sur le module de compression des céramiques HA poreuses, mais aucune influence sur la résistance à la compression.

En conclusion, il y a de nombreux facteurs tels que les pores (taille, fraction et morphologie), la taille des grains et la deuxième phase qui influent sur les propriétés mécaniques des biocéramiques.

Contrairement aux biocéramiques qui nécessitent un frittage à haute température pour être fabriquées, les CPC sont formés lors d'un processus de dissolution-reprécipitation à température ambiante ou corporelle. Au cours de ce processus, un réseau de cristaux d'apatite enchevêtrés est formé, qui est à l'origine des propriétés mécaniques du ciment.

Avec le temps, des cristaux d'apatite continuent de croître et le réseau enchevêtré devient plus dense (Fig.1-13) jusqu'à ce que le CPC atteigne sa résistance maximale.

Les propriétés mécaniques des CPC ont été largement étudiées. La plupart d'entre elles ont été évaluées à l'aide d'essais de résistance en compression ou en traction diamétrale (DTS) (Barralet et al., 2004 ; Bermudez et al., 1993 ; Chow et al., 2000 ; Fukase et al., 1990 ; Ginebra et al., 1997 ; Gbureck et al., 2003 ; Hofmann et al., 2009 ; Ishikawa et al., 1995A ; Martin et al., 1995 ; Pina et al., 2010). En revanche, peu d'études sur la ténacité et la fiabilité mécanique ont été publiées (Barralet et al., 2002A ; Barralet et al., 2002B ; Morgan et al., 1997 ; Zhang et al., 2006). Comme pour les biocéramiques, les propriétés mécaniques des CPC dépendent fortement des paramètres de leur microstructure tels que la porosité, la taille des cristaux ou la cristallinité. En outre, ces caractéristiques microstructurales sont liées à tous les facteurs technologiques impliqués dans la fabrication du ciment. Par conséquent, il est imaginable que des facteurs comme la composition chimique du ciment, la proportion relative des réactifs dans le mélange, les additifs liquides ou pulvérulents qui agissent comme accélérateurs ou retardateurs, la granulométrie, le ratio liquide/poudre (L/P), la pression appliquée lors de la préparation de l'échantillon ou les conditions de vieillissement, auront une incidence sur les propriétés mécaniques.

Une particularité des CPC est qu'ils sont intrinsèquement poreux. La porosité des CPC, variant habituellement entre 30% et 50%, dépend du rapport L/P : plus le rapport L/P est élevé, plus la microporosité est grande (Dorozhkin, 2008). Comme les biocéramiques, les CPC sont par nature assez fragiles et sont donc très sensibles à la présence de gros défauts qui peuvent être, par exemple, des pores. Les propriétés mécaniques des CPC sont inversement corrélées à la porosité (Fig.1-14).

Outre cette microporosité intrinsèque permettant l'imprégnation par les fluides biologiques, une certaine macroporosité (pores de plus de 100 μm) est également souhaitable afin de permettre la croissance osseuse ainsi que de favoriser la biorésorption et le remplacement du ciment par un nouvel os. De nombreuses méthodes ont été utilisées pour créer des macropores dans les CPC (Almirall et al., 2004 ; Cama et al., 2009 ; Barralet et al., 2002B). Bien que les macropres permettent de renforcer la croissance osseuse et l'ostéo-intégration, il est largement admis que, puisque les CPC sont fragiles et sensibles aux plus grands défauts, leur résistance pourrait être réduite de façon drastique par les macropores, la taille de ces derniers étant plusieurs de ordres de grandeur supérieure à celle des micropores. Xu (2001) a préparé des CPC macroporeux avec une

porosité totale voisine de 71%, en ajoutant du mannitol avec une fraction massique de 40%. Dans cette étude toutes les propriétés mécaniques mesurées, y compris le module d'Young, le travail de rupture et la résistance à la flexion, ont fortement diminué, passant respectivement de 8,5 GPa, 0,032 kJ/m^2 et 15 MPa sans macroporosité à 0,8 GPa, 0,005 kJ/m^2 et 1,5 MPa pour une macroporosité de 46%. La Fig.1-15 montre l'évolution de la résistance à la compression de ces CPC en fonction de la macroporosité.

Outre l'effet de la fraction des macropores, semblable à celui qui se manifeste dans les biocéramiques, la taille des macropores affecte également de manière significative les propriétés mécaniques des CPC. Bai et al. (2010) ont fabriqué des CPC macroporeux avec une porosité totale à peu près constante mais avec des tailles de macropores différentes, et ont trouvé que la résistance à la compression était inversement proportionnelle à la taille des macropores.

Différents additifs liquides ou pulvérulents, agissant comme accélérateurs ou retardateurs de prise, peuvent aussi avoir des effets importants sur les propriétés mécaniques des CPC en contrôlant le degré de prise et la microstructure. Les poudres de CDHA sont des additifs solides fréquemment utilisés comme germes pour favoriser la formation de l'apatite dans les CPC (Bermudez et al., 1993, 1994 ; Brown et al., 1991 ; Durucan et al., 2002B ; Liu et al., 1997 ; Yang et al., 2002). Brown et al (1991) ont indiqué que les germes de CDHA accéléraient les réactions initiales, mais ne semblaient pas avoir d'importants effets à long terme sur l'ampleur de la réaction ou sur le développement de la microstructure. Bermudez et al (1994) et Yang et al (2002) ont constaté que l'addition de certaines quantités de germes de CDHA diminuait le temps de prise et augmentait la résistance à la compression. Contrairement aux accélérateurs, les retardateurs ont pour conséquence de différer la prise, ce qui est néanmoins parfois positivement corrélé avec une plus grande résistance (Bohner et al., 2000; Durucan et al., 2002B ; Fernandez et al., 1998). Les améliorations de la résistance sont principalement imputables à un affinement de la structure du ciment (par exemple, l'incorporation de carbonate dans l'apatite provoque une diminution de la taille des cristallites, entraînant ainsi une augmentation des propriétés mécaniques finales). Par ailleurs, l'ajout d'ions libres (Sr^2+, Mg^{2+}, Si^{4+}) a également un effet retardateur, mais n'a pas toujours d'effet bénéfique sur la résistance du ciment (Lilley et al., 2005 ; Saint-Jean et al., 2005).

Comme mentionné précédemment, la taille des particules modifie significativement la cinétique de prise des CPC, contrôlant ainsi la quantité et la taille des cristaux enchevêtrés qui sont à l'origine de la résistance. Plus la taille des particules est petite, plus la

conversion des matières premières en produits d'hydratation est rapide, ce qui conduit à des cristaux plus enchevêtrés et donc à une augmentation de la résistance (Liu et al., 2003). En outre, le vieillissement est un autre facteur qui influe sur les propriétés mécaniques des CPC, bien que dans la plupart des cas, il est réalisé dans une solution de Ringer à 37 °C. À des températures plus élevées la vitesse de transformation des particules initiales en CDHA est plus rapide et la microstructure du CPC est plus homogène et dense, ce qui conduit à une plus grande résistance ; cet effet se manifeste surtout lors du stade de durcissement précoce (Ginebra et al., 1995).

En résumé, les propriétés mécaniques des CPC dépendent fortement de leur microstructure, qui est liée à tous les facteurs technologiques impliqués dans la fabrication, comme la composition chimique, les additifs liquides ou en poudre agissant comme accélérateurs ou retardateurs, la taille des particules, le rapport L/P et les conditions de vieillissement. Entre autres, les microstructures compactes avec de petits cristaux semblent posséder de meilleures propriétés mécaniques que les microstructures moins compactes avec de plus grands cristaux.

Malgré de nombreux avantages par rapport aux biocéramiques, il est largement admis que les CPC requièrent de nouvelles améliorations sur les propriétés mécaniques, en particulier sur la ténacité, afin d'élargir leurs applications cliniques potentielles telles que, par exemple, la réparation des fractures multiples des os longs, la fixation par ciment de prothèses d'articulations ou la substitution des corps vertébraux.

Pour atteindre ces objectifs, diverses méthodes ont été utilisées pour améliorer les propriétés mécaniques des CPC. Comme la porosité est le facteur le plus préjudiciable aux propriétés mécaniques, une stratégie simple et efficace pour les améliorer consiste à réduire la taille et la fraction volumique des pores pour obtenir une matrice dense.

Un compactage uniaxial, biaxial ou isostatique de la pâte de ciment avant hydratation s'est avéré être une méthode efficace pour réduire la porosité et améliorer les propriétés mécaniques (Chow et al., 2000 ; Barralet et al., 2002A). Cependant, ces méthodes ont globalement le même effet que la diminution du rapport L/P (Fig.1-17), ce qui influe sur l'aptitude à la mise en œuvre et l'injectabilité du ciment, et peut interdire son application en chirurgie mini-invasive. De plus, étant donné que ces procédés provoquent une diminution de la porosité, ils pourraient également affecter les performances biologiques. En ce sens, de nombreux additifs (Barralet et al., 2003 ; Gbureck et al., 2004B ; Sarda et al., 2002) ont été utilisés pour tenter de trouver un compromis entre facilité de mise en œuvre et propriétés mécaniques, ou de les améliorer simultanément.

Sarda et al (2002) ont ajouté de l'acide citrique à la phase liquide d'un ciment à base de α-TCP afin d'étudier son effet sur les propriétés d'injectabilité. Il a été constaté que l'acide citrique retarde la formation de HA, mais améliore l'injectabilité et la résistance. Par le biais d'une compétition entre répulsion de Coulomb et attraction de Van der Waals, en raison des ions citrate adsorbés sur la surface des réactifs, les particules, au lieu de s'agglomérer dans le liquide, glissent facilement les unes sur les autres et se dispersent de manière homogène (Fig.1-18). Par la suite, la croissance et l'enchevêtrement des cristaux d'apatite se font à partir de ces microstructures initialement plus homogènes, et produisent ainsi une matrice plus résistante.

Une autre stratégie pour améliorer les propriétés mécaniques des CPC consiste à ajouter des fibres dans la matrice. Il a été prouvé que l'incorporation de fibres dans la matrice d'un ciment fragile est une méthode efficace pour améliorer la ténacité ainsi que la résistance à la traction et à la flexion (Beaudoin et al., 1990). De manière générale, il est essentiel d'utiliser des fibres possédant une résistance élevée à la traction. Cependant, non seulement le type de fibres est important, mais d'autres facteurs tels que la longueur des fibres, leur fraction volumique, leur orientation et l'adhésion fibres/matrice sont également essentiels pour améliorer les propriétés finales du matériau composite. La pâte de ciment ou la poudre précurseur peut être mélangée avec des matières fibreuses ayant des structures différentes (Fig. 1-19).

En résumé, deux stratégies principales ont été proposées pour améliorer les propriétés mécaniques des CPC. Tout d'abord, en dépit des facteurs essentiels pour la croissance osseuse ou d'autres performances biologiques, une matrice plus dense et homogène, composée de petits cristaux, serait souhaitable afin d'améliorer les propriétés mécaniques intrinsèques des CPC. Ensuite, l'incorporation de renforts pourrait apporter une amélioration supplémentaire. Cependant, la sélection de fibres devrait prendre en compte leurs propriétés, leur fraction volumique et leur longueur.

Comme indiqué précédemment, les propriétés mécaniques des CPC sont essentielles pour leur application en chirurgie et ont souvent été étudiées. Cependant, elles ont été la plupart du temps évaluées à l'aide d'essais de résistance. Néanmoins, d'autres travaux ont mentionné la ténacité et la fiabilité comme représentant les réelles limites à l'utilisation des CPC, plutôt que la contrainte de rupture elle-même. Pour cette raison, quelques exemples sur la fiabilité de céramiques (Bhamra et al., 2002 ; Cordell et al., 2009 ; Salehi et al, 2008 ; Villora et al., 2004) et de ciments dentaires (Fleming et al., 1999), possédant diverses microstructures résultant de procédés de fabrication différents, permettent de

fournir des références utiles pour les CPC. En général, le module de Weibull, qui caractérise la fiabilité mécanique, dépend fortement de la microstructure du matériau. Globalement, plus la microstructure est homogène, plus le matériau est fiable, traduisant une faible dispersion statistique de la taille des défauts sur lesquels la rupture est susceptible de s'amorcer.

Comme mentionné ci-dessus, les propriétés mécaniques des CPC dépendent fortement de leur porosité (micropores et macropores). Pour optimiser le comportement mécanique des CPC, il est donc nécessaire de comprendre comment les paramètres microstructuraux que sont la microporosité ou la macroporosité influencent les propriétés mécaniques. À cette fin, il serait utile de modéliser les propriétés mécaniques des CPC en fonction de la porosité et de sa morphologie. Cependant, très peu d'études ont porté sur la modélisation des propriétés mécaniques des CPC en fonction de la porosité, qu'il s'agisse de microporosité, de macroporosité ou de porosité totale (Ginebra et al., 2007 ; Martin et al., 1995 ; Zhang et al., 2006). Martin et Brown (1995) ont mesuré la résistance à la compression de CPC avec différentes microporosités et ont décrit leurs résultats, ainsi que des résultats provenant d'autres études, en fonction de la microporosité l'aide d'une loi exponentielle. De même, Ginebra et al (2007) ont mesuré la résistance à la compression d'une mousse de CPC et l'ont décrite en fonction de la macroporosité au moyen d'une loi exponentielle. Zhang et al (2006) ont préparé des CPC renfermant différentes quantités de macropores créés par des particules de mannitol utilisées comme agent porogène soluble. Les auteurs ont mesuré le module d'Young, la résistance à la flexion et le travail de rupture de ces CPC macroporeux, et les ont décrits en fonction de la porosité totale à l'aide de lois puissance. Par le passé, de nombreux modèles ont été proposés pour décrire le comportement mécanique des matériaux poreux. Néanmoins, détailler l'intégralité de ces modèles serait à la fois extrêmement long et inapproprié, de sorte que seuls quelques modèles connus ou pertinents sont brièvement passés en revue ; les connaissances acquises pourraient nous aider à étendre l'application des principes de modélisation au cas des propriétés mécaniques des CPC, et à mieux les expliquer.

Suite à la revue bibliographique précédemment exposée, nous pouvons tirer quelques conclusions sur l'état actuel des connaissances dans le domaine des propriétés mécaniques des CPC. De nombreux matériaux à base de phosphates de calcium sont disponibles dans le commerce de nos jours. Parmi eux, les ciments à base de α-TCP ont suscité un grand intérêt en raison de leur biodégradabilité supérieure à celle de HA, de β-TCP ou des biocéramiques BCP actuellement utilisées. L'hydrolyse de α-TCP produit

de la CDHA, plus semblable à l'apatite biologique en termes de structure et de composition chimique que l'hydroxyapatite stoechiométrique HA. Les propriétés mécaniques des CPC sont essentielles pour une application réussie en chirurgie et ont été largement étudiées. Cependant, la plupart d'entre elles ont été évaluées en utilisant des tests de résistance telles que la résistance à la compression ou la résistance à la traction diamétrale. Néanmoins, des études ont mentionné que la ténacité et la fiabilité constituaient les réelles limites des CPC, plutôt que leur contrainte de rupture. Par ailleurs, outre l'absence d'une étude systématique sur les propriétés mécaniques des CPC, il n'existe aucune étude complète sur l'évolution des propriétés mécaniques avec la microporosité et la macroporosité considérées séparément, ainsi que sur sa modélisation qui peut constituer un outil utile non seulement pour une meilleure compréhension du comportement mécanique mais aussi pour aider à concevoir des matériaux aux propriétés optimisées. Par ailleurs, le rôle de la taille des particules sur les propriétés mécaniques des CPC n'a pas non plus été étudié avec une approche similaire, bien que son effet sur la cinétique de prise soit bien compris. À partir de ces constatations, il semble que l'une des principales faiblesses de la littérature existante est l'absence d'une étude approfondie, comparative et systématique sur les relations entre la fabrication, la microstructure et les propriétés mécaniques des CPC, produite par une équipe unique même si, bien sûr, chaque publication individuelle représente un apport scientifique précieux. De plus, comme indiqué dans la littérature, les CPC restent très fragiles de par leur nature, avec de très faibles propriétés mécaniques ; il serait donc nécessaire de développer de nouveaux matériaux avec des propriétés optimisées (mie en œuvre / propriétés biologiques / propriétés mécaniques), qui pourraient en particulier être moins fragiles et présenter une certaine tolérance à l'endommagement. Cependant, il apparaît que l'option « fibres » a été largement étudiée et semble compromettre les propriétés de mise en œuvre des CPC (injectabilité par exemple). En revanche, les ciments composites contenant des polymères de type HPMC (hydroxy-propyl-methyl-cellulose) semblent être intéressants du point de vue de la cohésion, même si, de nouveau, aucune étude systématique n'est disponible sur l'effet de l'ajout de HPMC à la fois sur la mise en œuvre et sur les propriétés mécaniques (par exemple sur la ténacité). Par ailleurs, les HPMC silanisés (Si-HPMC) sont des « nouveaux » biomatériaux actuellement au stade de la recherche et du développement, présentant des propriétés biologiques et rhéologiques intéressantes. Leur combinaison avec les phosphates de calcium pour la régénération osseuse et articulaire a été mentionnée, mais plutôt pour des matériaux riches en polymère (Si-HPMC constituant

alors une « matrice » dans laquelle des particules de phosphate de calcium sont intégrées) (Weiss et al., 2008). Compte tenu de ce qui a été vu dans la littérature sur le rôle de la viscosité sur la cohésion des pâtes cimentaires et sur leur injectabilité, il serait donc intéressant d'essayer d'intégrer ce type de polymère aux CPC pour produire des matériaux composites. Toutes les questions ci-dessus sont abordées dans cette thèse.

Chapitre 2 et Chapitre 3: Matériaux et méthodes – Influence de la microporosité et de la macroporosité sur les propriétés mécaniques des CPC

Le Chapitre 2 décrit les principales méthodes de fabrication des poudres et des ciments, ainsi que les techniques de mesure des propriétés mécaniques. Au début du Chapitre 3, avant d'aborder le cœur du sujet sur les relations entre procédé de fabrication, microstructure et comportement mécanique, une étude préliminaire est réalisée sur la cinétique de prise des CPC, qui est essentielle pour la préparation des échantillons et pour une comparaison valable des propriétés mécaniques mesurées. Les temps de prise initiale et finale des CPC préparés avec une poudre fine (Ciments F) ou grossière (Ciments C), ainsi qu'avec ajout de différentes quantités de mannitol (utilisé comme porogène), sont tout d'abord mesurés (Fig. 3-1). Les temps de prise initiale et finale des Ciments F et des Ciments C augmentent avec le rapport L/P (Fig. 3-1A, B). Ceci est simplement dû au fait qu'avec l'augmentation du rapport L/P, la distance entre les particules initiales de α-TCP augmente. Cela modifie l'interaction entre les particules de α-TCP, puis retarde la formation du réseau de cristaux d'apatite enchevêtrés qui est responsable des propriétés mécaniques; la conséquence est une prolongation du temps de prise. Pour les CPC préparés avec du mannitol comme porogène, les temps de prise initiale et finale augmentent avec la quantité de mannitol (Fig. 3-1C). Ces résultats peuvent être expliqués en termes de disponibilité de liquide: lorsque la quantité de mannitol ajoutée augmente, il y a moins de α-TCP disponible pour la réaction de dissolution, ce qui augmente la quantité de liquide disponible par rapport à α-TCP, et prolonge le temps de prise en raison des effets mentionnés pour les ciments F et C (augmentation du rapport L/P « effectif »).

En outre, à des fins de comparaison des propriétés mécaniques, le maximum de paramètres expérimentaux, tels que le temps de durcissement ou les dimensions de l'échantillon, devraient être choisis puis fixés pour l'ensemble de l'étude. À cet effet, comme précédemment, une étude cinétique sur le développement de la résistance à la compression en fonction du temps de durcissement a été réalisée jusqu'à 35 jours (Fig. 3-2). La poudre fine de α-TCP est sélectionnée en raison d'une vitesse de réaction plus élevée comme indiqué dans la section 3.1.1. Une forte corrélation est établie entre le

développement de la résistance et le degré de réaction, évalué à partir de l'évolution des phases en présence (Fig. 3-5). Pendant le durcissement, α-TCP réagit progressivement avec l'eau, et un réseau de cristaux d'apatite enchevêtrés est formé, qui est à l'origine des propriétés mécaniques. Avec le temps, α-TCP disparaît, des cristaux d'apatite continuent de croître et le réseau de cristaux devient de plus en plus enchevêtré, de sorte que le CPC devient plus résistant. En général, nous voulons toujours éviter la présence de réactif résiduel (dans notre cas du α-TCP n'ayant pas réagi) dans le produit final de réaction, mais cela semble être assez difficile à atteindre en cinq jours. Toutefois, un temps plus long, d'une part, n'apporte pas de changements notables dans la microstructure et les propriétés (Ginebra et al., 2004), et d'autre part entraînerait des expériences trop longues. Suite à cette étude, cinq jours sont considérés comme suffisants pour assurer à la fois un degré de réaction élevé et un durcissement complet en termes de résistance (Fig. 3-3). Un temps de durcissement de cinq jours peut donc être considéré comme un compromis optimal, et il sera utilisé tout au long de cette thèse.

La microstructure et les propriétés mécaniques des CPC microporeux (Ciments F et Ciments C) sont ensuite étudiées.

La porosité des ciments F a été mesurée pour différents rapports L/P (Fig. 3-6). Comme cela était prévisible, la porosité totale des ciments F augmente lorsque le rapport L/P augmente, allant de 36% à 51%. Cela est dû à une proportion plus élevée de liquide dans le volume constant du moule.

Les diagrammes de diffraction des rayons X (DRX) des ciments F préparés avec différents rapports L/P sont présentés sur la Fig. 3-8. Après cinq jours de durcissement, il est observé que la plupart de la poudre fine de α-TCP a réagi avec l'eau et s'est transformée en CDHA, et ce quel que soit le rapport L/P. Une faible quantité de α-TCP n'ayant pas réagi peut toutefois être détectée, mais cette quantité diminue globalement avec l'augmentation du rapport L/P. Deux hypothèses peuvent être formulées pour expliquer cette tendance. L'une peut être exprimée en termes de disponibilité de liquide : lorsque le rapport L/P augmente, il y a plus de liquide disponible pour la réaction de dissolution, ce qui pourrait conduire à moins de α-TCP n'ayant pas réagi dans le ciment final. L'autre explication serait fondée sur des caractéristiques « géométriques » : quand le rapport L/P augmente, la distance entre particules augmente, ainsi que la porosité (voir Fig. 3-6), laissant plus de place dans le matériau pour que la solution saline puisse s'écouler et réagir avec α-TCP, provoquant une diminution de la quantité de α-TCP ne réagissant pas.

Les surfaces de rupture de ciments F avec deux rapports L/P différents, observées par Microscopie Électronique à Balayage (MEB), sont présentées sur la Fig. 3-9. Des « cavités » de quelques dizaines de micromètres sont distribuées aléatoirement sur la surface du ciment F avec un rapport L/P de 0,30 (Fig. 3-9A). À un plus fort grossissement (Fig. 3-9C), des amas de particules composées de α-TCP n'ayant pas réagi peuvent être observés à l'intérieur de ces cavités ; ils sont séparés de la matrice d'apatite environnante par une sorte de « vide ». En revanche, aucune de ces cavités contenant des amas de α-TCP n'ayant pas réagi n'a été observée sur la surface de rupture du ciment F avec un rapport L/P de 0,4 (Fig. 3-9B et 3-9D). Cela est probablement dû à la très faible quantité de α-TCP qui n'a pas réagi pour ce rapport L/P (comme en témoigne la DRX), d'où la difficulté à l'observer par MEB. Malgré cette différence, la morphologie et la taille des cristaux d'apatite formés, qui sont principalement en forme d'aiguille et à l'échelle du nanomètre ou submicronique, semblent être similaires pour ces deux Ciments F fabriqués avec des rapports L/P de 0,3 (Fig. 3-9E) et de 0,4 (Fig. 3-9F).

Les propriétés mécaniques (module d'Young, ténacité et résistance à la compression) des ciments F, préparés en utilisant différents rapports L/P, sont présentées sur la Fig. 3-10. Comme attendu, toutes les propriétés mécaniques mesurées diminuent avec la porosité. Afin de mieux comprendre les phénomènes physiques et aider à la conception de CPC ayant des propriétés mécaniques optimisées, une loi puissance (Eq. 3-1) est délibérément choisie tout au long de l'étude pour décrire l'évolution avec la porosité des propriétés mécaniques des ciments.

La modélisation des propriétés mécaniques avec la porosité a été menée en deux étapes. La première consiste à confirmer la validité d'un modèle de loi puissance pour décrire les données mesurées. Comme le montre la Fig. 3-10, toutes les données mesurées pour les ciments F peuvent être décrites correctement, avec des coefficients de détermination R^2 = 0,97, 0,99 et 0,96, pour le module d'Young, la ténacité et la résistance à la compression, respectivement. En s'appuyant sur ce premier résultat encourageant, et afin d'établir une inter-relation entre les différentes propriétés mécaniques des ciments F, conformément aux hypothèses émises au Chapitre 1, la procédure d'ajustement des paramètres a ensuite été adaptée en utilisant le même exposant de loi puissance pour toutes les propriétés. La possibilité d'obtention d'un exposant commun à toutes les propriétés mécaniques et sa signification physique ont été examinées dans la section 1.5.3. Néanmoins, il est utile de rappeler les hypothèses nécessaires à l'obtention d'un exposant commun dans la loi puissance : la constance des micromécanismes de rupture sur toute la

plage de porosité et la constance de la taille du défaut critique. Dans le cas des ciments F, il s'est néanmoins avéré impossible de décrire les trois courbes avec la même valeur de l'exposant « a » de la loi puissance. Une description des trois courbes, utilisant le même exposant pour les trois propriétés, est néanmoins présentée sur la Fig. 3-11. Une valeur commune pour l'exposant a = 4,13 peut être trouvée pour la ténacité et la résistance à la compression, mais pas pour le module d'Young. Les courbes en traits pleins sur les Fig. 3-11B et 3-11C représentent cette description de la ténacité et de la résistance à la compression, avec K_{IC0} = 3,31 MP.m$^{1/2}$ et σ_{r0} = 730 MPa, respectivement. La courbe en trait plein sur la Fig. 3-11A montre l'évolution « virtuelle » du module de Young en utilisant la même valeur de « a » que pour la ténacité et la résistance à la compression, et pour une valeur ajustée de E_0 = 84 GPa. Si la tendance semble se justifier pour des porosités élevées (haut rapport L/P), il y a une surestimation évidente du module d'Young par ce modèle pour les porosités faibles (faible rapport L/P : 0,3 et 0,35). Cela peut s'expliquer si le α-TCP n'ayant pas réagi est pris en compte. En effet, comme indiqué sur la Fig. 3-8, du α-TCP n'ayant pas réagi a pu être détecté par DRX, en particulier pour les rapports L/P de 0,30 et 0,35. Par ailleurs, il a été observé que les particules de α-TCP qui n'ont pas réagi sont séparées de la matrice de CDHA par des espaces vides qui peuvent être comparés à des « fissures » (Fig. 3-9C). Plus il reste de α-TCP, plus la matrice du ciment contient de ces « fissures », ce qui provoque une diminution du module d'Young et ainsi l'écart observé sur la courbe entre le modèle et les mesures pour les faibles rapports L/P. Néanmoins, cette « microfissuration » ne semble pas influer sur la ténacité, ce qui est malgré tout en accord avec des cas signalés dans d'autres matériaux multi-fissurées (Tancret et al., 2001), ou avec le cas célèbre du titanate d'aluminium, qui possède une ténacité similaire à celle de l'alumine, mais un module d'Young dix fois plus faible en raison d'une forte microfissuration spontanée.

La porosité des ciments C préparés avec différents rapports L/P a été mesurée (Fig. 3-12). Comme pour les ciments F, la porosité totale des ciments C augmente avec le rapport L/P, allant de 38% à 52%. Cela peut également être attribué à une plus grande proportion de phase liquide dans le volume constant du moule lors de la fabrication. Toutefois, pour un même rapport L/P (sauf pour un rapport L/P de 0,3) la porosité totale des ciments C est nettement inférieure à celle des Ciments F, ce qui est probablement dû à une masse de pâte différente introduite dans le moule (la compacité de la pâte est différente).

Les diagrammes de DRX des ciments C préparés avec différents rapports L/P sont

présentés sur la Fig. 3-13. Comme on peut le voir, la poudre de α-TCP s'est transformée en CDHA, mais avec beaucoup de α-TCP n'ayant pas réagi. Cela peut être interprété par un simple effet de taille, de grosses particules étant évidemment plus longues à disoudre. De plus, comme pour les ciments F, la quantité de α-TCP qui n'a pas réagi diminue avec l'augmentation du rapport L/P ; cela peut être expliqué par les mêmes hypothèses que celles proposées pour les ciments F (voir 3.2.1.2).

Les surfaces de rupture de ciments C préparés avec deux rapports L/P différents, observées par MEB, sont présentées sur la Fig. 3-14. Du α-TCP qui n'a pas réagi peut être trouvé sur la surface de rupture du ciment C avec un rapport L/P de 0,3 (Fig. 3-14A). De même, des particules de α-TCP n'ayant pas réagi peuvent également être observées dans le Ciment C ayant un rapport L/P de 0,5, mais en proportion nettement moindre (Fig. 3-14B). À un plus fort grossissement, quel que soit le rapport L/P (0,3, Fig 3-14C ; 0.5, Fig 3-14D), on retrouve des fissures autour des particules de α-TCP n'ayant pas réagi, les séparant de la matrice de CDHA environnante, et indiquant un faible lien entre le α-TCP qui n'a pas réagi et les cristaux de CDHA. Ce constat est semblable à l'observation faite dans le ciment F préparé avec un rapport L/P de 0,3 (Fig. 3-9C). Par ailleurs, aucune différence notable ne peut être constatée entre les divers ciments C, ni dans la forme des cristaux de CDHA, qui sont la plupart du temps en forme de plaquettes, ni dans leur taille, qui est submicronique ou à une échelle nanométrique (Fig. 3-9E, F).

Les propriétés mécaniques (module d'Young, ténacité et résistance à la compression) des ciments C, préparés avec différents rapports L/P, sont tracées sur la Fig. 3-15. Comme attendu, toutes les propriétés mécaniques diminuent lorsque la porosité augmente. En outre, comme pour les ciments F, afin de mieux comprendre et expliquer les observations expérimentales, une loi puissance est également utilisée pour décrire l'évolution avec la porosité des propriétés mécaniques des ciments C. Comme pour les ciments F (section 3.2.1.3), la validité de la loi puissance a d'abord été testée sur les données mesurées sans tenir compte d'une éventuelle inter-relation entre propriétés.

Comme on peut le constater, toutes les données mesurées peuvent être assez bien décrites par une loi puissance, avec R^2 = 0,98, 0,99 et 0,97, pour le module d'Young, la ténacité et la résistance à la compression, respectivement, ce qui conforte la validité du modèle en loi puissance dans le cas des ciments C. Néanmoins, il est également souhaitable, d'un point de vue théorique, de tenter d'établir une inter-relation entre les trois propriétés mécaniques mesurées, dans laquelle le même exposant « a » pourrait être utilisé dans les équations du module d'Young, de la ténacité et de la résistance à la

compression.

Contrairement aux ciments F, les trois propriétés peuvent être décrites dans les ciments C avec le même exposant a = 3,77 (Fig. 3-16), bien que l'effet sur la rigidité de la « microfissuration » due à la présence de α-TCP n'ayant pas réagi puisse également être mise en évidence (Fig. 3-16A, Fig. 3-14). En effet, tous les ciments préparés avec de la poudre grossière contiennent des quantités importantes de α-TCP qui n'a pas réagi (Fig. 3-13), et sont donc tous plus « microfissurés » que les ciments F, ce qui est cohérent avec l'observation précédente sur les Ciments F : le α -TCP n'ayant pas réagi réduit le module d'Young par microfissuration, ce qui peut donc en partie expliquer pourquoi la valeur de E_0 = 26,9 GPa pour les ciments C est seulement le tiers du E_0 = 84 GPa des ciments F. Par ailleurs, le point correspondant au rapport L/P de 0,30 apparaît notablement plus bas que ce qu'on peut attendre de la courbe ajustée, ce qui est également compatible avec un plus haut degré de « microfissuration », associée à une plus grande fraction de α-TCP n'ayant pas réagi dans ce ciment (Fig. 3-13).

L'inter-relation entre propriétés donne aussi une valeur K_{IC0} = 2,31 MPa.m$^{1/2}$ pour les ciments C, qui est inférieure à celle des ciments F (3,31 MPa.m$^{1/2}$). Ceci peut être expliqué en considérant l'origine de la ténacité dans les CPC. En fait, les CPC sont naturellement fragiles et leur capacité de résistance à la fissuration provient principalement des cristaux d'apatite enchevêtrés. D'après les micrographies, il semble que les ciments C contiennent plus de plaquettes et de « grands » cristaux d'apatite que les ciments F, ces derniers étant plutôt constitués de petits cristaux d'apatite en forme d'aiguilles. Plus les cristaux d'apatite sont petits, plus les points de contact sont nombreux et peuvent ainsi contribuer à une ténacité plus élevée des ciments F. Un phenomène similaire a également été observé sur d'autres matériaux (Tancret et al., 2003). Par ailleurs, cet enchevêtrement dense de cristaux d'apatite dans les ciments F pourrait aussi contribuer à leur module d'Young plus élevé que celui des ciments C, en plus du mécanisme susmentionné. Enfin, une valeur de de σ_{r0} = 245 MPa a été obtenue pour les ciments C, nettement inférieure à celle des ciments F (730 MPa). Une telle différence de résistance ne peut pas être expliquée par les seules valeurs de ténacité. Ceci indique que la taille des défauts critiques dans les ciments C est significativement plus grande que dans les ciments F, ce qui est compatible avec une microstructure plus grossière qui de surcroît contient de nombreuses fissures.

La microstructure et les propriétés mécaniques des CPC macroporeux ont été étudiées. La macroporosité des CPC macroporeux préparés avec différentes fractions massiques de

mannitol a été déterminée par analyse d'image sur certains échantillons ; elle est tracée sur la Fig. 3-17 en fonction de la teneur en mannitol (voir lignes continues bleues). Comme on pouvait s'y attendre, la macroporosité augmente avec la fraction massique en mannitol, allant de 7% à 46%.

Les diagrammes de DRX des CPC macroporeux préparés avec différentes fractions massiques en mannitol sont présentés sur la Fig. 3-19. Ces diagrammes sont similaires à ceux des ciments F, ce qui indique que l'addition de mannitol n'affecte pas la réaction d'hydratation de α-TCP (Shimogoryo et al., 2009). Comme pour les ciments F, de petits pics de α-TCP n'ayant pas réagi sont présents, mais l'intensité des principaux pics de cette phase diminue lorsque la fraction massique en mannitol augmente. Deux hypothèses peuvent être avancées pour l'expliquer. Tout d'abord, la quantité totale d'eau introduite dans la pâte est déterminée à partir du poids total des poudres (α-TCP + mannitol) ; il est alors possible qu'une plus grande quantité d'eau soit disponible pour la réaction avec α-TCP lorsque la fraction massique en mannitol augmente, ce qui correspondrait à une augmentation du rapport L/P effectif de la partie minérale du ciment. La tendance observée serait alors en accord avec les résultats de la Fig. 3-6. La seconde hypothèse est basée sur la « géométrie » : quand la fraction massique en mannitol augmente, la macroporosité laissée par sa dissolution augmente et, par conséquent, la perméabilité du matériau augmente, permettant à l'eau de s'écouler plus facilement à l'intérieur du matériau et d'améliorer son contact avec α-TCP, favorisant ainsi la réaction chimique et conduisant à moins de α-TCP résiduel.

Les surfaces de rupture des CPC macroporeux, observées par MEB, sont présentées sur la Fig. 3-20. Sans surprise, le CPC fabriqué sans mannitol ne contient pas de macropores (Fig. 3-20A). En revanche, des macropores de plusieurs centaines de micromètres, résultant de la dissolution du mannitol, sont observables sur la surface de rupture du CPC fabriqué avec 10% en masse de mannitol (Fig. 3-20B). Lorsque la fraction massique en mannitol augmente (30%, figure 3-20C ; 50%, figure 3-20D), de plus en plus de macropores sont observés, avec des orientations à peu près aléatoires, indiquant que les particules de mannitol sont bien mélangées et réparties de manière homogène lors de la préparation des échantillons. Enfin, la microstructure de la matrice des CPC macroporeux a été examinée à un plus fort grossissement (Fig. 3-20F). Aucune différence notable n'existe entre la matrice microporeuse des ciments macroporeux et celle des ciments F. La morphologie et la taille des cristaux d'apatite formés sont comparables, indiquant que l'addition de mannitol n'affecte pas la formation et la croissance des cristaux de CDHA

(Shimogoryo et al., 2009).

Les propriétés mécaniques (module d'Young, ténacité et résistance à la compression) des CPC macroporeux fabriqués avec différentes fractions massiques en mannitol sont présentées sur la Fig. 3-21. Comme on pouvait s'y attendre, toutes les propriétés mécaniques mesurées diminuent quand la macroporosité augmente (c'est-à-dire quand la fraction massique en mannitol augmente). Comme dans le cas des CPC microporeux (Ciments F et C), afin de mieux appréhender les observations expérimentales, une approche de modélisation est utilisée. Pour ce faire, un nouveau modèle (Eq. 3-11), qui prend en compte séparément l'effet des macropores et des micropores, est développé pour décrire l'évolution avec la porosité (macroporosité et microporosité) des propriétés mécaniques des CPC macroporeux. Cependant, dans le cas particulier de nos ciments la macroporosité et la microporosité sont interdépendantes. En effet, en ajoutant du mannitol la macroporosité augmente, mais plus d'eau est également disponible pour la partie minérale du ciment, ce qui équivaut à un rapport L/P effectif plus élevé pour cette partie minérale et conduit à une microporosité plus grande. Par conséquent, le tracé des propriétés mécaniques en fonction de la seule macroporosité n'aurait pas de signification physique, puisque la microporosité varie en même temps. Pour cette raison, une autre méthode est utilisée pour afficher les résultats, en reportant les valeurs mesurées en fonction des valeurs calculées par le modèle (Fig. 3-22).

Comme le montre la Fig. 3-22, un bon accord est obtenu entre les valeurs mesurées et calculées, pour toutes les propriétés mécaniques étudiées (module d'Young, Eq. 3-12 ; ténacité, Eq. 3-13 ; résistance à la compression, Eq 3-14). Par ailleurs, les valeurs de référence déterminées pour le module d'Young et la ténacité sont respectivement de 96,6 GPa et 4,47 $MPa.m^{1/2}$, et sont comparables à celles des ciments F, confirmant la validité de l'équation 3-11, proposée et utilisée dans le cas des CPC macroporeux. En outre, comme cela apparaît dans les équations 3-12, 3-13 et 3-14, un exposant commun c = 1,55 peut être utilisé pour le module d'Young et la ténacité, mais pas pour la résistance à la compression, pour laquelle la valeur de « c » est de 2,5. Ce résultat est cohérent avec une étude récente concernant des céramiques BCP (Pecqueux et al., 2010), où l'exposant de la loi puissance associée à la résistance en compression est également plus élevé que ceux permettant de décrire le module d'Young et la ténacité, ces deux derniers exposants étant du reste identiques. Cette particularité avait été reliée à une augmentation de la taille des défauts critiques avec la macroporosité. Quand un nombre limité de macropores est présent dans l'échantillon, les macropores sont bien dispersés

dans le matériau (comme dans le cas des CPC, voir Fig. 3-20B) et n'interagissent pas fortement les uns avec les autres. Lorsque la macroporosité augmente, la distance moyenne entre les macropores voisins diminue, et leurs champs de concentration de contraintes associés commençent à interagir. Par ailleurs, d'un point de vue statistique, la probabilité de trouver des groupes de macropores dans certaines zones du matériau augmente avec le nombre total de macropores. Pendant le chargement en compression, ces groupes de macropores pourraient alors devenir des défauts critiques de grande taille grâce à la croissance sous-critique de microfissures reliant plusieurs macropores entre eux. Ainsi, ces amas de macropores (pour les fortes macroporosités) constitueraient des défauts critiques d'une taille plus importante que celle de macropores isolés (pour les faibles macroporosités), d'où une augmentation de la taille des défauts critiques avec la macroporosité. Il a également été suggéré que ce mécanisme puisse se produire dans d'autres céramiques macroporeuses (Pernot et al. 1999) ; il a aussi été étudié en utilisant la simulation par éléments finis (Cannillo et al., 2004). Il est donc possible qu'un mécanisme similaire agisse dans les CPC macroporeux.

L'hypothèse ci-dessus peut d'ailleurs être mise en évidence dans le cas de nos ciments en traçant la quantité $(K_{IC}/\sigma_r)^2$, qui est proportionnelle à la taille du défaut critique, en fonction de la macroporosité (Fig. 3-23). Comme le montre la Fig. 3-23, la gamme de valeurs est à peu près constante pour les ciments microporeux (ciments F d'une part et ciments C d'autre part, ces derniers ayant des tailles de défauts critiques un peu plus grandes, en raison de leur microstructure grossière comme nous l'avons déjà mentionné). En revanche, la taille des défauts critiques des CPC macroporeux augmente fortement avec la macroporosité, ce qui est semblable à l'observation faite dans le cas des céramiques BCP macroporeuses (Pecqueux et al., 2010), et vient appuyer l'hypothèse proposée précédemment.

Par conséquent l'hypothèse initiale, qui considérait qu'une taille de défaut critique indépendante de la porosité était associée à un exposant « c » commun pour la ténacité et la contrainte de rupture, ne s'applique pas dans le cas des ciments macroporeux, ce qui peut expliquer les différents exposants obtenus pour la ténacité et la résistance à la compression (Eq. 3-13, 3-14). De même, les tailles de défauts critiques à peu près constantes pour les ciments F ou les ciments C sont compatibles avec le fait que des exposants communs peuvent être utilisés pour décrire à la fois la ténacité et la contrainte de rupture (Ciment F, Fig. 3-11 ; Ciment C, Fig 3-16).

mécaniques et sur la fiabilité des CPC

Dans l'étude ci-dessus qui correspond au troisième chapitre de la thèse, les propriétés mécaniques, y compris le module d'Young, la ténacité et la résistance en compression ont été systématiquement étudiées sur les CPC préparés en faisant varier les rapports L/P, la taille des particules et les pourcentages de macroporosité.

Toutefois, par souci de simplicité expérimentale, toutes les mesures dans l'étude ci-dessus ont été réalisées à l'état sec, assez différent de l'environnement biologique humide où les CPC sont généralement implantés. Certaines propriétés mécaniques de l'apatite dense ayant été décrites comme dépendant fortement de l'eau et de l'humidité (Benaqqa et al., 2005) et en vue d'applications pratiques, il nous semble plus pertinent de mesurer les propriétés mécaniques des CPC à l'état humide. Par ailleurs, il est largement admis que la fiabilité mécanique est plus appropriée pour l'évaluation ou la conception de matériaux fragiles plutôt que la valeur moyenne de la contrainte de rupture, mais cette méthode est néanmoins rarement utilisée dans les CPC, qui sont aussi intrinsèquement fragiles.

Pour ces raisons, l'influence des conditions de fabrication et d'essai (degré d'humidité) sur les propriétés mécaniques et la fiabilité des CPC (microporeux et macroporeux) a donc été étudiée.

Avant de tester les éprouvettes en milieu biologique simulé (solution saline), des expériences préliminaires ont été réalisées afin de positionner précisément l'extensomètre sur des échantillons (préalablement humidifiés) pour obtenir une mesure de flexion la plus juste possible. Puis des éprouvettes immergées et fraîchement sorties de la solution saline ont été testées en compression. Aucune différence statistiquement significative n'a pu être mise en évidence (Fig. 4-2), indiquant la validité des mesures réalisées sur les échantillons humides non immergés.

En outre, parce qu' un grand nombre d'échantillons sont nécessaires pour la présente étude, tous n'ont pas pu être testés exactement cinq jours après immersion mais parfois après une période de strockage supplémentaire dans la solution saline ; il a été vérifié que cette courte période supplémentaire (de l'ordre d'une journée) n'avait pas d'influence sur les mesures (Fig. 4-3).

La porosité des CPC microporeux a été mesurée sur une plage étendue de rapport L/P (Fig. 4-4). Comme indiqué précédemment, la porosité des ciments augmente avec l'augmentation du rapport L/P. En comparaison avec les données des ciments F préparés dans le troisième chapitre, la gamme de porosité des ciments préparés ici est étendue de

près de 62%.

Les propriétés mécaniques (module d'Young, ténacité, résistance à la compression et résistance à la flexion) des CPC microporeux préparés avec différents rapports L/P ont été mesurées à l'état humide (Fig. 4-5). Globalement, et comme pour les CPC mesurés à l'état sec (Fig. 3-10), toutes les propriétés mécaniques mesurées diminuent avec l'augmentation de la porosité. Les modules d'Young mesurés dans des conditions humides et sèches sont comparés (Fig. 4-6) pour les rapports L/P où les deux mesures sont disponibles. Comme on le voit, le module d'Young mesuré à l'état sec est supérieur à celui mesurée à l'état humide. De façon surprenante, cette différence diminue avec l'augmentation de la porosité. En comparant la ténacité d'un même type d'échantillon dans les états sec et humide, on observe généralement que la présence d'eau diminue l'énergie de surface des fissures et donc la valeur mesurée. Cet effet néfaste de l'eau sur la ténacité a également été mesuré pour les céramiques d'hydroxyapatite (Benaqqa et al., 2005). De même, on observe une diminution des résistances à la compression et à la flexion en testant une éprouvette en conditions humides (Fig. 4-5C, Fig. 3-10C). Les résistances en flexion et en compression plus faibles mesurées à l'état humide sont principalement la conséquence de l'évolution de la ténacité, propriété intrinsèque du matériau. La fiabilité mécanique mesurée en compression sur les CPC microporeux a été analysée au moyen des statistiques de Weibull (Weibull, 1939, 1951). Les diagrammes de Weibull logarithmiques calculés en utilisant l'équation 4-3 pour les échantillons de compression des CPC préparés avec différents rapports L/P sont présentés (Fig. 4-10), et le module de Weibull pour chaque CPC a été déterminé. Comme on le voit, il existe un saut dans les valeurs du module de Weibull des CPC pour un rapport L/P compris entre 0,4 et 0,45. Plus précisément, les modules de Weibull pour les CPC ayant un rapport L/P compris entre 0,25 et 0,4 sont tous entre 8 et 9, ce qui est significativement supérieur aux valeurs des CPC présentant des rapports L/P compris entre 0,45 et 0,6, qui sont tous entre 5 et 6.

Afin de mieux expliquer les résultats ci-dessus, la quantité $(K_{IC}/\sigma_r)^2$, qui est proportionnelle à la taille moyenne du défaut critique sur lequel la rupture s'initie, est tracée en fonction du rapport L/P. Comme on le voit, la taille moyenne du défaut critique augmente avec le rapport L/P. Ceci met en évidence un changement de régime à partir de rapports L/P > 0,40 qui correspond au seuil observé dans l'évolution du module de Weibull.

En fait, lorsque le rapport L/P augmente, la taille des pores et l'interconnectivité des

pores augmentent, ce qui pourrait expliquer une légère augmentation de la taille du défaut critique, comme on l'observe pour les rapports L/P jusqu'à 0,4. Dans le même temps, la dispersion statistique de la contrainte de rupture, liée à la dispersion statistique des défauts, reste assez forte, peut-être simplement parce que les petits défauts sont statistiquement plus abondants et donc influencent de façon plus déterminante la résistance. Toutefois, lorsque le rapport L/P augmente au-delà de 0,4, la pâte devient de plus en plus fluide au cours de la fabrication, et des bulles d'air peuvent être facilement piégées dans la pâte de ciment, et donc agir comme de grands défauts critiques. Même si une table vibrante a été utilisée pour tenter de supprimer autant de bulles que possible, des bulles d'air seraitent susceptibles d'être piégées dans la pâte quand les rapports L/P augmentent, alors qu'il est assez facile d'enlever l'air dans les pâtes plus sèches grâce à densification par vibration ou par pression manuelle. En conséquence, parce que la probabilité de trouver de grandes bulles d'air dans la pâte augmente avec le rapport L/P (0,45 et au-dessus), la moyenne des tailles de défauts critiques mesurées commence également à augmenter très rapidement. En outre, seule une petite quantité de bulles d'air est susceptible d'être piégée dans chaque échantillon, ce qui donne au piégeage de bulles un fort caractère statistique, qui pourrait expliquer pourquoi la distribution statistique de la taille de défaut critique, et donc de la contrainte de rupture, devient plus large, à travers un module de Weibull inférieur, lorsque le rapport L/P passe le seuil où le piégeage de bulles commence (environ 0,4 ou 0,45).

Les propriétés mécaniques (module d'Young, ténacité, résistance à la compression et résistance à la flexion) ont également été mesurées sur les CPC macroporeux dans des conditions humides et sèches (Fig. 4-13). Comme prévu, toutes les propriétés mécaniques diminuent avec l'augmentation de la macroporosité quelles que soient les conditions d'essai. En outre, comme pour les CPC microporeux, les propriétés mécaniques mesurées à l'état mouillé sont généralement inférieures à celles mesurées à l'état sec, mais les différences entre elles ont tendance à diminuer avec l'augmentation de la macroporosité. Les propriétés mécaniques inférieures mesurées à l'état humide pour les CPC macroporeux pourraientt être attribuées à l'effet néfaste de l'eau existant dans les CPC, tel que discuté précédemment.

En outre, de façon similaire à la procédure menée dans le chapitre 3, la quantité $(K_{IC}/\sigma_f)^2$ (σ_f est la résistance à la flexion des CPC macroporeu), qui est proportionnelle à la taille du défaut sur lequel la rupture s'amorce, est tracée en fonction de la macroporosité (Fig. 4-14) afin d'étudier si la croissance stable des fissures pourrait se

produire lors d'un chargement en traction. Comme on peut le constater, la taille du défaut critique augmente de façon drastique avec l'augmentation de la macroporosité, ce qui est similaire à notre observation précédente, concernant la taille de défaut critique calculée à partir de la résistance à la compression, ce qui indique que la croissance stable des fissures peuvt aussi se produire lors d'un chargement en traction dans les CPC macroporeux.

La fiabilité des CPC macroporeux a également été analysée en utilisant les statistiques de Weibull. Comme pour les CPC microporeux, les diagrammes de Weibull logarithmiques pour les échantillons de compression des CPC macroporeux préparés avec des fractions massiques en mannitol différentes et mesurés dans diverses conditions sont représentées (Fig. 4-15, état humide ; Fig. 4-16, état sec), et le module de Weibull pour chaque CPC macroporeux a été calculé. En outre, afin de mieux expliquer les résultats ci-dessus, comme pour les CPC microporeux, la quantité $(K_{IC}/\sigma_r)^2$ (σr est la résistance à la compression) pour les CPC macroporeux dans des conditions différentes d'essai est représentée en fonction de la macroporosité (Fig. 4-17).

Comme on le voit, indépendamment des différentes conditions d'essai, la taille du défaut critique des CPC macroporeux augmente avec l'augmentation de la macroporosité. Ce résultat est cohérent avec qui a été montré dans le chapitre 3. En comparaison avec ce qui a été vu pour les CPC microporeux, le module de Weibull pour les CPC macroporeux est beaucoup moins variable et semble indépendant des conditions d'essai. Ceci peut être expliqué par le fait que les macropores agissent comme des défauts critiques, que ce soit seuls ou en groupes (Pecqueux et al., 2010), et parce qu'ils sont introduits en grand nombre dans chaque échantillon, la résistance devient plus « déterministe » (par exemple un haut module de Weibull), comme prédit par la théorie du « maillon faible » lorsque la quantité de défauts est grande.

Chapitre 5: Propriétés de mise en œuvre et propriétés mécaniques des CPC composites

Dans l'étude ci-dessus qui correspond au quatrième chapitre de la thèse, l'influence de la fabrication et des conditions d'essai (sec et humide) sur les propriétés mécaniques et la fiabilité des CPC (microporeux et macroporeux) a été étudiée. Toutefois, comme indiqué dans la littérature, nos CPC, sans exception, sont intrinsèquement fragiles. Par conséquent, il serait essentiel de développer de nouveaux matériaux moins fragiles présentant des propriétés biologiques, ergonomiques et mécaniques optimisées.

À cette fin, des solutions d'éthers de cellulose (HPMC/MC) biocompatibles

présentant des masses moléculaires différentes et des niveaux de substitution différents sont préparées et utilisées comme composantes liquides pour fabriquer des CPC composites. Ces composés ont largement été utilisés dans d'autres matériaux de type ciment (e.g. ciment Portland) pour améliorer les propriétés rhéologiques et mécaniques de ces derniers. Il sera donc intéressant d'étudier si ces éthers de cellulose peuvent jouer les mêmes rôles dans les CPC. Les effets de ces polymères sur l'ouvrabilité et les propriétés mécaniques des CPC composites ont été systématiquement étudiés.

L'injectabilité du CPC composite HPMC/MC a été évaluée (Fig. 5-1). Avant d'expliquer les résultats, il est utile de préciser que l'injectabilité de la pâte de CPC est définie ici comme sa capacité à rester homogène pendant l'injection, indépendamment de la force d'injection (Bohner et al., 2005A). Il est à noter que cette grandeur est différente de l'injectabilité liée à la force d'injection qui doit être appliquée à une seringue de façon à délivrer la pâte de ciment, quelle que soit sa qualité, l'homogénéité ou la quantité (Khairoun et al., 1998 ; Wang et al., 2006).

L'injectabilité des CPC composites HPMC/MC est significativement améliorée en ajoutant des quantités croissantes d'éthers de cellulose, comme indiqué dans la Fig. 5-1. Par exemple, en ajoutant seulement 0,25% d'E4M, l'injectabilité de la pâte peut être augmentée de 75%. L'amélioration significative de l'injectabilité est principalement attribuable à la viscosité améliorée de la pâte qui peut effectivement réduire ou même éliminer les phénomènes de démixion qui sont censés limiter l'injectablité d'une pâte de ciment (Habit et al., 2008). Selon cette étude, l'injectabilité des CPC composites préparés avec diverses solutions de cellulose de même concentration (par exemple 0,25%) peuvent être classés dans l'ordre ascendant : A15 < E4M ≈ K4M < K15M. Cependant, fait intéressant, le ciment composite préparé en ajoutant une solution de E4M (avec une viscosité similaire à celle K4M) semble démontrer une meilleure injectabilité, comme indiqué dans la Fig. 5-1.

Cet écart peut être expliqué par l'analyse des propriétés rhéologiques de la pâte composite de CPC HPMC/MC. En général, les solutions aqueuses de polymères (ici des solutions d'éthers de cellulose) sont des fluides non-newtoniens et présentent un comportement d'écoulement pseudoplastique (Holmberg et al., 2002). Les systèmes (se réfère ici aux CPC) modifiés avec des solutions de polymères visqueux présentent généralement également une pseudoplasticité (Khayay., 1998 ; Wang et al., 2007). En outre, cette pseudoplasticité augmente avec le poids moléculaire et avec la concentration. En ce qui concerne E4M, car il a un plus petit poids moléculaire que K15M, sa

pseudoplasticité est moins importante et devrait être du même ordre que celle de K4M. Cependant, comme indiqué dans le tableau 5-1, E4M a un degré plus élevé de substitution des groupes MeO et HPO que K4M et K15M, qui peut entraîner un effet stérique plus fort et qui réduit encore son comportement pseudoplastique. Selon les deux facteurs ci-dessus, il est très possible que la viscosité apparente de la pâte CPC composite avec une solution E4M à 0,25% soit supérieure à celle de la pâte CPC composite contenant du K4M à la même concentration, et même supérieure à celle de la pâte de ciment composite préparée avec une solution K15M à la même concentration, ce qui conduit finalement à une meilleure injectabilité (Fig. 5-1).

Comme prévu, l'addition de différents éthers de cellulose améliore fortement les performances de cohésion et la résistance au lessivage du CPC composite (Fig. 5-3). Ces performances sont liées aux propriétés rhéologiques améliorées (par exemple la viscosité) du CPC composite. Cette viscosité peut effectivement réduire l'influence de la pression osmotique et donc réduire la dilution liée au saignement (Khayat, 1998), et interdit également la libération des particules de CPC dans le liquide environnant, qui sont soupçonnés d'être les facteurs principaux provoquant des pertes de cohésion et une plus grande sensibilté au lessivage (Bohner et al., 2006B).

L’évolution des temps de prise initial et final des CPC préparés par addition de différentes quantités d'additifs d'éthers de cellulose est montrée dans la Fig. 5-4. Il est évident que les temps de prise initiale des ciments sont légèrement augmentés. En revanche, les temps de prise finale des ciments sont visiblement prolongés lorsque le montant des additifs augmente. En ce qui concerne le mécanisme de retard de prise dans ces CPC composites, il est considéré comme similaire à celui des ciments de Portland (Weyer et al., 2005; Khayat, 1998). Dans le système CPC en prenant, un point de vue imagé, l'éther de cellulose dans l'eau peut en effet être considéré comme un "boule" de taille nanométrique, qui se compose de longues chaînes de polymères et qui fixe l'eau à l'intérieur. Ces "boules" d’éther de cellulose s'adsorbent à la surface des micro-cristaux (6 μm) de α-TCP de taille micronique, agissant comme des écrans qui interfèrent avec la dissolution de Ca^{2+} et PO_4^{3-} dans l'eau, affectant ainsi la précipitation de l'apatite et prolongeant les temps de prise. Malgré l'effet retardateur observé sur la prise, aucune différence notable n’est observée entre les ciments comportant ou pas d’éther de cellulose, ce qui indique que ces additifs n’inhibent pas la formation finale de la CDHA (Fig. 5-5).

La porosité des CPC composites fabriqués avec les différents éthers de cellulose a été mesurée (Fig. 5-6). Comme on le voit, par rapport au ciment contrôle (fraction massique

= 0%), la porosité du CPC composite augmente de façon monotone avec la fraction massique croissante de chaque éther de cellulose ajouté. La porosité croissante est attribuée à des bulles d'air entraînées (Fig. 5-7). La capacité à former des bulles d'air et puis à les stabiliser est fortement dépendante des propriétés de la composante liquide du ciment. Dans la présente étude, les éthers de cellulose agissent comme agents tensio-actifs qui peuvent donc abaisser la tension superficielle de la solution liquide, et aident à la formation de bulles d'air. En outre, comme mentionné précédemment, les éthers de cellulose peuvent augmenter la viscosité de la solution liquide ce qui est utile pour la stabilisation de bulles d'air en les empêchant de se déplacer et d'être éliminées à la surface.

La ténacité des ciments composites préparés avec des différents éthers de cellulose est présentée sur la Fig. 5-8. Les valeurs mesurées sont généralement plus élevées que celles du ciment de contrôle, même si la différence est faible. Par ailleurs, afin de mieux comprendre l'influence des éthers de cellulose sur la ténacité, cette dernière a été tracée en fonction de la porosité totale (Fig. 5-9 A, C, E et G). Comme on peut le constater, la ténacité des CPC composites reste constante ou même augmente avec l'augmentation de la porosité, ce qui est toutefois différent de notre résultat précédent, à savoir que la ténacité diminue avec la porosité ; ceci indique que les éthers de cellulose ont un effet renforçant sur les CPC. Cependant, cette hypothèse n'est valable que si la ténacité des ciments composites est comparée à celle des ciments de contrôle ayant les mêmes porosités. Pour cette raison et pour favoriser la comparaison, une courbe correspondant à une loi puissance (comme les modèles présentés dans le Chapitre 3) a été ajustée pour passer par le point correspondant au ciment de contrôle (voir Fig. 5-9A, C, E et G). Comme on peut le constater, la ténacité de tous les ciments composites est plus élevée que celle des ciments de contrôle ayant les mêmes porosités.

En outre, l'augmentation relative de la ténacité des ciments composites (par rapport à des ciments de contrôle « virtuels » ayant des porosités identiques) est tracée en fonction de la fraction massique en polymère (Fig. 5-9B, D, F et H). La ténacité augmente continuellement et fortement avec la fraction massique en polymère, indiquant que les additifs d'éthers de cellulose conduisent à un renforcement significatif des CPC. Par ailleurs, l'augmentation relative de ténacité peut être globalement décrite par des lignes droites. Les pentes des droites (correspondant aux taux d'augmentation de la ténacité) sont tracées en fonction de la masse molaire des différents éthers de cellulose (Fig. 5-10). Comme on peut le constater, les pentes augmentent globalement avec la masse molaire

des éthers de cellulose, indiquant que celle-ci a également un effet significatif sur la ténacité des ciments composites.

Concernant cet effet de durcissement dans les CPC composites, deux mécanismes possibles sont proposés et peuvent être explicités ainsi : en raison des procédés de broyage et de la présence d'humidité dans l'atmosphère, les particules de α-TCP ont tendance à s'agglutiner et à former des agglomérats. Lorsqu'elles sont mélangées avec le α-TCP, les molécules d'éther de cellulose sont adsorbées à la surface des particules de α-TCP. En raison de leur effet stérique, les molécules de cellulose permettent de réduire les forces d'attraction de Van der Waals entre les particules, les séparant et les empêchant ainsi de former des agglomérats, ce qui aboutit à une répartition plus homogène des particules dans la pâte (Burguera et al., 2006). Par conséquent, on peut s'attendre à ce que la croissance des cristaux d'apatite à partir d'une pâte homogène puisse finalement former une microstructure uniforme et optimisée, contenant moins de défauts, conduisant ainsi à une meilleure résistance à la rupture (Sarda et al., 2002). En outre, on peut observer que des morceaux de polymère, probablement issus des éthers de cellulose ayant rétréci au séchage, sont « collés » à plusieurs cristaux d'apatite voisins (Fig. 5-11 C, D). Ces morceaux de polymère peuvent contribuer à atténuer la sollicitation mécanique subie par le fond de fissure, par le mécanisme de pontage de fissure (le polymère forme des ponts reliant les faces de la fissure et consommant une partie de l'énergie de rupture à fournir grâce à une déformation élastique-plastique), améliorant ainsi la ténacité (Launey et al., 2009). Ainsi, à la fois la microstructure optimisée possédant une meilleure homogénéité et le pontage de la fissure par des ligaments de polymère peuvent contribuer à une ténacité améliorée des ciments composites.

La résistance à la compression du composite CPC préparé avec différents additifs d'éthers de cellulose est présentée sur la Fig. 5-13. La résistance à la compression des ciments composites est dans tous les cas inférieure à celle du ciment de contrôle. De même, afin de mieux comprendre l'influence des éthers de cellulose sur la résistance à la compression des ciments composites, cette propriété a été tracée en fonction de la porosité (Fig. 5-14A, C, E et G).

Lorsque des éthers de cellulose sont ajoutés, la résistance des ciments composites diminue de manière concomittante. En outre, comme pour la ténacité, la résistance reste généralement constante ou augmente même avec la porosité, ce qui est également différent de notre précédent résultat, à savoir que la résistance diminue avec la porosité, indiquant que les éthers de cellulose peuvent avoir un effet de renforcement sur les CPC.

Une fois de plus, cette hypothèse ne peut être prouvée que si la résistance des ciments composites est comparée à celle des ciments de contrôle ayant les mêmes porosités. Ainsi, un peu à l'image de ce qui a été fait dans le cas de la ténacité pour favoriser la comparaison, une loi puissance a été ajustée pour passer par le premier point correspondant à chaque ciment composite (voir Fig. 5-14A, C, E et G). L'augmentation relative de résistance des ciments composites, par rapport à des ciments « virtuels » ayant des porosités identiques, est tracée en fonction de la fraction massique en polymère (Fig. 5-14B, D, F et H). En général, l'augmentation relative de résistance augmente continuellement et fortement avec la fraction massique, indiquant que les additifs d'éthers de cellulose ont également un effet de renforcement sur les CPC. Cet effet est attribué à la ténacité qui augmente (Fig. 5-9).

Par ailleurs, les courbes contrainte-déplacement, enregistrées au cours des essais de compression sur les ciments composites, sont présentées sur la Fig. 5-15. Une augmentation linéaire de la contrainte suivie par une chute brutale peut être observée pour le ciment de contrôle, correspondant à une fracture fragile typique (par exemple, le contrôle sur la Fig. 5-15A). Au contraire, une augmentation moins linéaire de la contrainte, suivie par une baisse légère et progressive, peut être observée pour les ciments composites, indiquant une rupture moins fragile et correspondant à une microfissuration / macrofissuration progressive de la matière, ce qui peut être considéré comme une sorte de tolérance à l'endommagement. Cette tolérance à l'endommagement peut également être associée à une ténacité améliorée.

L'HPMC silanisé (Si-HPMC) est synthétisé par greffage contrôlable de silane sur l'HPMC (Bourges et al., 2002). Comme son précurseur, HPMC, Si-HPMC est biocompatible et a été décrit comme présentant un potentiel pour la régénération du cartilage (Merceron et al., 2010). En outre, en solution il présente une viscosité élevée (Fatimi et al., 2008) et, en tant que gel, il présente un comportement auto-durcissant. Ainsi, il a été utilisé dans une deuxième génération de substituts osseux injectables, en association avec des BCP (Daculsi et al., 2010A ; Weiss et al., 2008), démontrant un avantage significatif sur la première génération non durcissante (Vinatier et al., 2009). La haute viscosité et la gélification de Si-HPMC pourraient être intéressantes pour préparer des ciments composites présentant des propriétés mécaniques et une ouvrabilité améliorées.

Pour ces raisons, l'effet de Si-HPMC sur l' ouvrabilité et les propriétés mécaniques des CPC composites Si-HPMC a été étudié de façon systématique.

L’ injectabilité du CPC composite Si-HPMC à 4% présentant différents rapports L/P et après des temps de gélification différents a été mesurée, et les résultats sont tracés sur la Fig. 5-19. De façon surprenante, le ciment composite ayant un rapport L/P de 0,4 peut difficilement être injecté. En revanche, tous les ciments composites préparés avec des rapports L/P plus élevés peuvent être extrudés, pour atteindre un maximum d’injectabilité d'environ 95%. Il convient de rappeler que les 5% de pâte restants sont laissés dans l'embout de la seringue, de sorte que 95% est en fait la limite supérieure de l'injectabilité mesurée par cette méthode. Comme pour les CPC composites HPMC/MC, l'injectabilité améliorée du CPC composite Si-HPMC est attribuée à l'augmentation de viscosité de la pâte qui peut effectivement prévenir la démixion qui est considérée comme le mécanisme provoquant l’injectablité limitée des pâtes de ciment. Quant aux CPC composites Si-HPMC avec un rapport L/P de 0,4, leur mauvaise injectabilité peut être liée à un seuil très haut (i.e. la force nécessaire pour mettre en mouvement le flux de pâte), ce qui pourrait surpasser la force d'extrusion maximale utilisée dans la présente étude (~ 100 N).

Lorsqu'il est injecté dans une solution saline immédiatement après la préparation (moins de trois minutes), le ciment de contrôle se désintègre complètement et des particules sédimentent au fond du bécher (Fig. 5-21A), quel que soit le rapport L/P (0,4 à 0,8). En revanche, les pâtes de ciment composites Si-HPMC peuvent maintenir leur forme jusqu'au durcissement et aucune désintégration n’est observée, indiquant une cohésion exceptionnelle (Fig. 5-21B). Comme pour les ciments composites HPMC, la bonne cohésion des ciments composites Si-HPMC peut être attribuée à l'augmentation de viscosité de la pâte.

Les temps de prise initiale et finale des CPC, sans ou avec 4% de Si-HPMC, ont été mesurés pour différents rapports L/P (Fig. 5-22). Contrairement à l’HPMC qui retarde la prise du ciment composite (Fig. 5-4), Si-HPMC semble légèrement raccourcir le temps de prise initial du ciment composite pour des rapports L/P allant jusqu'à 0,6, mais au-delà de 0,8 la réduction est très significative. Le phénomène de réduction du temps de prise devient beaucoup plus évident pour le temps de prise final avec l'augmentation du rapport L/P. Quant au mécanisme de prise accélérée dans le ciment composite, il peut être principalement attribué à l'effet de gélification de Si-HPMC.

Après un durcissement de cinq jours, les phases composant les ciments de contrôle et les ciments composites Si-HPMC ont été examinées par DRX (Fig. 5-23). Comme pour les ciments composites HPMC, la plupart de l’α-TCP dans les ciments composites

Si-HPMC se transforme également en CDHA. Toutefois, la formation finale de CDHA dans le ciment composite Si-HPMC semble être retardée. Cela peut être attribué au fait que Si-HPMC peut former un réseau d'hydrogel en trois dimensions qui interfère avec la dissolution de Ca^{2+} et PO_4^{3-} dans l'eau, ce qui affecte la formation finale de CDHA.

Comme prévisible, les porosités des ciments contrôles et composites Si-HPMC augmentent avec un rapport L/P croissant (Fig. 5-24A). En outre, la porosité des ciments composites est supérieure à celle des ciments de contrôle pour les mêmes rapports L/P, qui est, comme dans le cas des ciments composites HPMC, supposée provenir de bulles d'air introduites lors de la préparation (Jenni et al., 2005 ; Khayat, 1998 ; Pourchez et al., 2010B).

Les micrographies MEB des surfaces de rupture des ciments de contrôle et des composites Si-HPMC avec différents rapports L/P sont présentées sur la Fig. 5-25. Aucune bulle d'air entraînée n’a pu être observée dans le ciment de contrôle avec un rapport L/P de 0,4 (Fig. 5-25A). En revanche, comme pour les ciments composites HPMC (Fig. 5-7), une fois Si-HPMC ajouté, de nombreuses bulles d'air de tailles différentes peuvent être facilement trouvées (Fig. 5-25B). Avec l'augmentation du rapport L/P (1,0), très peu de bulles d'air entraînées peuvent être vues dans le ciment de contrôle, mais la matrice de ciment de contrôle semble être devenue moins dense (Fig. 5-25C). En comparant les ciments composites Si-HPMC de rapports L/P 0,4 et 1,0, on observe une augmentation de la taille des macropores au-delà de 100 μm.

Le module d’Young du ciment de contrôle et des composites Si-HPMC préparés avec différents rapports L/P est tracé en fonction de la porosité (Fig. 5-26). Comme prévu, le module d’Young des ciments de contrôle et des composites diminue avec l'augmentation de la porosité (Fig. 5-26). Afin d'étudier l'effet de Si-HPMC sur le module d’Young, il est donc nécessaire de comparer le module d’Young des ciments composites Si-HPMC avec celui des ciments de contrôle ayant les mêmes porosités. À cette fin, pour favoriser la comparaison, une loi puissance a été utilisée pour décrire le module d’Young du ciment de contrôle (Fig. 5-26). Comme on le voit, le module d’Young des ciments composites Si-HPMC est apparemment plus élevé que celui des ciments de contrôle avec les mêmes porosités. Par ailleurs, l’augmentation relative du module d’Young des ciments composites est tracée en fonction du rapport L/P (Fig. 5-27). L'augmentation relative du module d’Young augmente continuellement et fortement avec le rapport L/P. Ce résultat semble être en contradiction avec notre résultat précédent, à savoir que le module d’Young diminue avec la porosité. La raison précise de cette contradiction n'est pas claire,

mais peut être due aux différentes microstructures résultant de l'effet de Si-HPMC.

Comme pour HPMC, afin de révéler l'effet de Si-HPMC, la ténacité des ciments de contrôle et composites préparés avec différents rapports L/P et avec Si-HPMC en concentrations différentes est tracée en fonction de la porosité (Fig. 5-29). Comme on peut le constater, la ténacité des ciments composites augmente avec une porosité croissante quel que soit le rapport L/P. Ceci est différent de nos résultats précédents, à savoir que la ténacité diminue avec la porosité, indiquant que Si-HPMC a un effet de renforcement sur les CPC. Afin de prouver cette hypothèse, la ténacité des ciments composites devrait être comparée à celle de ciments de contrôle ayant les mêmes porosités. De même, pour favoriser la comparaison, une loi puissance a été utilisée pour décrire la ténacité des ciments de contrôle (Fig. 5-29). Le ténacité de tous les ciments composites est apparemment plus élevée que celle des ciments de contrôle ayant les mêmes porosités.

Par ailleurs, l'augmentation relative de la ténacité des ciments composites avec différentes concentrations en Si-HPMC est tracée en fonction du rapport L/P (Fig. 5-30). L'augmentation relative de la ténacité augmente significativement avec la concentration en polymère, montrant que Si-HPMC a bien un effet renforçant sur les CPC. En outre, cet effet de durcissement devient plus évident dans les ciments composites à rapport L/P élevé. Comme pour les ciments composites HPMC ou MC (Fig. 5-9), la ténacité améliorée des ciments composites Si-HPMC a été attribuée à un effet synergique d'une microstructure plus homogène et du pontage des fissures par des ligaments polymères (Fig. 5-31, Fig. 5-32).

La résistance à la flexion des ciments de contrôle et des composites Si-HPMC préparés avec des rapports L/P différents est tracée en fonction de la porosité (Fig. 5-34). Comme prévu, la résistance à la flexion des ciments de contrôle et des composites diminue avec l'augmentation de la porosité. Afin de déterminer l'influence de Si-HPMC sur la résistance à la flexion, une loi puissance a été utilisée pour décrire la résistance à la flexion des ciments de contrôle pour faciliter la comparaison entre ces derniers et les ciments composites ayant la même porosité (Fig. 5-34). Comme on le voit, à l'exception du rapport L/P de 0,4, la résistance à la flexion des ciments composites Si-HPMC est supérieure à celle des ciments de contrôle ayant les mêmes porosités. En outre, l'augmentation relative de la résistance à la flexion des ciments composites, par rapport à des ciments de contrôle « virtuels » ayant des porosités identiques, est tracée en fonction du rapport L/P (Fig. 5-35). L'augmentation relative de la résistance à la flexion augmente

continuellement et fortement avec l'augmentation du rapport L/P, indiquant que Si-HPMC a un effet de renforcement sur les CPC ; cette tendance devient plus importante dans les ciments composites à hauts rapports L/P.

La résistance à la compression des ciments de contrôle et des composites Si-HPMC préparés avec différents rapports L/P et avec Si-HPMC en concentrations différentes est également représentée en fonction de la porosité (Fig. 5-37). Deux tendances différentes peuvent être observées. Dans le cas des ciments composites avec des rapports L/P de 0,4 ou 0,45, la résistance à la compression diminue avec l'augmentation de la porosité. En revanche, pour les ciments composites avec des rapports L/P de 0,6 ou 1,0, la résistance à la compression reste constante, voire augmente légèrement avec la porosité, indiquant que Si-HPMC peut aussi avoir un effet de renforcement sur la résistance à la compression des CPC.

Pour vérifier cette hypothèse, la résistance à la compression des ciments composites Si-HPMC est comparée à celle des ciments de contrôle ayant les mêmes porosités. Comme on peut le constater, la résistance à la compression des ciments composites ayant des rapports L/P élevés (0,6, 0,8 et 1,0) est supérieure à celle des ciments de contrôle ayant les mêmes porosités. L'augmentation relative de la résistance à la compression des ciments composites préparés avec des concentrations différentes en Si-HPMC est tracée en fonction du rapport L/P (Fig. 5-38). Comme pour la résistance à la flexion, à l'exception des ciments composites avec des rapports L/P de 0,4 ou 0,45, l'augmentation relative de résistance à la compression augmente fortement avec la concentration en polymère, montrant que Si-HPMC a sûrement des effets de renforcement sur la résistance à la compression des CPC. Cet effet de renforcement est attribué à une ténacité améliorée.

Dans l'étude ci-dessus, il a été observé que des bulles d'air de tailles différentes peuvent être trouvées dans les CPC composites. D'une part, ces bulles se sont avérées très difficiles à éviter, indiquant qu'elles sont plutôt stables, et d'autre part leur taille, typiquement plusieurs dizaines de micromètres, est de l'ordre de la taille des macropores recherchés dans les phosphates de calcium (Hing et al., 1999), dans lesquels les cellules osseuses peuvent facilement se développer. Il est donc ici proposé d'exploiter les particularités de Si-HPMC pour entraîner volontairement un grand nombre de bulles d'air dans les ciments Si-HPMC, pour produire des matériaux macroporeux. Si-HPMC est donc préliminairement évalué comme agent entraîneur d'air pour produire des bulles d'air stables, qui seront ensuites mélangées avec une pâte CPC pour préparer une mousse macroporeuse. La porosité, les propriétés de mise en œuvre et les propriétés mécaniques

de ces CPC composites macroporeux ont été étudiées.

L'injectabilité de la mousse composite CPC Si-HPMC a été évaluée et toutes les mousses étudiées peuvent être extrudées complètement de la seringue. Comme pour les composites CPC HPMC ou Si-HPMC, l'injectabilité exceptionnelle des mousses composites est due à la viscosité améliorée de la pâte qui permet de réduire efficacement, voire de supprimer la séparation de phase lors du pressage.

Même avec une grande quantité de bulles d'air, la mousse de ciment composite Si-HPMC démontre une excellente cohésion (Fig. 5-43). La forte cohésion des mousses de ciment peut être attribuée à la viscosité améliorée de la pâte et à l'effet du réseau tri-dimensionnel de l'hydrogel.

Comme prévu, la porosité totale des mousses composites CPC Si-HPMC augmente avec le volume d'air introduit (Fig. 5-44). En outre, étant donnée la manière dont les macropores sont créés dans la présente étude, la macroporosité d'une mousse de ciment peut être estimée en soustrayant la porosité totale du ciment correspondant, fabriqué sans air, de la porosité totale de la mousse de ciment fabriquée avec de l'air, en utilisant l'équation 2-7 développée dans le Chapitre 2. La macroporosité augmente avec le volume d'air introduit (Fig. 5-44).

Les micrographies MEB de surfaces de rupture de mousses de ciments composites Si-HPMC sont présentées sur la Fig. 5-45. De nombreux macropores sphériques de tailles diverses sont arbitrairement distribués dans la mousse de ciment composite Si-HPMC ayant un rapport L/P de 0,8 et un rapport $V_{air}/V_{hydrogel}$ = 1 (Fig. 5-45A). Avec l'augmentation du ratio $V_{air}/V_{hydrogel}$, de nombreux macropores de grande taille et ayant des formes distordues sont observés (Fig. 5-45B). Par ailleurs, à plus fort grossissement on peut trouver, dans la matrice de ciment située entre les macropores, des ligaments de polymère adhérant aux cristaux d'apatite ; ils sont probablement issus de l'hydrogel Si-HPMC s'étant contracté au séchage (Fig. 5-45C). Comme mentionné précédemment, ces ligaments de polymères peuvent contribuer à accroître les propriétés mécaniques, en particulier la ténacité.

Les mousses composites CPC Si-HPMC ont été examinées par microtomographie X, pour une évaluation préliminaire de la taille et la distribution des bulles d'air introduites (Fig. 5-46 et 5-47). Seuls quelques macropores peuvent être observés dans une section transversale de la mousse de ciment ayant un rapport L/P de 0,6 et un rapport $V_{air}/V_{hydrogel}$ de 0,5 (Fig. 5-46A). Avec l'augmentation du rapport $V_{air}/V_{hydrogel}$, le nombre et la taille des macropores augmentent simultanément (Fig. 5-46B, C). Par contre, de plus

nombreux macropores sont observés dans la section transversale de la mousse de ciment ayant un rapport L/P supérieur (0,8) et un rapport $V_{air}/V_{hydrogel}$ de 0,5 (Fig. 5-46D). Par ailleurs, le nombre et la taille des macropores augmentent de façon significative avec l'augmentation de $V_{air}/V_{hydrogel}$ (Fig. 5-46E, F).

Comme prévu, toutes les propriétés mécaniques mesurées diminuent lorsque la macroporosité augmente (Fig. 5-48). Dans le cas de la résistance à la compression et avec un rapport L/P de 0,6, il semble qu'une forte diminution est provoquée dès que des bulles d'air sont introduites. Ce phénomène a également été observée dans tous les ciments macroporeux. Ceci est principalement attribué à la présence de grosses bulles d'air qui agissent comme défauts critiques de grande taille. Enfin, il convient de noter que, bien que les propriétés mécaniques des mousses de ciments soient très faibles, elles sont encore comparables aux valeurs rapportées pour l'os spongieux (Koester et al., 2008 ; Wagoner Johnson et al., 2011).

Enfin, des courbes contrainte-déplacement enregistrées au cours d'essais de compression de mousses de ciments composites Si-HPMC, renfermant différentes quantités d'air, sont présentées sur la Fig. 5-49. Un chute brutale de la contrainte peut être observée pour le ciment de contrôle ayant un rapport L/P de 0,8, ce qui est caractéristique d'une rupture fragile. Au contraire, une baisse légère et progressive de la contrainte se produit pour le ciment composite Si-HPMC ayant un rapport $V_{air}/V_{hydrogel}$ de 0 (pas de macropores), ce qui peut être assimilé à une sorte de tolérance à l'endommagement. Cette tolérance à l'endommagement devient encore plus prononcée dans les mousses de ciments composites Si-HPMC contenant diverses quantités d'air introduit. Ces courbes de rupture non fragile montrent l'effet bénéfique de Si-HPMC sur le comportement à la rupture des mousses de ciments composites Si-HPMC, ce qui est comparable avec les ciments composites HPMC/Si-HPMC dont il a été question précédemment.

Conclusion

Dans ce travail, des CPC présentant des microstructures contrôlables (porosité, taille des pores, forme et taille des cristaux) ont été préparés et leurs propriétés mécaniques (module d'Young, ténacité, résistance à la compression et à la flexion) ont été systématiquement étudiées. Par ailleurs, des CPC composites ont été développés en utilisant différents éthers de cellulose, et leurs propriétés mécaniques et de mise en œuvre ont été étudiées. Les principaux résultats de ces recherches ont déjà été décrits et discutés, mais les caractéristiques les plus importantes sont résumées ici.

Du phosphate tricalcique α (α-TCP) n'ayant pas réagi peut être détecté par divers

moyens (DRX et MEB), dans les ciments fabriqués avec un faible rapport L/P et d'une manière générale dans les ciments préparés avec de la poudre α-TCP grossière. Ces particules de α-TCP présentent des liens faibles avec la matrice de CDHA et sont habituellement entourées par des « espaces » qui les séparent de la matrice, ces espaces étant comparables à « microfissures ». Celles-ci peuvent provoquer une diminution du module d'Young, mais ne semblent pas influer sur la ténacité.

La taille des particules de la poudre α-TCP de départ a un effet important sur la microstructure du produit final (CDHA). Plus les particules initiales de α-TCP sont grosses, plus la microstructure finale de la CDHA est grossière, ce qui entraîne une taille de défaut critique plus importante et donc un résistance réduite par rapport aux ciments fabriqués avec une poudre fine. Dans le cas des CPC macroporeux obtenus en utilisant des particules de mannitol solubles comme agent porogène, la taille du défaut critique est de l'ordre de celle des plus grands macropores pour des macroporosités faibles, puis augmente de façon monotone avec l'augmentation de la macroporosité. Cette taille croissante du défaut critique est associée à la propagation sous-critique de microfissures, qui relieraient les macropores entre eux avant d'atteindre le pic de contrainte, comme cela avait été suggéré dans les céramiques macroporeuses BCP (Pecqueux et al. 2010). Cette croissance stables des fissures dans les CPC macroporeux semble d'ailleurs se produire lors d'un chargement en compression, mais également en traction (flexion). L'évolution de la plupart des propriétés mécaniques (module d'Young, ténacité et résistance à la compression), avec la microporosité et la macroporosité considérées séparément, peut être décrite avec des modèles en loi puissance à double échelle ; elle peut être interprétée en prenant en compte tous les phénomènes mentionnés ci-dessus.

Les conditions d'essai (sec ou humide) affectent fortement les propriétés mécaniques des CPC microporeux ou macroporeux. Les propriétés mécaniques mesurées à l'état humide sont généralement inférieures à celles qui sont mesurées à sec. Les propriétés de rupture inférieures obtenues dans des conditions humides sont principalement attribuées à la présence d'eau qui peut diminuer l'énergie de surface des fissures.

Le procédé de fabrication des CPC, en particulier le stade de mélange de la pâte de ciment, réduit la fiabilité mécanique des CPC microporeux ayant un rapport L/P élevé, en raison du caractère imprévisible d'un petit nombre de grosses bulles d'air piégées dans la pâte, agissant comme défauts critiques de taille fortement aléatoire. En revanche, le procédé de fabrication a moins d'effet sur la fiabilité des CPC macroporeux. Leur fiabilité est élevée et constante avec la macroporosité, en raison de la présence d'un grand nombre

de macropores de taille calibrée, conduisant à une taille de défaut critique plus déterministe.

L'addition d'éthers de cellulose HPMC/MC, possédant des paramètres structurels différents, et Si-HPMC, présentant un réseau tridimensionnel de chaînes polymères, modifie l'ensemble des performances des CPC, y compris la porosité ainsi que les propriétés mécaniques et de mise en œuvre.

La masse molaire des HPMC/MC et leur degré de substitution ont tous deux une grande influence sur l'injectabilité des CPC. Plus la solution de HPMC/MC est visqueuse, meilleure est l'injectabilité de la pâte de CPC composite. Pour différentes solutions de HPMC ayant des viscosités similaires, le degré de substitution par des groupes MeO ou HPO semble jouer un grand rôle. Les additifs HPMC/MC semblent représenter une excellente option, non seulement pour améliorer l'injectabilité mais aussi pour améliorer la cohésion et la résistance au lessivage. Par ailleurs, les HPMC/MC peuvent prolonger le temps de prise des ciments composites, et en particulier le temps de prise final. De même, l'ajout de Si-HPMC améliore significativement l'injection et la cohésion des pâtes de ciment composite. Cependant, contrairement aux HPMC/MC qui retardent la prise, Si-HPMC réduit le temps de prise apparent des CPC, probablement en raison de son comportement auto-durcissant lors de la gélification. Même une petite quantité de HPMC/MC ou de Si-HPMC suffit pour changer radicalement toutes les propriétés de mise en œuvre des pâtes de ciment étudiées.

Les HPMC/MC et Si-HPMC induisent un fort effet de renforcement des propriétés mécaniques ; cet effet devient plus important dans les ciments composites ayant des fractions massiques élevées en polymère, lorsque la masse molaire du polymère augmente, ou dans les ciments composites à rapport L/P élevé. Ce renforcement est attribué, entre autres, au pontage des fissures par des ligaments de polymère se déformant plastiquement ; l'évolution de la ténacité avec la fraction en polymère et sa masse molaire est conforme aux descriptions existantes. Si-HPMC améliore également le module d'Young et la ténacité grâce à une meilleure homogénéité de la structure microporeuse. Cependant, dès que de petites quantités de HPMC/MC ou Si-HPMC sont ajoutées aux ciments, une baisse soudaine de la résistance à la compression est provoquée par l'apparition de bulles d'air, entraînées lors de la préparation de la pâte et agissant comme des défauts critiques de grande taille. Néanmoins, par rapport aux ciments de contrôle macroporeux ayant la même porosité, la résistance a ensuite généralement tendance à augmenter avec la fraction massique en polymère, ce qui peut être attribuée à

l'augmentation de ténacité précédemment identifiée. L'ajout de polymères confère également au matériau une certaine tolérance à l'endommagement, permettant une déformation et une fissuration progressives lors du chargement, au lieu d'une rupture fragile, ce qui peut être intéressant pour les applications biologiques, en empêchant la libération de débris dans le corps en cas de surcharge.

L'hydrogel Si-HPMC semble être un agent moussant prometteur pour la préparation de CPC macroporeux. Les CPC macroporeux démontrent d'excellentes propriétés de mise en œuvre telles que l'injectabilité et la cohésion. Leurs propriétés mécaniques (module d'Young et résistance à la compression) sont comparables à celles de l'os spongieux. Par ailleurs, ils présentent également une certaine tolérance à l'endommagement, qui est généralement aussi liée à une amélioration de la ténacité, même si cette dernière n'a pas encore été mesurée. Compte tenu des exigences principales rapportées pour l'application des CPC en chirurgie (macropores, propriétés de mise en œuvre et propriétés mécaniques), les CPC composites macroporeux contenant Si-HPMC, développés dans cette étude, peuvent représenter une alternative intéressante aux greffes d'os spongieux.

Sur la base des constatations ci-dessus, en particulier celles concernant les ciments composites macroporeux Si-HPMC, des recherches supplémentaires sont donc à mener.

La fiabilité mécanique et la ténacité sont les limites réelles des CPC. Ainsi, il serait très intéressant d'étudier la fiabilité et la ténacité des CPC macroporeux Si-HPMC et, si nécessaire, d'essayer de les améliorer.

Si-HPMC a été évalué comme agent moussant pour produire des macropores dans les CPC, mais les quantités et les tailles de ces macropores ne sont pas bien contrôlées ni caractérisées. Ce travail restera à mener à l'avenir.

La prochaine étape de l'étude consistera à étudier les comportements in vitro & in vivo des CPC macroporeux Si-HPMC, en particulier leur effet sur la conductivité osseuse. Dans cet objectif, une formulation expérimentale de CPC composite Si-HPMC va être prochainement implantée dans des fémurs de lapins pendant huit semaines afin d'examiner si les mousses de CPC macroporeux Si-HPMC sont bénéfiques pour la colonisation cellulaire. Si les résultats sont positifs, une étude biologique plus complète sera menée pour mesurer la sécurité et l'efficacité des composites contenant du Si-HPMC chez le grand animal (par exemple, la brebis ou le chien).

References

Almirall, A., Larrecq, G., Delgado, J. A., Martinez, S., Planell, J. A., Ginebra, M. P. Fabrication of low temperature macroporous hydroxyapatite scaffolds by foaming and hydrolysis of an alpha-TCP paste. Biomaterials 25, 3671-3680 (2004)

Andrianjatovo, H., Lemaitre, J. Effects of polysaccharides on the cement properties in the monocalcium phosphate/ β-tricalcium phosphate system. Innovation and Technology in Biology and Medicine 16, 140-147 (1995)

Arato, P. Comment on ‘dependence of ceramics fracture properties on porosity’. Journal of Materials Science Letters 15, 32-33 (1996)

Ashby, M. F. Criteria for selecting the components of composites. Acta Metallurgica et Materialia 41, 1313-1335 (1993)

Ashby, M. F., Jones, D. R. H., Bréchet, Y., Courbon, J., Dupeux, M. Matériaux. Tome 1, Propriétés, applications et conception. Dunod 2008

Bai, F., Meng, G., Yuan, Y., Liu, C., Wang, Z., Liu, J. Role of macropore size in the mechanical properties and in vitro degradation of porous calcium phosphate cements. Materials Letters 64, 2028-2031 (2010)

Baroud, G., Cayer, E., Bohner, M. Rheological characterization of concentrated aqueous beta-tricalcium phosphate suspensions: The effect of liquid-to-powder ratio, milling time, and additives. Acta Biomaterialia 1, 357-363 (2005)

Barralet, J. E., Gaunt, T., Wright, A. J., Gibson, I. R., Knowles, J. C. Effect of porosity reduction by compaction on compressive strength and microstructure of calcium phosphate cement. Journal of Biomedical Research Part b: Applied Biomaterials 63, 1-9 (2002A)

Barralet, J. E., Grover, L., Gaunt, T., Wright, A. J., Gibson, I. R. Preparation of macroporous calcium phosphate cement tissue engineering scaffold. Biomaterials 23, 3063-3072 (2002B)

Barralet, J. E., Hofmann, M., Grover, L. M., Gbureck, U. High strength apatitic cement by modification with α-hydroxy acid salts. Advanced Materials 15, 2091-2094 (2003)

Barralet, J. E., Grover, L. M., Gbureck, U. Ionic modification of calcium phosphate cement viscosity. Part II: hypodermic injection and strength improvement of brushite cement. Biomaterials 25, 2197-2203 (2004)

Barriga, A., Diaz-de-Rada, P., Barroso, J. L., Alfonso, M., Lamata, M., Hernaez, S., Beguiristain, J. L., San-Julian, M., Villas, C. Frozen cancellous bone allografts:

Positive cultures of implanted grafts in posterior fusions of the spine. European Spine Journal.13, 152-156 (2004)

Bazant, Z. P., Xiang, Y. J. Size effect in compression fracture: Splitting crack band propagation. Journal of Engineering Mechanics 123, 162-172 (1997)

Beaudoin, J. J. Handbook of fibre-reinforced concrete. Noyes publications, New Jersey 1990

Benaqqa, C., Chevalier, J., Saadaoui, M., Fantozzi, G. Slow crack growth behavior of hydroxyapatite ceramics. Biomaterials 26, 6106-6112 (2005)

Bermudez, O., Boltong, M. G., Driessens, F. C. M., Planell, J. A. Compressive strength and diametral tensile strength of some calcium-orthophosphate cements: a pilot study. Journal of Materials Scienece: Materials in Medicine 4, 389-393 (1993)

Bermudez, O., Boltong, M. G., Driessens, F. C. M., Planell, J. A. Development of some calcium phosphate cements from combination of α-TCP, MCPM, and CaO. Journal of Materials Scienece: Materials in Medicine 5, 160-163 (1994)

Bernards, C. M., Chapman, J. R., Mirza, S. K. Lethality of embolized Norian bone cement varies with the time between mixing and embolization. Proceeding of the 50th annual meeting of the orthopaedic research society (ORS), San Francisco, P254 (2005)

Bhamra, G., Palin, W. M., Fleming, G. J. P. The effect of surface roughness on the flexure strength of an alumina reinforced all-ceramic crown material. Journal of Dentistry 30, 153-160 (2002)

Bignon, A., Chouteau, J., Chevalier, J., Fantozzi, G., Carret, J. P., Chavassieux, P., Boivin, G., Melin, M., Hartmann, D. Effect of micro- and macroporosity of bone substitutes on their mechanical properties and cellular response. Journal of Materials Scienece: Materials in Medicine 14, 1089-1097 (2003)

Blakeslee, K. C., Condrate Sr, R. A. Vibrational spectra of hydrothermally prepared hydroxyapatites. Journal of the American Ceramic Society 54, 559-563 (1971)

Boger, A., Bohner, M., Heini, P., Verrier, S., Schneider, E. Properties of an injectable low modulus PMMA bone cement for osteoporotic bone. Journal of Biomedical Materials Research Part B- Applied Biomaterials 86B, 474-482 (2008)

Bohner, M. Physical and chemical aspects of calcium phosphates used in spinal surgery. European Spine Journal 10, 114-121 (2001)

Bohner, M. Reactivity of calcium phosphate cements, Journal of Materials Chemistry 17, 3980-3986 (2007)

Bohner, M. Resorbable biomaterials as bone graft substitutes. Materials Today 13, 24-30 (2010A)

Bohner, M. Design of ceramic-based cements and putties for bone graft substitution. European Cells and Materials 20, 1-12 (2010B)

Bohner, M., Merkle, H. P., Landuyt, P. V., Trophardy, G., Lemaitre, J. Effect of several additives and their admixtures on the physico-chemical properties of a calcium phosphate cement. Journal of Materials Scienece: Materials in Medicine 11, 111-116 (2000)

Bohner, M. and G. Baroud, Injectability of calcium phosphate pastes. Biomaterials 26, 1553-1563 (2005A)

Bohner, M., Gbureck, U., Barralet, J.E. Technological issues for the development of more efficient calcium phosphate bone cements: A critical assessment. Biomaterials 26, 6423-6429 (2005B)

Bohner, M., Malsy, A. K., Camire, C. L., Gbureck, U. Combining particle size distribution and isothermal calorimetry data to determine the reaction kinetics of alpha-tricalcium phosphate-water mixtures. Acta Biomaterialia 2, 343-348 (2006A)

Bohner, M., Doebelin, N., Baroud, G. Theoretical and experimental approach to test the cohesion of calcium phosphate pastes. European Cells and Materials 12, 26-35 (2006B)

Bohner, M., Luginbuhl, R., Reber, C., Doebelin, N., Baroud, G., Conforto, E. A physical approach to modify the hydraulic reactivity of alpha-tricalcium phosphate powder. Acta Biomaterialia 5, 3524-3535 (2009)

Bouler, J. M., et al., Macroporous biphasic calcium phosphate ceramics: Influence of five synthesis parameters on compressive strength. Journal of Biomedical Materials Research 32, 603-609 (1996)

Bourges, X., Weiss, P., Daculsi, G., Legeay, G. Synthesis and general properties of silated-hydroxypropyl methylcellulose in prospect of biomedical use. Advances in Colloid and Interface Science 99, 215-228 (2002)

Brown, P. W., Fulmer, M. Kinetics of hydroxyapatite formation at low temperature. Journal of American Ceramic Society 74, 934-940 (1991)

Brown, W. E., Chow, L. C. A new calcium phosphate setting cement. Journal of Dental Research 62, 672-679 (1983)

Brunner, T.J., Grass, R. N., Bohner, M., Stark, W. J. Effect of particle size, crystal phase and crystallinity on the reactivity of tricalcium phosphate cements for bone reconstruction. Journal of Materials Chemistry 17, 4072-4078 (2007A)

Brunner, T. J., Bohner, M., Dora, C., Gerber, C., Stark, W. J. Comparison of amorphous TCP nanoparticles to micron-sized alpha-TCP as starting materials for calcium phosphate cements. Journal of Biomedical Materials Research Part B- Applied Biomaterials. 83B, 400-407 (2007B)

Burguera, E. F., Xu, H. H. K., Takagi, S., Chow, L. C. High early strength calcium phosphate bone cement: Effects of dicalcium phosphate dihydrate and absorbable fibers. Journal of Biomedical Materials Research Part A 75, 966-975 (2005)

Burguera, E. F., Xu, H. H. H., Weir, M. D. Injectable and rapid-setting calcium phosphate bone cement with dicalcium phosphate dihydrate. Journal of Biomedical Materials Research Part B-Applied Biomaterials 77, 126-134 (2006)

Cama, G., Barberis, F., Botter, R., Cirillo, P., Capurro, M., Quarto, R., Scaglione, S., Finocchio, E., Mussi, V., Valbusa, U. Preparation and properties of macroporous brushite bone cements. Acta Biomaterialia 5, 2161-2168 (2009)

Camire, C. L., Gbureck, U., Hirsiger, W., Bohner, M. Correlating crystallinity and reactivity in an alpha-tricalcium phosphate. Biomaterials 26, 2787-2794 (2005)

Canal, C., Ginebra, M. P. Fibre-reinforced calcium phosphate cements: A review. Journal of the Mechanical Behavior of Biomedical Materials 4, 1658-1671 (2011)

Cannillo, V., Manfredini, T., Montorsi, M., Boccaccini, A. R. Use of numerical approaches to predict mechanical properties of brittle bodies containing controlled porosity. Journal of Materials Science 39, 4335-4337 (2004)

Carrodeguas, R. G., Aza, S. D. α-Tricalcium phosphate: Synthesis, properties and biomedical applications. Acta Biomaterialia 7, 3536-3546 (2011)

Charnley, J. Anchorage of the femoral head prosthesis to the shaft of the femur. The journal of Bone and Joint Surgery (British volume) 42B, 28-30 (1960)

Chen, G. X., Li, W. W., Yu, X. M., Sun, K. Study of the cohesion of TTCP/DCPA phosphate cement through evolution of cohesion time and remaining percentage. Journal of Materials Science 44, 828-834 (2009)

Cherng, A., Takagi, S., Chow, L. C. Effects of hydroxypropyl methylcellulose and other gelling agents on the handling properties of calcium phosphate cement. Journal of Biomedical Materials Research 35, 273-277 (1997)

Chevalier, J., Gremillard, L. Ceramics for medical applications: A picture for the next 20 years. Journal of the European Ceramic Society 29, 1245-1255 (2009)

Cho, S. J., Yoon, K. J., Kim, J. J., Kim, K. H. Influence of humidity on the flexural strength of alumina. Journal of the European Ceramic Society 20, 761-764 (2000)

Cho, S. J., Yoon, K. J., Lee, Y. C., Chu, M. C. Effects of environmental temperature and humidity on the flexural strength of alumina and measurement of environment-insensitive inherent strength. Materials Letters 57, 2751-2754 (2003)

Chow, L. C., Hirayama, S., Takagi, S., Parry, E. Diametral tensile strength and compressive strength of a calcium phosphate cement: effect of applied pressure.

Journal of Biomedical Materials Research Part B: Applied Biomaterials 53, 511-517 (2000)

Chow, L. C., Eanes, E. D. Octacalcium phosphate. Monographs in Oral Science Karger 18, (2001)

Chow, L. C. Next generation calcium phosphate-based biomaterials. Dental Materials Journal 28, 1-10 (2009)

Claussen, N., Petzow, G. Strengthening and toughening models in ceramics based on ZrO_2 inclusions. Proceeding of the 4^{th} international meeting on modern ceramics technologies, 680-691 (1980)

Cordell, J. M., Vogl, M. L., Johnson, A. J. W. The influence of micropore size on the mechanical properties of bulk hydroxyapatite and hydroxyapatite scaffolds. Journal of the Mechanical Behavior of Biomedical Materials 2, 560-570 (2009)

Cordier, P., Tournilhac, F., Soulie-Ziakovic, C., Leibler, L. Self-healing and thermoreversible rubber from supramolecular assembly. Nature 451, 977-980 (2008)

Daculsi, G., Baroth, S., LeGeros, R. 20 years of biphasic calcium phosphate bioceramics development and applications. Westerville: American Ceramic Society 45-58 (2010A)

Daculsi, G., Uzel, A. P., Weiss, P., Goyenvalle, E., Aguado, E. Developments in injectable multiphasic biomaterials. The performance of microporous biphasic calcium phosphate granules and hydrogels. Journal of Materials Science-Materials in Medicine 21, 855-861 (2010)

Davies D. G. S. The statistical approach to engineering design in ceramics. Proceedings of the British Ceramic Society 22, 429-452 (1973)

De With, G., Van Dijk, H. J. A, Hattu, N., Prijs, K. Preparation, microstructure and mechanical properties of dense polycrystalline hydroxy apatite. Journal of Materials Science 16, 1592-1598 (1981)

Del Real, R. P., Wolke, J. G. C., Vallet-Regi, M., Jansen, J. A. A new method to produce macropores in calcium phosphate cements. Biomaterials 23, 3673-3680 (2002)

Deville, S., Saiz, E., Tomsia, A. P. Freeze casting of hydroxyapatite scaffolds for bone tissue engineering. Biomaterials 27, 5480-5489 (2006)

Dlouhy, I., Holzmann, M., Man, J., Valka, L. Using chevron notched specimens for determining fracture toughness of bearing steels. Metallic Materials 32, 5-10 (1994)

Dorozhkin, S. V. Calcium orthophosphate cements for biomedical application. Journal of Materials Science 43, 3028-3057 (2008)

Dorozhkin, S. V. Bioceramics of calcium orthophosphates. Biomaterials 31, 1465-1485 (2010)

Dos Santos, L. A., de Oliveira, L. C., Rigo, E. C. D., Carrodeguas, R. G., Boschi, A. O., de Arruda, A. C. F. Fiber reinforced calcium phosphate cement. Artificial Organs 24, 212-216 (2000)

Dow Chemical Company, METHOCEL Cellulose Ethers Technical Handbook. Form No. 192-01062-0902 AMS, USA (2002)

Driessens, F. C., Boltong, M. G., Bermudez, O., Planell, J. A., Ginebra, M. P., Fernandez, E. Effective formulations for the preparation of calcium-phosphate bone cements. Journal of Materials Scienece: Materials in Medicine 5, 164-170 (1994)

Driessens, F. C., Planell, J. A., Boltong, M. G., Khairoun, I., Ginebra, M. P. Osteotransductive bone cements. Proceeding of the Institution of Mechanical Engineers Part H: Journal of Engineering in Medicine 212, 427-435 (1998)

Dunne, N. J., Orr, J. F. Curing characteristics of acrylic bone cement. Journal of Materials Scienece: Materials in Medicine 13, 17-22 (2002)

Durucan, C., Brown, P.W. alpha-Tricalcium phosphate hydrolysis to hydroxyapatite at and near physiological temperature. Journal of Materials Scienece: Materials in Medicine 11, 365-371 (2000)

Durucan, C., Brown, P.W. Kinetic model for alpha-tricalcium phosphate hydrolysis. Journal of the American Ceramic Society 85, 2013-2018 (2002A)

Durucan, C., Brown, P.W. Reactivity of alpha-tricalcium phosphate. Journal of Materials Science 37, 963-969 (2002B)

Eden, N. B., Bailey, J. E. Cellulose and its derivatives. Ellis Horwood (1985)

Espanol, M., Perez, R. A., Montufar, E. B., Marichal, C., Sacco, A., Ginebra, M. P. Intrinsic porosity of calcium phosphate cements and its significance for drug delivery and tissue engineering applications. Acta Biomaterialia 5, 2752-2762 (2009)

Eyre, D. R., Paz, M. A., Gallop, P. M. Cross-linking in collagen and elastin. Annual Review of Biochemistry 53, 717-748 (1984)

Fantner, G.E., Hassenkam, T., Kindt, J. H., Weaver, J. C., Birkedal, H., Pechenik, L., Cutroni, J.A., Cidade, G. A. G., Stucky, G. D., Morse, D. E., Hansma, P. K. Sacrificial bonds and hidden length dissipate energy as mineralized fibrils separate during bone fracture. Nature Materials 4, 612-616 (2005)

Fatimi, A., Tassin, J., Axelos, M. A. V., Weiss, P. The stability mechanisms of an injectable calcium phosphate ceramic suspension. Journal of Materials Science-Materials in Medicine 21, 1799-1809 (2010)

Fatimi, A., Tassin, J. F., Quillard, S., Axelos, M., Weiss, P. The rheological properties of silated hydroxypropylmethylcellulose tissue engineering matrices. Biomaterials 29, 533-543 (2008)

Fatimi, A., Tassin, J. F., Turczyn, R., Axelos, M., Weiss, P. Gelation studies of a cellulose-based biohydrogel: The influence of pH, temperature and sterilization. Acta Biomaterialia 5, 3423-3432 (2009)

Fernandez, E., Ginebra, M. P., Boltong, M. G., Driessens, F. C. M., Ginebra, J., De Maeyer, E. A. P., Verbeeck, R. M. H., Planell, J. A. Kinetic study of the setting reaction of a calcium phosphate bone cement. Journal of Biomedical Materials Research 32, 367-374 (1996)

Fernandez, E., Gil, F. J., Best, S. M., Ginebra, M. P., Driessens, F. C. M., Planell, J. A. Improvement of the mechanical properties of new calcium phosphate bone cements in the CaHPO4-alpha-Ca-3(PO4)(2) system: Compressive strength and microstructural development. Journal of Biomedical Materials Research 41, 560-567 (1998)

Fernandez, E., Gil, F. L., Ginebra, M. P., Driessens, F. C. M., Planell, J. A. Calcium phosphate bone cements for clinical applications Part I: Solution chemistry. Journal of Materials Science: Materials in Medicine 10, 169-176 (1999A)

Fernandez, E., et al., Production and characterization of new calcium phosphate bone cements in the CaHPO4-alpha-Ca-3(PO4)(2) system: pH, workability and setting times. Journal of Materials Science: Materials in Medicine 10, 223-230 (1999B)

Fernandez, E., Sarda, S., Hamcerencu, M., Vlad, M. D., Gel, M., Valls, S., Torres, R., Lopez, J. High-strength apatitic cement by modification with superplasticizers. Biomaterials 26, 2289-2296 (2005)

Fleming, G. J. P., Shortall, A. C. C., Shelton, R. M., Marquis, P. M. Encapsulated verses hand-mixed zinc phosphate dental cement. Biomaterials 20, 2147-2153 (1999)

Frankenburg, E.P., et al., Biomechanical and histological evaluation of a calcium phosphate cement. Journal of Bone and Joint Surgery-American volume 80, 1112-1124 (1998)

Fratzl, P., Groschner, M., Vogl, G., Plenk H. J., Eschberger, J., Fratzl-zelman, N., Koller, K., Klaushofer, K. Mineral crystalsS in calcified tissues: A comparative study by SAXS. Journal of Bone and Mineral Research 7, 329-334 (1992)

Friel, J. J. Practical guide to image analysis. ASTM international, Materials Park 101-128 (1992)

Fukase, Y., Eanes. E. D., Takagi, S., Chow, L. C., Brown, W. E. Setting reactions and compressive strengths of calcium phosphate cements. Journal of Dental Research 69, 1852-1856 (1990)

Galibert, P., Deramond, H., Rosat, P., Legars, D. Note préliminaire sur le traitement des angiomes vertébraux par vertébroplastie percutanée. Neurochirurgie 33, 166-168 (1987)

Gauthier, O., Bouler, J. M., Aguado, E., Pilet, P., Daculsi, G. Macroporous biphasic calcium phosphate ceramics: influence of macropore diameter and macroporosity percentage on bone ingrowth. Biomaterials 19, 133-139 (1998)

Gbureck, U., Barralet, J. E., Radu, L., Klinger, H. G., Thull, R. Amorphous alpha-tricalcium phosphate: Preparation and aqueous setting reaction. Journal of the American Ceramic Society 87, 1126-1132 (2004A)

Gbureck, U., Barralet, J. E., Spatz, K., Grover, L. M., Thull, R. Ionic modification of calcium phosphate cement viscosity. Part I: hypodermic injection and strength improvement of apatite cement. Biomaterials 25, 2187-2195 (2004B)

Gbureck, U., Grolms, O. Barralet, J. E., Grover, L. M., Thull, R. Mechanical activation and cement formation of beta-tricalcium phosphate. Biomaterials 24, 4123-4131 (2003)

Gibson, L. J. The mechanical behavior of cancellous bone. Journal of Biomechanics 18, 317-328 (1985)

Gibson, L. J., Ashby, M. F. The mechanics of three-dimensional cellular materials. Proceedings of the Royal Society of London. Series A, Mathematical and Physical Sciences 382, 43-59 (1982)

Gibson, L. J., Ashby, M. F. Cellular solids: structure and properties. Cambridge university press 1999

Ginebra, M. P., Delgado, J. A., Harr, I., Almirall, A., Del Valle, S., Planell, J. A. Factors affecting the structure and properties of an injectable self-setting calcium phosphate foam. Journal of Biomedical Materials Research Part A 80, 351-361 (2007)

Ginebra, M.P., Driessens, F., Planell, J.A. Effect of the particle size on the micro and nanostructural features of a calcium phosphate cement: a kinectic analysis. Biomaterials 25, 3453-3462 (2004)

Ginebra, M. P., Fernandez, E., DeMaeyer, E. A. P., Verbeeck, R. M. H., Boltong, M. G., Ginebra, J., Driessens, F. C. M., Planell, J. A. Setting reaction and hardening of an apatitic calcium phosphate cement. Journal of Dental Research 76, 905-912 (1997)

Ginebra, M. P., Fernandez, E., Driessens, F. C. M., Boltong, M. G., Muntasell, J., Font, J., Planell, J. A. The effects of temperature on the behavior of an apatitic calcium phosphate cement. Journal of Materials Science-Materials in Medicine 6, 857-860 (1995)

Ginebra, M.P., Fernandez, E., Driessens, F. C. M., Planell, J. A. Modeling of the hydrolysis of alpha-tricalcium phosphate. Journal of the American Ceramic Society 82, 2808-2812 (1999)

Ginebra, M. P., Rilliard, A., Fernandez, E., Elvira, C., San Roman, J., Planell, J. A. Mechanical and rheological improvement of a calcium phosphate cement by the addition of a polymeric drug. Journal of Biomedical Materials Research 57, 113-118 (2001)

Glimcher, M. J., Bonar, L. C., Grynpas, M. D., Landis, W. J., Roufosse, A. H. Recent studies of bone mineral: Is the amorphous calcium phosphate theory valid?. Journal of Crystal Growth 53, 100-119 (1981)

Gorst, N. J. S., Perrie, Y., Gbureck, U., Hutton, A. L., Hofmann, M. P., Grover, L. M., Barralet, J. E. Effects of fibre reinforcement on the mechanical properties of brushite cement. Acta Biomaterialia 2, 95-102 (2006)

Grados, F., Depriester, C., Cayrolle, G., Hardy, N., Deramond, H., Fardellone, P. Long-term observations of vertebral osteoporotic fractures treated by percutaneous vertebroplasty. Rheumatology 39, 1410-1414 (2000)

Greenwald, A. S., Boden, S. D., Goldberg, V. M., Khan, Y., Laurencin, C. T., Rosier, R. N. Bone-graft substitutes: Facts, fictions, and applications. Journal of Bone and Joint surgery-American 83, 98-103 (2001)

Gross, K. A., Rodriguez-Lorenzo, L. M. Sintered hydroxyfluorapatites. Part II: Mechanical properties of solid solutions determined by microindentation. Biomaterials 25, 1385-1394 (2004)

Griffith A. A. The phenomenon of rupture and flow in solids. Philosophical Transactions of the Royal Society of London A221, 163-198 (1920)

Habib, M., Baroud, G., Gitzhofer, F., Bohner, M. Mechanisms underlying the limited injectability of hydraulic calcium phosphate paste. Acta Biomaterialia 4, 1465-1471 (2008)

Hallam, M. A., Pollard, G., Ward, I. M. Relationship between tensile-strength and molecular-weight of highly drawn polyethylenes. Journal of Materials Science Letters 6, 975-976 (1987)

Heikkila, J. T., Aho, A. J., Kangasniemi, I., YliUrpo, A. Polymethylmethacrylate composites: Disturbed bone formation at the surface of bioactive glass and hydroxyapatite. Biomaterials 17, 1755-1760 (1996)

Hing, K. A. Best, S. M., Bonfield, W. Characterization of porous hydroxyapatite. Journal of Material Science: Materials in Medicine 10, 135-145 (1999)

Hing, K. A. Bone repair in the twenty-first century: biology, chemistry and engineering?. Philosophical Transactions of the Royal Society A 362, 2821-2850 (2004)

Hing, K. A. Bioceramic bone graft substitutes: Influence of porosity and chemistry. International Journal of Applied Ceramic Technology 2, 184-199 (2005A)

Hing, K. A., Annaz, B., Saeed, S., Revell, P. A., Buckland, T. Microporosity enhances bioactivity of synthetic bone graft substitutes. Journal of Material Science: Materials in Medicine 16, 467-475 (2005B)

Hofmann, M. P., Mohammed, A. R., Perrie, Y., Gbureck, U., Barralet, J. E. High-strength resorbable brushite bone cement with controlled drug-releasing capabilities. Acta Biomaterialia 5, 43-49 (2009)

Holmberg, K., Jonsson, B., Kronberg, B., Lindman, B. Surfactants and polymers in aqueous solution. John Wiley (2002)

Ikenaga, M., Trecant, M., Delecrin, J., Royer, J., Passuti, N., Daculsi, G. Biomechanical characterization of a biodegradable calcium phosphate hydraulic cement: A comparison with porous biphasic calcium phosphate ceramics. Journal of Biomedical Materials Research 40, 139-144 (1998)

Ishikawa, K. Effect of spherical tetracalcium phosphate on injectability and basic properties of apatitic cement. Key Engineering Materials 240-242; 269-272 (2003)

Ishikawa, K., Asaoka, K. Estimation of ideal mechanical strength and critical porosity of calcium phosphate cement. Journal of Biomedical Materials Research 29, 1537-1543 (1995B)

Ishikawa, K., Miyamoto, Y., Kon, M., Nagayama, M., Asaoka, K. Non-decay type fast-setting calcium phosphate cement: composite with sodium alginate. Biomaterials 16, 527-532 (1995A)

Ishikawa, K., Takagi, S., Chow, L. C., Ishikawa, Y. Properties and mechanisms of fast-setting calcium phosphate cements. Journal of Material Science: Materials in Medicine 6, 528-533 (1995C)

Jenni, A., Holzer, L., Zurbriggen, R., Herwegh, M. Influence of polymers on microstructure and adhesive strength of cementitious tile adhesive mortars. Cement and Concrete Research 35, 35-50 (2005)

Jernot, J. P., Coster, M., Chermant, J. L. Model to describe the elastic modulus of sintered materials. Physica Status Solidi A 72, 325-332 (1982)

Julien, M., Khairoun, I., LeGeros, R. Z., Delplace, S., Pilet, P., Weiss, P., Daculsi, G., Bouler, J. M., Guicheux, J. Physico-chemical-mechanical and in vitro biological properties of calcium phosphate cements with doped amorphous calcium phosphates. Biomaterials 28, 956-965 (2007)

Jyoti, M. A., Thai, V. V., Min, Y. K., Lee, B. T., Song, H. Y. In vitro bioactivity and biocompatibility of calcium phosphate cements using

Hydroxy-propyl-methyl-Cellulose (HPMC). Applied Surface Science 257, 1533-1539 (2010)

Kai, D., Li, D. X., Zhu, X. D., Zhang, L., Fan, H. S., Zhang, X. D. Addition of sodium hyaluronate and the effect on performance of the injectable calcium phosphate cement. Journal of Materials Science-Materials in Medicine 20, 1595-1602 (2009)

Karageorgiou, V., Kaplan, D. Porosity of 3D biomaterial scaffolds and osteogenesis. Biomaterials 26, 5474-5491 (2005)

Keary, C. M. Characterization of METHOCEL cellulose ethers by aqueous SEC with multiple detectors. Carbohydrate polymers 45, 293-303 (2001)

Khairoun, I., Boltong, M. G., Driessens, F. C. M., Planell, J. A. Some factors controlling the injectability of calcium phosphate bone cements. Journal of Materials Science-Materials in Medicine 9, 425-428 (1998)

Khairoun, I., Driessens, F. C. M., Boltong, M. G., Planell, J. A., Wenz, R. Addition of cohesion promoters to calcium phosphate cements. Biomaterials 20, 393-398 (1999)

Khairoun, I., Magne, D., Gauthier, O., Bouler, J. M., Aguado, E., Daculsi, G., Weiss, P. In vitro characterization and in vivo properties of a carbonated apatite bone cement. Journal of Biomedical Materials Research 60, 633-642 (2002)

Khayat, K. H. Effects of anti-washout admixtures on fresh concrete properties. American concrete institute-materials journal 92, 164-171 (1995)

Khayat, K. H. Viscosity-enhancing admixtures for cement-based materials-An overview. Cement and Concrete Composites 20, 171-188 (1998)

Khayat, K. H., Yahia, A. Effect of welan gum-high-range water reducer combinations on rheology of cement grout. American concrete institute-materials journal 94, 365-372 (1997)

Kingery, W. D. Introduction of ceramics. Wiley, New York (1976)

Knott, L., Bailey, A. J. Collagen cross-links in mineralizing tissues: A review of their chemistry, function, and clinical relevance. Bone 22, 181 (1998)

Koester, K.J., Ager J.W., Ritchie, R.O. The true toughness of human cortical bone measured with realistically short cracks. Nature Materials 7, 672-677 (2008)

Konigsberger, E., Konigsberger, L. C. Biomineralization: Medical aspects of solubility. Wiley, England (2006)

Launey, M.E., Ritchie, R.O. On the Fracture Toughness of Advanced Materials. Advanced Materials 21, 2103-2110 (2009)

LeGeros, R. Z., Chohayeb, A., Shulman, A. Apatitic calcium phosphates: possible dental restorative materials. Journal of Dental Research 61, 343 (1982)

Le Huec, J. C., Schaeverbeke, T., Clement, D., Faber, J. Le Rebeller, A. Influence of porosity on the mechanical resistance of hydroxyapatite ceramics under compressive stress. Biomaterials 16, 113-118 (1995)

Lewis, G. Properties of acrylic bone cement: State of the art review. Journal of Biomedical Materials Research 38, 155-182 (1997)

Lewis, G., Mladsi, S. Correlation between impact strength and fracture toughness of PMMA-based bone cements. Biomaterials 21, 775-781 (2000)

Li, M., Liu, X. Y., Liu, X. D., Ge, B. F., Chen, K. M. Creation of macroporous calcium phosphate cements as bone substitutes by using genipin-crosslinked gelatin microspheres. Journal of Materials Science-Materials in Medicine 20, 925-934 (2009)

Lilley, K. J., Gbureck, U., Knowles, J. C., Farrar, D. F., Barralet, J. E. Cement from magnesium substituted hydroxyapatite. Journal of Materials Science-Materials in Medicine 16, 455-460 (2005)

Link, D.P., et al., Mechanical evaluation of implanted calcium phosphate cement incorporated with PLGA microparticles. Biomaterials 27, 4941-4947 (2006)

Liu, C. S., Shao, H. F., Chen, F. Y., Zheng, H. Y. Effects of the granularity of raw materials on the hydration and hardening process of calcium phosphate cement. Biomaterials 24, 4103-4113 (2003)

Liu, C. S., Shao, H. F., Chen, F. Y., Zheng, H. Y. Rheological properties of concentrated aqueous injectable calcium phosphate cement slurry. Biomaterials 27, 5003-5013 (2006)

Liu, D. M. Influence of porosity and pore size on the compressive strength of porous hydroxyapatite ceramic. Ceramics International 23, 135-139 (1997)

Liu, D. M. Preparation and characterization of porous hydroxyapatite bioceramic via a slip-casting route. Ceramics International 24, 441-446 (1998)

Liu, H., Li, H., Cheng, W. J., Yang, Y., Zhu, M. Y., Zhou, C. R. Novel injectable calcium phosphate/chitosan composites for bone substitute materials. Acta Biomaterialla 2, 557-565 (2006)

Lowenstam, H. A., Weiner, S. On biomineralization. Oxford, (1989)

Lu, W.W., Zhao, F., Luk, K. D. K., Yin, Y. J., Cheung, K. M. C., Cheng, G. X., Yao, K. D., Leong, J. C. Y. Controllable porosity hydroxyapatite ceramics as spine cage: fabrication and properties evaluation. Journal of Materials Science-Materials in Medicine 14, 1039-1046 (2003)

Maravic, M., Le Bihan C, Landais, P., Fardellone, P. Incidence and cost of osteoporotic fractures in France during 2001. A methodological approach by the national hospital database. Osteoporosis International 16, 1475-1480 (2005)

Marino, F.T., Torres, J., Hamdan, M., Rodriguez, C. R., Cabarcos, E. L. Advantages of using glycolic acid as a retardant in a brushite forming cement. Journal of Biomedical Materials Research Part B- Applied Biomaterials 83, 571-579 (2007)

Martin, R. I., Brown, P. W. Mechanical properties of hydroxyapatite formed at physiological temperature. Journal of Materials Science-Materials in Medicine 6, 138-143 (1995)

Meeder, P. J., Eggers, C. The history of autogenous bone grafting. Injury 25(suppl. 1), A2-A3 (1994)

Merceron, C., Portron, S., Masson, M., Fellah, B. H., Gauthier, O., Lesoeur, J., Chérel, Y., Weiss, P., Guicheux, J., Vinatier, C. Cartilage tissue engineering: From hydrogel to mesenchymal stem cells. Bio-medical Materials and Engineering 20, 159-166 (2010)

Merkert, P., Hoffman, M., Rodel, J. Detection of prefracture microcracking in Al_2O_3 by acoustic emission. Journal of the European Ceramic Society 18, 1645-1654 (1998)

Meyer, P. R., Lautenschlager, E.P., Moore, B.K. On the setting properties of acrylic bone cement. The Journal of Bone and Joint Surgery (American volume) 55, 149-56 (1973)

Metsger, D. S., Rieger, M. R., Foreman, D. W. Mechanical properties of sintered hydroxyapatite and tricalcium phosphate ceramic. Journal of Materials Science-Materials in Medicine 10, 9-17 (1999)

Milosevski, M., Bossert, J., Milosevski, D., Gruevska, N. Preparation and properties of dense and porous calcium phosphate. Ceramics International 25, 693-696 (1999)

Miranda, P., Pajares, A., Saiz, E., Tomsia, A. P., Guiberteau, F. Mechanical properties of calcium phosphate scaffolds fabricated by robocasting. Journal of Biomedical Materials Research Part A 85, 218-227 (2008)

Monma, H., Ueno, S., Kanazawa, T. Properties of hydroxyapatite prepared by hydrolysis of tricalcium phosphate. Journal of Chemical Technology and Biotechnology 31, 15-24 (1981)

Montufar, E. B., Traykova, T., Gil, C., Harr, I., Almirall, A., Aguirre, A., Engel, E., Planell, J. A., Ginebra, M. P. Foamed surfactant solution as a template for self-setting injectable hydroxyapatite scaffolds for bone regeneration. Acta biomaterialia 6, 876-885 (2010)

Morgan, E. F., Yetkinler, D. N., Constantz, B. R., Dauskardt, R. H. Mechanical properties of carbonated apatite bone mineral substitute: strength, fracture and fatigue behavior. Journal of Materials Science-Materials in Medicine 8, 559-570 (1997)

Munz, D., Fett, T. Ceramics: mechanical properties, failure behavior, materials selection. Springer 2001

Nalla, R. K., Kruzic, J. J., Ritchie, R. O. On the origin of the toughness of mineralized tissue: microcracking or crack bridging? Bone 34, 790-798 (2004A)

Nalla, R. K., Kruzic, J. J., Kinney, J. H., Ritchie, R. O. Effect of aging on the toughness of human cortical bone: evaluation by R-curves. Bone 35, 1240-1246 (2004B)

Nalla, R. K., Kruzic, J. J., Kinney, J. H., Ritchie, R. O. Mechanistic aspects of fracture and R-curve behavior in human cortical bone. Biomaterials 26, 217-231 (2005)

Nyman, J.S., Roy, A., Shen, X. M., Acuna, R. L., Tyler, J. H., Wang, X. D. The influence of water removal on the strength and toughness of cortical bone. Journal of Biomechanics 39, 931-938 (2006)

Olszta, M. J., Cheng, X. G., Jee, S. S., Kumar, R., Kim, Y. Y., Kaufman, M. J., Douglas, E. P., Gower, L. B. Bone structure and formation: A new perspective. Materials Science & Engineering R-Reports 58, 77-116 (2007)

Ormsby, R., McNally, T., Mitchell, C., Dunne, N. Incorporation of multiwalled carbon nanotubes to acrylic based bone cements: Effects on mechanical and thermal properties. Journal of the Mechanical Behavior of Biomedical Materials 3, 136-145 (2010)

Osmers, H. R., Metzner, A. B. Diffusion in dilute polymeric solutions. Industrial & Engineering Chemistry Fundamentals 11, 161-169 (1972)

Otsuka, M., Matsuda, Y., Suwa, Y., Fox, J. L., Higuchi, W. I. Effect of particle size of metastable calcium phosphates on mechanical strength of a novel self-setting bioactive calcium phosphate cement. Journal of Biomedical Materials Research 29, 25–32 (1995)

Pecqueux, F. Elaboration et propriétés mécaniques de biocéramiques macroporeuses pour la substitution osseuse. PhD Thesis, Universite de Nantes (2009)

Pecqueux, F., Tancret, F., Payraudeau, N., Bouler, J. M. Influence of microporosity and macroporosity on the mechanical properties of biphasic calcium phosphate bioceramics: Modelling and experiment. Journal of the European Ceramic Society 30, 819-829 (2010)

Pernot, F., Etienne, P., Boschet, F., Datas, L. Weibull parameters and the tensile strength of porous phosphate glass-ceramics. Journal of the American Ceramic Society 82, 641-648 (1999)

Peterlik, H, Roschger, P., Klaushofer, K., Fratzl, P. From brittle to ductile fracture of bone. Nature Materials 5, 52-55 (2006)

Pietak, A. M. et al Silicon substitution in the calcium phosphate bioceramics. Biomaterials 28, 4023-4032 (2007)

Pina, S., Torres, P. M., Goetz-Neunhoeffer, F., Neubauer, J., Ferreira, J. M. F. Newly developed Sr-substituted [alpha]-TCP bone cements. Acta Biomaterialia 6, 928-935 (2010)

Pourchez, J., Grosseau, P., Ruot, B. Changes in C3S hydration in the presence of cellulose ethers. Cement and Concrete Research 40, 179-188 (2010A)

Pourchez, J., Ruot, B., Debayle, J., Pourchez, E., Grosseau, P. Some aspects of cellulose ethers influence on water transport and porous structure of cement-based materials F-4976-2011. Cement and Concrete Research 40, 242-252 (2010B)

Qi, X. P., Ye, J. D. Mechanical and rheological properties and injectability of calcium phosphate cement containing poly (lactic-co-glycolic acid) microspheres. Materials Science & Engineering C-Materials for Biological Applications 29, 1901-1906 (2009)

Raynaud, S., Champion, E., Lafon, J. P., Bernache-Assollant, D. Calcium phosphate apatites with variable Ca/P atomic ratio III. Mechanical properties and degradation in solution of hot pressed ceramics. Biomaterials 23, 1081-1089 (2002)

Reddi, A. H. Morphogenesis and tissue engineering of bone and cartilage: inductive signals, stem cells and biomimetic biomaterials. Tissue Engineering 6, 351-359 (2000)

Rho, J. Y., Kuhn-Spearing, L., Zioupos, P. Mechanical properties and the hierarchical structure of bone. Medical Engineering & Physics 20, 92-102 (1998)

Rice, R. W. Comparison of stress concentration versus minimum solid area based mechanical property-porosity relations. Journal of Materials Science 28, 2187-2190 (1993)

Rice, R. W. Evaluation and extension of physical property-porosity models based on minimum solid area. Journal of Materials Science 31, 102-118 (1996)

Rice, R. W. Porosity of ceramics. CRC, USA (1998)

Rice, R. W., Freiman, S. W. Grain-size dependence of fracture energy in ceramics: II, a model for noncubic materials. Journal of American Ceramic Society 64, 350-354 (1981B)

Rice, R. W., Freiman, S. W., Becher, P. F. Grain-size dependence of fracture energy in ceramics: I, experiment. Journal of American Ceramic Society 64, 345-350 (1981A)

Ritchie, R. O. The conflicts between strength and toughness. Nature Materials 10, 817-822 (2011)

Rödel, J. Crack closure forces in ceramics: characterization and formation. Journal of the European Ceramic Society 9, 323-334 (1992)

Rodriguez-Lorenzo, L. M., Vallet-Regi, M., Ferreira, J. M. F., Ginebra, M. P., Aparicio, C., Planell, J. A. Hydroxyapatite ceramic bodies with tailored mechanical properties for different applications. Journal of Biomedical Materials Research 60, 159-166 (2002)

Rupprecht, S., Merten, H. A., Kessler, P., Wiltfang, J. Hydroxyapatite cement (BoneSource™) for repair of critical sized calvarian defects--an experimental study. Journal of Cranio-Maxillofacial Surgery 31, 149-153 (2003)

Saha, S., PAL, S. Improvement of mechanical properties of acrylic bone cement by fiber reinforcement. Journal of Biomechanics 17, 467-478 (1984)

Saimoto, A., Imai, Y., Hashida, T., Nisitani, H. Simulation of compressive fracture of brittle and disordered solids. Key Engineering Materials 243, 285-290 (2003)

Saint-Jean, S. J., Camire, C. L., Nevsten, P., Hansen, S., Ginebra, M. P. Study of the reactivity and in vitro bioactivity of Sr-substituted alpha-TCP cements. Journal of Materials Science-Materials in Medicine 16, 993-1001 (2005)

Salehi, M., Salem, A. Effect of moisture content on extrusion process of kaolinitic-illitic clay in manufacturing of ceramic Raschig ring. Journal of Materials Processing Technology 200, 232-237 (2008)

Sammis, C. G., Ashby, M. F. The failure of brittle porous solids under compressive stress states. Acta Metallurgica 34, 511-526 (1986)

Sarda, S., Fernandez, E., Nilsson, M., Balcells, M., Planell, J. A. Kinetic study of citric acid influence on calcium phosphate bone cements as water-reducing agent. Journal of Biomedical Materials Research 61, 653-659 (2002)

Shimogoryo, R., Eguro, T., Kimura, E., Maruta, M., Matsuya, S., Ishikawa, Kunio. Effects of added mannitol on the setting reaction and mechanical strength of apatite cement. Dental Materials Journal 28, 627-633 (2009)

Steinbrech, R.W. “Toughnening mechanisms for ceramic materials”. Journal of the European Ceramic Society 10, 131-142 (1992)

Ström, O., Borgström, F., Kanis, John A., Compston, J., Cooper, C., McCloskey, Eugene V. and Jönsson, B. Osteoporosis: burden, health care provision and opportunities in the EU- A report prepared in collaboration with the International Osteoporosis Foundation (IOF) and the European Federation of Pharmaceutical Industry Associations (EFPIA). Archives of Osteoporosis 6, 59-155 (2011)

Swain, M. V., Rose, L. R. F. Toughening of ceramics. Proceeding of the 6th international conference on fracture 473-494 (1984)

Tajima, S., Kishi, Y., Makoto, O. D. A., Maruta, M., Matsuya, S., Ishikawa, K. Fabrication and biporous low-crystalline apatite based on mannitol dissolution from apatite cement. Dental Materials Journal 25, 616-620 (2006)

Takagi, S., Chow, L. C. Formation of macropores in calcium phosphate cement implants. Journal of Materials Science-Materials in Medicine 12, 135-139 (2001)

Tancret, F., Bouler, J. M., Chamousset, J., Minois, L. M. Modelling the mechanical properties of microporous and macroporous biphasic calcium phosphate bioceramics. Journal of the European Ceramic Society 26, 3647-3656 (2006)

Tancret, F., Desgardin, G., Osterstock, F. Influence of porosity on the mechanical properties of cold isostatically pressed and sintered $YBa_2Cu_3O_{7-x}$ superconductors. Philosophical Magazine A 75, 505-523 (1997)

Tancret, F., Monot, I., Osterstock, F. Toughness and thermal shock resistance of $YBa_2Cu_3O_{7-x}$ composite superconductors containing Y_2BaCuO_5 or Ag particles. Materials Science and Engineering A 298, 268-283 (2001)

Tancret, F., Osterstock, F. Modelling the toughness of porous sintered glass beads with various fracture mechanism. Philosophical Magazine 83, 137-150 (2003)

Taylor, D., Hazenberg, J. G., Lee, T. C. Living with cracks: Damage and repair in human bone. Nature Materials 6, 263-268 (2007)

TenHuisen, K.S., Brown, P.W. The effects of citric and acetic-acids on the formation of calcium-deficient hydroxyapatite at 38℃ Journal of Materials Science-Materials in Medicine 5, 291-298 (1994)

TenHuisen, K.S., Brown, P.W. Formation of calcium-deficient hydroxyapatite from alpha-tricalcium phosphate. Biomaterials 19, 2209-2217 (1998)

TenHuisen, K.S., Brown, P.W. Hydrolysis of alpha-tricalcium phosphate in NaF solutions. Biomaterials 20, 427-434 (1999)

Thangamani, N., Chinnakali, K., Gnanam, F. D. The effect of powder processing on densification, microstructure and mechanical properties of hydroxyapatite. Ceramics International 28, 355-362 (2002)

Togawa, D., Bauer, T. W., Lieherman, I. H., Sakai, H. Lumbar intervertebral body fusion cages: histological evaluation of clinically failed cages retrieved from humans. Journal of Bone and Joint Surgery America 86, 70-79 (2004)

Trojani, C., Boukhechba, F., Scimeca, J. C., Vandenbos, F., Michiels, J. F., Daculsi, G., Boileau, P., Weiss, P., Carle, G. F., Rochet, N. Ectopic bone formation using an

injectable biphasic calcium phosphate/Si-HPMC hydrogel composite loaded with undifferentiated bone marrow stromal cells. Biomaterials 27, 3256-3264 (2006)

Ueyama, Y., Ishikawa, K., Mano, T., Koyama, T., Nagatsuka, H., Matsumura, T. Initial tissue response to anti-washout apatite cement in the rat palatal region: comparison with conventional apatite cement. Journal of Biomedical Materials Research 55, 652-660 (2001)

Vallet-Reg, M., Gonzalez-Calbet, J.M. Calcium phosphates as substitution of bone tissues. Progress in Solid State Chemistry 32, 1-31 (2004)

Vallo, C. I., Montemartini, P. E., Fanovich, M. A., Porto-Lopez, J. M., Cuadrado, T. R. Polymethylmethacrylate-based bone cement modified with hydroxyapatite. Journal of Biomedical Materials Research 48, 150-158 (1999)

Vashishth, D., Rising crack-growth-resistance behavior in cortical bone: implications for toughness measurements. Journal of Biomechanics 37, 943-946 (2004)

Villora, J. M., Callejas, P., Barba, M. F., Baudin, C. Statistical analysis of the fracture behavior of porous ceramic Raschig rings. Journal of the European Ceramic Society 24, 589-594 (2004)

Vinatier, C., Gauthier, O., Fatimi, A., Merceron, C., Masson, M., Moreau, A., Moreau, F., Fellah, B., Weiss, P., Guicheux, J. An injectable celllose-based hydrogel for the transfer of autologous nasal chondrocytes in articular cartilage defects. Biotechnology and Bioengineering 102, 1259-1267 (2009)

von Doernberg, M. C., von Rechenberg, B., Bohner, M., Grunenfelder, S., van Lenthe, G. H., Muller, R., Gasser, B., Mathys, R., Baroud, G., Auer, J. In vivo behavior of calcium phosphate scaffolds with four different pore sizes. Biomaterials 27, 5186-5198 (2006)

Wagoner Johnson, A. J., Herschler, B.A. A review of the mechanical behavior of CaP and CaP/polymer composites for applications in bone replacement and repair. Acta Biomaterialia 7, 16-30 (2011)

Wagh, A. S., Poeppel, R. B., Singh, J. P. Open pore description of mechanical properties of ceramics. Journal of Materials Science 26, 3862-3868 (1991)

Wagh, A. S., Singh, J. P., Poeppel, R. B. Dependence of ceramic fracture properties on porosity. Journal of Materials Science 28, 3589-3593 (1993)

Wang, L., D'Alpino, P. H. P., Lopes, L. G., Pereira, J. C. Mechanical properties of dental restorative materials: relative contribution of laboratory tests. Journal of Applied Oral Science 11, 162-167 (2003)

Wang, X. P., Chen, L., Xiang, H., Ye, J. D. Influence of anti-washout agents on the rheological properties and injectability of a calcium phosphate cement. Journal of Biomedical Materials Research Part B-Applied Biomaterials 81, 410-418 (2007)

Wang, X. P., Ye, J. D., Wang, Y. J. Reinforcement of calcium phosphate cement by bio-mineralized carbon nanotube. Journal of American Ceramic Society 90, 962-964 (2007)

Weibull, W. A. A statistical theory of the strength of materials. Ingeniörs Vetenskaps Akademien – Hanlingar 151, 1-45 (1939)

Weibull, W. A statistical distribution function of wide applicability. Journal of Applied Mechanics 18 (1951) 293-305.

Weiss, P., Gauthier, O., Bouler, J. M., Grimandi, G., Daculsi, G. Injectable bone substitute using a hydrophilic polymer. Bone 2, 67-70 (1999)

Weiss, P., Lapkowski, M., Legeros, R. Z., Bouler, J. M., Jean, A., Daculsi, G. Fourier-transform infrared spectroscopy study of an organic–mineral composite for bone and dental substitute materials. Journal of Materials Science: Materials in Medicine 8(10), 621-629 (1997)

Weiss, P., Vinatier, C., Sohier, J., Fatimi, A., Layrolle, P., Demais, V., Atmani, H., Basle, M. F., Guicheux, J. Self-hardening hydrogel for bone tissue engineerin. Macromolecular Symposia 266, 30-35 (2008)

Weyer, H. J., Muller, I., Schmitt, B., Bosbach, D., Putnis, A. Time-resolved monitoring of cement hydration: Influence of cellulose ethers on hydration kinetics. Nuclear instrument and methods in physics B 238, 102-106 (2005)

Woodard, J.R., Hilldore, A.J., Lan, S.K., Park, C.J., Morgan, A.W., Eurell, J.A.C., Clark, S.G., Wheeler, M.B., Jamison, R.D., Wagoner Johnson, A.J., The mechanical properties and osteoconductivity of hydroxyapatite bone scaffolds with multi-scale porosity, Biomaterials 28, 45-54 (2007)

Xie, B. Q., Nancollas, G. H. How to control the size and morphology of apatite nanocrystals in bone. Proceedings of the National Academy of Sciences of the United States of America107, 22369-22370 (2010)

Xu, H. H. K., Eichmiller, F. C., Giuseppetti, A. A. Reinforcement of a self-setting calcium phosphate cement with different fibers. Journal of Biomedical Materials Research 52, 107-114 (2000).

Xu, H. H. K., Quinn, J. B. Calcium phosphate cement containing resorbable fibers for short-term reinforcement and macroporosity. Biomaterials 23, 193-202 (2002)

Xu, H. H. K., Quinn, J. B., Takagi, S., Chow, L. C., Eichmiller, F. C. Strong and macroporous calcium phosphate cement: Effects of porosity and fiber reinforcement on mechanical properties. Journal of Biomedical Materials Research 57, 457-466 (2001)

Xu, H. H. K., Simon, C. G. Self-hardening calcium phosphate cement-mesh composite : reinforcement, macropores, and cell response. Journal of Biomedical Materials Research 69, 267-278 (2004A)

Xu, H. H. K., Simon, C. G. Fast setting calcium phosphate-chitosan scaffold: mechanical properties and biocompatibility. Biomaterials 26, 1337-1348 (2005)

Xu, H. H. K., Takagi, S., Quinn, J. B., Chow, L. C. Fast-setting calcium phosphate scaffolds with tailored macropore formation rates for bone regeneration. Journal of Biomedical Materials Research Part A 68, 725-734 (2004B)

Xu, H. H. K., Weir, M. D., Burguera, E. F., Fraser, A. M. Injectable and macroporous calcium phosphate cement scaffold. Biomaterials 27, 4279-4287 (2006)

Yamamoto, H., et al., Mechanical strength of calcium phosphate cement in vivo and in vitro. Biomaterials 19, 1587-1591 (1998)

Yang, Q. Z., Troczynski, T., Liu, D. M. Influence of apatite seeds on the synthesis of calcium phosphate cement. Biomaterials 23, 2751-2760 (2002)

Yashima, M., Sakai, A. High-temperature neutron powder diffraction study of the structural phase transition between α and α’ phases in tricalcium phosphate Ca3(PO4)2. Chemical Physics Letters 372, 779-783 (2003)

Yokoyama, A., Yamamoto, S., Kawasaki, T., Kohgo, T., Nakasu, M. Development of calcium phosphate cement using chitosan and citric acid for bone substitute materials. Biomaterials 23, 1091-1101 (2002)

Zhang, Y., Xu, H. H. K. Effect of synergistic reinforcement and absorbable fiber strength on hydroxyapatite bone cement. Journal of Biomedical Materials Research 75, 832-840 (2005)

Zhang, Y., Xu, H. H. K., Takagi, S., Chow, L. C. In-situ hardening hydroxyapatite-based scaffold for bone repair. Journal of Materials Science-Materials in Medicine 17, 437-445 (2006)

Zuo, Y., Yang, F., Wolke, J. G. C., Li, Y. B., Jansen, J. A. Incorporation of biodegradable electrospun fibers into calcium phosphate cement for bone regeneration. Acta Biomaterialia 6, 1238-1247 (2010)